Neural stem cells from embryonic brain of mice and neural cell adhesion molecule L1 and projection aberrations to the hippocampus in NCAM deficient mice (Mus musculus L., 1758)

Dissertation

zur Erlangung des Doktorgrades im Department Biologie der Fakultät für Mathematik, Informatik und Naturwissenschaften an der Universität Hamburg
vorgelegt von Yuliya Tereshchenko

Hamburg 2008

Genehmigt vom Department Biologie
der Fakultät für Mathematik, Informatik und Naturwissenschaften
an der Universität Hamburg
auf Antrag von Frau Professor Dr. M. SCHACHNER
Weiterer Gutachter der Dissertation:
Herr Professor Dr. K. WIESE
Tag der Disputation: 08. Februar 2008

Hamburg, den 25. Januar 2008

Professor Dr. Jörg Ganzhorn
Leiter des Departments Biologie

Contents

Abstract

Cell recognition molecules comprise a prominent group of molecules regulating cell-cell or cell-matrix interactions in the developing, adult and pathologically altered nervous system. They have been implicated in several critical processes of nervous system development, including cell migration, axon outgrowth and fasciculation, myelination and synapse formation. Cell recognition molecules of the immunoglobulin superfamily are characterized by the existence of at least one immunoglobulin like domain, enabling them to mediate cell adhesion in a calcium independent manner.

The neural cell adhesion molecule (NCAM) is implicated in nervous system development and plasticity and its ablation in mice causes a range of functional abnormalities. In this study we performed quantitative immunohistochemical analyses of catecholaminergic and cholinergic nuclei and their hippocampal projections in NCAM deficient (NCAM-/-) mice and wild-type (NCAM+/+) littermates with the aim to identify structural aberrations underlying abnormal functions. It was found that total numbers of cholinergic neurons in the medial septa / diagonal band nuclear complex and dopaminergic neurons in the A9-A10 nuclei were by 18-27% decreased in both young and adult (2- and 13-month-old, respectively) NCAM-/- mice versus NCAM+/+ littermates. The number of noradrenergic neurons in the locus coeruleus was not affected by the mutation. Despite reduced numbers of projecting neurons, length densities and total length of catecholaminergic and cholinergic axons in the hippocampus were normal in young NCAM-/- mice. In adult NCAM -/- mice, however, the abnormally small dentate gyrus was deficiently innervated by catecholaminergic fibers (by 27% lower fiber length compared to NCAM+/+ littermates), while the cornu ammonis received abnormally higher cholinergic input (by 27% and 47% in CA1 and CA3, respectively). These results indicate early developmental loss of cholinergic and dopaminergic cells in NCAM-/- mice and differential age-related effects of the mutation on two types of hippocampal projections.

The functions of a second member of the Ig superfamily, the neural recognition molecule L1, were also investigated. L1 is implicated in migration of nerve cells, outgrowth, pathfinding, fasciculation and regeneration of axons, adhesion between neurons and between neurons and Schwann cells, neuronal cell survival, and proliferation and fate decision of neural precursor cells. Neural stem cells (NSCs) are characterized by their multipotentiality and capability for self-renewal, and are considered as candidate cells to develop cell-based

therapies for the treatment of neurodegenerative disorders. Genetic manipulations of these cells prior to transplantation might improve their therapeutic potential by, for instance, enhancing their migratory capacity, influencing their differentiation potential or improving their survival. These aims might be achieved by transfecting these cells with the neural recognition molecule L1. To test this hypothesis, we established a method that allows efficient non-viral stable transfection of mouse NSCs using the nucleofection technique. To characterize the properties of L1-nucleofected NSCs *in vivo*, cells were grafted into the quinolinic acid-lesioned striatum of adult mice. In this animal model, stably L1-nucleofected NSCs showed improved migratory capacity when compared to control NSCs. Moreover, stably L1-nucleofected NSCs showed increased neuronal and decreased astrocytic differentiation when compared to control cells.

Zusammenfassung

Zellerkennungsmoleküle stellen eine bedeutende Gruppe von Molekülen dar, die Zell-Zell- oder Zell-Matrix-Interaktionen im sich entwickelnden, adulten und pathologisch veränderten Nervensystem regulieren,. Diese Moleküle steuern verschiedene wichtige Abläufe während der Entwicklung des Nervensystems wie das Wandern von Zellen, das Auswachsen und Bündeln von Neuriten, Myelinisierung und die Bildung von Synapsen. Zellerkennungsmoleküle der Immunglobulin-Superfamilie sind durch die Existenz von mindestens einer Immunglobulin-ähnlichen Domäne gekennzeichnet, welche es ihnen ermöglicht, eine Calcium-unabhängige Zelladhäsion vermitteln.

Das neurale Zelladhäsionsmolekül (NCAM) spielt eine Rolle bei der Entwicklung und Plastizität des zentralen Nervensystems, und seine Ablation in Mäusen verursacht eine Reihe von funktionellen Störungen. In dieser Studie haben wir quantitative immunhistochemische Analysen von catecholaminergen und cholinergen Kernen und deren hippocampalen Projektionen in NCAM-defizienten (NCAM-/-) und Wildtyp (NCAM+/+) Mäusen mit dem Ziel durchgeführt, strukturelle Aberrationen zu identifizieren, welche die gestörten Funktionen bedingen. Es wurde gefunden, dass die Gesamtzahl der cholinergen Neurone im Kernkomplex des medialen Septums / diagonalen Bandes und die der dopaminergen Neurone in den A9-A10 Kernen sowohl in jungen als auch adulten (2 beziehungsweise 13 Monate alten) NCAM-/- Mäusen um 18-27% im Vergleich zu deren NCAM+/+ Geschwistertieren reduziert war. Demgegenüber war die Zahl der noradrenergen Neurone im Locus coeruleus durch die Mutation nicht verändert. Trotz der reduzierten Anzahl an Projektionsneuronen waren Dichte und Gesamtlänge der catecholaminergen und cholinergen Axone im Hippocampus von jungen NCAM-/- Mäusen normal. In adulten NCAM-/- Mäusen hingegen zeigte der abnormal verkleinerte Gyrus dentatus eine verminderte Innervation durch catecholaminerge Fasern (eine um 27% geringere Faserlänge im Vergleich zu NCAM+/+ Geschwistertieren), während das Cornu ammonis eine abnormal erhöhte cholinerge Innervation aufwies (um 27% und 47% höher in der CA1- beziehungsweise in der CA3-Region). Diese Ergebnisse zeigen eine Reduktion von cholinergen und dopaminergen Zellen in NCAM-/- Mäusen während der frühen Entwicklung und differentielle, altersabhängige Effekte der Mutation auf zwei Formen hippocampaler Projektionen.

Die Funktionen eines zweiten Mitglieds der Immunglobulin-Superfamilie, die des neuralen Erkennungsmoleküls L1, wurden ebenfalls untersucht. L1 beeinflußt die Migration

von Nervenzellen, das Auswachsen, die Wegfindung, Bündelung und Regeneration von Axonen, die Adhäsion zwischen Neuronen sowie zwischen Neuronen und Schwann`schen Zellen, das Überleben von neuronalen Zellen und die Proliferation und die Differenzierung von neuralen Vorläuferzellen. Neurale Stammzellen (NSCs) sind durch ihre Multipotenz und ihre Fähigkeit zur Selbsterneuerung charakterisiert und werden als potentielle Kandidatenzellen für die Entwicklung zellbasierter Therapien zur Behandlung neurodegenerativer Erkrankungen betrachtet. Die genetische Manipulation dieser Zellen vor deren Transplantation könnte ihr therapeutisches Potential verbessern, zum Beispiel durch Erhöhung ihrer Migrationsfähigkeit, durch Beeinflussung ihres Differenzierungspotentials oder durch Verbesserung ihres Überlebens. Diese Ziele könnten durch eine Transfektion mit dem neuralen Erkennungsmolekül L1 erreicht werden. Zur Überprüfung dieser Hypothese haben wir eine Methode etabliert, die eine effiziente nicht-virale, stabile Transfektion von Maus-NSCs unter Anwendung der Nucleofektionstechnik erlaubt. Um die Eigenschaften von L1-transfizierten NSCs *in vivo* zu testen, wurden die Zellen in das Quinolinsäure-lädierte Striatum adulter Mäuse transplantiert. In diesem Tiermodell wiesen stabil L1-transfizierte NSCs ein verbesserte Migrationvermögen im Vergleich zu Kontrollzellen auf. Weiterhin zeigten L1-transfizierte NSCs eine verstärkte neuronale und eine verminderte astrozytäre Differenzierung im Vergleich zu Kontrollzellen.

Study one: Hippocampal dysplasia and aberrations in cholinergic and catecholaminergic nuclei and their hippocampal projections in NCAM-deficient mice

1. Introduction

1.1. General Introduction

During development of the nervous system, neurons migrate and extend axons in order to find their final functional position and to innervate their appropriate targets. These developmental processes are crucially dependent on cell-cell and cell-matrix interactions. Migrating cells and outgrowing processes orient themselves along short-range and long-range, attractive or repulsive guidance cues. These guidance cues can be expressed on the cell surface of, for instance, glial cells or pioneering axons, or they are secreted into the extracellular matrix.

One prominent group of molecules regulating cell-cell or cell-matrix interactions are the cell recognition molecules. There exist three main families of recognition molecules, the integrins, the cadherins and the immunoglobulin superfamily (Ig superfamily). Characteristic for the members of the Ig superfamily is the existence of at least one Ig-like domain, which allows them to mediate cell adhesion via a calcium independent mechanism. Three subfamilies have been distinguished within the Ig superfamily: (1) molecules, that contain only Ig-like domains, (2) molecules that possess Ig and fibronectin type III- (FN III) like domains and (3) molecules with Ig-like and various other domains (Brümmendorf et al., 1998). This work focuses on the neural cell adhesion molecule (NCAM), a transmembrane protein belonging to the second subgroup of Ig superfamily members (Cunningham et al., 1987; Walmod et al., 2004).

1.2. NCAM

1.2.1. Structure of NCAM

NCAM was the first cell adhesion molecule identified in the nervous system. It consists of five Ig-like domains and two fibronectin type III like domains (Fig. 1). From all members of the Ig-superfamily, it displays the highest homology to the myelin-associated glycoprotein (MAG) both with respect to sequence and overall structure (Salzer et al., 1987).The NCAM gene, which is located on chromosome 9 in mice (D'Eustachio et al., 1985) and on chromosome 11 in humans (Nguyen et al., 1986), gives rise to several different protein isoforms by alternative splicing of the primary transcript. The major isoforms have a size of 180, 140 and 120 kD and differ only in the size of their cytoplasmic domain (Fig.1). The 180 kD and the 140 kD forms are transmembrane molecules, whereas the 120 kD form is attached to the membrane by a glycosylphosphaditylinositol (GPI) anchor (Gennarini et al., 1984 a, b).

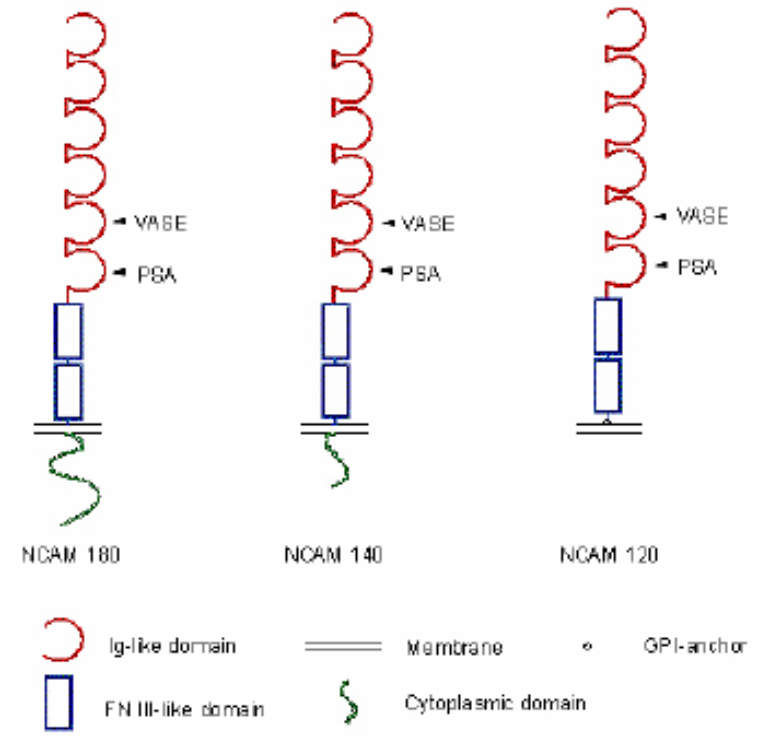

Figure 1: Modular structure of the major isoforms of NCAM. The schematic drawing displays the modular structure of the three major isoforms of NCAM. The different domains are described underneath the scheme. PSA stands for polysialic acid and VASE is an acronym for variable alternative spliced exon. Arrowheads indicate the attachment site of PSA and the insertion site of VASE.

NCAM is involved in signal transduction (Schuch et al., 1989; Walsh et al., 1997; Niethammer et al., 2002; Walmod et al., 2004) and promotes a variety of developmental processes such as neurite outgrowth and fasciculation (Rutishauser and Edelman, 1980; Doherty et al., 1990), neural crest cell migration (Bronner-Fraser et al., 1992), muscle innervation (Landmesser et al., 1988), as well as adult neurogenesis (Kim et al., 2005; Seki and Arai, 1991).

1.2.2. NCAM expression

Expression of NCAM starts very early during development. In Xenopus, for instance, the first NCAM transcripts can be detected already 2 hours after neural induction (Balak et al., 1987). Generally, NCAM is very ubiquitously expressed. It can be found on nearly all postmitotic neurons, on Schwann cells, oligodendrocytes, astrocytes and denervated or developing skeletal muscle fibers (Moore and Walsh, 1986; Neugebauer et al., 1988; Seilheimer and Schachner, 1988). Some cell types or subcellular structures specifically express one of the three main isoforms. The 180 kD form, for instance, is strongly associated with synapses. Its long cytoplasmic tail interacts with the spectrin-actin cytoskeleton and thereby stabilizes synapses (Pollerberg et al., 1987; Persohn et al. 1989). Of the three major isoforms of NCAM, NCAM-120 is not detectable in synaptosomal membranes, whereas NCAM-140 is expressed on both pre- and postsynaptic membranes and NCAM-180 is restricted to postsynaptic sites, with localization of the NCAM-180 specific epitope in postsynaptic densities. Interestingly, NCAM-180 is only detectable in subpopulations of synapses in the adult rat hippocampus (Schuster et al., 1998; Schuster et al., 2001) and becomes upregulated after the induction of LTP (Schuster et al., 1998).

Astrocytes mainly express the 140 kD form while the 120 kD form is strongly expressed by oligodendrocytes and muscle cells and within the axons of the white matter, and in Lamina X of the gray matter of the spinal cord (Chuong and Edelman, 1984; Walsh and Doherty 1991; Filiz at al., 2002).

Immunostaining with polyclonal antibodies that recognize all NCAM isoforms is intense in the hilus and inner molecular layer of the dentate gyrus with lighter staining in the dentate outer molecular layer. The mossy fiber tract, comprising axons traveling from the dentate granule cells to CA3 pyramidal cells, is strongly stained. There is abundant staining of the stratum radiatum and stratum oriens of CA1, but the stratum lacunosum-moleculare shows very little staining. A monoclonal antibody, which recognizes specifically NCAM-140 and NCAM-180, intensely stains the mossy fiber tract, hilus, and inner molecular layer (Miller et al., 1993).

1.2.3. PSA-NCAM and VASE

An interesting feature of NCAM is its developmentally regulated post-translational modification, which has an important impact on its functional properties. Two different mechanisms are known. The first occurs very early during development. After translation, a

2,8-polysialic polymer is attached to the fifth Ig-like domain. This process is calcium dependent and is regulated by two different enzymes, designated ST8SiaII/STX and ST8SiaIV/PST (Ong et al., 1998). While all isoforms of NCAM might be sialylated, the 180kD form is the main carrier of polysialic acid (PSA) (Franceschini et al., 2001b). The PSA polymer is negatively charged and it is strongly hydrated. Both its size and its negative charge are believed to reduce NCAM-mediated cell-cell adhesion, but also cell-cell interactions mediated by other cell surface associated ligands, including L1 (reviewed in Rutishauser and Landmesser 1996; Kiss et al., 2001). By attenuating cell-cell contacts, the polysialylated form of NCAM is thought to be involved in dynamic processes, such as cell migration, axonal growth, pathfinding and synaptic plasticity (Bruses and Rutishauer, 2001). After contact formation and establishment of axonal projections, the amount of NCAM-associated PSA decreases. However, PSA-NCAM remains expressed in adult brain regions exhibiting a permanent capacity for structural and synaptic plasticity, including the olfactory bulb, the hippocampus and the pituitary gland (Bonfanti et al., 1992; Gubkina et al., 2001).

Coinciding with the decrease of PSA, expression of the second type of NCAM modification becomes pronounced, an alternatively spliced NCAM mRNA variant characterized by a 10 amino acid sequence insert within the fourth Ig-like domain, the so called variable alternative spliced exon (VASE) (Fig. 1). The VASE insert has been found in every major isoform of NCAM (Small and Akeson, 1990). Its presence correlates with a decreased capacity of NCAM to promote neurite outgrowth without, however, affecting its adhesive properties (Lahrtz et al., 1997). At the beginning of neural development, only less than 3% of the NCAM transcripts contain this exon. With ongoing developmental progress, the amount of VASE-bearing transcripts increases up to 50% of all NCAM molecules in the adult, although at this time point, it is never found in brain regions characterized by synaptic and morphogenic plasticity, like the hippocampus and the olfactory bulb (Small et al., 1988). Together, the shift of the functional properties of NCAM nicely correlates with the shift of its structural features, without changing the overall expression levels of NCAM. At the beginning of development, dynamic processes like axon outgrowth, pathfinding, migration and synaptic plasticity are relevant, involving the PSA polymer. Later on, maintenance of fasciculation and stabilization of synaptic contacts are of greater importance, which correlates with an increase of the VASE insert-bearing form of NCAM.

1.2.4. NCAM deficient mice

Despite of its presumed versatile roles in CNS development, disruption of the NCAM gene in mice evokes only subtle morphological changes in the adult nervous system (Cremer et al., 1994; 1997). The olfactory bulb of NCAM deficient (NCAM$^{-/-}$) mice is reduced in size, probably as a result of disturbed cell migration. Similar observations have been reported for adult mice deficient for NCAM180 (Tomasiewicz et al., 1993) and for wild-type mice treated with endoneuraminidase-N to remove NCAM-associated polysialic acid (Ono et al., 1994), indicating that absence of PSA on migrating granule cells is a major factor for such abnormal development. Furthermore, disorganization of the pyramidal cell layer in the hippocampal area CA3 and disorganized growth of mossy fiber bundles, with reduced fasciculation and quantitative reduction of mossy fibers and their terminals have been observed in NCAM$^{-/-}$ mice (Cremer et al., 1994; 1997).

In addition to such altered morphology, behavioral changes are apparent in NCAM$^{-/-}$ mice. Modest alteration of exploratory activity, deficits in spacial learning and strongly increased intermale aggression associated with increased activation of the limbic system have been observed in NCAM-/- mice (Cremer et al., 1994; Stork et al., 1997). Furthermore, NCAM$^{-/-}$ mice show increased anxiety-like behavior compared with wild-type mice that could be reduced by systemic administration of the 5-HT1A –(serotonin 1A) receptor agonists buspirone and 8-OH-DPAT. This behavior could be related to increased cell surface expression of the downstream signaling target of both NCAM and the 5-HT1A receptor, the Kir3.1/2 inwardly rectifying K^+ channels (Delling et al., 2002). Anxiolysis in NCAM-/- mice is achieved at lower doses of buspirone and 8-OH-DPAT compared with wild-type mice (Stork et al., 1999). Such increased response to 5-HT1A receptor stimulation suggests a functional change in the serotonergic system of NCAM-/- mice, likely involved in the control of anxiety and aggression (for review, see Graeff et al., 1996).

1.3. Anatomy of the septo-hippocampal system

In rodents, the septo-hippocampal system includes the hippocampal formation, the septal area, their interconnections and the afferent and efferent pathways that connect them to other brain areas. The septum and the hippocampus are connected mainly by the fimbria and the dorsal fornix bundles (Fig. 2)

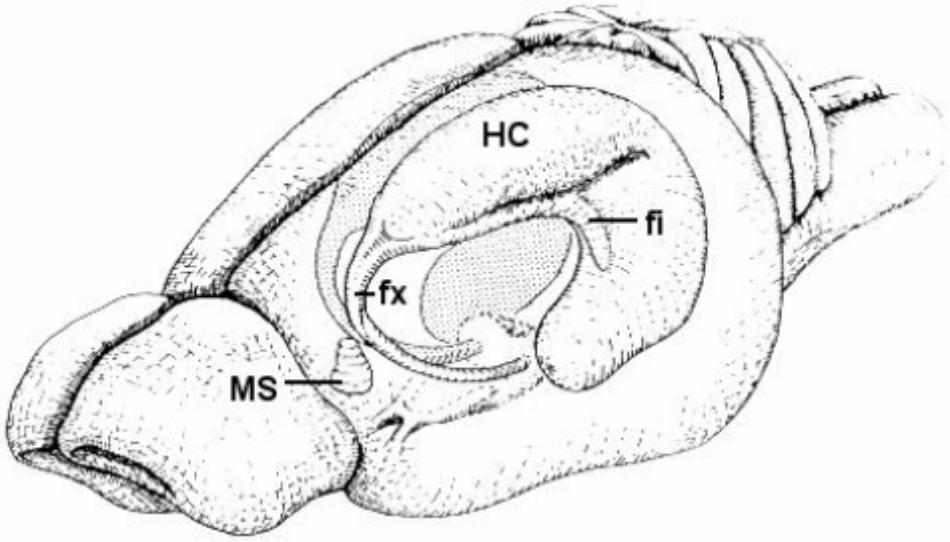

Figure 2: A three-dimensional organization of the septo-hippocampal system in the rat brain. The hippocampus is the C-shaped structure. Abbreviations: fx = fornix; fi = fimbria; HC = hippocampus; MS = medial septum (modified from Amaral and Witter 1995).

1.3.1. The hippocampus

The hippocampus is a specialized part of the limbic cortex, which is located in the temporal lobe in humans. It is known to function in the formation of memory. The formation of new memories requires the function of the hippocampus, but eventually the memory trace is stored in another part of the brain and is no longer dependent on the hippocampus (Scoville and Milner, 1957; Morris et al., 1982; Zola-Morgan and Squire, 1986; Squire and Zola-Morgan, 1991)

The notion that the hippocampus is mainly involved in spatial encoding in rodents has been challenged by studies showing that the pyramidal cells of the hippocampus can have other than spatial learning functions (Bunsey and Eichenbaum, 1996; Dusek and Eichenbaum, 1997; Wood et al. 1999; for review, see Eichenbaum and Cohen, 1988). These results indicate that the function of the hippocampus in animals is not limited to spatial encoding alone, but also non-spatial declarative processing takes place in the hippocampus, as does in humans (Scoville and Milner, 1957). However, spatial memory is still the most universally accepted critical function of the hippocampus in rodents, monkeys and humans.

The term hippocampal formation encompasses six subregions: the dentate gyrus, hippocampus proper, subiculum, presubiculum, parasubiculum and the entorhinal cortex (Amaral and Witter, 1989; 1995). Often, as here, the word *hippocampus* is used to refer to a structure that is composed of the hippocampus proper and the dentate gyrus. The

hippocampus is a C-shaped structure (Fig. 2) that has a characteristic laminar organization: if the hippocampus is cross-sectioned at any septo-temporal level, it can be seen that the cells are packed into distinct layers. In rodents, the hippocampus proper comprises of three parts: CA1, CA2 and CA3. In humans, there are four parts: CA1, CA2, CA3 and CA4. The abreviation CA stands for the Latin words *cornu ammonis*; "Ammon's horn" in English.

The intrahippocampal connections form a tri-synaptic loop, which is composed of the cells of the dentate gyrus, CA3 and CA1 and their interconnections (Fig. 3) (Amaral and Witter, 1995).

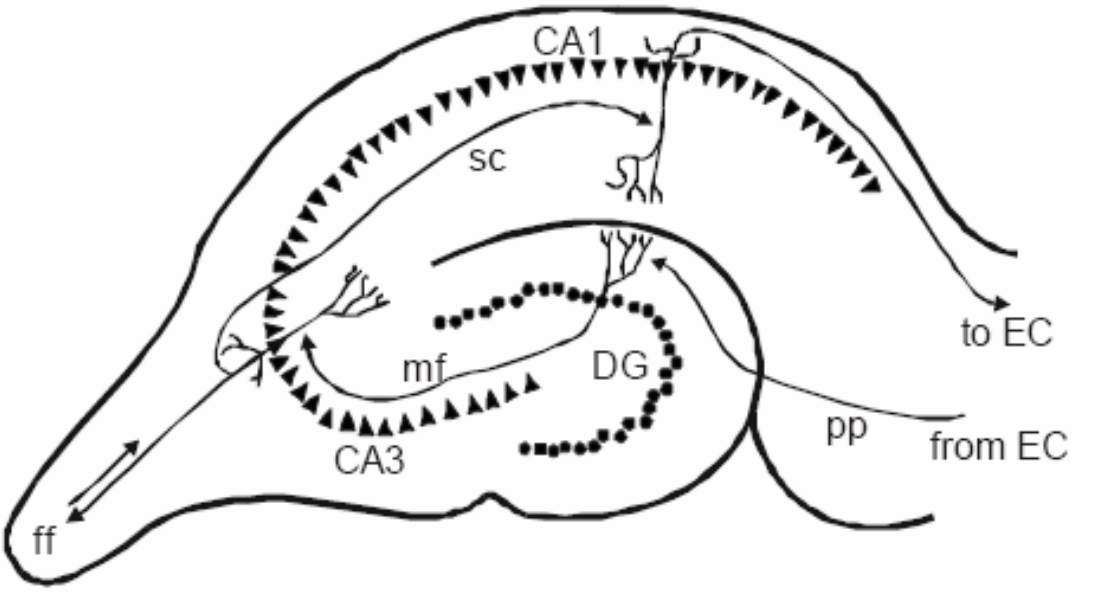

Figure 3: The tri-synaptic loop of the hippocampus. The filled triangles represent the pyramidal cell layer (CA1 and CA3) and the filled circles represent the granular cell layer of the dentate gyrus. Abbreviations: EC = entorhinal cortex; DG = dentate gyrus; pp = perforant pathway; mf = mossy fibers; sc = Schaffer collaterals; ff = fimbria fornix (modified from Amaral and Witter 1995).

The first synaptic connections of the loop are formed between the entorhinal cortex and dentate gyrus. The cells in the superficial layers (mainly layer II) of the entorhinal cortex send their axons to the molecular layer of the dentate gyrus and provide the main glutamatergic input to the hippocampus. This pathway is called the perforant pathway. Collaterals of the same axons form also connections with CA3 pyramidal cells. The second synaptic connection is formed between the dentate gyrus and the CA3. The axons from the granular cells of the dentate gyrus innervate the dendrites of the CA3 pyramidal cells. These axons are called mossy fibers. As in the case of the perforant pathway, also mossy fibers form connections with another cell population, namely the mossy cells of the dentate gyrus. These

interneurons provide feedback excitation back to the granule cells. In the third and last stage of the tri-synaptic loop, the axons of the CA3 pyramidal cells form connections with the dendrites of the CA1 pyramidal cells in the layers stratum radiatum and stratum oriens. These axons are called Schaffer collaterals, and they also branch to form connections with other cell population: the cells of the lateral septum and the mammillary bodies. These axons pass through the fimbria/fornix. Thus, the tri-synaptic loop is closed, but the information that is processed in the loop by the principal cells and the interneurons is projected back to the entorhinal cortex by the CA1 pyramidal cell axons, either directly or via the subiculum. While the input cells to the hippocampus are located in the superficial layers of the entorhinal cortex, the output axons from the hippocampus project to the deep layers of the entorhinal cortex (Amaral and Witter, 1995).

While the tri-synaptic loop is the main circuit of the hippocampus, it is still only one part of the entire circuitry. There are several other connections with important contributions to the function of the hippocampus such as connections from the entorhinal cortex to the CA1 and the subiculum, connections between the two hippocampi via the commissures, and the subcortical connections via the fimbria/fornix, mostly with the septum. Other connections that pass via the fimbria/fornix are noradrenergic connections from the locus coeruleus, serotonergic connections from the raphe nuclei, histaminergic connections from the supramammillary nucleus and dopaminergic connections from the ventral tegmental area and the substantia nigra (see Dutar et al., 1995). A common feature of the hippocampal connections other than the tri-synaptic loop is that they provide, in addition to some sparse excitation, massive inhibition of the pyramidal cells of the hippocampus enabling synchronization of the pyramidal cell firing (Freund and Gulyas, 1997).

1.3.2. Classification of the cholinergic nuclei in the central nervous system

According to the classification by Satoh (Satoh et al., 1983), there are four main groups of cholinergic cells in the rat brain. The first group is composed of cells of the basal forebrain that constitute the “rostral column”. The second group is composed of cells that are located in the pons and midbrain, and which are called the “caudal column”. The cells in the neostriatum, nucleus accumbens and olfactory tubercle constitute the third group, and the fourth groups of cholinergic cells are in the spinal cord and the nuclei of the cranial nerves. Another, more commonly used classification by Mesulam (Mesulam et al., 1983), classifies the cholinergic cells into six groups (Fig. 4). This classification is based on topographical

variations in the projection fields. The first group (Ch1) is composed of the cholinergic cells of the medial septum (MS) and cells in the vertical limb of diagonal band, DB (vDB, Ch2). These two groups project mainly to the hippocampus. The horizontal limb of the DB (hDB) that projects to the olfactory bulb is classified as Ch3. The neocortex and amygdala are innervated by the fourth group of cells, Ch4. These Ch4 cells constitute a large group that is located in the nucleus basalis (NB), the preoptic magnocellular nucleus and some parts of the hDB. The thalamus is innervated by the two remaining groups of cells, Ch5 and Ch6. They are located in the pedunculopontine nucleus and laterodorsal tegmental nucleus. Although these nuclei (Ch1-6) are generally considered to be cholinergic, they contain also other types of cell (Mesulam et al., 1983). For example, only 10-20 % of the cells in the Ch3 nucleus are cholinergic, whereas in Ch4 the proportion of cholinergic cells is 80-90 %. Most of the studies concerning the role of the cholinergic system in learning and memory have concentrated on Ch1/Ch2 and Ch4, because they are supposed to be the most important ones based on their projection areas (hippocampus and cortex).

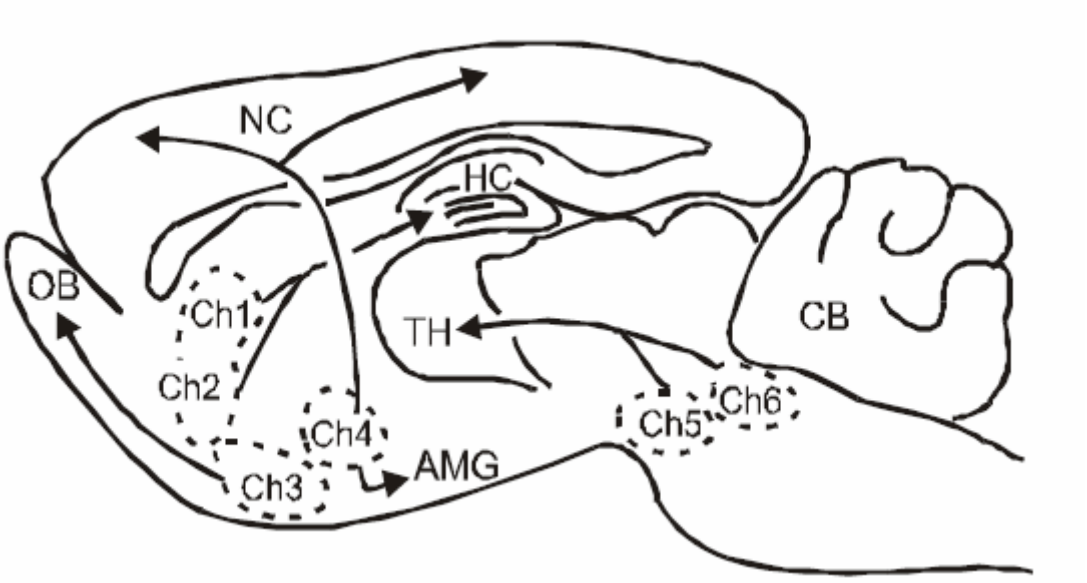

Figure 4: The cholinergic nuclei of the rodent brain (Ch1-6). Abbreviations: AMG = amygdala; CB = cerebellum; HC = hippocampus; NC = neocortex; OB = olfactory bulb; TH = thalamus (modified from Mesulam et al., 1983).

1.3.3. The septum

Already in the second century A.D. the Greek neuroanatomist Galen has defined the septum as a separate brain structure including the area which is located between the anterior horns of the lateral ventricles (septum = from Latin, *saeptum*: a dividing wall or membrane especially between bodily spaces or masses of soft tissue). The first detailed description of the

anatomy of the septum was provided in 1901 by Cajal, who was also the first to classify it as a part of the basal ganglia on the contrary to the previous generally accepted notion that it is a specialized part of cerebral cortex. Even today, a general agreement about the classification has not been accomplished. Furthermore, not even the exact boundaries defining the septum are generally agreed upon. What is generally accepted is that the septum can be viewed as an interface or a relay station between the evolutionarily "old brain" (diencephalon) and "new brain" (telencephalon). It is assumed to maintain the balance between the endocrine and emotional components of the central nervous system.

The septal complex is usually divided into three parts: the medial septum / diagonal band of Broca (MSDB), the lateral septum (LS) and the posterior septum. The two subnuclei of the MSDB are the medial septal nucleus (MS) and the nucleus of the diagonal band of Broca (DB). DB is further composed of two parts: the horizontal limb of DB (hDB) and vertical limb of DB (vDB). MS and DB are often classified as separate nuclei even though they are actually continuous and no anatomical boundary can be determined between them (Fig. 5). In fact, a more functional classification would be to combine MS and the vertical limb of the DB. Therefore, in this text, this complex is considered to be one functional unit and is called medial septum / diagonal band of Broca nuclear complex (MSDbBnc). The second part of the entire septal complex, the lateral septum can be divided into three main parts: dorsal, intermediate and ventral parts. The third part, posterior septum is composed of two parts: the bilateral septofimbrial nucleus and triangular septal nucleus (Jakab and Leranth, 1995).

As most brain structures, the septum was originally defined on the basis of gross dissections rather than any rational structure-based principle. As a result, the septal complex is actually a group of functionally unrelated nuclei that are considered under one category only for historical reasons. For example, the functions of MSDbBnc and LS are quite different. MSDbBnc primarily relays the ascending information from the diencephalon to the telencephalic structures, whereas LS mediates the descending information from the telencephalon to the diencephalon (Jakab and Leranth, 1995). Furthermore, connections between the MSDbBnc and lateral septum are very sparse (Jakab and Leranth, 1995).

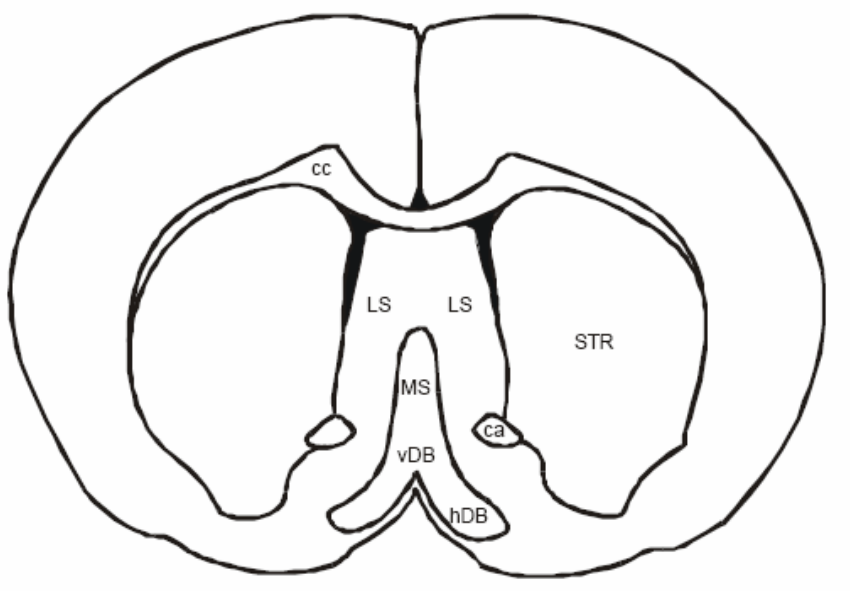

Figure 5: Coronal section of the rat brain. Abbreviations: MS = medial septum; vDB = vertical limb of the diagonal band of Broca; hDB = horizontal limb of the diagonal band of Broca; STR = striatum; ca = commissura anterior; cc = corpus callosum. Adapted from Paxinos and Watson (1986).

The cells of the MSDbBnc project mainly to the hippocampus and less extensively to the entorhinal cortex and the cingulate cortex (Gaykema et al., 1990). Approximately 40-50% of the cells in this area that project to the hippocampus are cholinergic and 10-20% are GABAergic (Linke et al., 1994). The cholinergic cells of the MSDbBnc have long been considered its functionally most important cell type, since it provides most of the cholinergic innervation of the hippocampus. However, the GABAergic cells have been shown to contribute to the maintenance of the hippocampal theta activity (Lee et al., 1994; Wenk et al., 1994).

The septum is involved in the regulation of the hippocampal rhythmic electrical activities. The theta rhythm is a regular electroencephalographic 4-12 Hz oscillation in the hippocampus and related structures. There are two types of theta rhythm: Type I theta has an overall frequency range of 6-12 Hz and it occurs mainly during walking and running. Type II theta has a lower frequency range of 4-9 Hz and it occurs during immobility (Kramis et al., 1975). The septum is considered the pacemaker of the theta rhythm since the discovery of pacemaker cells in the septum by Petsche (Petsche et al., 1962). This view has been confirmed by studies showing that lesions of the septal area completely eliminate the theta rhythm in the hippocampus of experimental animals (Andersen et al., 1979; Leung et al., 1994). Pharmacological studies of the theta rhythm have revealed that the cholinergic innervation from the MS is the most important input that regulates the hippocampal theta rhythm. Indeed, various cholinergic agonists produce theta activity when administered

systemically (Teitelbaum et al., 1975), when microinfused into the septum (Monmaur and Breton, 1991) or hippocampus (Rowntree and Bland, 1986; Colom et al., 1991) and even *in vitro*, when applied to hippocampal slices (Konopacki et al., 1987). Conversely, cholinergic antagonists attenuate the theta rhythm (Bennett et al., 1971; Kramis et al., 1975). In conclusion, the most convincing view is that the theta rhythm is crucial for the proper function of the hippocampus and that the septum is crucial for the generation of theta activity but that the cholinergic cells are not the only determinant of the theta rhythm. It is the complex circuitry of the entire septal area that orchestrates the function of hippocampal pyramidal cells and interneurons in a way that allows the hippocampus to function properly and that this orchestration can be recorded as an oscillation that can be called the hippocampal theta rhythm.

1.3.4. Interconnections

The interconnections between the septum and the hippocampus are reciprocal. The ascending connections from the septum to the hippocampus arise from the MSDbBnc. There are two types of connections: cholinergic and GABAergic. About 90 % of the cholinergic innervation of the hippocampus comes from the MSDbBnc. The cholinergic input provides a modulatory input to principal cells and GABAergic interneurons of the hippocampus (Wainer et al., 1984; Frotscher and Leranth, 1985). The GABAergic projections terminate at GABAergic interneurons of the hippocampus and thus provide a massive disinhibition of the pyramidal cells (Freund and Antal, 1988). Both the cholinergic and the GABA-to-GABAergic input provide a synchronous orchestration of the entire hippocampal formation (see Chrobak, 2000). The hippocampus projects descending connections back to the septum. The main target area of the hippocampal projections is the LS. The CA1 pyramidal cells project to the entire LS whereas CA3 pyramidal cells project only to the caudal part of the LS (Jakab and Leranth, 1995). Although the LS is the main target of the hippocampal projections, there are also some connections to the MSDbBnc from the (mainly GABAergic) interneurons of the hippocampus. These projections arise from the calbindin-containing interneurons and they terminate at both cholinergic and GABAergic cells of the MSDbBnc (Jakab and Leranth, 1995). The fiber bundles that contain the main projections between the septum and the hippocampus are called the fimbria/fornix, the dorsal fornix and the supracallosal striae. A fourth ventral route passing through the amygdala has also been described (Milner and

Amara, 1984). These bundles contain also other projections, for example noradrenergic and serotonergic projections from the brain stem to the hippocampus.

1.4. Anatomy of substantia nigra

The substantia nigra and its adjacent dopaminergic cell groups have attracted the interests of many researchers since the discovery that degeneration of one chemically defined cell types – the dopaminergic neuron – causes Parkinson's disease (Zold et al., 2007; Chen et al., 2007). One of the major inputs of sunstantia nigra – the striato-nigral pathway – degenerates during the course of Huntington's chorea (Petersén et al., 2001; Yohrling et al., 2003; Tang et al., 2007). In addition to these largely extrapyramidal motor disorders, the substantia nigra and its adjacent nuclei in the ventral tegmental area have been strongly implicated in thought and affective disorders such as schizophrenia, manic-depressive illness, and tardive dyskinesia (Lauterbach 1996; Mitchell et al., 2002; McCormick and Stoessl, 2002; Andreassen et al., 2003; Mueller et al., 2004; Fachinetto et al., 2005; Kumamoto et al., 2006; Ulla et al., 2006; Murray et al., 2007). The substantia nigra and the adjacent cell group also play key roles in generation of pleasure and in the development of drug addiction (Belin et al., 2007; Iacovelli et al., 2006; Sun et al., 2005; Shepard et al., 2006; Berretta et al., 2001). This area also involved in the control of gonadal hormones, the autonomic nervous system, reinforcement behavior, stress, and a broad array of behavioral processes and clinical disorders (Fallon and Loughlin, 1995).

The substantia nigra (Latin for "black substance") is a heterogeneous structure in the midbrain, and lies in the ventral tegmentum of the mesencephalon. In rat, it is 2.5 mm long in the rostro-caudal plane, and 3 mm wide in the medio-lateral plane. The substantia nigra (SN) consists of two ensembles, the pars compacta (SNC) and related adjacent dopaminergic groups, and another ensemble made up of the pars reticulata and the pars lateralis. SN pars reticulata and pars lateralis, along with the pallidal nuclei, are elements of the core of the basal ganglia. Although intricate and interconnected, the two ensembles must be clearly distinguished. The SNC has a volume of 0.3 mm^3 in rat and contains 10,000-12,000 neurons on each side, whereas VTA is 1,2 mm^3 in volume and contains 27,000 neurons on each side (Halliday and Tork, 1986).

1.4.1. Pars compacta and adjacent dopaminergic groups

1.4.1.1. Anatomy

Substantia nigra pars compacta contains neurons which, in humans, are colored black by the pigment neuromelanin which accumulates intracellularly with age. This pigmentation is visible as a distinctive black stripe in brain sections and is the origin of the name given to this area. The neurons in SNC have particularly long and thick dendrites (Francois et al., 1984). The ventral dendrites go down deeply into the pars reticulata. Neurons with similar morphology are sparsely distributed in the mesencephalon outside SNC and constitute "groups" with no clear borders, although continuous to the pars compacta, in prerubral positions. In early works in rats these cell groups have been given the names "area A8" and "A10". The pars compacta itself ("A9") is usually subdivided into a ventral and a dorsal tier, the last being calbindin positive (Francois et al., 1987). The ventral tier is considered as A9v. The dorsal tier A9d is linked to an ensemble comprising also A8 and A10 (Langer et al., 1991), A8, A9d and A10 representing 28% of all dopaminergic neurons in the monkey brain. The long dendrites of pars compacta neurons receive striatal innervation. This cannot be the case for the more posterior groups that are located outside the striato-pallidonigral bundle territory. Neurons of the pars compacta receive inhibiting signals from the collateral axons from the neurons of the pars reticulata (Hajos and Greenfield., 1994). All these neurons send their axons along the nigrostriatal pathway to the striatum where they release the neurotransmitter dopamine. Dopaminergic axons also innervate other elements of the basal ganglia system including the lateral and medial pallidum (Lavoie et al., 1989), substantia nigra pars reticulata and the subthalamic nucleus (Cragg et al., 2004).

1.4.1.2. Function

The function of the dopamine neurons in the substantia nigra pars compacta is complex (Fallon and Loughlin, 1995). Contrary to what has been thought initially, it is not directly linked to movements. Dopamine neurons are activated by novel, unexpected stimuli, by primary rewards in the absence of predictive stimuli and during learning. Dopamine neurons are thought to be involved in learning to predict which behaviors will lead to a reward (for example food or sex). In particular, it is suggested that dopamine neurons fire when a reward is greater than that previously expected, a key component of many reinforcement learning models. This signal can then be used to update the expected value of

that action. Many drugs of abuse, such as cocaine, mimic this reward response which provides an explanation for their addictive nature (Fallon and Loughlin, 1995).

1.4.1.3. Pathology

Degeneration of pigmented neurons in the substantia nigra is the principal pathology that underlies the Parkinson's disease (Zold et al., 2007; Chen et al., 2007). In some patients the cause of the Parkison's disease is genetic, but in most cases the reason for the death of these dopamine neurons is unknown. Parkinsonism can also be produced by viral infections such as encephalitis or a number of toxins, such as MPTP, an industrial toxin which can be produced during synthesis of the meperidine analog MPPP. Many such toxins appear to work by producing reactive oxygen species. Binding to neuromelanin by means of charge transfer complexes may concentrate radical-generating toxins in the substantia nigra. Pathological changes to the dopaminergic neurons of the pars compacta are also thought to be involved in schizophrenia (the dopamine hypothesis of schizophrenia) and psychomotor retardation sometimes seen in clinical depression (Lauterbach 1996; Mitchell et al., 2002; McCormick and Stoessl, 2002; Andreassen et al., 2003; Mueller et al., 2004; Fachinetto et al., 2005; Kumamoto et al., 2006; Ulla et al., 2006; Murray et al., 2007).

1.4.2. Pars reticulata and lateralis

1.4.2.1. Anatomy

Neurons in the pars reticulata and lateralis are much less densely packed than those in pars compacta and therefore sometimes named pars diffusa. The neurons are smaller than the dopaminergic neurons and morphologically similar to the pallidal neurons. Their dendrites are preferentially perpendicular to the striatal afferents which arise from the medial end of the striato-pallidonigral bundle (Francois et al., 1999). Nigral neurons in pars reticulata and lateralis make synaptic connections with the dopamine neurons of pars compacta at the level of their long dendrites that plunge deeply into pars reticulata. The neurons of the pars reticulata and lateralis produce the neurotransmitter gamma-aminobutyric acid (GABA). In addition, pars reticulata sends axons to the pars parafascicularis of the central region of the thalamus and to the pedunculopontine complex. The particularity of the pars lateralis is that it innervates the superior colliculus (Atherton and Bevan, 2005).

1.4.2.2. Function

The neurons of the pars reticulata are fast-spiking pacemakers, generating action potentials in the absence of synaptic input (Schultz, 1986). In primates, they discharge at a mean rate of 68 Hz in contrast to dopaminergic neurons (below 8 Hz) (Hikosaka and Wurtz, 1983). Pars reticulata neurons receive abundant afferrents from the striatum (mainly from the associative striatum), the subthalamic nucleus and dopaminergic innervation from the dopaminergic ensemble.

The pars reticulata is one of the two primary output nuclei of the basal ganglia system to the motor thalamus. The second output of the basal ganglia is the internal segment of the globus pallidus.

1.4.2.3. Pathology

The function of the neurons of the pars reticulata is profoundly changed in parkinsonism and epilepsy (Lauterbach 1996; Mitchell et al., 2002; McCormick and Stoessl, 2002; Andreassen et al., 2003; Mueller et al., 2004; Fachinetto et al., 2005; Kumamoto et al., 2006; Ulla et al., 2006; Murray et al., 2007). These changes are thought to be mostly secondary to pathology elsewhere in the brain, but may be crucial to understanding the generation of the symptoms of these disorders.

2. Rationale and aims of the study

Different behavioral and physiological abnormalities have been identified so far in NCAM deficient mice. The morphological substrates of these anomalies are largely unknown. This study was designed to address the question of the structural basis of functional impairments. In particular, analysis of cholinergic nuclei and their hippocampal projections appeared warranted with a view to the major impact of the cholinergic system on hippocampal functions. The methodological approach applied in this study has been previously described (Irintchev et al., 2005). It is based on immunohistochemical visualization of defined cell types and stereological estimation of cell densities and volumes of structures. In addition, densities of immunohistochemically visualized projecting axons in the hippocampus were estimated using a stereological approach. The particular aims of these investigations were to determine whether NCAM deficiency causes:

1. Changes in the number of cholinergic cells in the medial septum / diagonal band of Broca nuclear complex, dopaminergic cells in substantia nigra/ ventral tegmental area and noradrenergic cells in locus coeruleus.

2. Alterations in the cholinergic and catacolaminergic fiber densities in different subfields and layers of the hippocampus.

Both young (2 months of age) and adult (13 months) NCAM deficient mice and wild-type littermates were analyzed in order to detect possible age-related impacts of the NCAM deficiency.

3. Materials and methods

3.1. Chemicals

The chemicals used in this study were obtained from the following companies: Dianova (Hamburg, Germany), donkey serum; Fluka (Buchs, Germany), paraformaldehyde, cacodylate, sucrose; Merck (Darmstadt, Germany), 2-methyl-butane; Roth (Karlsruhe, Germany), sodium citrate.

3.2. Solutions and buffers

Antigen retrieval buffer	10	mM	sodium citrate in H_2O
Blocking buffer	0.2	% (v/v)	Triton X-100
	0.02	% (w/v)	sodium azide
	5	% (v/v)	normal donkey serum
Cacodylate buffer	0.1	M	sodium cacodylate in H_2O, pH 7.3
Cryoprotection buffer	15	% (w/v)	in 0.1 M cacodylate buffer
Fixative	4	% (w/v)	formaldehyde
	0.1	(w/v)	$CaCl_2$
			in cacodylate buffer, pH 7.3
Phosphate-buffered saline (PBS)	150	mM	NaCl
	20	mM	Na3PO4, pH 7.4
PBS-carrageenan	0.5	% (w/v)	lambda-carrageenan
	0.02	(w/v)	sodium azide
Post-fixation solution	15	% (w/v)	sucrose in fixative

3.3. Animals

Male and female NCAM deficient (NCAM-/-) mice (n = 9) and wild-type (NCAM+/+) littermates (n = 9) were used at the age 2 months. Only male NCAM-/- (n = 9) and NCAM+/+ mice (n = 7) were used at the age 13 months. The generation of the NCAM-deficient mice has been described previously (Cremer et al., 1994). Prior to the experiments, the genotype of the animals had been determined by a polymerase-chain reaction assay using

tissue samples taken after birth as described previously (Cremer et al., 1994). To confirm the results of the first genotyping, second biopsy and genotyping were performed after sacrificing of the animals. The 2-month-old animals were bred in the animal facility of the Univeritätsklinikum Hamburg and delivered to the Institute several days before sacrifice. The 13-month-old animals, also bred in the animal facility of the Univeritätsklinikum Hamburg, were used for behavioral analysis prior to morphological analysis and kept in the animal facility of the Institut für Biosynthese neuraler Strukturen until sacrifice. All animals used appeared healthy and were treated in accordance to the German law on protection of experimental animals.

3.4. Tissue processing

Tissue processing, sectioning and immunohistochemical stainings were performed as described (Irintchev et al., 2005). Mice were weighed and anesthetized with 16% w/v (weight/volume) solution of sodium pentobarbital (Narcoren, Merial, Hallbergmoos, 5 µl g^{-1} body weight, i.p.). After surgical tolerance was achieved, the animals were transcardially perfused with physiologic saline for 60 seconds followed by fixative consisting of 4% formaldehyde and 0.1% $CaCl_2$ in 0.1M cacodylate buffer, pH 7.3, for 30 minutes at room temperature (RT). Cacodylate buffer supplemented with calcium was selected for use in order to ensure optimal tissue fixation including preservation of highly soluble antigens. Following perfusion, the animals were left *in situ* for 2 hours at RT to reduce fixation artifacts. Subsequently, the brains were dissected out without the olfactory bulbs and post-fixed overnight (18-22 hours) at 4°C in the formaldehyde solution used for perfusion. Tissue was then immersed into 15% sucrose solution in 0.1M cacodylate buffer, pH 7.3, at 4°C for two days for cryoprotection. Fixed and cryoprotected (sucrose-infiltrated) brains were carefully examined under a stereomicroscope and hair, rests of dura mater or other tissue debri were removed with fine tweezers. Following this, the brains were placed in a mouse brain matrix (World Precision Instruments, Berlin) and the caudal end was cut at a defined level (1 mm from the most caudal slot of the matrix). Then brain mass and volume were measured (see 3.6.2 and 3.6.3). Finally, the brains were frozen by insertion into 2-methyl-butane (isopentane) which had been precooled to -30°C in the cryostat. The brains were stored in liquid nitrogen until sectioned.

3.5. Preparation of cryostat sections

For sectioning, the caudal pole of each brain was attached to a cryostat specimen holder using a drop of distilled water placed on a pre-frozen layer of Tissue Tek (Sakura Finetek Europe, Zoeterwoude, The Netherlands). The ventral surface of the brain was oriented to face the cryostat knife edge and serial coronal sections were cut in a cryostat Leica CM3050 (Leica Instruments, Nußloch, Germany). Sections of 25-µm thickness for immunohistochemical analysis were prepared. Sections were collected on SuperFrost Plus glass slides (Roth, Karlsruhe, Germany). Since stereological analyses require extensive sectioning of the structures studied and use of spaced-serial sections (Howard and Reed, 1998) sampling was always done in a standard sequence so that 4 sections that were 250 apart from each otherwere present on each slide (Figure 6).

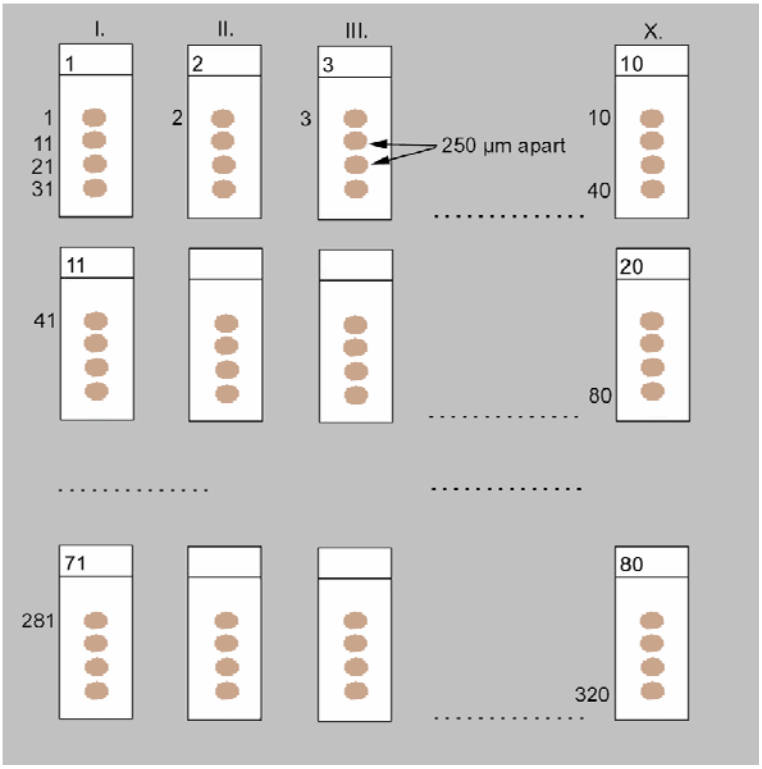

Figure 6: Standardized sequence of collecting sections (25-µm thickness) on glass slides. Staining of slides from one row (e.g. 1, 11, etc.) with a given antibody gives the opportunity to evaluate a cell population using randomly spaced samples from a brain structure of interest.

3.6. Analysis of anatomical variables

3.6.1 Body weight

The body weight of the animals was measured after anesthesia for perfusion fixation using a digit scale (Mettler Toledo, Switzerland).

3.6.2 Brain volume

Brain volume was determined by measurement of volume displacement using a 5-ml measuring cylinder (Roth) prefilled with 4 ml sucrose/cacodylate solution.

3.6.3 Brain weight

Brains were blotted with filter paper to remove excess liquid from the surface and the brain mass was measured using a fine 4-digit scale (BP61, Sartorius, Göttingen, Germany).

3.7. Analysis of immunohistochemically defined cell density and fiber

3.7.1. Antibodies

3.7.1.1. Primary antibodies

Goat anti-ChAT (choline-acetyltransferase) affinity-purified Ig polyclonal antibody (Chemicon, Hofheim, Germany) was used at dilution of 1:100 in PBS containing 0.5% lambda-carrageenan and 0.2% sodium azide. Choline acetyltransferase is found in cholinergic neurons in the central nervous system.

Rabbit anti-TH (tyrosine hydroxylase) affinity-purified polyclonal antibody (Chemicon, Hofheim, Germany) was used at a dilution of 1:500 in PBS containing 0.5% lambda-carrageenan and 0.2% sodium azide. Tyrosine hydroxylase is the rate-limiting enzyme in the synthesis of the catecholamine neurotransmitters (dopamine, epinephrine, and norepinephrine) and is present in catacalominergic neurons.

3.7.1.2. Secondary antibodies

Donkey anti-goat IgG - Alexa Fluor® 555 (Molecular Probe, Mo Bi Tec, Göttingen, Germany) was used diluted 1:200 in PBS containing 0.5% lambda-carrageenan and 0.2% sodium azide.

Goat anti-rabbit IgG conjugated with Cy3 (Jackson ImmunoResearch Laboratories) was used diluted 1:200 in PBS containing 0.5% lambda-carrageenan and 0.2% sodium azide.

3.7.2. Immunohistochemical stainings

For immunohistochemical staining, a method described by Irintchev and colleagues (Irintchev et al., 2005) was used because it allows repeated use of antibody solutions (stabilized by the non-gelling vegetable gelatin lambda-carrageenan), convenient incubation in jars and high reproducibility. Sections, stored at -20°C, were air-dried for 30 minutes at 37°C. A 10mM sodium citrate solution (pH 9.0, adjusted with 0.1M NaOH) was freshly prepared and sections were immersed for antigen de-masking in the solution preheated in a water bath to 80°C for 30 minutes. Afterwards, the jar was taken out of the water bath and left to cool down at room temperature. Sections were briefly rinsed with PBS to prevent contamination of the jars with sodium citrate. Then blocking of unspecific binding sites was performed. The sections were incubated at room temperature for two hours in PBS containing 0.2% v/v Triton X-100 (Fluka, Buchs, Germany), 0.02 w/v sodium azide (Merck, Darmstadt, Germany) and 5% v/v normal donkey serum (NDS) or normal goat serum (NGS, Jackson Immuno Research Laboratories, Dianova, Hamburg, Germany). After one hour, the blocking solution was aspired and the slides were incubated with the primary antibody against choline acetyltransferase (ChAT, Chemicon, goat polyclonal antibody) diluted 1:100 in PBS containing 0.5% w/v lamda-carrageenan and 0.02% w/v sodium azide in PBS or against tyrosine hydroxylase (anti-TH, Chemicon, rabbit polyclonal antibody) in dilution 1:500 in PBS containing 0.5% lambda-carrageenan and 0.2% sodium azide The slides were incubated for 3 days at 4°C in a well closed plastic staining jar (Roth). Following this, the sections were washed 3 times in PBS (15 minutes each) before secondary antibody was applied. The sections were incubated with donkey anti-goat IgG - Alexa Fluor® 555 (Molecular Probe, Mo Bi Tec, Göttingen, Germany) for cholinergic staining or goat anti-rabbit IgG conjugated with Cy3 (Jackson ImmunoResearch Laboratories) for tyrosine hydroxylase staining, both diluted 1:200 in PBS containing 0.5% lambda-carrageenan and 0.2% sodium azide, at RT for 2 hours. After a subsequent wash in PBS, cell nuclei were stained for 10 minutes at room temperature with bis-benzimide solution (Hoechst 33258 dye, 5 µg/ml in PBS, Sigma, Deisenhofen, Germany). Finally the sections were washed again 3 times (10 minutes each), mounted with anti-fading medium (Fluoromount G, Southern Biotechnology Associates, Biozol, Eching, Germany) and stored in the dark at 4°C.

Specificity of staining was tested by omitting the first antibody or replacing it by variable concentrations of normal serum or IgG (1 – 30 µg/ml). In both mutant and wild-type animals the morphology of the immunofluorescent cells appeared to be characteristic of the cell type expected to be labeled.

3.7.3. Stereological analysis

3.7.3.1 Cavalieri method

This method of volume estimation is named after the Italian mathematician Bonaventura Cavalieri (1598-1647), a student of Galileo. Being very straightforward to apply, it is the most commonly used method for the estimation of reference volume (Howard and Reed, 1998). According to the Cavalieri method, an unbiased estimate of the volume, V, of a structure of interest may be obtained by sectioning it from end to end with a series of systematic sections a constant distance, T, apart and measuring the area, A, of the transect through the object on each section, whereby:

$est_1V = T (A_1 + A_2 + A_3 + ... + A_m)$

Volume estimates were performed using bis-benzimide stained spaced-serial sections with T = 250 μm. The area of each transect was measured with an Axioskop microscope (Zeiss, Oberkochen, Germany, objective 10x) equipped with a motorized stage and a Neurolucida software-controlled computer system (MicroBrightField Europe, Magdeburg, Germany).

3.7.3.2 Volume of the hippocampus

The areas of the hippocampal subfields CA1, CA3 and the dentate gyrus (DG) and their layers, strata oriens, pyramidale and stratum radiatum in CA1, srata pyramidale, oriens and lucidum in CA3 and strata polymorphe, granulosum and moleculare in DG were measured bilaterally in three coronal sections from each animal stained with bis-bensimide using the Neurolucida system. The criterion for the selection of the mid-section was similarity in appearance to that of section (Bregma –2,10 mm) shown in the mouse brain atlas of Sidman (Sidman et al., 1971). The other two sections were 250 μm apart from the mid-section, one rostral to it, one caudal. The average of three values per animals and area was used to calculate group mean values.

3.7.3.3 Estimation of cell numbers

Numerical density and total cell number were estimated using the optical dissector and Cavalieri methods (Gundersen, 1986). The optical disector method was chosen for quantitative analysis because of its efficiency (Howard and Reed, 1998), an important prerequisite when aiming to quantify numerical densities of a variety of cell types in a given brain region (Irintchev et al., 2005). The method consists of direct counting of objects in relatively thick sections (e.g. 25–50 μm) under the microscope using a three-dimensional counting frame (“counting brick” of Howard and Reed, here simply referred to as disector) to

"probe" the tissue at random. The base of the frame (dimensions in the x/y plane) is defined by the size of the squares formed by a grid projected into the visual field of the microscope. The height of the disector is a portion of the section thickness defined by two focus planes in the z axis at a distance of x µm. Objects, for example, cells, within each disector are counted according to stereological rules: those entirely within the disector as well as those touching or being dissected by the "acceptance", but not the "forbidden" planes of the frame are counted. The cell counts and area estimation were performed on a Ziess Axioskop microscope (Zeiss) equipped with a motorized stage and Neurolucida software controlled computer system (Neurolucida, MicroBrightField Europe). For the identification of medial septal/diagonal band of Broca nuclear complex, the immunohistochemical ChAT staining was used. The viewed area was randomized by setting a reference point at an arbitrary place resulting in an overlay of the visible field by a grid with lines spaced 30 µm in both axes. The contours of the area of interest were outlined with the cursor using 10x objective. Squares within the marked area separated by distances of 60 µm were labeled with a symbol starting from the uppermost left side of the field. A dissector depth of 10 µm was chosen since antibody penetration was sufficient to enable clear recognition of stained objects within a depth of at least 15 µm. The sections were viewed with the 40x magnification objective and 546/590nm excitation/emission filter set (15, Zeiss, red fluorescence) for cell counting. The marked disectors were meander scanned to view all marked frames consecutively. Immunolabeled cell profiles that were entirely within the counting frame at any focus level, as well as those attaching to or intercrossed by the forbidden or acceptance lines were marked with a symbol. Then by repeated switching between the red and blue filter sets and changing the focus plane, the nuclei of the labeled cells were identified. All nuclei that were in focus beyond a guard space (depth 0-2 µm from the section surface), i.e. lying within 2 and 12 µm below the top of the section, were counted except for those at the "look-up" level (2 µm) and such intercrossed by or touching the forbidden lines.

3.7.3.4. Cell profile density

The locus coeruleus was too small, with regard to outlines in coronal sections and rostro-caudal extent, to apply in a straightforward manner the three-dimensional counting strategy used for the other nuclei. Therefore, analysis here was reduced to counting of cell profiles which has been shown to correlate well with stereological estimates (Irintchev et al., 2005). The locus coeruleus was outlined using the immunofluorescence staining to define the

boundaries of the nucleus. All cell profiles in the outlined area were counted using the 40x objective.

3.7.3.5 Length density and total length of fibers

To estimate the densities of projecting immunolabeled fibers, 2 µm-thick optical slices were obtained, assuring a guard distance of about 2 µm from the section's surface, on a Zeiss confocal laser scanning microscope (LSM510, Zeiss, Oberkochen, Germany). Images from the following subdivisions and layers of the hippocampus were taken: strata moleculare, granulosum and polymorphe of the dentate gyrus, strata oriens, pyramidale and lucidum of the CA3 region and strata oriens, pyramidale and radiatum of the CA1 region (Fig. 7A). For each animal and layer, four pictures per field were taken from the left and right hippocampus. Bis-benzimide nuclear staining was used to aid delineation of the hippocampal layers (Fig. 7B). The confocal images were saved in TIFF format.

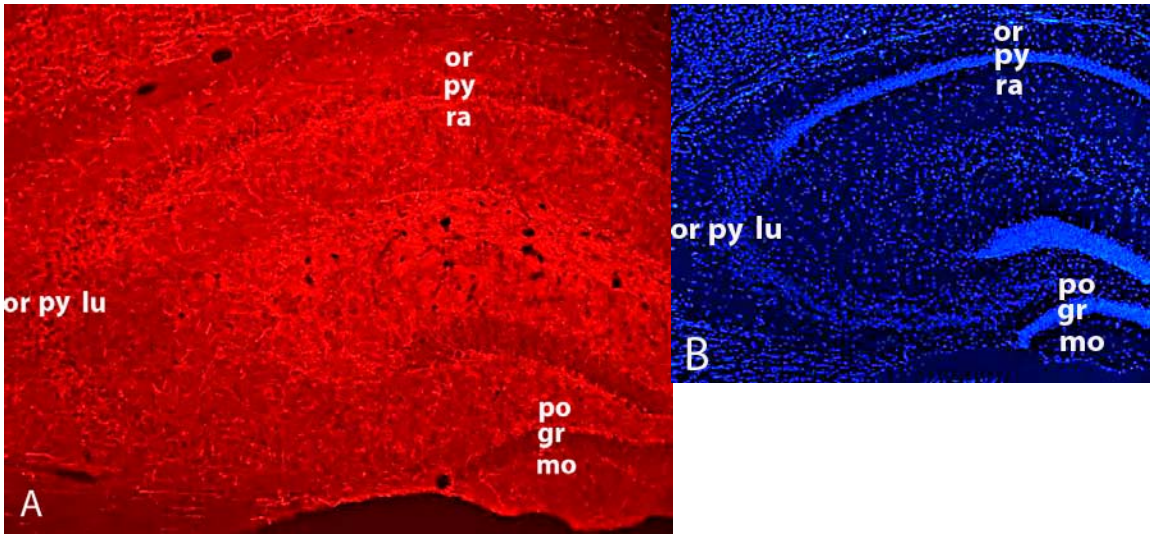

Figure 7: A coronal section from the hippocampus of a 2-month-old wild-type mouse stained for ChAT (A) and nuclei (B) viewed at low-power magnification using appropriate filter sets. Layers in CA1, CA3 and dentate gyrus are indicated: (or) statum oriens, (py) stratum pyramidale, (ra) stratum radiatum, (lu) stratum lucidum, (po) stratum polymorphe, (gr) stratum granulosum, (mo) stratum moleculare.

The digital images were overlaid with a stereological test grid (grid C4; Howard and Reed, 1998, Figure 8) using Adobe Photoshop, and the number of intersections of fibers with the grid or touching point with the curved side of grid were counted. Length densities of projecting fibers were calculated in m per m^3, i.e. m^{-2} according to the formula:

$$L_v = 2/t \times PL$$

where L_V is the length density, t is the thickness of slice and PL is the number of crosses divided by the summed length of the grid arcs. Total fiber length is in for given structure was calculated using the formula:

$$TL_V = L_V \times V$$

where TL_V is total length density, L_V is length density and V is the volume the structure of interest.

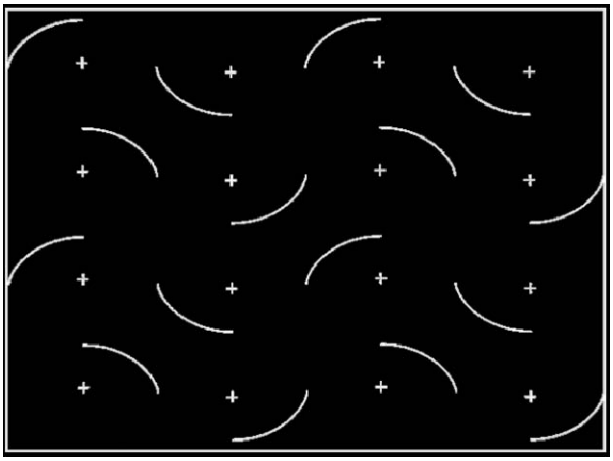

Figure 8: Stereological test grid. Counting interceptions of fibers with curved side allows calculate length density.

3.7.4. Photographic documentation

Photographic documentation was made on an Axiophot 2 microscope equipped with a digital camera AxioCam HRC and AxioVision software (Zeiss) at highest resolution (2300 x 2030 pixel, RGB) or a Zeiss confocal laser scanning microscope (LSM510) at resolution 1024 x 1024 pixel for fiber density estimation. The images were processed using LSM 5 Image Browser (Zeiss) and Adobe® Photoshop® 6.0 software (Adobe Systems Inc., San Jose, California).

3.7.5. Statistical analysis

Statistical analysis was restricted to comparisons of mean values of age-matched groups, i.e. littermates, using the two-sided *t* test for independent groups. By two or more measurements per parameter and animal, the mean was used as a representative value. Thus, for all comparisons the degree of freedom was determined by the number of animals. Regression analyses were performed with SigmsPlot 8.0 software (SPSS Inc., Chicago, Illinois). The accepted level of significance for all tests was 5%.

4. Results

4.1 Body weight

Body weights were estimated separately for female and male two-month-old animals (Figure 9). For both genders, knock-out animals had 13% smaller body weight compared with wild-type mice. This finding is in correspondence to a previous observation (Cremer et al., 1994). Similar tendency for smaller body mass was observed for thirteen-month-old NCAM-/- mice (-10% compared with wild-type littermates) but this difference was not statistically significant because of the large variability within the groups (Fig. 9).

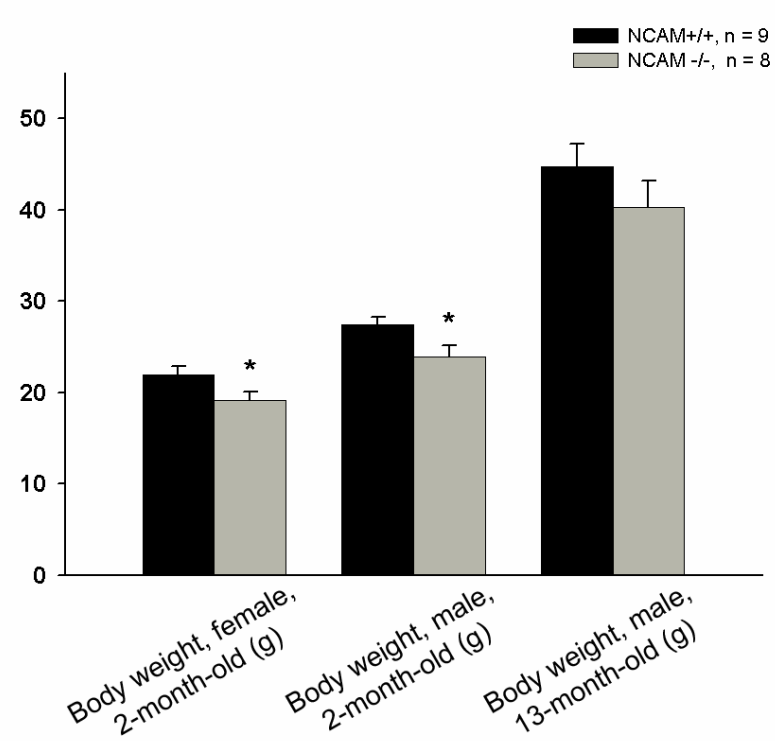

Figure 9: Body mass in NCAM deficient (NCAM-/-) mice and wild-type littermates (NCAM+/+) studied at 2 months (females and males) and 13 months of age. Shown are mean values + SEM. Number of animals studied per genotype and age are indicated. Asterisks indicate significant differences between groups mean values ($p < 0.05$, two-sided *t* test for independent samples).

4.2. Brain mass and volume

Whole brain mass in NCAM-/- mice (mean 352 mg at 9 weeks old and 365 mg at 13 months) was 11% smaller compared with wild-type (NCAM+/+) littermates (372 mg and 387 mg, respectively) at both ages studied (Fig. 10). Estimation of brain volume produced similar results (Fig. 10). These observations are consistent with previous results (Cremer et al., 1994).

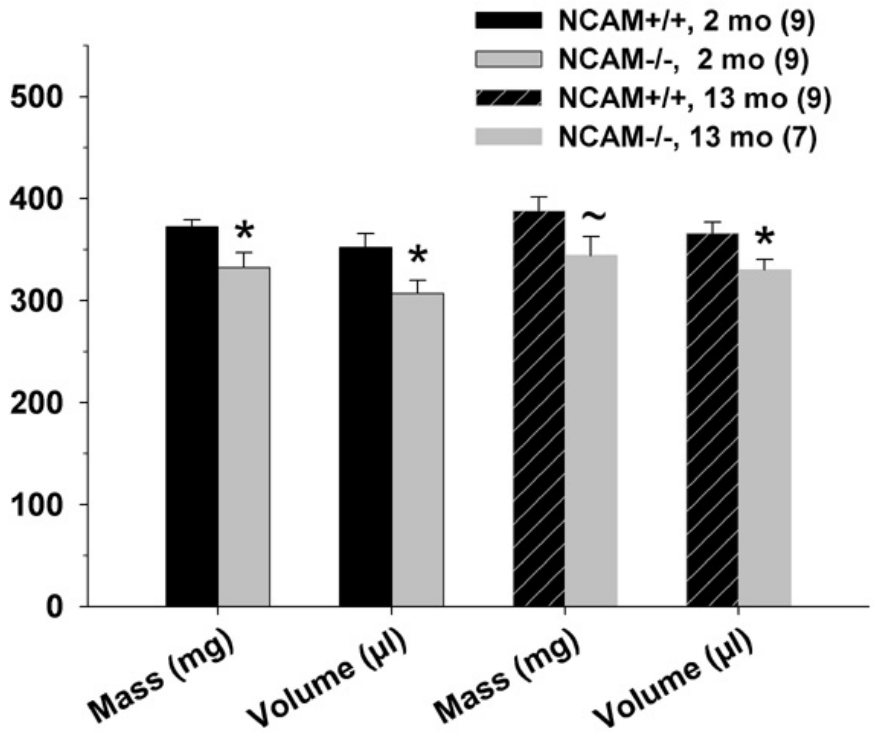

Figure 10: Brain mass and volume in NCAM deficient (NCAM-/-) mice and wild-type littermates (NCAM+/+) studied at 2 months (2 mo, two column pairs on the left hand side) and 13 months (13 mo, column pairs on the right hand side) of age. Shown are mean values + SEM. Number of animals studied per group are indicated in the legend. Asterisks indicate significant differences between group mean values ($p < 0.05$, two-sided *t* test for independent samples, ~ - $p < 0.08$).

4.3. General immunohistochemical observations

For a particular antigen, all sections were stained in the same primary and secondary antibody solutions kept in staining jars and stabilized to enable repeated long-term usage (Sofroniew and Schrell, 1984; Irintchev et al., 2005). The previously documented reproducibility of this staining technique was also apparent in this study: the quality of staining remained constant for all batches of slides processed over a period of several months. No qualitative differences between NCAM+/+ and NCAM-/- animals were noticed in the characteristic staining pattern for each of the detected antigens. Examples of the stainings are shown in Fig. 11.

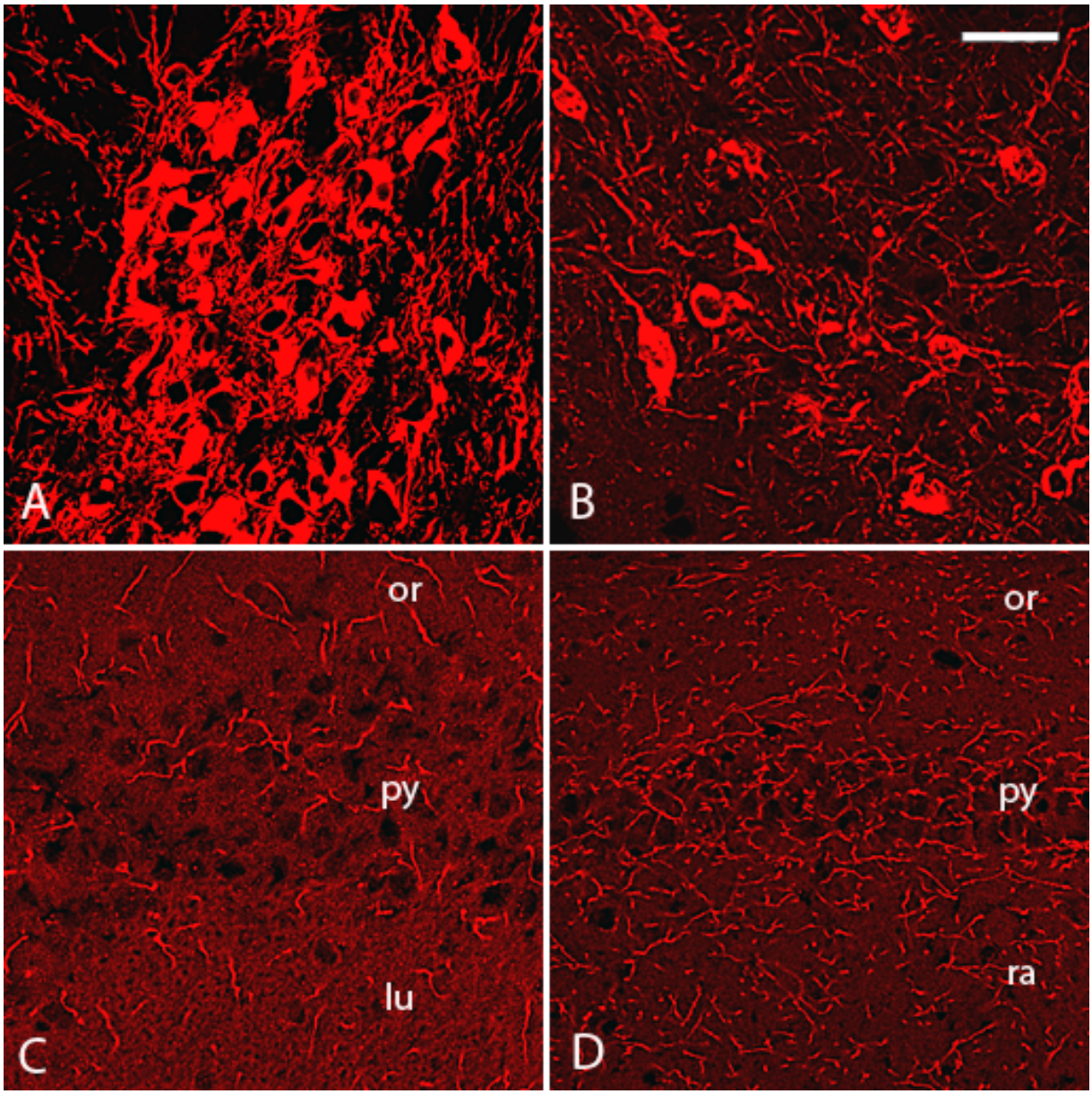

Figure 11: TH immunofluorescence stainings of cell bodies in substantia nigra pars compacta (A9 cell group) (A) and projection fibers in the CA3 subfield of the hippocampus (C).ChAT immunofluorescence stainings of cell bodies in the medial septal/ diagonal band of Broca cell complex (B) and projection fibers in the CA1 subfield of the hippocampus (D) of a 2-month-old wild-type mouse. Strata oriens (or), pyramidale (py) and lucidum (lu) of the CA3 region are indicated in B and strata oriens (or), pyramidale (py) and radiatum (ra) of the CA1 region are indicated in D. Scale bar in B indicates 20 µm for A and B and 50 µm for C and D.

4.4. Volume of the hippocampus and its subdivisions

The cross-sectional area of the structures was measured in three spaced-serial sections (250 µm apart) from the dorsal hippocampus cut at defined levels (see Materials and Methods). The values of the three sections were averaged. Since spacing between the evaluated sections was equal and relatively large (250 µm), the area estimates are proportional to the volume of a significant portion of the dorsal hippocampus. All measurements were

performed bilaterally and evaluated separately for the left and right hippocampus. Since the results for the left and the right hippocampus and the degree of asymmetry were similar with respect to genotype-related differences, for clarity and brevity the averaged bilateral values are presented here.

The total area of the hippocampus, CA1 and CA3 regions were similar in 2-month-old animals indicating a normal size of these structures in mutant animals (Fig. 12). In contrast, the DG in NCAM-deficient animals was smaller (15%). Also in 13-month-old mice, the area of the whole hippocampus and the CA1 subfield were similar in the two groups and the DG of NCAM-/- mice was smaller (11%). In contrast to 2-month-old animals, however, the CA3 area was larger (16%) in adult NCAM-/- mice compared with wild-type littermates (Fig. 13).

The areas of all tree layers of the DG in 2-month-old animals (Fig. 14) were smaller in NCAM-deficient animals (by 21%, 11% and 10% for stratum moleculare, stratum granulosum and stratum polymorphe compared with wild-type mice, respectively). In 13-month-old mice (Fig. 15), reduced area of stratum moleculare (-11%) and stratum granulosum (-16%) of NCAM-/- animals was also observed. A tendency for smaller stratum polymorphe in NCAM-/- compared with NCAM+/+ mice was also present but the difference (8 %) was not statistically significant.

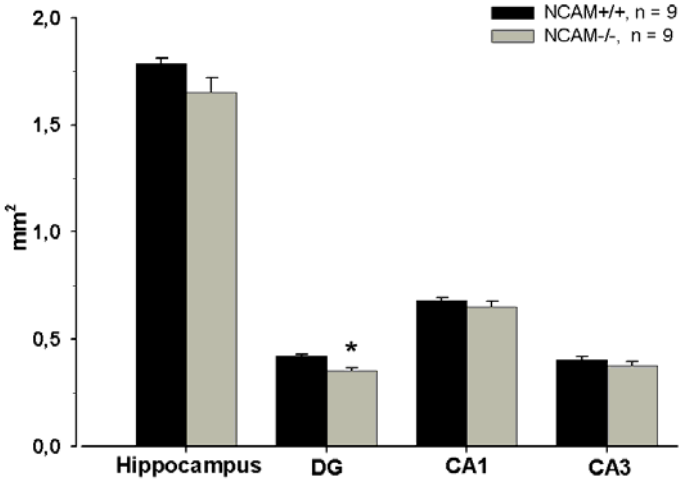

Figure 12: Cross-sectional area of the whole hippocampus and its subdivisions in coronal brain sections of NCAM+/+ (black bars) and NCAM-/- animals (grey bars) studied at the age of 2 months. Shown are averaged bilateral mean values + SEM. Number of animals studied per group are indicated. Asterisk indicates significant difference between the group mean values ($p < 0.05$, *t* test).

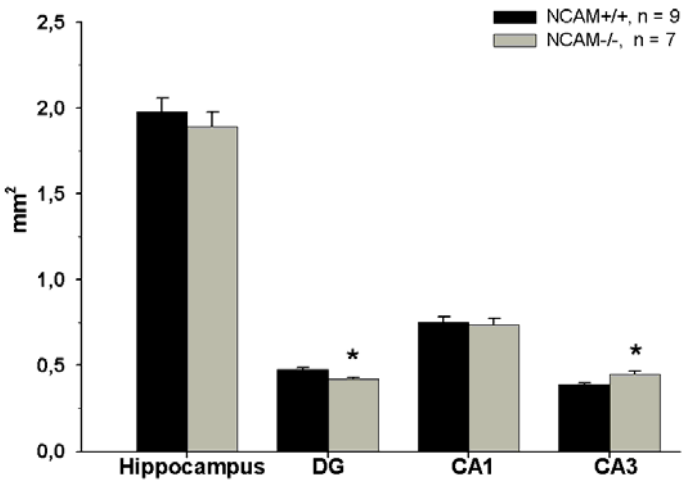

Figure 13: Cross-sectional area of the whole hippocampus and its subdivisions in coronal brain sections of NCAM+/+ (black bars) and NCAM-/- animals (gray bars) studied at the age of 13 months. Shown are averaged bilateral mean values + SEM. Number of animals studied per group are indicated. Asterisks indicate significant difference between group mean values ($p < 0.05$, *t* test).

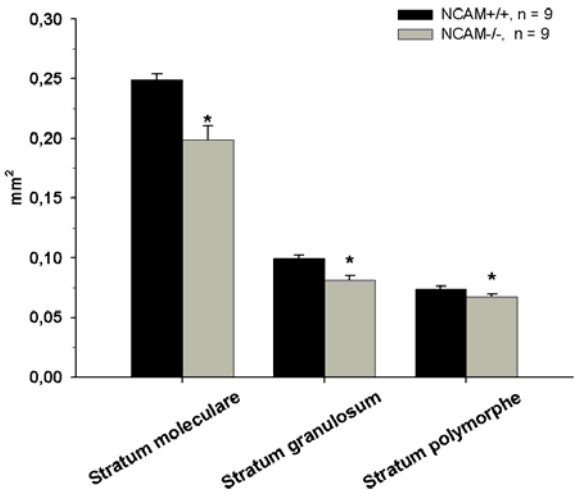

Figure 14: Cross-sectional areas of the DG layers in NCAM+/+ (black bars) and NCAM-/- animals (gray bars) studied at the age of 2 months. Shown are averaged bilateral mean values + SEM. Number of animals studied per group are indicated. Asterisks indicate significant difference between group mean values ($p < 0.05$, *t* test).

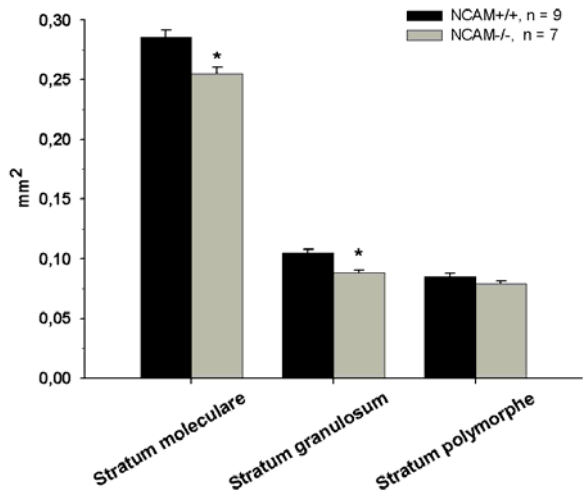

Figure 15: Cross-sectional areas of the DG layers in NCAM+/+ (black bars) and NCAM-/- animals (gray bars) studied at the age of 13 months. Shown are averaged bilateral mean values + SEM. Number of animals studied per group are indicated. Asterisk indicates significant difference between the group mean values ($p < 0.05$, *t* test).

Stratum pyramidale of the CA1 region of NCAM-/- mice was by 13% smaller compared with wild-type littermates at both ages studied (Fig. 16 and Fig. 17). No significant differences were found for stratum oriens and stratum radiatum of the CA1 region for both ages studied (Fig. 16 and Fig. 17).

Two-month-old NCAM deficient animals had smaller size of the stratum lucidum in the CA3 region (12%) while the areas of the stratum oriens and stratum pyramidale were similar in the two genotype groups (Fig. 18). In contrast to the young animals, 13-month-old NCAM-/- mice had reduced size of the stratum pyramidale (-20% compared with wild-type littermates) and stratum lucidum (-18%) while stratum oriens was not affected (Fig. 19).

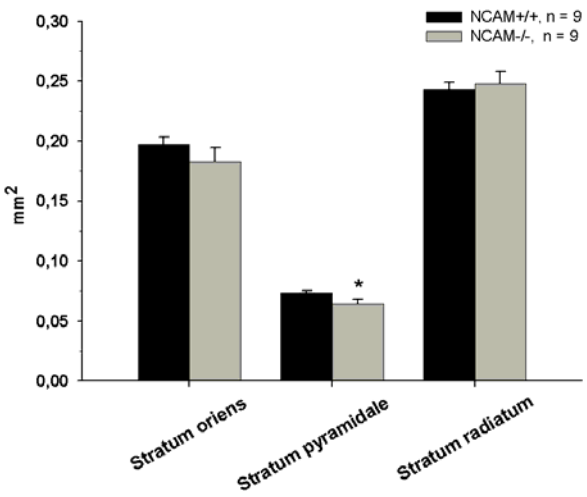

Figure 16: Cross-sectional areas of the CA1 layers in NCAM+/+ (black bars) and NCAM-/- animals (gray bars) studied at the age of 2 months. Shown are averaged bilateral mean values + SEM. Number of animals studied per group are indicated. Asterisk indicates significant difference between the group mean values ($p < 0.05$, *t* test).

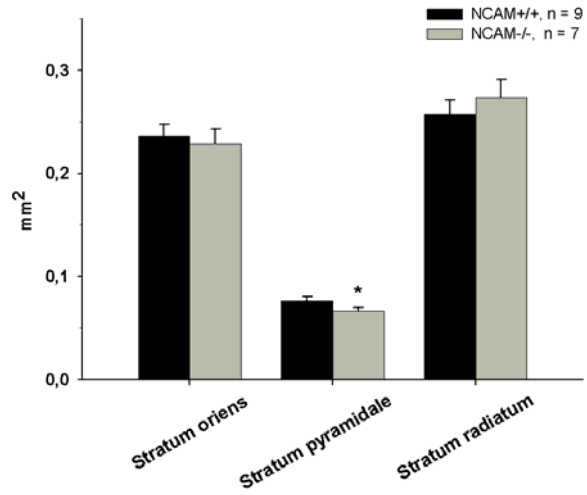

Figure 17: Cross-sectional areas of the CA1 layers in NCAM+/+ (black bars) and NCAM-/- animals (gray bars) studied at the age of 13 months. Shown are averaged bilateral mean values + SEM. Number of animals studied per group are indicated. Asterisk indicates significant difference between the group mean values ($p < 0.05$, *t* test).

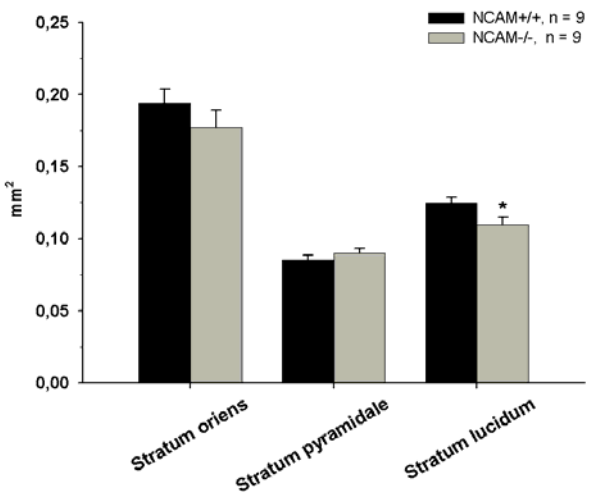

Figure 18: Cross-sectional areas of the CA3 layers in NCAM+/+ (black bars) and NCAM-/- animals (gray bars) studied at the age of 2 months. Shown are averaged bilateral mean values + SEM. Number of animals studied per group are indicated. Asterisk indicates significant difference between the group mean values ($p < 0.05$, *t* test).

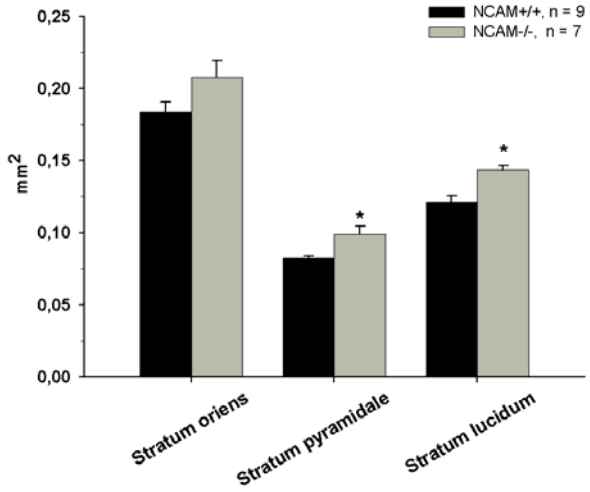

Figure 19: Cross-sectional areas of the CA3 layers in NCAM+/+ (black bars) and NCAM-/- animals (gray bars) studied at the age of 13 months. Shown are averaged bilateral mean values + SEM. Number of animals studied per group are indicated. Asterisks indicate significant difference between group mean values ($p < 0.05$, *t* test).

4.5. Cholinergic cells in the medial septal/ diagonal band of Broca nuclear complex

To get an insight into the structural integrity of the cholinergic system, the density and total cell number of ChAT-positive neurons was evaluated in the medial septal/diagonal band of Broca nuclear complex. This complex provides the major cholinergic innervation of the hippocampus.

Total numbers of choline acetyltransferase immunoreactive ($ChAT^+$) neurons were significantly lower in NCAM-/- animals compared with NCAM+/+ mice at both ages studied (-23% and 18% at 2 and 13 months, respectively, Fig. 20 and 21, bar pairs on the right hand side). These differences were due to a reduced volume of the nuclear complex in the mutant animals (Fig. 20, 21, bar pairs in the middle). Cell densities were similar in the two groups.

The numbers of cholinergic neurons estimated in this study (about 12000 at both ages in wild-type animals) was higher than the previously reported numbers in different inbred mouse strains (1200 – 2200, Beck et al., 2002; Boncristiano et al., 2002; Schwegler et al., 1996b). These differences could be attributed to the exclusion of the horizontal limb of the diagonal band from quantitative analyses in the earlier studies, as opposed to the present investigation, as well as to methodological differences (e.g., variance in the depth of antibody penetration into the sections due to different incubation time periods and types of section used (Irintchev et al., 2005).

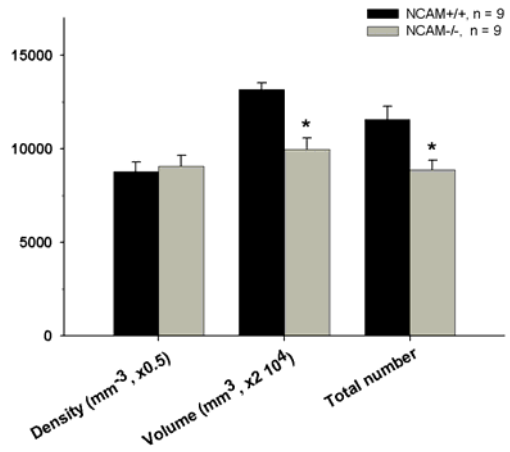

Figure 20: Numbers of ChAT$^+$ cells in the medial septal/ diagonal band of Broca nuclear of young (2 month-old) NCAM+/+ and NCAM-/- mice. Shown are mean values + SEM for numerical cell density (Density), total nuclear volume (Volume) and total cell number. Numbers of animals studied per group are indicated in the legend. Asterisks indicate significant differences between groups mean values ($p < 0.05$, two-sided *t* test for independent samples).

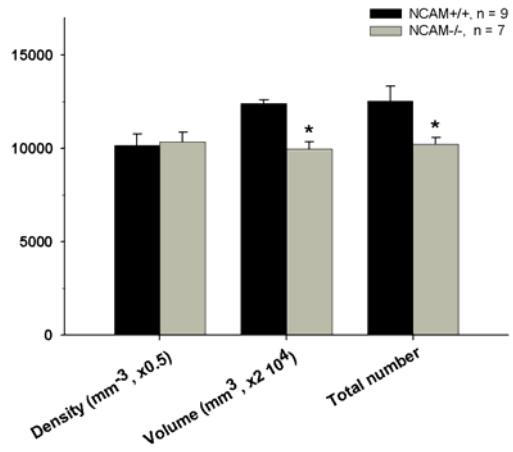

Figure 21: Numbers of ChAT$^+$ cells in the medial septal/ diagonal band of Broca nuclear complex of adult (13-month-old) NCAM+/+ and NCAM-/- mice. Shown are mean values + SEM for numerical cell density (Density), total nuclear volume (Volume) and total cell number. Numbers of animals studied per group are indicated in the legend. Asterisks indicate significant differences between groups mean values ($p < 0.05$, two-sided *t* test for independent samples).

4.6. Length densities of cholinergic axons in the hippocampus

Length density (density per unit volume) was measured in most regions and layers of hippocampus: molecular, granular and polymorph layer, in the dentate gyrus, strata oriens, pyramidale and lucidum in CA3 and oriens, pyramidale and radiatum of CA1.

In contrast to the numbers of cholinergic neuronal cell bodies, an overall tendency for higher ChAT$^+$ fiber densities were found in the hippocampus of NCAM-/- mice compared with wild-type littermates at both ages (Fig. 22-27). This increase was significant at both ages for the granular (27-35% higher in NCAM-/- *versus* NCAM+/+ mice) and polymorph (by +33-35%) layers of the dentate gyrus (Fig.22, 23), and the oriens (+19-29%) and pyramidal cell layer (+21-29%) of CA1 (Fig. 24, 25). In addition, increased densities were found in the NCAM-/- mice at 13 months in the stratum lucidum of CA3 (by 74%, Fig.27) and the stratum radiatum of CA1 (by 44%, Fig. 25). Comparisons of previous data on cholinergic axon densities in the hippocampus of inbred mice (see, for example, Schwegler et al., 1996a; Aznavour et al., 2002) with our results is difficult because largely different methodologies have been used.

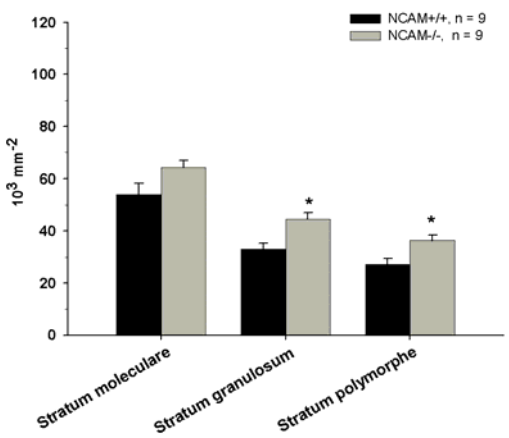

Figure 22: Length densities of ChAT$^+$ fibers (mean values + SEM) in the dentate gyrus of NCAM+/+ and NCAM-/- mice studied at the age of 2 months. Shown are mean values + SEM. Fiber densities were analyzed in the molecular, granular and polymorph layers. Asterisks indicate significant differences between group mean values ($p < 0.05$, *t* test).

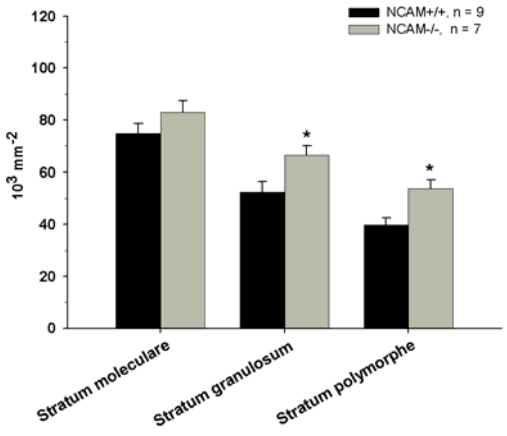

Figure 23: Length densities of ChAT$^+$ fibers (mean values + SEM) in the dentate gyrus region of NCAM+/+ and NCAM-/- mice studied at the age of 13 months. Shown are mean values + SEM. Fiber densities were analyzed in the molecular, granular and polymorph layers. Asterisks indicate significant differences between group mean values ($p < 0.05$, *t* test).

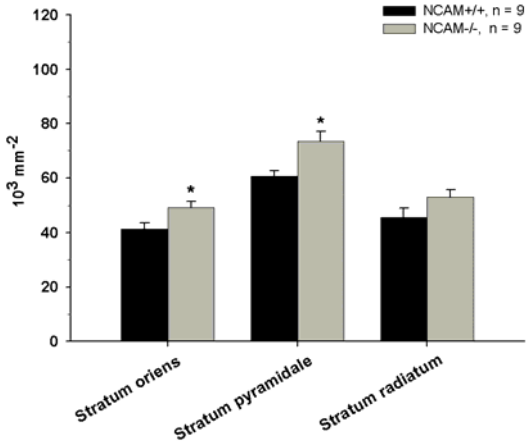

Figure 24: Length densities of ChAT$^+$ fibers (mean values + SEM) in the CA1 region of NCAM+/+ and NCAM-/- mice studied at the age of 2 months. Shown are mean values + SEM. Fiber densities were analyzed in the strata oriens, pyramidale and radiatum. Asterisks indicate significant differences between group mean values ($p < 0.05$, *t* test).

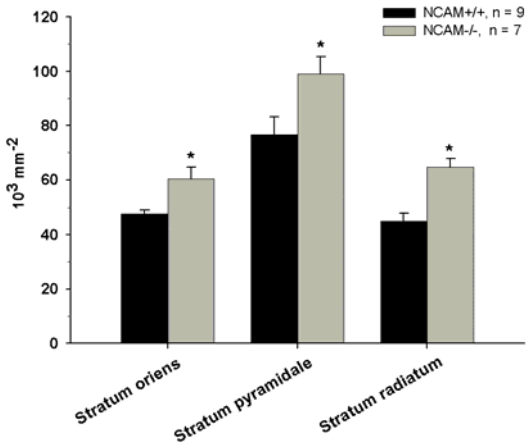

Figure 25: Length densities of ChAT$^+$ fibers (mean values +SEM) in the CA1 of NCAM+/+ and NCAM-/- mice studied at the age of 13 months. Shown are mean values + SEM. Fiber densities were analyzed in the strata oriens, pyramidale and radiatum. Asterisks indicate significant differences between group mean values ($p < 0.05$, *t* test).

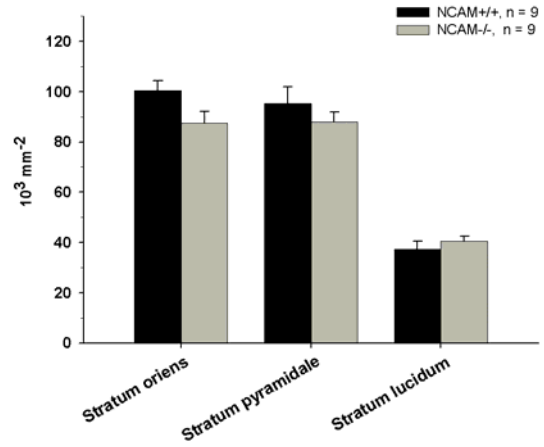

Figure 26: Length densities of ChAT$^+$ fibers (mean values + SEM) in the CA3 region of NCAM+/+ and NCAM-/- mice studied at the age of 13 months. Shown are mean values + SEM. Fiber densities were analyzed in the strata oriens, pyramidale and lucidum. No significant differences between the groups were found ($p > 0.05$, *t* test)

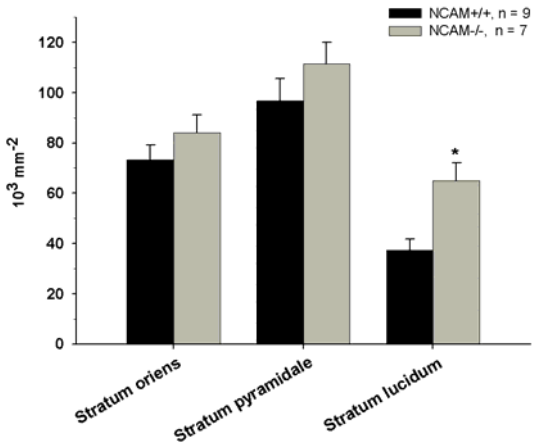

Figure 27: Length densities of ChAT$^+$ fibers (mean values + SEM) in the CA3 region of NCAM+/+ and NCAM-/- mice studied at ages of 13 months. Shown are mean values + SEM. Fiber densities were analyzed in the strata oriens, pyramidale and lucidum. Asterisk indicates a significant difference between the group mean values ($p < 0.05$, *t* test).

4.7. Total length of cholinergic axons in the hippocampus and its subdivisions

The total lengths of cholinergic fibers, calculated using length densities and volumes of the structures, in the whole hippocampus or separately in the dentate gyrus and the CA3 and CA1 regions of were similar in young NCAM-/- and NCAM+/+ mice (Fig. 28). In adult NCAM-deficient mice, total fiber lengths in the hippocampus and its subdivisions CA3 and CA1, but not in the dentate gyrus, were significantly increased (by +17%, +47% and +27%, respectively) as compared with wild-type littermates (Fig. 29).

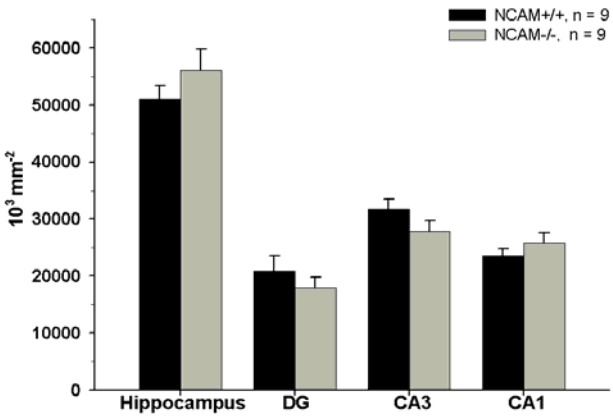

Figure 28: Total lengths of ChAT$^+$ fibers in the hippocampus and its subdivisions of young (2-month-old) NCAM+/+ and NCAM-/- mice. Shown are mean values + SEM. Number of animals studied per group are indicated. No significant differences between the groups were found ($p > 0.05$, *t* test)

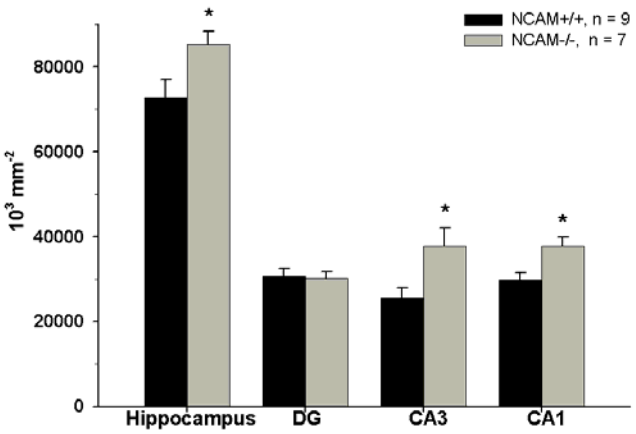

Figure 29: Total lengths of ChAT$^+$ fibers in the hippocampus and its subdivisions of adult (13-month-old) NCAM+/+ and NCAM-/- mice. Shown are mean values + SEM. Number of animals studied per group are indicated. Asterisks indicate significant differences between group mean values ($p < 0.05$, *t* test).

In contrast to length density in the DG, total length of cholinergic fibers in this region was not affected in two-month old NCAM-/- animals (Fig. 30). In thirteen-month-old animals no statistically significant difference was found in NCAM-/- animals compared with wild-type littermates either (Fig. 31).

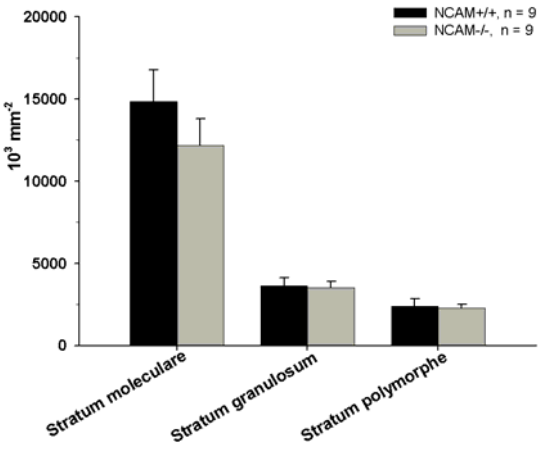

Figure 30: Total lengths of ChAT$^+$ fibers in the DG of young (2-month-old) NCAM+/+ and NCAM-/- mice. Shown are mean values + SEM. Number of animals studied per group are indicated. No significant differences between the groups were found ($p > 0.05$, *t* test)

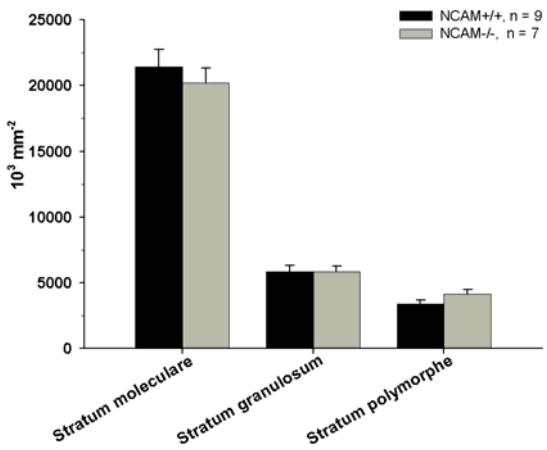

Figure 31: Total lengths of ChAT$^+$ fibers in the DG of adult (13-month-old) NCAM+/+ and NCAM-/- mice. Shown are mean values + SEM. Number of animals studied per group are indicated. No significant differences between the groups were found ($p > 0.05$, *t* test)

In the CA1 region, total length of ChAT fibers in two-month-old NCAM-/- animals was similar to that in wild-type littermates (Fig. 32). In contrast, in thirteen-month-old NCAM-/- mice the total fiber length in stratum radiatum of the CA1 region was increased by 42% compared with NCAM+/+ mice (Fig. 33).

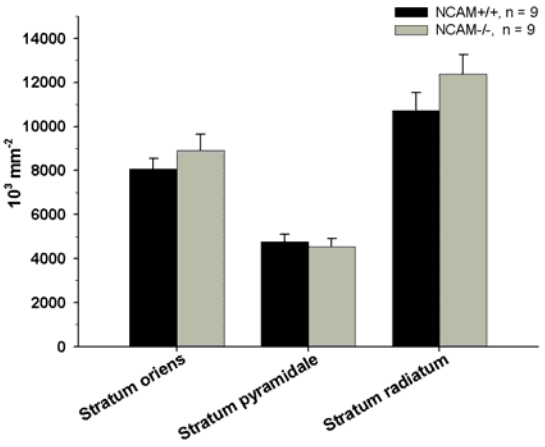

Figure 32: Total lengths of ChAT$^+$ fibers in the CA1 region of young (2-month-old) NCAM+/+ and NCAM-/- mice. Shown are mean values + SEM. Number of animals studied per group are indicated. No significant differences between the groups were found ($p > 0.05$, *t* test)

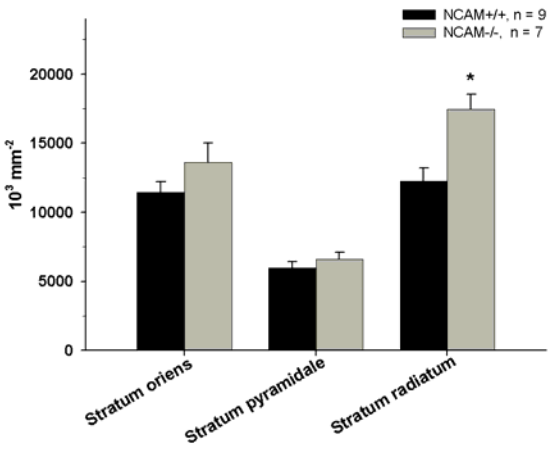

Figure 33: Total lengths of ChAT$^+$ fibers in the CA1 region of adult (13-month-old) NCAM+/+ and NCAM-/- mice. Shown are mean values + SEM. Number of animals studied per group are indicated. Asterisks indicate significant differences between group mean values ($p < 0.05$, *t* test).

The total fiber length in stratum oriens of the CA3 region of two-month-old animals was reduced (- 23%) in NCAM-/- animals as compared with wild-type littermates (Fig. 34). In contrast, no differences were observed in stratum pyramidale and stratum lucidum. Thirteen-month-old NCAM-/- mice had increased total length in stratum pyramidale (+ 38%) and stratum lucidum (+ 118%) of CA3 region as compared with NCAM+/+ mice (Fig. 35).

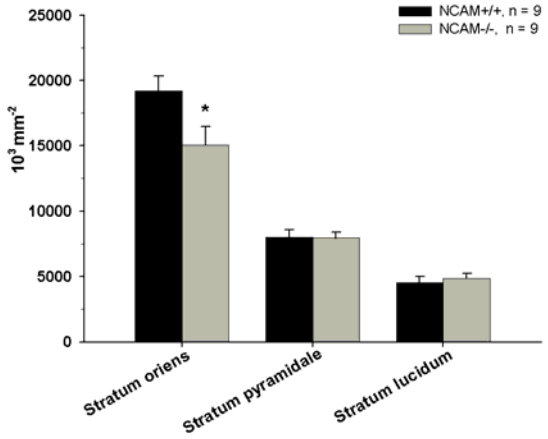

Figure 34: Total lengths of ChAT$^+$ fibers in the CA3 of young (2-month-old) NCAM+/+ and NCAM-/- mice. Shown are mean values + SEM. Number of animals studied per group are indicated. Asterisks indicate significant differences between group mean values ($p < 0.05$, *t* test).

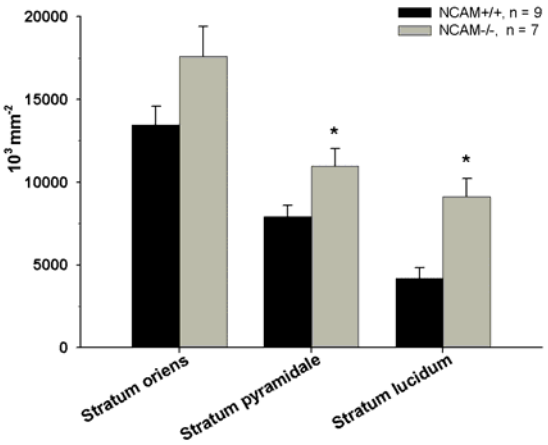

Figure 35: Total lengths of ChAT$^+$ fibers in the CA3 region of adult (13-month-old) NCAM+/+ and NCAM-/- mice. Shown are mean values + SEM. Number of animals studied per group are indicated. Asterisks indicate significant differences between group mean values ($p < 0.05$, *t* test).

4.8. Dopaminergic cells in substantia nigra/ ventral tegmental area

The estimated numerical densities of tyrosine hydroxylase (TH$^+$) immunoreactive neurons in the substantia nigra/ ventral tegmental area (A9-A10 groups) were lower in the NCAM-/- animals compared with NCAM+/+ mice (-27% and -21% at 2 and 13 months, respectively, Fig. 36, 37). The volume of the nuclear complex was similar in the two genotype groups and, therefore, the size of the cell population in individual groups reflects differences in cell densities (Fig. 36, 37). Total cell number was lower in the NCAM-/- animals compared with NCAM+/+ animals (-22% at 2 month and -21% at 13 month). The estimated numbers of TH$^+$ cells in the A9-A10 groups in wild-type mice (29000 and 33000 cells at 2 and 13 months, respectively) are within the range of values previously reported for different inbred mouse strains (20000 – 35000 cells, Zaborszky and Vadasz, 2001).

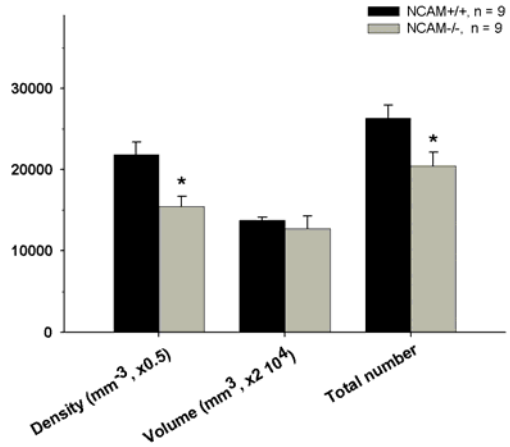

Figure 36: Numbers of TH^+ cells in the substantia nigra/ ventral tegmental area of young (2 month-old) NCAM+/+ and NCAM-/- mice. Shown are mean values + SEM for numerical cell density (Density), total nuclear volume (Volume) and total cell number. Numbers of animals studied per group are indicated in the legend. Asterisks indicate significant differences between groups mean values ($p < 0.05$, two-sided *t* test for independent samples).

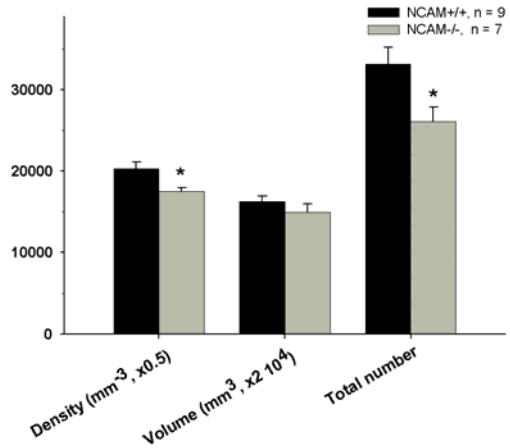

Figure 37: Numbers of TH^+ cells in the substantia nigra/ ventral tegmental area of adult (13 month-old) NCAM+/+ and NCAM-/- mice. Shown are mean values + SEM for numerical cell density (Density), total nuclear volume (Volume) and total cell number. Numbers of animals studied per group are indicated in the legend. Asterisks indicate significant differences between groups mean values ($p < 0.05$, two-sided *t* test for independent samples).

4.9. Noradrenergic cells in locus coeruleus

Locus coerulleus is too small for total cell number estimates and, therefore, profile density (number of cells in certain volume) estimates were performed. The estimates of profile densities of TH^+ cell bodies in the locus coeruleus (noradrenergic cells) did not reveal genotype-specific differences (-7% at 2 month and -8% at 13 month NCAM-/- compared with NCAM+/+ animals, respectively, Fig. 38). Also, the size of the nucleus, as indicated by area measurements, was not affected by the NCAM deficiency (+1% at 2 month and +11% at 13 month NCAM-/- compared with NCAM+/+ animals, respectively, Fig. 38).

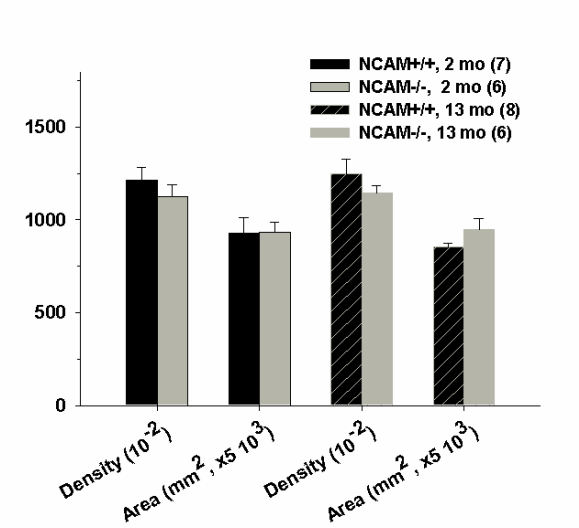

Figure 38: Profile density of TH^+ cells in the locus coeruleus and area of the locus coeruleus of young (2 month-old) and adult (13 month-old) NCAM+/+ and NCAM-/- mice. Shown are mean values + SEM for prifile cell density (Density) and area of locus coerulleus (Area). Numbers of animals studied per group are indicated in the legend. No significant differences between the groups were found ($p > 0.05$, *t* test).

4.10. Length densities of catecholaminergic axons in the hippocampus

Length densities of TH^+ fibers were studied in the molecular, granular and polymorph layers of the dentate gyrus (Fig. 39, 40), in the oriens, pyramidal and radiatum layers of CA1 (Fig. 41, 42) and in the oriens, pyramidal and lucidum layers of CA3 (Fig. 43, 44). Fiber density was significantly reduced in the pyramidal layer of CA3 in NCAM deficient mice at both ages (Fig. 43, 44, -25% and -33% compared with the NCAM+/+ group at 2 and 13 months, respectively). In all other areas, densities were similar in NCAM-/- and NCAM+/+ mice at both ages. Since TH is present in dopaminergic as well as noradrenergic axons, and no antibody against the noradrenergic cell-specific marker dopamine beta-hydroxylase suitable for axonal visualization was available, we could not dissociate between these two types of projections.

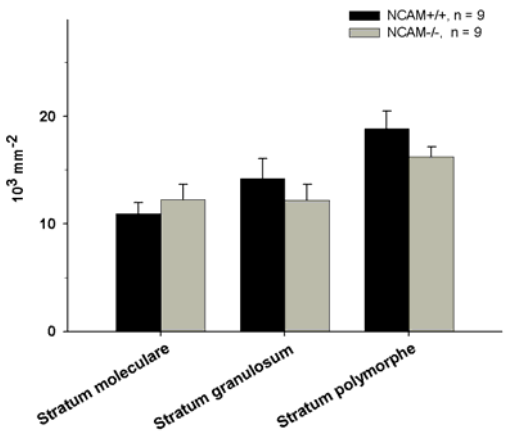

Figure 39: Length densities of TH^+ fibers in the DG region of NCAM+/+ and NCAM-/- mice studied at ages of 2 months. Shown are mean values + SEM. Fiber densities were analyzed in the molecular, granular and polymorph layers. No significant differences between the groups were found ($p > 0.05$, *t* test)

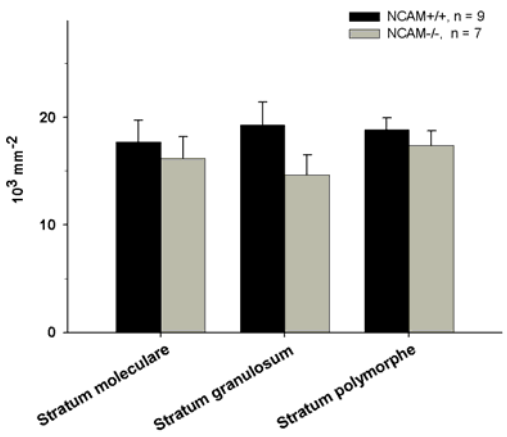

Figure 40: Length densities of TH^+ fibers in the DG region of NCAM+/+ and NCAM-/- mice studied at ages of 13 months. Shown are mean values + SEM. Fiber densities were analyzed in the molecular, granular and polymorph layers. No significant differences between the groups were found ($p > 0.05$, *t* test)

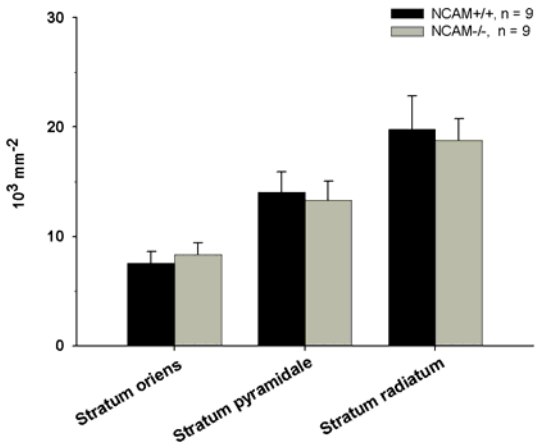

Figure 41: Length densities of TH^+ fibers in the CA1 region of NCAM+/+ and NCAM-/- mice studied at the age of 2 months. Shown are mean values + SEM. Fiber densities were analyzed in the strata oriens, pyramidale and radiatum. No significant differences between the groups were found ($p > 0.05$, *t* test)

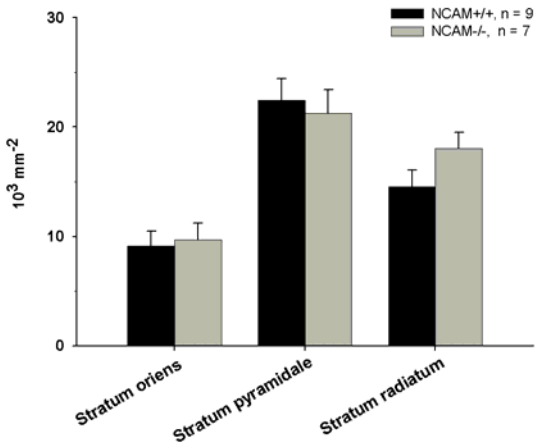

Figure 42: Length densities of TH^+ fibers in the CA1 region of NCAM+/+ and NCAM-/- mice studied at the age of 13 months. Shown are mean values + SEM. Fiber densities were analyzed in the strata oriens, pyramidale and radiatum. No significant differences between the groups were found ($p > 0.05$, *t* test)

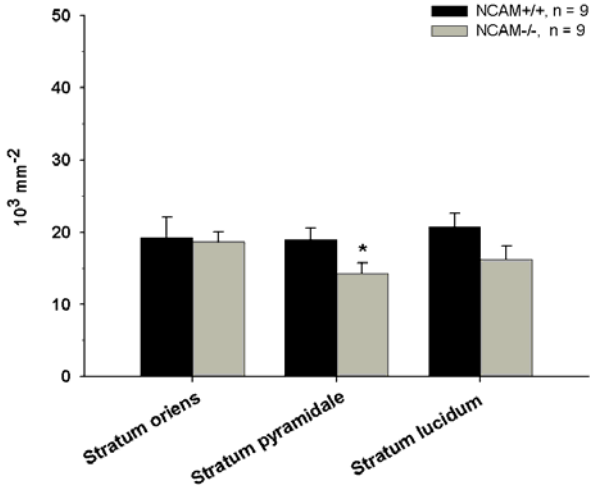

Figure 43: Length densities of TH^+ fibers in the CA3 region of NCAM+/+ and NCAM-/- mice studied at the age of 2 months. Shown are mean values + SEM. Fiber densities were analyzed in the strata oriens, pyramidale and lucidum. The asterisk indicates a significant difference between the group mean values ($p < 0.05$, two-sided *t* test for independent samples).

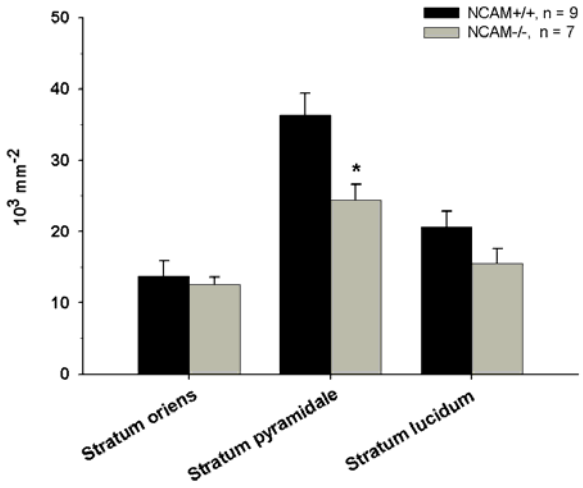

Figure 44: Length densities of TH^+ fibers in the CA3 region of NCAM+/+ and NCAM-/- mice studied at the age of 13 months. Shown are mean values + SEM. Fiber densities were analyzed in the strata oriens, pyramidale and lucidum. The asterisk indicates a significant difference between the group mean values ($p < 0.05$, two-sided *t* test for independent samples).

4.11. Total length of catecholaminergic axons in the hippocampus

Total lengths of TH+ fibers calculated for the whole hippocampus and it's subdivisions, DG, CA3 and CA1, were similar in 2-month-old NCAM-/- and NCAM+/+ mice (Fig. 45). At the age of 13 months, the total length was significantly smaller in the DG (-28%), but not in the CA3 and CA1 region, of NCAM-/- mice compared with wild-type littermates (Fig. 46).

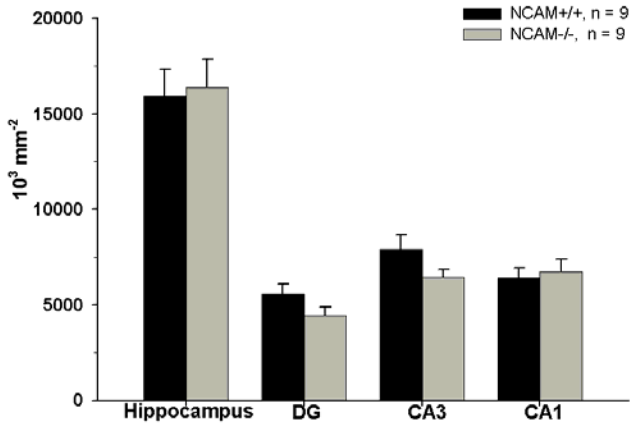

Figure 45: Total lengths of TH$^+$ fibers in the whole hippocampus and its subdivisions of young (2-month-old) NCAM+/+ and NCAM-/- mice. Shown are mean values + SEM. Number of animals studied per group are indicated. No significant differences between the groups were found ($p > 0.05$, *t* test)

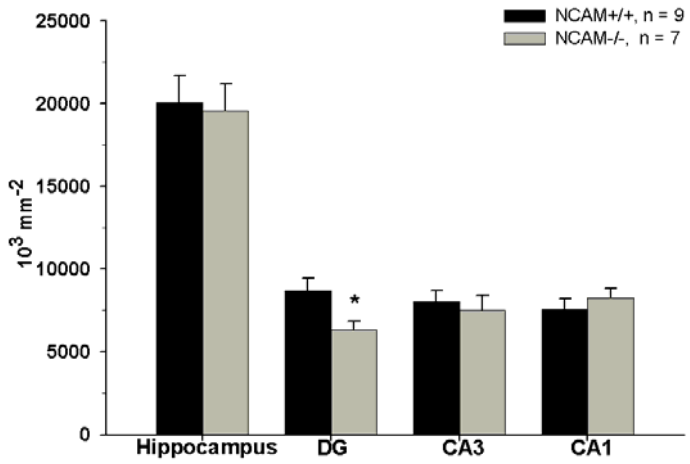

Figure 46: Total lengths of TH$^+$ fibers in the whole hippocampus and its subdivisions of adult (13-month-old) NCAM+/+ and NCAM-/- mice. Shown are mean values + SEM. Number of animals studied per group are indicated. The asterisk indicates a significant difference between the group mean values ($p < 0.05$, *t* test).

The total fiber length was significantly lower in NCAM-/- compared with NCAM+/+ mice at the age of two-month in stratum granulosum (- 37%) and stratum polymorphe (- 24%) of the DG (Fig. 47). At the age of 13 months, a significant reduction, as compared with NCAM+/+ littermates, was found in stratum granulosum (- 43%) of the DG of NCAM-/- mice (Fig. 48).

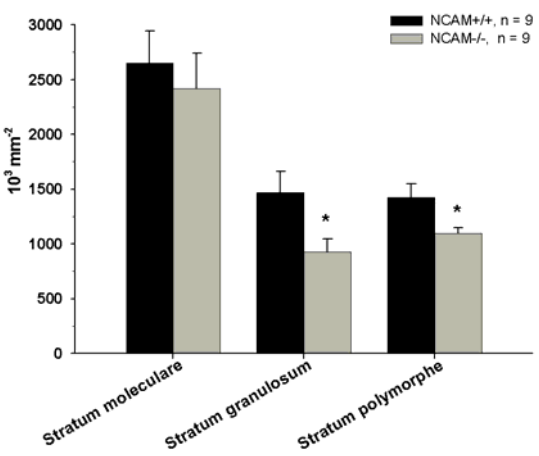

Figure 47: Total lengths of TH^+ fibers in the DG layers of young (2-month-old) NCAM+/+ and NCAM-/- mice. Shown are mean values + SEM. Number of animals studied per group are indicated. Asterisks indicate significant differences between group mean values ($p < 0.05$, *t* test).

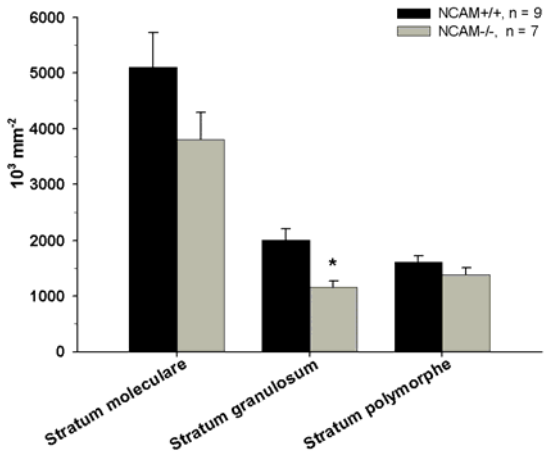

Figure 48: Total lengths of TH^+ fibers in DG layers of adult (13-month-old) NCAM+/+ and NCAM-/- mice. Shown are mean values + SEM. Number of animals studied per group are indicated. The asterisk indicates a significant difference between the group mean values ($p < 0.05$, *t* test).

For all layers (strata oriens, pyramidale and radiatum) of the CA1 region, no difference between the genotypes was found for total fiber length at both ages studied (Fig. 49 and Fig. 50).

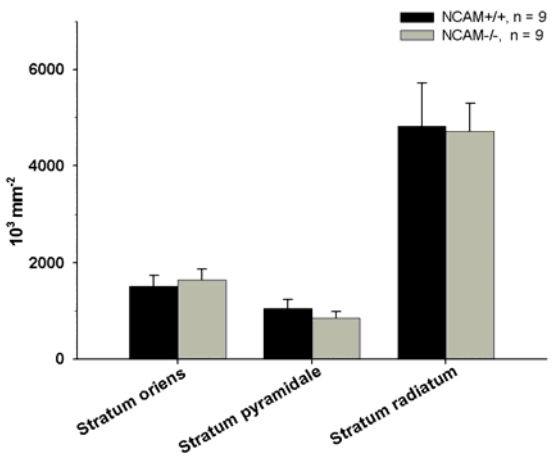

Figure 49: Total lengths of TH^+ fibers in the CA1 layers of young (2-month-old) NCAM+/+ and NCAM-/- mice. Shown are mean values + SEM. Number of animals studied per group are indicated. No significant differences between the groups were found ($p > 0.05$, *t* test)

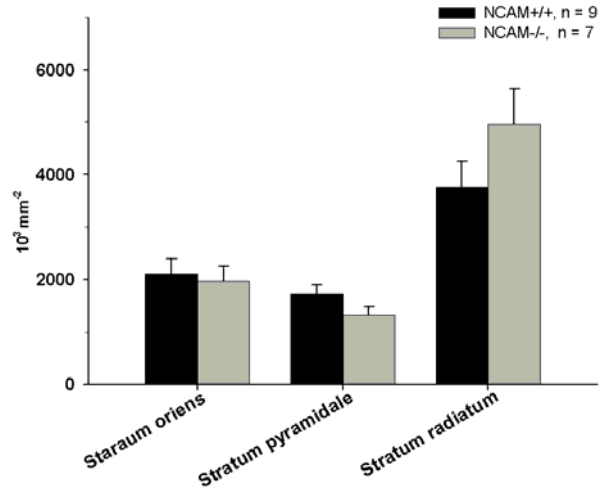

Figure 50: Total lengths of TH^+ fibers in the CA1 layers of adult (13-month-old) NCAM+/+ and NCAM-/- mice. Shown are mean values + SEM. Number of animals studied per group are indicated. No significant differences between the groups were found ($p > 0.05$, *t* test).

In the CA3 area, a difference between the genotypes in total fiber length was found only in stratum lucidum at 2 months of age (- 33% in NCAM-/- versus NCAM+/+ mice) (Figs. 51, 52).

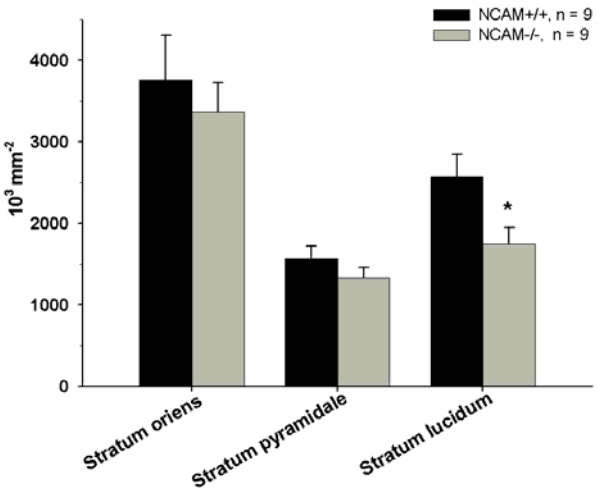

Figure 51: Total lengths of TH^+ fibers in the CA3 layers of young (2-month-old) NCAM+/+ and NCAM-/- mice. Shown are mean values + SEM. Number of animals studied per group are indicated. The asterisk indicates a significant difference between the group mean values ($p < 0.05$, *t* test).

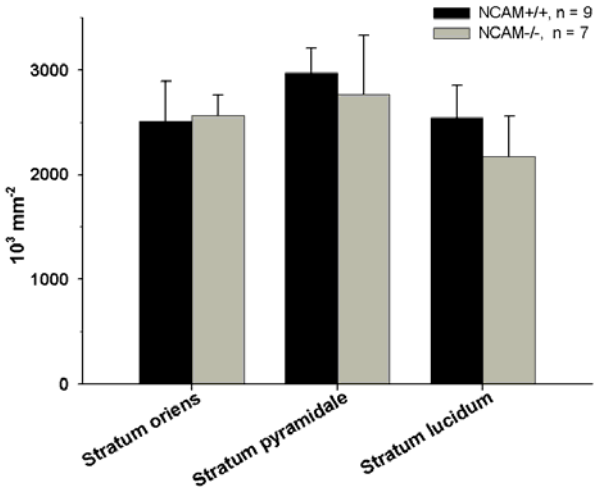

Figure 52: Total lengths of TH^+ fibers in CA3 layers of adult (13-month-old) NCAM+/+ and NCAM-/- mice. Shown are mean values + SEM. Number of animals studied per group are indicated. No significant differences between the groups were found ($p > 0.05$, *t* test)

5. Discussion

The results of this study show that deficient expression of the cell recognition molecule NCAM in the mouse causes a range of abnormalities in different brain regions. Apart from discrete gross structural abnormalities in hippocampal subfields, cholinergic neurons in the medial septal / diagonal band of Broca nuclear complex and A9 – A10 cell groups (substantia nigra/ventral tegmental area) and their hippocampal projections are affected by the mutation. The study provides evidence for the importance of NCAM in early development and structural maintenance during adulthood of the cholinergic and dopaminergic systems of the mouse.

A brief summary of results is shown in Table 1.

Table 1: Summary of differences found between NCAM-/- and NCAM+/+ mice in different brain regions and at different ages. Arrows indicate significantly lower or higher values in mutant animals as compared with wild-type animals, = indicates that there is no significant difference.

Parameter	**2 month**	**13 month**
Body weight	↓	=
Brain mass	↓	=
Brain volume	↓	↓
Cholinergic cells in the medial septal/ diagonal band of Broca nuclear complex		
Density of cells	=	=
Volume of the structure	↓	↓
Total number of cells	↓	↓
Length densities of cholinergic axons in the hippocampus		
DG		
Stratum moleculare	=	=
Stratum granulosum	↑	↑
Stratum polymorphe	↑	↑
CA1		
Stratum oriens	↑	↑
Stratum pyramidale	↑	↑
Stratum radiatum	=	↑
CA3		

Stratum oriens	=	=
Stratum pyramidale	=	=
Stratum lucidum	=	↑
Total length densities of cholinergic axons in the hippocampus and its subdivisions		
Hippocampus	=	↑
DG	=	=
CA1	=	↑
CA3	=	↑
DG		
Stratum moleculare	=	=
Stratum granulosum	=	=
Stratum polymorphe	=	=
CA1		
Stratum oriens	=	=
Stratum pyramidale	=	=
Stratum radiatum	=	↑
CA3		
Stratum oriens	↓	=
Stratum pyramidale	=	↑
Stratum lucidum	=	↑
Dopaminergic cells in substantia nigra/ ventral tegmental area		
Density of cells	↓	↓
Volume of the structure	=	=
Total number of cells	↓	↓
Noradrenergic cells in locus coeruleus		
Density of cells	=	=
Area of the structure	=	=
Length densities of catecholaminergic axons in the hippocampus		
DG		
Stratum moleculare	=	=
Stratum granulosum	=	=

Stratum polymorphe	=	=
CA1		
Stratum oriens	=	=
Stratum pyramidale	=	=
Stratum radiatum	=	=
CA3		
Stratum oriens	=	=
Stratum pyramidale	↓	↓
Stratum lucidum	=	=
Total length densities of catecholaminergic axons in the hippocampus and its subdivisions		
Hippocampus	=	=
DG	=	↓
CA1	=	=
CA3	=	=
DG		
Stratum moleculare	=	=
Stratum granulosum	↓	↓
Stratum polymorphe	↓	=
CA1		
Stratum oriens	=	=
Stratum pyramidale	=	=
Stratum radiatum	=	=
CA3		
Stratum oriens	=	=
Stratum pyramidale	=	=
Stratum lucidum	↓	=
Volume of the hippocampus and its subdivisions		
Hippocampus	=	=
DG	↓	↓
CA1	=	=
CA3	=	↑
Volume of DG layers		
Stratum moleculare	↓	↓

Stratum granulosum	↓	↓
Stratum polymorphe	↓	=
Volume of CA1 layers		
Stratum oriens	=	=
Stratum pyramidale	↓	↓
Stratum radiatum	=	=
Volume of CA3 layers		
Stratum oriens	=	=
Stratum pyramidale	=	↑
Stratum lucidum	↓	↑

5.1. Hippocampal dysplasia in NCAM deficient mice

The size of the dentate gyrus, as opposed to CA1 and CA3, was found to be specifically reduced in both young and adult NCAM-/- mice. Since NCAM is involved in neurogenesis, neurite outgrowth and synaptogenesis, the deficit in volume of the dentate gyrus may reflect either a reduction in the number of granule cells, size of their dendritic trees and/or number of synapses on these. In contrast to the dentate gyrus, the CA1 and CA3 regions in young and the CA1 region in adult NCAM-/- mice were normal in size. Even more surprisingly, the volume of the CA3 region was increased in adult NCAM-/- compared with NCAM+/+ mice. The latter finding can be interpreted as a sign of an age-related adaptive response the reasons for which, however, are not known. For further understanding of the role of NCAM in early hippocampal development and during adulthood, detailed quantitative analyses of defined cell populations such as principal cells, interneuronal subpopulations, glial cells and perisomatic synaptic coverage in NCAM-/- and NCAM+/+ mice, as performed in earlier studies on transgenic mice (Irintchev *et al.*, 2005; Nikonenko *et al.*, 2006), appear warranted.

5.2. Reduced numbers of cholinergic neurons in NCAM deficient mice

This study provides novel evidence for aberrations in defined neuronal populations and axonal projections in NCAM deficient mice. Numbers of cholinergic neurons in the medial septal/diagonal band complex were significantly lower in NCAM deficient mice (by

23% and 18% at 2 and 13 months, respectively). The similar differences detected at both ages studied indicate a lack of age-related decline in cell numbers in NCAM deficient animals between 2 and 13 months. These findings show that NCAM deficiency affects the embryonic and/or early postnatal development of the cholinergic neurons in the medial septal/diagonal band complex.

Normal volume of the medial septal/diagonal band complex and lower cell density in the NCAM -/- mice may indicate that NCAM is involved more in maturation and survival than in migration of cells. This notion is strongly supported by recent findings that glia-cell-line-derived neurotrophic factor (GDNF), a survival factor for cholinergic cells in the basal forebrain as indicated by *in vitro* experiments, tissue transplantation and lesion studies (Price et al., 1996; Weis et al., 2001; Williams et al., 1996), signals through, among other receptors, NCAM (Chao et al., 2003; Paratcha et al., 2003; Sariola and Saarma, 2003). Therefore, we can speculate that a failure in GDNF/NCAM signaling in NCAM deficient mice is a reason for the developmental loss of cholinergic cells in the medial septal/diagonal band complex. NCAM is also modulating brain derived neurotrophic factor (BDNF) signaling (Vutskits et al., 2001) that is essential for development of basal ganglia cholinergic neurons (Ward and Hagg, 2000) and different types of catecholaminergic neurons (Murer et al., 2001). NCAM also interacts with FGF receptors and this interaction is required for NCAM stimulated neurite outgrowth (Niethammer et al., 2002). In this respect it is remarkable that FGF enhances survival of cholinergic neurons and up-regulates their ChAT activity (Kanda et al., 2000).

Beyond development, one has to consider that the septo-hippocampal systems is more susceptible to genetic and environmental influences than other neural systems and is preferentially affected, like the nigro-striatal dopaminergic system, in neurodegenerative diseases. We can thus speculate that polymorphisms in the NCAM gene, alone or in conjunction with other genetic and epigenetic factors, may have relevance for neurodegenerative disorders in humans. Relevance of NCAM for the pathogenesis of Alzheimer type dementia has been recently suggested based on the observation that NCAM serum concentrations are increased in patients with this disease (Todaro et al., 2004; Strekalova et al., 2005). Moreover, a potential consequence of amyloid beta-mediated oxidative stress, a process implicated in the pathogenesis of Alzheimer's disease, is impaired synthesis of the HNK-1 glycan, a functionally important carbohydrate associated with NCAM (Kruse et al., 1984; Thomas et al., 2005). From an experimental point of view, it thus appears

interesting to investigate the effects of aging and environmental factors, such as toxic substances and stress on cholinergic systems in NCAM homozygous and heterozygous mice.

5.3. Impacts of NCAM deficiency on dopaminergic and noradrenergic neuronal populations

The observed reduction in the number of dopaminergic neurons in the A9-A10 groups of NCAM-/- mice was considerable compared with NCAM+/+ mice (by 27% and 21% at 2 and 13 months, respectively) and larger than could be expected if solely related to the deficit of 11% in brain mass observed at both ages. In contrast to cholinergic and dopaminergic cells, no genotype-related differences were found for noradrenergic neurons in the locus coeruleus. The numbers of dopaminergic and noradrenergic cell types analyzed were similar in young and adult NCAM-/- mice indicating a lack of age-related cell loss between 2 and 13 months of age. These findings and the observations on the cholinergic neurons, indicate that NCAM deficiency differentially affects the embryonic and/or early postnatal development of different cell groups with different origin, location and function.

Previous observations of high levels of NCAM expression in dopaminergic neurons during embryonic development (Shults and Kimber, 1992) and of PSA-NCAM mediated enhancement of cell contact-dependent dopaminergic cell maturation *in vitro* (Loudes *et al.*, 1997) have suggested that NCAM may be important for the development of the dopaminergic system. Normal volume of and lower cell density in the A9-A10 nuclei of NCAM -/- mice may indicate that NCAM is involved in maturation and survival rather than migration of dopaminergic cells. This notion is supported by findings that glia-cell-line-derived neurotrophic factor (GDNF), a survival factor for midbrain dopaminergic neurons during development (Burke, 2004), signals through, among other receptors, NCAM (Chao *et al.*, 2003; Paratcha *et al*., 2003; Sariola and Saarma, 2003). Trophic effects of GDNF have additionally been shown for noradrenergic cells of the locus coeruleus after lesion and fetal tissue transplantation (Arenas *et al.,* 1995; Quintero *et al.,* 2004). The impact of GDNF on the early development of the locus coeruleus, however, appears to be limited (Granholm *et al.,* 1997; Holm *et al.,* 2003), an observation which may explain why the locus coeruleus is not affected in NCAM-/- mice. NCAM modulates also brain derived neurotrophic factor (BDNF) signaling (Vutskits *et al*., 2001) that is essential for development subpopulations of catecholaminergic neurons (Murer *et al*., 2001). NCAM also interacts with FGF receptors, and this interaction is required for NCAM-stimulated neurite outgrowth (Niethammer *et al*.,

2002). Thus, NCAM may affect development of catecholaminergic neurons and their hippocampal projections via modulation of receptors to several growth factors and neurotrophins.

5.4. Aberrations in the cholinergic innervation of the hippocampus of NCAM deficient mice

The density of cholinergic axons was higher in most fields and layers of the hippocampus and total fiber length was much larger in the CA1 and CA3 regions of NCAM-/- mice compared with NCAM+/+ littermates. This appears to some extent surprising in view of the reduced numbers of cholinergic cell bodies. However, the idea that fewer neurons can produce a denser, as compared with normal, axonal network in the target area is not altogether surprising. A well known example is the adaptive and thus compensatory axonal sprouting of motoneurons in disease and aging (Gordon et al., 2004). More intriguing is the question as to the reasons for the enhanced cholinergic innervations which are variable in its degree in different hippocampal subfields. A possible explanation is that NCAM may regulate membrane targeting, clustering or functional properties of particular neurotransmitter receptors, for example, the alpha7 nicotinic acetylcholine receptor (Bruses et al., 2001a). In this case, NCAM deficiency would cause an impairment of cholinergic signaling which, in turn, may induce compensatory growth of the cholinergic axonal arborization. Differences in receptor types and densities in different hippocampal areas would thus result in subregion-specific responses. Several observations lend support to the plausibility of our speculation. NCAM regulates important signaling molecules, such as AMPA and NMDA receptors (Vaithianathan et al., 2004; Hammond at al., 2006; Sytnyk at al., 2006) and the Kir3.1/2 inwardly rectifying K^+ channels via lipid rafts (Delling et al., 2002). These observations are noteworthy since lipid rafts are important for the maintenance of alpha7 nicotinic receptors in the plasma membrane as shown for the somatic spines of ciliary ganglionic neurons (Bruses et al., 2001a). Another possibility is that NCAM may be important for acetylcholine release and, thus, the compensatory elaboration of cholinergic fibers reflects a deficit in release. This hypothesis is strongly supported by data on abnormal organization of the neuromuscular junction and impaired evoked release of acetylcholine vesicles at physiological rates of motor nerve stimulation (Rafuse et al., 2000; Polo-Parada et al., 2001). At motor endplates, NCAM interacts with agrin which is crucial for organization of cholinergic synapses (Huh and Fuhrer, 2002). The hypothesis that cholinergic transmission is impaired in the absence of NCAM is

also attractive in functional terms: cholinergic transmission modulates anxiety as well as learning and memory formation (File et al., 2000; Gold, 2003) and previous work has shown that NCAM deficient mice are more anxious and have memory deficits as compared with wild-type littermates (Cremer et al., 1994; Stork et al., 1997; 1999; Bukalo et al., 2004). These possibilities warrant further investigations on the cholinergic transmitter system under conditions of NCAM deficiency.

5.5. Aberrations in the catacholaminergic innervations of the hippocampus of NCAM deficient mice

In contrast to cholinergic axons, the total length of catecholaminergic fibers was reduced in the dentate gyrus of NCAM-/- *versus* NCAM+/+ mice. However, this was due to a smaller size of the dentate gyrus in NCAM-/- mice and not due to changes in fiber density. We could not dissociate between dopaminergic and noradrenergic axons because of lack of appropriate antibodies. If we assume that the normally sized noradrenergic cell population in the locus coeruleus of NCAM-/- mice innervates the hippocampus normally, overall normal catecholaminergic fiber densities should indicate a compensatory increase in dopaminergic axonal branching similar to that observed for cholinergic axons in young NCAM-/- mice. Electrophysiological studies will be useful to investigate whether the dopaminergic and noradrenergic innervation of the hippocampus of NCAM-/- mice are normal.

The structural abnormalities in hippocampal subfields observed in this study may be related to previously reported functional deficits in the hippocampus of NCAM-/- mice. *In vivo* electrophysiological analyses of mice deficient in expression of NCAM or PSA have indicated that LTP in the dentate gyrus depends on the NCAM glycoprotein backbone rather than on its associated PSA, while polysialylation of NCAM expressed by immature granule cells supports the development of basal excitatory synaptic transmission in this region (Stoenica *et al.*, 2006). The increased length density of cholinergic axons in the dentate gyrus and the CA1 area of the hippocampus may reflect homeostatic changes in the hippocampal circuitry to compensate deficits in synaptic plasticity in these two regions (Muller *et al*., 1996; Bukalo *et al.*, 2004; Stoenica *et al*., 2006). LTP is also impaired at mossy fiber synapses in the CA3 region of NCAM-/- mice (Cremer *et al*., 1997). This is remarkable in light of our present data showing a deficit in catecholaminergic innervation of the CA3 pyramidal cell layer in NCAM-/- mice and the reported enhancement of mossy fiber LTP by noradrenergic activation (Hopkins and Johnston, 1988).

6. Summary

The neural cell adhesion molecule is implicated in the development and synaptic plasticity of the central nervous system. Although NCAM deficiency in mice causes a range of functional abnormalities, the underlying morphological aberrations have remained largely unknown. Here we addressed the question whether NCAM is important for the development and maintenance during postnatal life of the cholinergic, dopaminergic and catacolaminergic neurotransmitter system in the forebrain. Major cell nuclei containing cholinergic, dopaminergic and catacolaminergic neurons and their hippocampal projections were studied in NCAM deficient (NCAM-/-) and wild-type (NCAM+/+) littermates aged 2 or 13 months using immunohistochemistry and stereology. The total number of choline acetyltransferase-immunoreactive neurons in the medial septal / diagonal band of the Broca nuclear complex was found to be lower in the mutant compared with wild-type animals at both ages studied. Despite deficient numbers of cholinergic neurons, the total lengths of cholinergic fibers projecting to the dentate gyrus and the CA1 and CA3 subfields of the hippocampus were normal at 2 months of age in NCAM-/- mice. At 13 months of age, the total length of cholinergic axons in the CA1 and CA3 region, but not in the dentate gyrus, of NCAM-/- mice was increased both compared with NCAM+/+ littermates and 2-month-old NCAM deficient animals indicating a region-specific compensatory response. The total number of dopaminergic neurons in A9-A10 cell group was found to be significantly reduced in NCAM-/- animals at both ages studied. Noradrenergic cells in locus coerulleus were not affected by the mutation. These finding demonstrate that NCAM is essential for the normal development of the forebrain cholinergic system and dopaminergic neurons. The observed abnormalities in the cholinergic system may underlie physiological and behavioral abnormalities previously reported for NCAM deficient mice.

Study two: Cell recognition molecule L1 and neural stem cells

1. Introduction

1.1. Cell adhesion molecules in the nervous system

One of the major challenges in developmental neurobiology is a full understanding of the molecular mechanisms that allow for the formation of specific synaptic connections in the central and peripheral nervous system. The development of the nervous system depends on a coordinate sequence of morphoregulatory processes, such as neural induction, proliferation and differentiation of cells, their migration to final destinations, and the patterning of neuronal connectivities (Purves and Lichtman, 1983; Goodman and Shatz, 1993; Edelman, 1986). In the adult nervous system glial cells and, in certain brain regions, also neurons are continuously generated and have to be integrated into the existing tissue. In addition, mature neurons have the capacity to change their synaptic connectivities and the efficacy of synaptic transmission, a process termed synaptic plasticity. A key step in all these processes is the ability of cells and their outgrowing axons and dendrites to interact with other cells and the extracellular matrix (Kater and Rehder, 1995; Gordon-Weeks and Fischer, 2000). Many of these interactions are mediated by a variety of integral membrane proteins, collectively termed cell adhesion molecules (CAMs).

Cell adhesion molecules (CAMs) are integral membrane proteins, which play important role in interactions between cells or/and cells and extracellular matrix elements (Gordon-Weeks and Fischer, 2000; Kater and Rehder, 1995). Sequence analysis indicated that many proteins evolved from common precursors by duplication and subsequent diversification of genes. Therefore they were grouped into families and subfamilies according to their structural similarities (Dayhoff et al., 1983). Neural CAMs are divided into three main classes: the Ca^{2+}-dependent cadherins (more than 40 members; Angst et al., 2001; Tepass et al., 2000; Fannon and Colman, 1996; Tang et al., 1998), the heterodimeric integrins (about 17 α- and 8 β-subunits; Clark and Brugge, 1995; Staubli et al., 1998), and the Ca^{2+}-independent

molecules of the immunoglobulin (Ig) superfamily (Aplin et al., 1998; Juliano, 2002; Dityatev et al., 2000; Luthi et al., 1994; Eckhardt et al., 2000; Muller et al., 1996; Perrin et al., 2001).

1.1.1. The immunoglobulin superfamily

Members of the Ig superfamily of cell recognition molecules are characterized by the presence of one or more immunoglobulin modules. Prototypical examples of this family are the immunoglobulins themselves (Edelman et al., 1969) and the MHC-antigens (major histocompatibility complex; Orr et al., 1979) of the immune system. In contrast to these molecules, which are specialized for highly specific antigen recognition, the polypeptide chains constructed by Ig-modules in CAMs (Williams and Barclay, 1988) do not form intermolecular, but intramolecular disulfide bridges within a module. Most cell recognition molecules in the nervous system combine their Ig-like modules with other repeated structures. One of these structures is the fibronectin repeat of the subtype III (FNIII domain). This motif was originally identified as a repeated module of 90 residues in the ECM molecule fibronectin (Kornblihtt et al., 1985) and was later also found in other ECM proteins (Engel, 1991). Functional analysis of fibronectin revealed that FNIII domains are involved in interactions of cells with the ECM (Ruoslahti and Pierschbacher, 1987).

The Ig superfamily is further divided into several subgroups according to the number of Ig-domains, the presence and number of FNIII-domains, the mode of attachment to the cell membrane, and the presence of a catalytic cytoplasmic domain (Cunningham, 1995). The first isolated and characterized Ig-like CAMs were the neural cell adhesion molecule (N-CAM; Brackenbury et al., 1977; Thiery et al., 1977) and L1 (Salton et al., 1983; Rathjen and Schachner, 1984), representative molecules of two different subgroups. F3 (mouse F3/chicken F11/human contactin), DCC (deleted in colonrectal carcinoma), MAG (myelin associated glycoprotein), and FGF-R (fibroblast growth factor-receptor) represent additional subgroups that occur in the brain.

1.1.2. The L1 family

The L1 family consists of six members, among which four are found in vertebrates. All members of the L1 family display high similarity in the composition and conformation of their modules and are composed of six amino-terminal Ig-domains, four to five FNIII-repeats,

a single hydrophobic membrane-spanning region and a short, phylogenetically highly conserved cytoplasmic tail at the carboxyl terminus (Brummendorf and Rathjen, 1995). These molecules display a widespread expression throughout the developing nervous system and are involved in a variety of morphogenetic processes, such as cell migration, axon outgrowth, myelination, pathfinding, fasciculation and synaptic plasticity. Members of the L1 family are mainly found on the surface of axons and at sites of cell-cell contact and are expressed by neurons and glial cells (Hortsch, 1996).

1.1.3. The neural cell adhesion molecule L1

L1 is one of the first isolated and characterized cell adhesion molecules, and has been found in variety of species (Rathjen and Schachner, 1984). In humans, the molecule is termed L1CAM or L1, in chicken Ng-CAM (neuron-glia CAM), in rats NILE (nerve growth factor-inducible large external glycoprotein), in drosophila neuroglian, in mice L1, in goldfish E587, and in zebrafish L1.1 and L1.2. There is a high sequence similarity among species homologous that ranges between 30 to 60 % with the intracellular domain showing the highest degree of interspecies homology. The amino acid sequence of L1 from human and mouse, for instance, is 92 % identical, and that between mouse and rat is 97 % identical. The intracellular domain of L1 from these three species shows complete identity. The presence of homologues across diverse species and the high degree of conservation in the course of evolution is indicative for the functional importance of this member of the Ig supefamily (Hortsch, 1996; Hortsch, 2000; Hlavin and Lemmon, 1991).

1.1.4.1. Characteristics of L1

Mammalian L1 consists of six Ig-domains of the C2-type, which are folded into a horseshoe shaped rather than an extended conformation (Schurmann et al., 2001), five FNIII repeats, a single membrane-spanning region followed by a short cytoplasmic tail. The size of fulllength L1 is approximately 200 kD. Proteolytic cleavage gives rise to smaller forms with a molecular weight of 180, 140, 80 and 50 kD (Sadoul et al., 1988). Twenty one putative sites for asparagine-(N-) linked glycosylation are distributed over the extracellular domain of L1. Since deglycosylation results in a molecular mass of about 150 kD, glycans comprise about 25% of the total molecular mass of L1 (Lindner et al., 1983; Rathjen and Schachner, 1984). Substantial portions of the glycans are O-linked which is indicated by tunicamycin inhibition of cotranslational N-glycosylation (Faissner et al., 1985).

Two tissue and cell specific isoforms are known for L1, resulting from alternative splicing, which are expressed in a tissue- and cell type-specific pattern. The L1 protein is encoded by a single gene, which is located on the X-chromosome and contains 29 exons. 28 exons encode the protein (designated 1b-28) while one exon contains 5´untranslated sequences (exon 1a) (Kallunki et al., 1997; Kohl et al., 1992). The mRNA provides an open reading frame of 3783 nucleotides. The encoded 1260 amino acids comprise a 19 amino acid signal peptide and a mature protein of 1241 amino acids (Moos et al., 1988).

Neurons utilize the entire 28 exon coding sequence of L1 (Takeda et al., 1996). A shorter isoform of L1 (sL1), exclusively expressed in non-neuronal cells, lacks exon 2 and 27. This form was found on cells of hematopoetic origin, in intestinal crypt cells and in the male urogenital tract (Kowitz et al., 1992; Thor et al., 1987; Kujat et al., 1995), in the epidermis and in the kidney (Nolte et al., 1999; Debiec et al., 1998). More recently also oligodendrocytes were found to express sL1, regulated in a maturation-dependent manner (Itoh et al., 2000).

Differential use of exons 2 and 27 is conserved for L1 orthologous in rodents (Jouet et al., 1995; Miura et al., 1991), and teleost fish (Coutelle et al., 1998) suggesting that it is of functional importance. Exon 27 encodes for the four amino acids RSLE within the cytoplasmic domain, which is important as a tyrosine-based sorting motif (YRSL) for clathrin-mediated endocytosis (Kamiguchi et al., 1998). Inclusion of exon 2 into the mRNA provides the six amino acids YEGHHV in human or YKGHHV in mouse, respectively, in place of a single leucine residue immediately amino-terminal to the first Ig-domain (Jouet et al., 1995).

1.1.4.2. Expression and function of L1 in the nervous system

While the following chapter focuses on the expression of L1 in the nervous system, the molecule is also expressed in other tissue such as the crypt cells of the intestine (Thor et al., 1987), the epithelia of the kidney (Nolte et al., 1999), T- and B-cells of the immune system (Ebeling et al., 1996) and tumor cells (Meli et al., 1999).

In the nervous system L1 expression is temporally and spatially regulated. It is detected from embryonic day 10 onwards in the central nervous system on postmitotic neurons and the distribution in the developing nervous system already suggests its role in late cell migration (Rathjen and Schachner, 1984; Fushiki and Schachner, 1986). Studies in young mice showed that expression of L1 in the hippocampus is restricted to fasciculating axons forming the stratum moleculare and the hilus where expression increases with age while

dendrites and regions rich in cell body remain negative for L1 (Persohn and Schachner, 1990). Again the expression profile is indicative of one of its functions, here fasciculation of axons. In the developing cerebral cortex, L1 is expressed by postmitotic, premigratory granule cells in the inner part of the external granular layer, but is absent from proliferating neuroblasts in the out part of the external layer (Persohn and Schachner, 1987), suggesting a role of L1 in migration of nerve cells. In adulthood expression of L1 is continued on unmyelinated axons, but it disappears from myelinated axons (Bartsch et al., 1989). In the peripheral nervous system L1 is also found on non-myelinating Schwann cells and unmyelinated axons (Martini and Schachner, 1986). L1 has never been detected in synapses (Schuster et al., 2001).

Several functional assays have demonstated a role of L1 in migration of postmitotic neurons (Lindner et al., 1983; Asou et al., 1992), axon outgrowth, pathfinding and fasciculation (Fischer et al., 1986; Lagenaur and Lemmon, 1987; Chang et al., 1987; Kunz et al., 1998), growth cone morphology (Payne et al., 1992; Burden-Gulley et al., 1995), adhesion between neurons and between neurons and Schwann cells (Rathjen and Schachner, 1984; Faissner et al., 1984; Persohn and Schachner, 1987), and myelination (Seilheimer et al., 1989). In addition, L1 has been implicated in axonal regeneration (Martini and Schachner, 1988), neuronal cell survival (Chen et al., 1999; Nishimune et al., 2005), and proliferation and differentiation of neural precursor cells (Dihne et al., 2003). Furthermore learning and memory formation (Rose, 1995; Venero et al., 2004) and the establishment of long-term potentiation in the hippocampus (Luthi et al., 1996) are modulated by L1.

1.1.4.3. Neurological disorders caused by mutations in the L1 gene

The human gene encoding L1 is located near the long arm of the X-chromosome (Djabali et al., 1990) in Xq28 (Chapman et al., 1990). A high number of different pathogenic mutations have been identified in virtually all regions of the gene, including missense, nonsense, and frame shift mutations, deletions, duplications, insertions, and splice site mutations. The syndromes caused by mutation in the L1 gene include HSAS (hydrocephalus due to stenosis of the aqueduct of Sylvius; Bickers and Adams, 1949; Rosenthal et al., 1992), MASA (mental retardation, aphasia, shuffling gait and adducted thumbs; Bianchine and Lewis, 1974), X-linked complicated spastic paraplegia (SP-1; Kenwrick et al., 1986) or ACC (agenesis of the corpus callosum; Fransen et al., 1994; Jouet et al., 1994; Kaplan, 1983; Vits et al., 1994). The fact that all of these conditions are allelic disorders proved that HSAS, MASA, SP-1, and ACC represent overlapping clinical spectra of the same disease, and are therefore now summarized under the term “L1 spectrum” (Moya et al., 2002). This term

might be more widely acceptable than the previously proposed term CRASH – corpus callosum agenesis, retardation, adducted thumbs, shuffling gait, and hydrocephalus (Fransen et al., 1995).

L1 mutations account for 5 % of all cases with hydrocephalus and are the most frequent genetic cause of this pathology. The incidence of pathological L1 mutations is generally estimated to be around 1 in 30,000 male births (Halliday et al., 1986; Schrander-Stumpel and Fryns, 1998). In general, the patients show a broad spectrum of clinical and neurological abnormalities, already reflected by the varying nomenclature. The severity of the disease varies significantly between patients with different L1 mutations and might also vary between patients carrying the same mutation (Serville et al., 1992). The most consistent features of affected patients are varying degrees of lower limb spasticity, mental retardation with IQs ranging between 20 and 50, enlarged ventricles or hydrocephalus, and flexion deformities of the thumbs. Those that develop hydrocephalus in utero or soon after birth have a low life expectancy and many of them die neonatally. Another striking morphological abnormality is a hypoplasia of the corticospinal tract (CST) and the corpus callosum. Other brain malformations of affected patients include hypoplasia of the septum pellucidum and the cerebellar vermis, and fusion of the thalami and colliculi (Wong et al., 1995a,b; Fransen et al., 1996 and 1997; Kenwrick et al., 2000).

1.1.4.4. The L1-deficient mouse

Two mouse L1 knock-out (L1ko) lines were independently generated in two laboratories by targeted disruption of the L1 gene (Dahme et al., 1997; Cohen et al., 1998). Many of the pathological features observed in human patients with L1 mutations were also seen in these L1ko mice, and their analysis provided important insights into the functions performed by L1 *in vivo* (Dahme et al., 1997; Cohen et al., 1998; Fransen et al., 1998; Demyanenko et al., 1999; Haney et al., 1999; Rolf et al., 2001). The phenotypes of the two independently generated L1 mutants showed many similarities. The body size of both mutants was significantly reduced when compared with wild-type littermates, the eyes were lacrimous and further back in their sockets and thus appeared smaller, and both mutants showed difficulties to use their hind legs (Dahme et al., 1997; Cohen et al., 1998). The latter observation may parallel the shuffling gait of patients with L1 spectrum. L1 mutant mice also showed a decreased sensitivity to touch and pain (Dahme et al., 1997). Although a few L1 mutants were able to breed, the vast majority of them were sterile (Cohen et al., 1998). Compared to a 129Sv genetic background, the mortality of the mutants was increased when

bred in a C57 genetic background. The higher mortality on a C57 strain correlated with a more severe phenotype when compared to mutants with a 129-background. When L1 mutants and wild-type mice were subjected to a passive avoidance-learning task, both genotypes showed a similar learning ability (Fransen et al., 1998). However, experiments in the Morris water maze revealed impaired spatial learning of L1 mutants compared to wild-type controls (Fransen et al., 1998).

The L1ko mice showed diverse morphological abnormalities. The CST of L1-deficient mice was reduced in size by about 40 % (Dahme et al., 1997). The hypoplasia of the CST was shown to result from pathfinding errors of corticospinal axons (Cohen et al., 1998). In wild-type mice, the majority of these axons turns dorsally at the pyramidal decussation and extends into the contralateral dorsal column. In L1-deficient mice, however, the majority of axons stayed ventrally and entered the contralateral pyramid or turned dorsally, but entered the ipsilatral instead of the contralateral dorsal column (Cohen et al., 1998). The abnormalities of the corticospinal tract might explain the locomotor deficits of L1 mutants and also of patients with L1 spectrum.

Significant hypoplasia was also reported for the corpus callosum, the major commissure of the brain (Demyanenko et al., 1999). This defect apparently resulted from a failure of callosal axons to cross the midline of the brain and is also found in patients with L1 spectrum. Other abnormalities of L1 mutants include abnormal morphology of septal nuclei, an approximately 30 % reduction in the number of hippocampal pyramidal and granule cells, and an abnormal orientation and undulating appearance of apical dendrites of a fraction of pyramidal cells in motor, visual, and somatosensory cortices (Demyanenko et al., 1999).

Given that anti-L1 antibodies interfere with the migration of granule cells in cerebellar explant cultures and with the elongation and fasciculation of neurites of cerebellar nerve cells, it is remarkable that the cytoarchitecture of the cerebellar cortex of L1 mutants showed no evidence for disturbed cell migration, axon outgrowth, or axon fasciculation (Dahme et al., 1997). The only abnormality reported for the cerebellum of L1 mutants was a hypoplasia of the cerebellar vermis (Fransen et al., 1998), a defect also frequently observed in patients with L1 spectrum (Yamasaki et al., 1995). In addition to the unexpectedly mildly affected cerebellum, axon tracts other than the CST and the corpus callosum appear to develop normal in L1-mutant mice (Dahme et al., 1997; Cohen et al., 1998). One explanation might be that other molecules, which perform similar functions as L1, might compensate for the lack of L1 and thus allow normal development of the cerebellum and of the majority of axon tracts in the mutant.

A striking defect of L1 mutant mice is a significant enlargement of the ventricular system (hydrocephalus). This abnormality is again reminiscent of pathological alterations reported for brains of patients with L1 spectrum. Massively enlarged lateral ventricles were observed in L1 mutants with a C57 genetic background, whereas only slightly enlarged ventricular were found in mutants with a 129 background (Dahme et al., 1997; Fransen et al., 1998; Demyanenko et al., 1999). The strong dependence of this defect on the genetic background suggests that modifier genes, together with the mutated L1 gene, determine the severity of this morphological abnormality.

In the PNS L1 deficient mice show reduced numbers of unmyelinated axons per nonmyelinating Schwann cell, Schwann cell processes extending into the endoneurial space, and the presence of incompletely ensheathed unmyelinated axons (Dahme et al., 1997; Haney et al., 1999). These defects demonstrate that L1 is essential for normal interactions between nerve cells and nonmyelinating Schwann cells and probably also for the long-term maintenance of unmyelinated axons.

Altogehter, the clinical of patients carrying L1 mutation and the phenotype of mice with a targeted disruption of the L1 gene both demonstrate the critical role of L1 for normal brain development.

1.2. Huntington's disease and animal models of Huntington's disease

Huntington's disease (HD) is an autosomal dominantly inherited progressive neuropsychiatric disorder, which starts in mid-life and inevitably leads to death. Although the causative mutation was already identified in 1993, the disease mechanism is not entirely understood and there is, as is true for all neurodegenerative diseases, no curative therapy available (The Huntington's Disease Collaborative Research Group, 1993).

Since in early disease stages, neurodegeneration is mainly confined to a distinct population of GABAergic projection neurons within the striatum, cell replacement therapies have been proposed for the treatment of this disorder (Clarke et al., 1988; Dunnett et al., 1988; Sirinathsinghji et al., 1988; Brasted et al., 1999). Successful experimental approaches using human fetal tissue as a graft source have resulted in ongoing clinical trials (Bachoud-Levi et al., 2000; Peschanski et al., 2004). However, the use of human fetal tissue has raised a number of ethical concerns and the availability of material is rather limited. Several researchers have thus started to investigate neural stem cells as an *in vitro* expandable

alternative source for cell replacement therapy in HD (Fricker et al., 1999; Hurelbrink et al., 2002; Fricker-Gates et al., 2004; McBride et al., 2004).

In order to investigate cell replacement therapies in HD it is essential to use animal models which closely resemble the striatal neuropathological characteristics of this disorder, i.e., selective neurodegeneration of GABAergic projection neurons with relative sparing of interneurons (Sharp and Ross, 1996; Li, 1999). Stereotactic injection of glutamate agonists such as quinolinic acid (QA) into the striatum is the most commonly used approach to investigate HD in animal models since glutamatergic excitotoxic cell damage has been postulated to play a role in the pathogenesis of HD and also because it reproduces the selective loss of striatal GABAergic projection neurons (Beal et al. 1986, 1989).

Although the QA-lesion model mimics many of the neuropathological features of HD, it does not reproduce the pathogenetic process of the human condition. In contrast to this model, the R6/2 transgenic mice carrying the human exon 1 with a greatly expanded (115–150) CAG repeat develop a progressive phenotype (Mangiarini et al., 1996). Since these mice show rather little overt cell death, but a shrinkage and dysfunction of the projection neurons, they represent the neuropathology of a very early stage of HD.

Experiments with NSC transplants into the QA lesioned striatum have shown that cell survival is, by far, not as good as the survival of fetal tissue transplants (Svendsen et al., 1996; Lundberg et al., 1997). Thus it is crucial to identify the factors that potentially increase survival. One of the critical factors which may influence cell survival is the method of stem cell preparation *in vitro* prior to transplantation. In culture, NSCs grow as neurospheres (Reynolds et al., 1992; Reynolds and Weiss, 1992). Some groups dissociate these cells via different techniques before transplantation in order to promote better integration and possible migration into the host tissue whereas other groups transplant intact neurospheres (Carpenter et al., 1997; Hammang et al., 1997; Winkler et al., 1998; Ader et al., 2001, 2004; Eriksson et al., 2003).

Furthermore, the survival of grafted NSCs may depend more on environmental factors than fetal transplants do, which are usually transplanted as a suspension of the entire striatal eminence (Dunnett and Bjorklund 1992; Dunnett et al., 2000; Dobrossy and Dunnett 2004). However, the changes occurring in the host after striatal injection of QA are only partly understood. QA injection induces acute cell death of striatal projection neurons (Beal et al., 1986, 1989). In parallel, astrocytes react to the tissue damage by dedifferentiation and proliferation leading to striatal astrogliosis—a feature of HD pathology (Isacson et al., 1987; Dusart et al., 1991). Also activated microglias migrate into the lesioned striatal parenchyma

and proliferate as a reaction to QA induced neuronal degeneration (Marty et al., 1991; Topper et al., 1993). This morphological disintegration of the normal striatal anatomic architecture is accompanied by changes in expression of a variety of inflammatory and neurotrophic factors (Canals et al., 1998; Schiefer et al., 1998; Acarin et al., 2000; Haas et al., 2004). One of these growth factors, known to be of specific importance for differentiation and survival of striatal neurons, is brain-derived neurotrophic factor (BDNF) (Mizuno et al., 1994; Nakao et al., 1995; Ventimiglia et al., 1995; Perez-Navarro et al., 2000).

1.3. Stem cells and their definitions

The nature of stem cell function dictates the complement of specific functional attributes that stem cells must be endowed with. In the absence of any identifying antigenic markers, these functional attributes provide the only basis for a reliable identification of stem cells. The most widely accepted definition identifies stem cells as: a) undifferentiated cells, that lack markers of differentiated tissue-specific cells, b) capable of proliferation and, more importantly, c) possessing self-renewal capacity, d) able to generate functionally differentiated progeny and e) able to regenerate tissue after injury (Loeffler et al., 1997). Some terms are given greater weight in identifying a candidate stem cell: either self-renewal or the capacity to generate a wide array of differentiated progeny, or the ability to regenerate a tissue may be accepted, even on it is own, to identify a stem cell (Morrison et al., 1997a,b). The proof for stem cell identity relies on the *in vitro* demonstration that different phenotypic cells can be generated from of a single cell and that this multipotentiality is maintained by the cells over time undergoing several subcloning steps.

1.3.1. Stem cells in the developing and adult nervous system

With the closure of the neural tube in the early vertebrate development the neural crest cells start migrating and give rise, among others, to the cells of the peripheral nervous system. At this stage (at embryonic day 8 (E8) in mouse) the lumen of the neural tube is lined with a ventricular layer of primitive neuroepithelial cells. They have a columnar appearance, touching ventricle and pial surface during the cell cycle (Fig. 53).

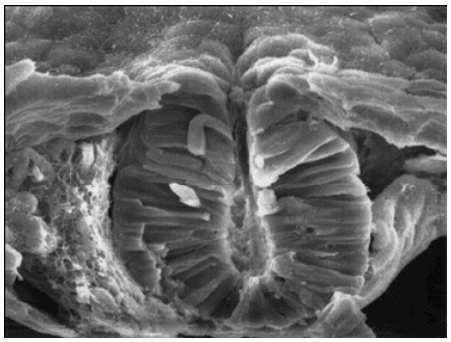

Figure 53: Neural tube.
Electron raster microscopic picture of a mouse neural tube at E8. The transverse section shows the long columnar neuroepithelial cells lining the lumen of the tube.

These cells proliferate and produce most of the cell types of the future central nervous system. The majority of these cells inherits a pluripotent potential with the ability to give rise to neuronal and glial lineages and to regenerate themselves and therefore can be described as neural stem cells (NSCs) (Kalyani et al., 1997). In a first wave of proliferation, during the neurogenic phase from E12 to E20 in rodents, the ventricular layer within the spinal cord produces neuroblasts (future neurons) that migrate peripherally to form an outer mantle zone, the future grey matter of spinal cord and brainstem. The nerve fibres from the neuroblasts form a marginal zone, superficial to the mantle zone, which contains fibre tracts (future white matter of the spinal cord and brainstem). The second wave of proliferation, the gliogenic phase starts around birth and produces glioblasts that migrate peripherally and become astrocytes and oligodendrocytes (Das, 1977). In the cerebral cortex the neuroepithelial cells lining the ventricles form the ventricular zone. Organized migration processes lead to the typically six-layered cortex. Hereby the first postmitotic cells migrating in a radial fashion out of the ventricular zone are forming the later on innermost layers. Later born neurons bypass earlier-generated neurons to form the cortical layers in an inside-out sequence (Brown et al., 1991). Throughout embryonic development radial glia cells continue to contact both ventricle and pia, guiding neuronal migration and also producing cortical neurons and glia (Tamamaki et al., 2001).

At mid-gestation around E13 in mouse, a second layer of proliferating cells appears between the ventricular zone and the adjacent intermediate zone, the subependymal or subventricular zone (Fig. 54).

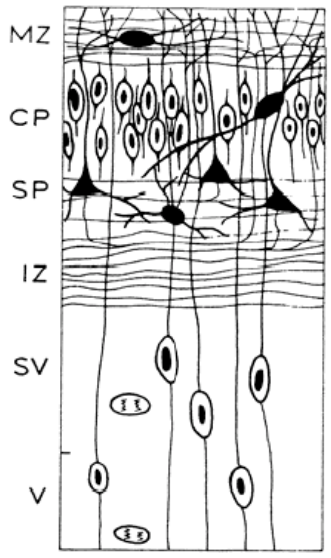

Figure 54: Schematic drawing of the cortical lamination in mouse at E14. MZ: marginal zone; CP: cortical plate; SP: subplate; IZ: intermediate zone; SV: subventricular zone; V: ventricular zone From Uylings et al., 1994.

This germinal zone contains cells, produced in the ventricular zone, which after the neurogenic period ceased, mainly give rise to glia. The subventricular zone expands greatly in late gestation and in early postnatal life. At postnatal ages the radial glia have transformed into astrocytes and the ventricular zone disappears but the subventricular zone remains into adulthood in some areas harbouring stem cells that have the potential to give rise to glia and neurons (Super et al., 1998).

De novo neurogenesis has been shown to occur in two discrete areas of the adult CNS of mammals, namely the subventricular zone and the dentate gyrus of the hippocampus (Altman and Das, 1965; Altman, 1969; Kaplan and Hinds, 1977; Reynolds and Weiss, 1992; Corotto et al., 1993; Lois and Alvarez-Buylla, 1993; Luskin, 1993; Palmer et al., 1995; McKay, 1997; Gage, 2000; van der Kooy and Weiss, 2000; Alvarez-Buylla et al., 2001). The neural precursor cells in the subventricular zone provide a supply of interneurons for the olfactory bulb (Altman, 1969; Corotto et al., 1993; Luskin, 1993; Lois and Alvarez-Buylla, 1994). In the adult hippocampus neural precursor cells are generated in the subgranular zone of the dentate gyrus and differentiate into neuronal and glial cells in the granular layer of the dentate gyrus (Cameron et al., 1993) and the cortex (Kaplan, 1981; Huang and Lim, 1990; Gould et al., 1999). The fact that *in vivo* newly generated neurons could be identified does not mean that the precursor cells were stem cells as evidence for multipotentiality and/or self-renewal capacity for these cells is lacking. Multipotentiality and ability to self-renew could be validated for cells isolated from the striatum, subventricular zone, hippocampus, olfactory bulb and cortex of adult rodents and humans, and the spinal cord of adult mice and rats (Reynolds and Weiss, 1992; Weiss et al., 1996a,b; Gritti et al., 1996, 1999; Johansson et al., 1999a,b; Taupin and Gage, 2002).

1.3.2. Neural stem cells

NSCs are characterized by two cardinal features: they are self-renewing, with the theoretical ability to produce unlimited progeny indistinguishable from themselves; and they are capable to give rise to the three principal cell types of the CNS: neurons, astrocytes and oligodendrocytes (Gage et al., 1995; Weiss et al., 1996b; McKay, 1997). NSC have been isolated from the fetal (Reynolds et al., 1992; Kilpatrick and Bartlett, 1993; Davis and Temple, 1994; Johe et al., 1996; Vescovi et al., 1999; Uchida et al., 2000) and adult (Reynolds and Weiss, 1992; Lois and Alvarez-Buylla, 1993; Gritti et al., 1996; Weiss et al., 1996a,b; Palmer et al., 1997, 1999; Johe et al., 1996; Johansson et al., 1999a,b) mammalian central nervous system. Embryonic stem (ES) cells provide another source of neural stem cells (Tropepe et al., 2001; Ying et al., 2003).

Adult neurogenesis comprises the entire set of events of neuronal development beginning with the division of a precursor cell and ending with the presence and survival of a mature, integrated, functional new neuron. True neuronal integration depends on many complex variables and progressive events. Even in the absence of a completely detailed molecular characterization, neural stem cells of the adult brain clearly possess features that justify considering these cells as extremely promising candidate cells for the aims of CNS cellular repair. They are undifferentiated, often highly mobile cells, relatively resistant to hypoxia and other injury, proliferatively active, and able to produce mature neurons and glia. Their variable specialization and differentiation competence provides great promise for application in medicine.

Neural precursor cells can be propagated in two main forms: in adherent cultures (Conti et al., 2005; Pollard et al., 2006; Glaser et al., 2007) and under floating conditions, in which they aggregate to form heterogeneous ball-like structures, termed “neurospheres” (Reynolds and Weiss, 1992). While it has become standard for some groups to use the so-called “neurosphere-forming” assay as a key criterion to identify a “neural stem cell”, the ability of a cell to form a neurosphere alone is not a sufficiently reliable hallmark of stem cells and does not completely differentiate between various mitotic and precursor cell populations (Seaberg and van der Kooy, 2003). Clonal analysis provides important additional information. By subcloning individual cells, one can test whether an individual cell from these spheres can again give rise to secondary spheres, which upon transfer into differentiation conditions can produce all neural lineages. Although these studies all contribute useful information, one should not forget that cell culture systems are highly artificial in many respects. *In vivo*, precursor cells are not isolated cells, and their relationship to a neurogenic microenvironment

might thus be inseparable from their inherent properties. Survival, proliferation and differentiation of stem cells appear to be regulated by both cell-autonomous and environmental signals (Morrison et al., 1997a,b; Watt and Hogan, 2000). Intrinsic regulators include proteins involved in asymmetric cell division or nuclear factors controlling gene expression. *In vivo*, the external signals that control stem cell fate collectively make up the stem cell 'niche' (Fuchs et al., 2004; Li and Xie, 2005). This niche has powerful effects on their resident stem cells in maintaining a balance of quiescence, self-renewal, and cell fate commitment. Signals generated from the niche include a wide range of secreted factors, cell-cell interactions mediated by integral membrane proteins and the extracellular matrix. Neurosphere cultures are supposed to provide some of these niche signals that may be relevant for neural stem cell maintenance, survival and proliferation.

In addition to maintaining neural precursor cells as neurophere cultures, these cells might also propagated under adherent culture conditions. Initially, adherent NSC was derived from ES cells that were differentiated into heterogeneous neuroepithelial progenitors in adherent monolayer cultures (Ying et al., 2003). Fibroblast growth factor (FGF-2) and epidermal growth factor (EGF) supported expansion of a distinct subset of progenitor cells attached to tissue culture plastic in a defined basal media. These cells lost the heterogeneous morphology and marker expression of the primary neuroepithelial population (Li et al., 1998; Ying et al., 2003). Instead, over several passages, the cultures acquired a homogeneous morphology and were shown to uniformly express nestin and Sox2, but lost expression of Sox1. These cells showed characteristics of stem cells as they were clonogenic and maintained the capacity to generate both neurons and astrocytes over multiple passages. Furthermore, they displayed many hallmarks of radial glia by morphology and molecular markers, including brain lipid binding protein (BLBP), RC2, GLAST, and Pax6 (Götz, 2003; Rakic, 2003). Thus, neural differentiation of ES cells initially entails conversion to a transient Sox1-positive panneural progenitor cell population, containing a subpopulation of cells that mature to a specific Sox1-negative state without differentiation which then can be stably maintained and expanded using EGF and FGF-2. Similar NSC lines were also isolated from fetal brain tissue. Either primary cell cultures or long-term expanded neurospheres allowed to settle onto gelatin-coated flasks and cultured in the presence of EGF and FGF-2 will reproducibly give rise to NSCs that are indistinguishable in all essential features from those derived from ES cells (Conti et al., 2005). Some observations suggest that such cells, rather than being differentiation products of the neurosphere are in fact the resident stem cells of neurospheres. Indeed, NSC will readily form neurospheres if detached from a culture

substrate. The finding that the complexity of neurosphere cultures, which contain a mixture of stem cells, committed progenitors, and differentiated cells (Suslov et al., 2002; Bez et al., 2003), can be eliminated by adherent culture parallels observations with ES cells. In adherent culture, ES cells self-renew with minimal differentiation, whereas suspension culture induces aggregation and differentiation into embryoid bodies (Doetschman et al., 1985).

1.3.3. Neural stem cell therapy

The rise of precursor cell biology has brought new life to neural transplantation and the consideration of cellular replacement strategies to treat diseases of the brain. The idea of "making new neurons" is appealing for neurodegenerative diseases, or selective neuronal loss associated with chronic neurological or psychiatric disorders. One goal of neural precursor biology is to learn from this regionally limited, constitutive neurogenesis how to manipulate neural precursors towards therapeutically useful neuronal or glial population. Elucidation of the relevant molecular control of neurogenesis, morphological maturation of newly generated neural cell types and their functional insertion into the adult brain might result in the development of cell replacements paradigm either by transplantation of cells or by recruitment of endogenous cells.

Some studies reported a surprisingly broad differentiation potential of neural stem cells into cell types of other organs or even other germ layers, but these observations remain a source of debates and controversies (Anderson et al., 2001). In fact, some reports have raised concerns that the broader potential of neural stem cells could derive from phenomenon like cell transformation, transdifferentiation or fusion, all of which can affect the use of neural stem cells for therapy. For example, cell transformation may be associated with aberrant cell growth, and with the risk of tumor formation upon grafting. Thus, neuronal replacement therapies based on manipulation of endogenous precursors may be an attractive aim in the future. However, many questions must be answered before neuronal replacement therapies using endogenous precursors become reality. The multiple signals that are responsible for endogenous precursor division, migration, differentiation, axon extension, circuit integration and survival will need to be elucidated in order for such therapies to be developed efficiently. These challenges also exist for neuronal replacement strategies based upon transplantation of precursors, because donor cells, whatever may be their source, must interact with an extremely complex and intricate mature CNS environment in order to functionally integrate into the brain.

Altogether, NSCs might be considered as candidate cells to develop cell-based therapies for neurological disorders. While ES can be efficiently expanded *in vitro* and are capable to give rise to all cell types of the body, these cells might form tumors upon transplantation. A mulitpotent cell type for the development of cell based therapies is NSC that is considered not to form tumours (Winkler et al., 1998; Englund et al., 2002). Futhermore, the use of human ES cells is limited because of ethical concerns. Similarly, the use of fetal-derived primary cells for cell-based therapies is associated with ethical and also logistic problems. Efficient cell replacement strategies require widespread integration, long-term survival and differentiation of grafted cells and, in particular, cell types that are capable to functionally integrate into the host tissue. Manipulation of NSCs prior to transplantation might be one strategy to achieve this aims. Indeed, several studies have demonstrated that neural stem/precursor cells might be "optimized" for cell based therapies by genetic manipulations. For instance, overexpression of PSA in neural precursor cells has been demonstrated to play an instructive role on the choice of a cells migration pathway depending on the environment (Franceschini et al., 2004). Furthermore, forced expression of the transcription factor Nurr1 has been shown to direct the differentiation of NSCs into dopaminergic neurons (Andersson et al., 2007; Li et al., 2007; Shim et al., 2007). Another example is the directed differentitation of neural precursor cells into actively myelinating oligodendrocytes by overexpression of the transcription factor olig2 (Copray et al., 2006).

Neural precursor cells derived from L1-transfected embryonic stem cells showed decreased cell proliferation *in vitro*, enhanced neuronal differentiation *in vitro* and *in vivo*, and decreased astrocytic differentiation *in vivo* without influencing cell death. L1 overexpression also resulted in an increased yield of GABAergic neurons and enhanced migration of embryonic stem cell-derived neural precursor cells into the excitotoxicly lesioned striatum. Mice grafted with L1-transfected cells showed recovery in rotation behavior 1 and 4 weeks, but not 8 weeks, after transplantation compared with mice that had received nontransfected cells, thus demonstrating for the first time that neural precursor cells with a transgenic expression of a recognition molecule are capable to improve functional recovery during the initial phase in a syngeneic transplantation paradigm (Bernreuther et al., 2006).

In another study, precursor cells derived from L1-transfected embryonic stem cells and injected into the lesion site after spinal cord injury migrated rostrally and caudally from the lesion. Anterogradely labeled corticospinal tract axons showed interdigitation with L1-positive donor cells and extended into the lesion site 1 month after transplantation and, in some cases, extended beyond the lesion site (Chen et al., 2005).

The fate and behaviour of stem cells evidently depends on environmental cues and cell intrinsic properties that probably interact with each other. Which are the environmental factors that influence the migration and differentiation of endogenous and transplanted stem cells and which mechanisms are employed? Understanding which cellular characteristics make a NSC and which events guide them to different neural cell fates could also open up strategies in the therapeutic use of stem cells which is engaging the endogenous pool of NSCs in the CNS. The aim of the study was reveal L1 role in controlling or influencing NSC fate decisions and behaviour following transplantation into a diseased adult brain region.

2. Rationale and aims of the study

NSCs are among the candidate cell type to develop cell-based therapies for a variety of neurological disorders. Strategies dependent on efficient cell replacement, widespread integration, long-term survival and directed differentiation of grafted cells into particular neutal cell types. During the development of the nervous system, L1 has ben implicated in migration of postmitotic neurons, outgrowth, pathfinding and fasciculation of axons, growth cone morphology and myelination. In addition, L1 has been implicated in axonal regeneration, neuronal cell survival, and proliferation and fate decision of neuronal precursor.

The aim of the present study was to generate stably L1-transfected neural precursor population, and to analyze the impact of ectopic L1 expression on the functional properties of these cells *in vitro* and after transplantation *in vivo*. The specific aim included:

1. To generate stably L1-transfected neural precursor population.
2. To analyze the effect of ectopic L1 expression on fate decision of NSCs *in vivo*.
3. To study the migrating capacity, fate decision and the survival of L1-positive NSCs after transplantation into a mouse model for Huntingtons disease.

3. Materials and methods

3.1. Materials

3.1.1. Reagents, disposables, etc.

All chemicals were purchased in pro analysis quality from the following manufacturers/vendors: Amersham Pharmacia Biotech (APB, Freiburg, Germany), Bio-Rad (Munich, Germany), GibcoBRL (Life Technologies, Karlsruhe, Germany), Life Technologies (Karlsruhe, Germany), Macherey-Nagel (Dueren, Germany), Merck (Darmstadt, Germany), Roche (Mannheim, Germany), Carl Roth (Karlsruhe, Germany), Serva (Heidelberg, Germany), and Sigma-Aldrich (Deisenhofen, Germany).

Cell culture material was supplied from Nunc (Roskilde, DK), Life Technologies, Invitrogen and Euroclone S.p.A. (Pero (MI), Italy).

Plasmids and molecular cloning reagents were obtained from Ambion, Ltd. (Cambridge, UK), APB, BD Biosciences, Clontech (Heidelberg, Germany), Invitrogen (Karlsruhe, Germany), Pharmacia Biotech, Promega (Mannheim, Germany), Qiagen (Hilden, Germany), and Stratagene (Amsterdam, NL).

DNA purification systems were purchased from APB, Life Technologies, Pharmacia Biotech (Freiburg, Germany), Macherey & Nagel and Qiagen (Hilden, Germany).

Nucleic acid molecular weight markers were purchased from Roche and NEB (Frankfurt a.M., Germany).

Restriction enzymes were obtained from New England biolabs (Frankfurt am Main, Germany), MBI Fermentas (St. Leon-Rot, Germany), and AGS (Heidelberg, Germany).

Molecular weight standards were obtained from GibcoBRL.

Oligonucleotides were ordered from metabion (Munich, Germany) or MWG biotech AG (Ebersberg, Germany).

CELLection™ Biotin Binder Kit which contain CELLection™ Dynabeads® and a Releasing Buffer were purchased form DYNAL® A.S, Oslo, Norway.

Roti-Fect transfection reagent was purchased from Roth (Karlsruhe, Germany).

Mouse NSC (Neural Stem Cell) Nucleofector Kit was obtained from AMAXA biosystems (Cologne, Germany).

Lipofectamin 2000 reagent was purchased by GibcoBRL (Life Technologies, Karlsruhe, Germany).

3.1.2. Enzymes and reaction kits

DNA polymerases		
Taq DNA Polymerase	Life Technologies	Karlsruhe, Germany
Advantage™ -GC 2	BD Biosciences Clontech	Heidelberg, Germany
HotStarTaq™	Qiagen	Hilden, Germany
Klenow enzyme	Roche	Mannheim, Germany
Restriction endonucleases		
various	AGS	Heidelberg, Germany
various	MBI Fermentas	St. Leon-Rot, Germany
various	NEB	Frankfurt a. M., Germany

3.1.3. Instruments

Particular devices are referenced throughout the respective protocols.

Centrifuges		
Sorvall	Kendro, Hanau, Germany	RC50plus with SLA3000, SLA1500, SA600 and HB-6 rotors
Eppendorf	Hamburg, Germany	Microcentrifuge 5415D, Bench-top centrifuges 5417R and 5403
Jouan, Inc.	Winchester, VA, USA	Bench-top centrifuge CR422
Miscellaneous		
Leica	Bensheim, Germany	Vibratome VT1000S, Cryostat CM3050
Zeiss	Goettingen, Germany	Axiophot, Confocal Laser Scanning Microscope (LSM 510)
DYNAL® A.S	Oslo, Norway	Dynal MPC
Power supplies		
Bio-Rad	Munich, Germany	Power-Pac series
Spectrophotometer, etc.		
APB	Freiburg, Germany	Ultrospec 3000/DPV-411 printer
Merlin	Bornheim-Hesel, Germany	MIKRONAUT Skan
Thermal cyclers		
Eppendorf	Hamburg, Germany	Mastercycler gradient
MJ Research, Inc.	Waltham, MA, USA	USA PTC-200 DNA ENGINE™ *calssic*

3.1.4. Software

Adobe	San Jose, CA, USA	Photoshop CS
DNASTAR, Inc.	Madison, WI, USA	Lasergene suite 4.05
ISI Researchsoft	Berkeley, CA, USA	Reference Manager 9.5

Sci&Ed Software	Durham, NC, USA	Clonemanage

3.1.5. Oligonucleotides

Oligonucleotides/primers were purchased from MWG biotech AG (Ebersberg, Germany) or Metabion (Planegg-Martinsried, Germany).

3.1.6. Antibodies

3.1.6.1. Primary antibodies

anti-L1	polyclonal antibody raised against the extracellular domain of mouse L1-Fact (produced in the lab of M. Schachner) Imunositochemistry 1:1000
mc-αL1-555	monoclonal rat anti-mouse L1 antibody clone 555. Supernatant of rat hybridoma cell line (produced in the lab of M. Schachner; Appel et al., 1993). Imunositochemistry 1:10 Western Blots 1:10000
mc-αL1-557	monoclonal rat anti-mouse L1 antibody clone 557. Supernatant of rat hybridoma cell line (produced in the lab of M. Schachner). Imunositochemistry 1:5
mc-αL1-324	monoclonal rat anti-mouse L1 antibody clone 324. Supernatant of rat hybridoma cell line (produced in the lab of M. Schachner) Imunositochemistry 1:5

3.1.6.2. Secondary antibodies

For immunocytochemistry, Cy2, Cy3 and Cy5-labeled secondary antibodies were obtained from Dianova (Hamburg, Germany) and used in a dilution of 1:200.

All horseradish-coupled secondary antibodies were purchased from Dianova (Hamburg, Germany) and used in a dilution of 1:10000.

3.1.7. Bacterial strains and eukaryotic cell lines

Bacterial strains	
E. coli DH5α	Invitrogen
Cell lines	
Hybridoma cells L1 AB producing cell line	Hybrydoma cells, producing monoclonal rat anti-mouse L1 antibody 555.

3.1.8. Bacterial media

Luria broth (LB-medium, per liter)	10 g NaCl 10 g tryptone/peptone 5 g yeast extract → pH 7.0 with 5N NaOH (optional) and autoclaved
LB agar (per liter)	10 g NaCl 10 g tryptone or peptone 5 g yeast extract 20 g agar → pH 7.0 with 5N NaOH (optional)
LB-MM broth (per liter)	10 g NaCl 10 g tryptone/peptone 5 g yeast extract 10mM MgSO4 2 g/l maltose → pH 7.0 with 5N NaOH (optional)
LB-MM agar	→ prepare LB agar, autoclave, cool to 50^{o}C , and add the following components 10mM MgSO4 2 g/l maltose

The following antibiotics were added when needed (1000-fold stock solutions : 100 mg/l ampicillin (LB-amp), 25 mg/l tetracycline (LB-tet), 25 mg/l kanamycin (LB-kan) and 25 mg/ml chloramphenicol (LB-cm).

3.1.9. Plasmids

pcDNA3	Mammalian expression vector. Ampicillin-resistance (Invitrogen).
pcDNA3-L1WT	Mammalian expression vector encoding murine L1. Ampicilin-resistance.
pEGFP-N1	Mammalian expression vector encoding the enhanced green fluorescent protein. Kanamycin-resistance (Clontech).

3.1.10. Buffers and stock solutions

Buffers and solutions are listed below. All more method-specific solutions are specified in the accompanying sections.

Antibody buffer	0.3 % (w/v)	BSA in PBS pH 7,4
(Immunocytochemistry)	0.02 % (w/v)	Triton X-100

Blocking buffer (Immunocytochemistry)	3 % (w/v) 0. 2 % (w/v)	BSA in PBS pH 7,4 Triton X-100
Blocking buffer (Western Blot)	1-4 % (w/v) 1 % (v/v)	instant milk powder in TBS block solution (boehringer) in TBS
Blocking buffer (Western Blot)	25 mM 192 mM	Tris Glycin
DNA elution buffer (DNA-preparation)	1mM	Tris-HCl (pH 8.0)
DNA-sample buffer (5x) (DNA-gels)	20 % (w/v) 0,025 % (w/v)	glycerol in TAE buffer orange G
dNTP-stock solution (PCR)	5mM	dATP
Ethidiumbromide staining solution (DNA-gels)	10 µg/ml	ethidiumbromide in 1xTAE
PCR (PCR)	5mM 5mM 5mM	dTTP dGTP dCTP or stock solution with 25 mM of each dNTP
EDTA stock solution	0.5 M	EDTA → pH 8.0
Phosphate-buffered saline (PBS, 10x, Biochemistry)	1.5 M 81mM 17.39mM	NaCl Na_2HPO_4 NaH_2PO_4 →pH 7.5
Phosphate-buffered saline (PBS, 10x, Morphology)	27mM 18mM	KCl KH_2PO_4 → pH 7
Citrate buffer (SSC, 20x) (DNA-preparation)	0.3 M	tri-sodium citrate → pH 7.0
Tris-acetate buffer (TAE; 50x)	2 M 50mM 1 M	Tris EDTA acetic acid (glacial: 17.4 M)
TE	10mM 1mM	Tris-HCl (pH 8.0) EDTA
Tris-buffered saline (TBS)	10mM 150mM	Tris-HCl (pH 7.4) NaCl

Running Gel 10% (8%)	3.92 ml (4.89 ml)	deionized water
(protein gels)	5.26 ml (5.26 ml)	1 M Tris pH 8.8
	0.14 ml (0.14 ml)	10% SDS
	4.70 ml (3.73 ml)	30% Acrylamide – Bis 29:1
	70.0 µl (70 µl)	10% APS
	7.00 µl (7 µl)	TEMED
Sample buffer (5x)	0.312 M	Tris-HCl pH 6.8
(protein-gels)	10 % (w/v)	SDS
	5 % (w/v)	β-Mercaptoethanol
	50 % (v/v)	Glycerol
	0.13 % (w/v)	Bromphenol blue
SDS running buffer (10x)	0.25 M	Tris-HCl, pH 8.3
(protein-gels)	1.92 M	Glycine
	1 M	SDS
Stacking Gel 5%	3.77 ml	deionized water
(protein gels)	0.32 ml	1 M Tris pH 6.8
	0.05 ml	10% SDS
	0.83 ml	30% Acrylamide – Bis 29:1
	25.0 µl	10% APS
	7.00 µl	TEMED
Staining solution	40 % (v/v)	Ethanol
(Protein-gels)	10 % (v/v)	acetic acid
	0,1 % (w/v)	Serva Blue R250
Stripping buffer	0.5 M	NaCl
(Western blots)	0.5 M	acetic acid

3.1.11. Cell culture media

DMEM F-12

Medium composed of a 1:1 mixture of Dulbecco's Modified Eagle's Medium and F-12 (Gibco, New York, USA) supplemented with glucose (0.3 %), sodium bicarbonate (3 mM), B27 (2%; Gibco, New York, USA), glutamine (2 mM), HEPES buffer (0,5 M), penicillin (1%), epidermal growth factor (EGF; 10 ng/ml; TEBU, Offenbach, Germany) and fibroblast growth factor-2 (FGF-2; 10 ng/ml; TEBU).

Euromed-N

Medium Euromed-N (Euroclone S.p.A. Pero (MI), Italy) supplemented with B27 (2%; Gibco, New York, USA), N2 (2%, self-made mixture) glutamine (2 mM), penicillin (1%), epidermal growth factor (EGF; 10 ng/ml; TEBU, Offenbach, Germany) and fibroblast growth factor-2 (FGF-2; 10 ng/ml; TEBU).

Cell culture medium for hydridoma cells

RPMI 1640 (Gibco/Invitrogen, New York, USA) supplemented with L-Glutamin (1-2%), Penicillin/Streptomycin (2%) and FCS (10%).

Production media for antibody production with hydridoma cells

Serum free hybridoma medium (Gibco/Invitrogen, New York, USA) supplemented with L-Glutamin (2-5%), Penicillin/Streptomycin (2%).

3.1.12. Animals

NSCs were isolated from spinal cords of 14-day-old mouse embryos. Transgenic mice ubiquitously expressing EGFP under control of a chicken β-actin promoter (Okabe et al., 1997) were used as donors. EGFP-transgenic mice were maintained on a C57BL/6J genetic background and their genotype was determined by analysing tail biopsies for the presence of EGFP-fluorescence.

As hosts for transplantation experiments C57BL/6J mice were used.

3.2. Methods

3.2.1. Molecular biological methods

If not indicated otherwise, standard molecular biological techniques were carried out as described by Sambrook (Sambrook et al., 1989).

3.2.1.1. Production of competent bacteria

E. coli DH5α bacteria (Invitrogen) were grown on LB-agar dishes overnight at 37°C. 50 ml of LB-medium was inoculated with 5 colonies and grown at 37°C under constant shaking (>200 rpm) until the culture reached an optical density (OD_{600}) of 0.35-0.45. Growth of bacteria was stopped by incubation on ice for 4 min. Bacteria were pelleted at 1000 x g for 15 min at 4°C and – after aspiration of the supernatant – resuspended in 17 ml pre-chilled buffer RF 1 (4°C). Following 15 min incubation on ice, the centrifugation was repeated. The cell pellet was resuspended in 4 ml pre-chilled RF 2 (4°C) and incubated again for 15 min on ice. 100 µl aliquots were frozen in liquid nitrogen and stored at -80°C. Transformation efficiency of cells was determined by transformation with a distinct quantity (pg-ng) of purified supercoiled plasmid DNA.

RF 1: 100 mM RbCl **RF 2:** 10 mM MOPS (pH 6.8)
50 mM $MnCl_2$ 10 mM RbCl
30 mM KOAc 75 mM $CaCl_2$
10 mM $CaCl_2$ 150 g/l glycerol
→ pH 5.8 (with 0.2 M acetic acid)

3.2.1.2. Transformation of DNA into bacteria

10 ng of plasmid DNA were added to 100 µl of competent DH5α bacteria and incubated for 20 min on ice. A heat-shock was performed at 42°C for 2 min followed by incubation on ice for 2 min. 900 µl of LB-medium were added and bacteria were kept at 37°C for 20 minutes under constant agitation. Then cells were centrifuged (10 000 x g, 1 min, RT), resuspended in 100 µl LB-medium after removal of the supernatant, plated on selective agar plates, and incubated at 37°C for 12-16 h.

3.2.1.3. Maintenance of bacterial strains

Selected bacterial strains transformed with plasmids of interest were stored as glycerol stocks (LB-medium, 25 % (v/v) glycerol) at -80°C for up to one year or at -20°C for up to 2 months. Bacteria grown on agar plates containing antibiotics were stored up to 6 weeks at 4°C.

3.2.1.4. Small scale plasmid isolation (Miniprep)

In order to purify 10-20 µg of plasmid DNA for further restriction analysis and sequencing reactions, minipreps were carried out. 4 ml LB-amp-medium (with appropriate selection antibiotic) were inoculated with a bacteria colony and incubated over night at 37°C with constant agitation. Cultures were transferred into 2 ml Eppendorf tubes and cells were pelleted by centrifugation (12 000 rpm, 1 min, RT). The procedure was repeated for amounts of more than 2 ml. Plasmids were isolated from the bacteria using the Quagen Miniprep kit system, according to the manufacturer's protocol. The DNA was eluted from the columns by addition of 50 µl Tris-HCl (10 mM, pH 8.0) with subsequent centrifugation (12 000 rpm, 2 min, RT). Plasmid DNA was stored at -20°C.

3.2.1.5. Large scale plasmid isolation (Maxiprep)

For preparation of large quantities of DNA, the Qiagen Maxiprep kit was used. 300 ml LB-amp-medium (with appropriate selection antibiotic) was inoculated with 5 µl bacteria

suspension of the glycerol stocks. This culture was incubated at 37°C with constant agitation overnight. The cells were pelleted in a Sorvall centrifuge (6 000 g, 15 min, 4°C) and the DNA was isolated as according to the manufacturer's protocol. The DNA pellet was resuspended in 100 µl of pre-warmed (70°C) Tris (10 mM, pH 8.0) followed by determination of the DNA concentration.

3.2.1.6. Determination of DNA concentration and purity

DNA molecules absorb UV light of a wavelength of 260 nm (A260), whereas proteins show strongest absorbtion at 280 nm (A280). The absorption of 1 OD (A) is equivalent to approximately 50 g/ml dsDNA. Additionally interference by protein contamination can be estimated by the ratio of A260/A280. Pure DNA has a ratio of 1.8. Absorption at 320 nm reflects contamination of the sample by substances such as carbohydrates, peptides, phenols or aromatic compounds. In pure samples, the ratio A260/A320 is approximately 2.2. Concentration and purity was determined spectrometrically using an Amersham-Pharmacia spectrometer.

3.2.1.7. Endonuclease restriction analysis

Endonuclease restriction enzymes were used to digest and analyze the sequence of plasmids or DNA fragments as well for preparation of DNA for transfection. Digestions were performed by incubating dsDNA molecules with an appropriate amount of restriction enzyme, the respective buffer as recommended by the supplier (New England Biolabs), and at the optimal temperature for the specific enzyme, usually at 37°C. In general, reaction volume was 20 µl. For preparative restriction digestions for transfection the reaction volume was 400 µl. Digestions were composed of DNA, 1 x restriction buffer, the appropriate amount of the respective restriction enzyme (due to glycerol content the volume of the enzyme stock solution added should not exceed 1/10 of the reaction volume) and reaction volume was adjusted with nuclease-free H_2O. After incubation at the optimal temperature for 2-3 h, digestion was terminated by addition of sample buffer and DNA was analyzed by agarose gel electrophoresis.

3.2.1.8. DNA agarose gel electrophoresis

To analyze restriction digestions and the quality of nucleic acid preparations horizontal agarose gel electrophoresis was performed. Gels were prepared by heating 0.8-1 % (w/v) agarose (Gibco) in Tris-acetate buffer (TAE), depending on the size of fragments to be

separated. DNA samples were adjusted to 1 x DNA sample buffer and were subjected to electrophoresis at 10 V/cm in BIO-Rad gel chambers in 1 x TAE running buffer. Afterwards, gels were stained in 0.5 µg/ml ethidium bromide in 1 x TAE solution for approximately 20 min up to tree hours for preparative restriction. Thermo-photographs of transilluminated gels were taken, or bands were made visible on an UV-screen (λ = 360 nm).

3.2.1.9. DNA fragment extraction from agarose gels

For isolation and purification of DNA fragments from agarose gels, ethidium bromide stained gels were transilluminated with UV-light and the appropriate DNA band was excised from the gel with a clean scalpel and transferred into an Eppendorf tube. The fragment was isolated using the silica matrix-based QIAquick Gel Extraction kit (Qiagen) following the manufacturer's instructions. The fragment was eluted from the column by addition of 50 µl pre-warmed (70°C) Tris-HCl (10 mM, pH 8.0) and the DNA concentration was determined.

3.2.1.10. Precipitation of DNA

The salt concentration of an aqueous DNA solution was adjusted by adding 1/10 volume of sodium acetate, pH 5.2, or 0.15 volume of 10M ammonium acetate. 2.5 volumes of cold ethanol, -20 °C, were added and the samples were mixed thoroughly. 5 - 10 µg tRNA was added to increase recovery from dilute solutions. Following incubation on ice for 30 min, samples were centrifuged for 10 - 15 min (16,000xg, RT). Supernatants were carefully aspirated and 1 ml cold 75% (v/v) ethanol, -20 °C, was added to each sample. Tubes were inverted several times and centrifuged for 5 min (16,000xg, RT). For optimal purity, the pellet was loosened from the tube during inverting and was resuspended in ethanol. After removal of the supernatant, a 1 - 2 s centrifugation was performed and residual ethanol was aspirated. Supernatants were removed and DNA pellets were air dried (approximately 5 min at RT). DNA was resuspended in an appropriate volume of prewarmed nuclease-free water (70 °C).

3.2.1.11. Sequencing of DNA

Sequence determination of dsDNA was performed by the sequencing facility of the ZMNH (Dr. W. Kullmann, M. Daeumigen). Fluorescent-dye labeled chain-termination products (ABI Prism Dye Terminator Cycle Sequencing Ready Reaction Kit, Perkin Elmer, Wellesly, MA, USA) were analyzed with an ABI Prism 377 DNA Sequencer (Perkin Elmer). For preparation, 0.8-1 µg of DNA was diluted in 7 µl ddH_20 and 1 µl of the appropriate sequencing primer (10 pM) was added.

3.2.2. Protein-biochemical methods

3.2.2.1 SDS-polyacrylamide gel electrophoresis

Separation of proteins was performed by means of the discontinuous SDS-polyacrylamide gel electrophoresis (SDS-PAGE) using the Mini-Protean III system (BioRad). The size of the running and stacking gel were as follows:

Running gel:	height 4.5 cm, thickness 1 mm
	8 % or 10 % (v/v) acrylamide solution
Stacking gel:	height 0.8 cm, thickness 1 mm
	5% (v/v) acrylamide solution 15-well combs

After complete polymerization of the gel, the chamber was assembled as described by the manufactures protocol. Up to 25 µl sample were loaded in the pockets and the gel was run at constant 80 V for 10 min and then at 140V for the remainder. The gel run was stopped when the bromphenolblue line had reached the end of the gel. Gels were then either stained or subjected to Western blotting (Laemmli, 1970).

3.2.2.1.1 Coomassie-staining of polyacrylamide gels

After SDS-PAGE, the gels were stained in staining solution (1h, RT) with constant agitation. The gels were then incubated in destaining solution until the background of the gel appeared nearly transparent (Ausrubel, 1996).

3.2.2.2 Western Blot-analysis

3.2.2.2.1 Electrophoretic transfer

Proteins were transferred from the SDS-gel on a Nitrocellulose membrane (Protran Nitrocellulose BA 85, 0.45 µm, Schleicher & Schüll) using a MINI TRANSBLOT-apparatus (BioRad, Munich, Germany). After equilibration of the SDS-gel in blot buffer for 5 min, the blotting sandwich was assembled as described in the manufactures protocol. Proteins were transferred electrophoretically at 4°C in blot buffer at constant voltage (80 V for 180 min or 35 V overnight). The prestained marker BenchMark (Gibco BRL; Invitrogen, Karlsruhe, Germany) was used as a molecular weight marker and to monitor electrophoretic transfer (Towbin et al., 1979).

3.2.2.2.2 Immunological detection of proteins on nitrocellulose membranes

After electrophoretic transfer, the membranes were removed from the sandwiches and placed protein-binding side up in glass vessels. Membranes were washed once in TBS and incubated in 8 ml blocking buffer (3% skim milk powder in TBS) for 1 h at room

temperature. Afterwards, the primary antibody was added in the appropriate dilution either for 2 h at RT or overnight at 4°C. The primary antibody was removed by washing the membrane 5 x 5 min with TBST. The appropriate secondary antibody was applied for 2 h at RT. The membrane was washed again 5 x 5 min with TBST and immunoreactive bands were visualized using the enhanced chemiluminescence detection system (Ausrubel, 1996).

3.2.2.2.3 Immunological detection using enhanced chemiluminescence

The antibody bound to the membrane was detected using the enhanced chemiluminescence detection system (Pierce, Bonn, Germany). The membrane was soaked for 1 min in detection solution (1:1 mixture of solutions I and II). The solution was removed and the blot was placed between two saran warp foils. The membrane was exposed to a light sensitive film (Biomax-MR, Kodak) for several time periods, starting with a 2 min exposure.

3.2.2.3. Antibody biotinylation

L1555 monoclonal antibody was dialyzed against carbonate buffer and the antibody concentration was adjusted to 1mg/ml. A solution of 1 mg/ml NHS-Biotin (N-Hydroxysuccinimidobiotin, Sigma, Deisenhofen, Germany) in DMSO was added to the dialyzed antibody solution with a ratio of 1:8 and incubated overnight at 4^{o}C. Samples were afterwards dialyzed against PBS to remove free Biotin.

3.2.2.4. Determination of protein concentration (BCA)

The protein concentration was determined using the BCA kit (Pierce). Solution A and B were mixed in a ratio of 1:50 to give the BCA solution. 10 µl of the sample were mixed with 200 µl BCA solution in 96-well microtiter plates and incubated for 30 min at 37°C. A BCA standard curve was co-incubated ranging from 0.1 mg/ml to 2 mg/ml. The extinction of the samples was determined at 560 nm in a microtiter plate reader (µQuant, BioTek Instruments GmbH, Bad Friedrichshall, Germany).

3.2.2.5. Enzyme-linked immunosorbent assay (ELISA), binding assay

Several antigens (concentrations 5-10 µg/ml) were immobilized on polystyrol Immuno MaxiSorb® 96-well plates (MaxiSorb F96, Nunc, Wiesbaden, Germany) for overnight at 4^{o}C. To remove non-absorbed proteins the wells were washed five times for 5 min with TBS-T and then free binding places on the wells were blocked with 2% BSA in TBS for one hour at RT. After washing, the wells were subsequently incubated with putative binding proteins diluted

in a wide range (from 70 ng/ml to 20 µg/ml) in TBS-T containing 1% BSA, 1mM $CaCl_2$, 1mM $MgCl_2$ and 1mM $MnCl_2$ for a further hour at RT. The wells were then washed again five times for 5 min at RT to remove unspecifically bound proteins. Specifically bound proteins were detected with streptavidin coupled to horseradish peroxidase (in case of biotinylated binding partners) or with specific primary antibodies and the appropriate HRP-linked secondary antibodies. Protein binding was visualized after reaction of HRP with ABTS reagent that resulted into a colored product that was quantified at 405 nm using an ELISA reader (µQuant).

3.2.3. Cell culture

3.2.3.1. Hybridoma cell culture

Hybridoma cells were thawed and cultured in RPMI media supplemented with L-Glutamin (1-2%), Penicillin/Streptomycin (2%) and FCS (10% fetal calf serum) in 25 cm^2 culture flasks or 6-well plates. Cells were passaged at confluence. Cells were centrifuged (1000xg, 5 min, RT) and the pellet was resuspended in fresh medium. Cells were split 1:2-1:5 and placed in production serum free hybridoma medium (Gibco/Invitrogen, New York, USA) supplemented with L-Glutamin (2-5%), Penicillin/Streptomycin (2%) in 75 cm^2 or 150 cm^2 culture flasks. Cells were passaged when necessary (usually every 3-4 days).

Production media were collected and stored in -20 ^oC before antibody purification.

3.2.3.2. Prepation of neural stem cell culture

Pregnant mice were sacrificed; embryos were removed and placed in sterile PBS. Genotypes of embryos were determined by analysing the tails biopsies under the microscope for the presence of EGFP. Brains of embryos were taken out and striata were removed and placed into a defined medium composed of a 1:1 mixture of Dulbecco's Modified Eagle's Medium and F-12 supplemented with penicillin (2 mM), glucose (0.6 %), sodium bicarbonate (3 mM), B27 (2%; Gibco, New York, USA), glutamine (2 mM), HEPES buffer (5 mM), epidermal growth factor (EGF; 20 ng/ml; TEBU, Offenbach, Germany) and fibroblast growth factor-2 (FGF-2; 20 ng/ml; TEBU) . The tissue was mechanically dissociated and cells were plated in uncoated tissue culture flasks at a density of 200,000 cells/ml. Neural stem cells of two types were used in experiments: GFP-NSCs from transgenic GFP-transgenic embryos and WT-NSCs. Cultures were passaged when necessary, approximately every three to five days.

3.2.3.3. Cultivation of neural stem cells.

NSCs were cultivated either as free-floating neurospheres or as adherent cells.

For free-floating neurosphere cultivation cells were plated in uncoated tissue culture flask at a density of 100,000 cells/ml into defined medium composed of a 1:1 mixture of Dulbecco's Modified Eagle's Medium F-12 supplemented with glucose (0.6 %), sodium bicarbonate (3 mM), B27 (2%; Gibco, New York, USA), glutamine (2 mM), HEPES buffer (5 mM), epidermal growth factor (EGF; 20 ng/ml; TEBU, Offenbach, Germany) and fibroblast growth factor-2 (FGF-2; 20 ng/ml; TEBU).

For adherent neural stem cells culture, cells were plated in Matrigel-coated flasks (0,1-1%) precoated with PLL(1%) at a density 50,000 cells/ml and in Euro Med-N media supplemented with B27 (2%; Gibco, New York, USA), N2 (self made mixture), glutamine (2 mM), penicillin (2mM), epidermal growth factor (EGF; 20 ng/ml; TEBU, Offenbach, Germany) and fibroblast growth factor-2 (FGF-2; 20 ng/ml; TEBU). Cells were passaged at confluence and plated at a density of 50,000 cells/ml.

As optional in some cases before transfection cells have been cultivated as free-floating neurospheres before transfection and as adherent cell culture after transfection.

3.2.4. Selection of stably transfected cells.

In order to obtain populations of cells that homogeneously express L1 molecule several methods for selection of L1-transfected cells were attempted.

3.2.4.1. Dynabeads selection

Single cells suspension (2 x 10^6) target cells/ml in sterile PBS with 0,1% BSA were used for selection according to manufacturer protocol. In brief, 2 x 10^6 cells were mixed with 1 x 10^7 Dynabeads precoated with L1555 biotinylated antibodies (ratio of cells:Dynabeads 1:5). Following incubation for 15 minutes at 4^oC tubes, mixture was rotated, placed in Dynal MPC and left for separation of cells connected with Dynabeads for 1 minute. Supernatant was discarded and Dynabeads were released with Releasing Buffer for 15 minutes at RT and placed in Dynal MPC for 1 minute. Supernatants with isolated cells were removed and resuspended in culture media.

3.2.4.2. Antibiotic selection

For selection of stably transfected NSCs with antibiotic, geneticin was added to the medium two days after manipulation (Gibco, New York, USA). Selection was started with a concentration of 100 µg/ml, geneticin concentration was increased to 200 µg/ml after two days, in two days up to 300 µg/ml and then up to 400 µg/ml. Positively selected cells were than further cultured in presence of geneticin in concentration of 400 µg/ml.

3.2.5. Immunocytochemistry

3.2.5.1. Immunocytochemistry of live cells

On the day before immnunostaining cells were placed on 12 mm coverslips pre-covered with PLL and covered with Marigel. Plates with coverslips were placed on ice and coverslips were incubated with blocking solutions (PBS 5 % FCS) for 15 minutes. 400 µl of mc-αL1-555 or 557 or 324 or polyclonal anti-L1 antibodies were added on the coverslips and incubated at 4°C for 20 min. Coverslips were washed once with PBS. Subsequently coverslips were covered with 400 µl PBS containing the appropriate secondary antibody for 15 min in the dark. Finally, coverslips were washed three times with PBS, fixed with 4 % PFA in PBS for 20 minutes, washed with PBS and mounted on slides using Fluromount G (Southern Biotechnology Associates, Biozol, Eching, Germany). Nuclear staining was done after fixation. In this case DAPI or biz-benzimide dilution of 1:2000 were applied on coverslips and incubated for 5-10 minutes. Then coverslips were washed tree times with PBS, and mounted.

3.2.5.2. Immunocytochemistry of fixed cells

On the day before immnunostaining cells were placed on 12 mm coverslips precovered with PLL and covered with Marigel. Cells were fixed with 1 ml of 4 % PFA in PBS for 15-30 min and washed twice with PBS. Coverslips were incubated with 300 µl 0,1 % BSA in PBS for 1 h at RT. The blocking buffer was removed and coverslips were covered with 300 µl of primary antibodies for 2-3 h at RT. Coverslips were washed three times with PBS and incubated with 300 µl secondary antibody for 1 h at room temperature in the dark. Finally, cells were washed three times with PBS and mounted on slides using Fluromount G (Southern Biotechnology Associates, Biozol, Eching, Germany).

3.2.5.3. Immunocytochemistry of brain sections

Cryostat sections, stored at -20°C, were air-dried for 30 minutes at 37°C. A 10mM sodium citrate solution (pH 9.0, adjusted with 0.1M NaOH) was freshly prepared and sections were immersed for antigen de-masking in the solution preheated in a water bath to 80°C for 30 minutes. Afterwards, the jar was taken out of the water bath and left to cool down at room temperature. Sections were briefly rinsed with PBS to prevent contamination of jar with blocking buffer. Then blocking of unspecific binding sites was performed. The sections were incubated at room temperature for two hours in PBS containing 0.2% v/v Triton X-100 (Fluka, Buchs, Germany), 0.02 w/v sodium azide (Merck, Darmstadt, Germany) and 5% v/v normal donkey serum (NDS) or normal goat serum(NGS) (Jackson Immuno Research Laboratories, Dianova, Hamburg, Germany). After one hour the blocking solution was aspired and the slides were incubated with the primary antibody diluted in PBS containing 0.5% w/v lamda-carrageenan and 0.02% w/v sodium azide. The slides were incubated for 1-3 days at 4°C in a well closed staining jar. Subsequently, the sections were washed 3 times in PBS (15 minutes each) before secondary antibody was applied. Incubation with secondary antibodies was performed in PBS containing 0.5% lambda-carrageenan and 0.2% sodium azide at RT for 2 hours. After a subsequent wash in PBS, cell nuclei were stained for 10 minutes at room temperature with bis-benzimide solution (Hoechst 33258 dye, 5 µg/ml in PBS, Sigma, Deisenhofen, Germany). Finally, sections were washed 3 times (10 minutes each), mounted with anti-fading medium (Fluoromount G, Southern Biotechnology Associates, Biozol, Eching, Germany) and stored in the dark at 4°C.

3.2.5.4. Confocal laser-scanning microscopy

Some of images of L1-transfected NSCs were obtained with a Zeiss LSM510 argon-crypton confocal laser-scanning microscope equipped with a 40x and 63x oil-immersion objective in order to prove transgenic L1 cell surface expression. Images were scanned at a resolution of 1024x1024. Detector gain and pinhole were adjusted to give an optimal signal to noise ratio.

3.2.6. Transfection

In order to establish stably transfected NSCs cultures several trasfection techniques were attempted.

3.2.6.1 AMAXA transfection

For nucleofection of adherently cultivated NSCs cells were deattached from the substrate using acutase for 5 min 37^{o}C. In case of free-floating neurospheres cells were centrifuged for 5 min at 900g and at the 4^{o}C, pellet was incubated with acutase for 5 min 37^{o}C. 1 000 000 cells were resuspended in 90 µl transfection solution and then mixed with 10 µl of transfection solution containing 10 µg linearized CMV-L1-SV40-neo, SV40-neo or CMV-EGFP-SV40-neo. Solution with cells was placed in the cuvette and transfections were performed with a program (A33) that was proven to result in the highest transfection efficacy for NSCs (Richard et al., 2005). Directly after transfection, NSCs were placed into culture medium in uncoated flasks in case of free-floating neurospheres and in 0,1% Matrigel coated flasks in case of adherent NSCs.

3.2.6.2. Lipofectamin transfection

Lipofectamin 2000 transfection was done on adherently cultivated NSCs. On the day before transfection cells were passage into 6 well plates coated with 1% PLL 50 000 cells/ml. Transfection was done according to the manufacturer's protocol. On the next day media were replaced and after further two days antibiotic were added to the media.

3.2.6.3. Roti-Fect and Fugene taransfection

Transfection was done with Roti-Fect transfection reagent (Roth, Karlsruhe, Germany) or with Fugene (Roche, Basel, Schweiz) on free-floating neurosphere according to the manufacturer's protocol. On the next day media were replaced.

3.2.7. Transplantation

3.2.7.1. Inraretinal transplantation

Intraretinal transplantation of NSCs was performed with stably L1-nucleofected and sham transfected NSCs. L1-transfected cells from EGFP-transgenic mice were transplanted into retinas of 1-day-old and adult wild-type mice. Transplantations were performed as described (Laeng et al., 1996; Ader et al., 2000). In brief, cells were centrifuged and resuspended in sterile media. Animals were deeply anaesthetized by an intraperitoneal injection of Ketanest/Rompun™, a glass micropipette was inserted into the vitreous of the eye, about 1 µl of vitreous fluid was removed and the same volume of a cell suspension

(approximately 50,000 cells/µl) was injected. Intraretinal transplantations were achieved by gently lesioning the retina with the micropipette at the time of cell transplantation.

Mice were sacrificed 2 weeks after transplantation and fixed by perfusion. Eyes were quiqly removed and sectioned at thickness of 25 µm using a vibrotom or cryostat.

3.2.7.2 Transplantation into lateral ventricles

On the day of transplantation, NSC were harvested using accutase, centrifuged and resuspended in $HBSS^-$ at a density of 100,000 viable cells per microliter. Animals were deeply anaesthetized by an intraperitoneal injection of Ketanest/Rompun™. Approximately 100,000 cells were injected into the lateral ventricles of 7-day-old wild-type mice using a glass micropipette. Mice were sacrificed 2 weeks after transplantation and fixed by perfusion. Brains were sectioned at a thickness of 25 µm using a cryostat.

3.2.7.3. Transplantation into lesioned striatum

Three days before transplantation, the right striatum of 3-month-old C57BL/6J mice was lesioned by a stereotaxic injection of 1µl of 60 nmol of quinolinic acid (Sigma) at the following coordinates in relation to bregma: 0.4 mm anteroposterior, 1.8 mm mediolateral, and 3.0 mm dorsal. On the day of transplantation, NSCs were harvested using acutase and resuspended in $HBSS^-$ at a density of 150,000 viable cells per microliter. One microliter cell suspension was injected into the lesioned striatum using the same coordinates as for the lesion. All animal experiments were approved by the University and State of Hamburg Animal Care Committees.

3.2.8. Stereological analysis

3.2.8.1. Cell migration

The lesion side was delineated at low magnification at an Axioskop microscope (Carl Zeiss Microimaging) and a Neurolucida software-controlled computer system were used (MicroBrightField Europe, Magdeburg, Germany) to measure the shortest distance between EGFP-positive cells and the lesion side. All cells thet had infiltrated the host brain were analythed.

3.2.8.2. Cell profile density

All cell profiles representing EGFP/NeuN in case of neurons or EGFP/S100 in case of astrocytes were counted with the 40x objective usind the Neurolucida software-controlled computer system (MicroBrightField Europe, Magdeburg, Germany).

3.2.8.3. Estimation of cell numbers

See chapter 3.7.3.3. Estimation of cell numbers study one.

4. Results

4.1. Production monoclonal L1 antibody and antibody biotinylation

Hybrydoma cells secreting the monoclonal rat anti-mouse L1 antibody clone 555 (L1555) raised against the 2-3 fibronectin domains of murine L1 were cultured in serum free medium (HybridomaSFM, Invitrogen) and supernatants containing the antibody were collected. L1555 antibody was isolated from these supernatants using a Protein G Sepharose 4 fast flow column (GE Healthcare, Freiburg, Germany). Bound antibody was eluted from the Protein G column by pH shift and the eluate was concentrated using VivaSpin centrifugation units with a 100 kD cut off membrane (Viva Science, VWR, Darmstadt, Germany). After purification and concentrating of the antibody the BCA assay was used to determine the concentration of the eluted antibody. Target specificity was determined by Western blot analysis on brain homogenates of WT and L1 knock-out mice (Fig. 55).

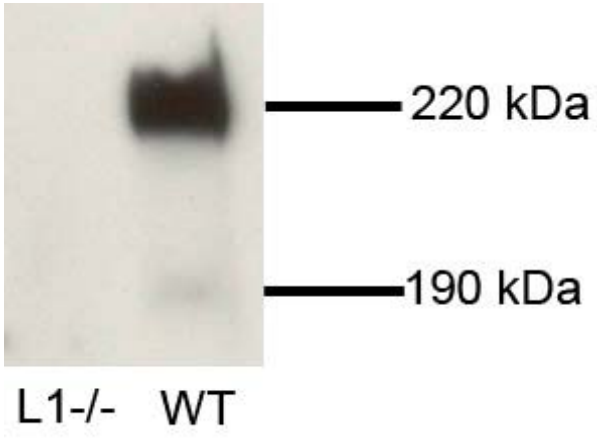

Figure 55: Western blot analysis of brain homogenates of L1-/- and WT mice stained with L1555. L1-immunoreactive bands at 220 and 190 kDa are detectable in brain homogenate of WT mice but not in L1 knock out mice.

Experiments revealed two specifically stained bands with molecular weights of 190 and 220 kDa in the wild type brain. As expected no bands in the L1 deficient brain was detectable, showing that the L1555 antibody was functional active and target specific. For later Dynabead assays part of the L1555 antibody was biotinylated (see 4.3.3). Efficiency of biotinylation and purity of the biotinylated antibody was examined by Western blot analysis and a single band of approximately 50 kDa on the stained gels (Figure 56) could be observed.

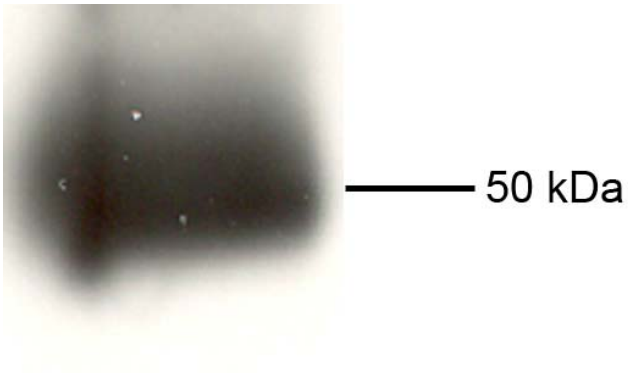

Figure 56: Immunoblot analysis of biotinylated L1555. Secondary antibody was anti-biotin HRP-coupled. A single 50 kDa band was visible which corresponds to expected weight of biotinylated L1 antibody.

Next, the binding efficiency of the biotinylated L1555 antibody was evaluated. Therefore both L1555 and biotinylated L1555 were applied to a direct binding Elisa experiment. L1-Fc (10 µg/ml) was coated on Immuno MaxiSorb® 96-wells and incubated with either L1555 or biotinylated L1555. Detection of the potential interaction partner was carried out using the rat coupled HRP or neutravidin coupled HRP antibodies. Both L1555 and biotinylated L1555 antibody bound to the target L1 fragment in a concentration dependent manner (Figure 57).

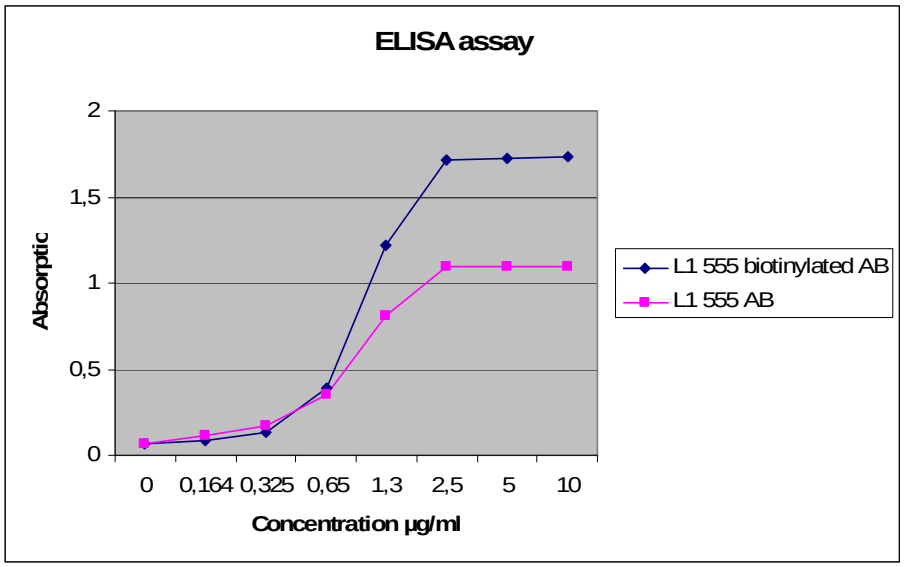

Figure 57: ELISA binding assay for evaluation of direct binding. L1-Fc (10 µg/ml) was incubated with L1555 or biotinylated L1555 antibody. Detection of bound proteins was carried out using the anti-rat HRP coupled secondary antibody for detection of L1555 or neutravidin coupled with HRP to detect biotinylated L1555.

4.2. Cloning of CD 24.

CD24 was recloned from pTZ19-mCD24a to the eukaryotic expression vector pcDNA3. A 0,4 kb kB-*Bcl*I-*Eco*RV-fragment was cut from pTZ19-mCD24a and ligated into pcDNA3. 14 positive clones were obtained and plasmid miniprep was performed followed by digestion with *Eco*RI and *Eco*RV (Fig. 58).

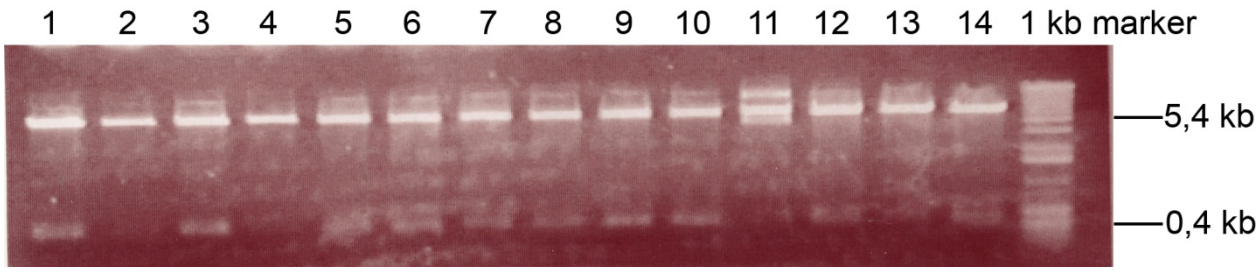

Figure 58: Agarose gel-electrophoresis (1%) minipreps of positive clones after ligation pcDNA3 and CD24. DNA was digested with *Eco*RI and *Eco*RV. Clones number 1, 2, 5-10, 12, 14 had expected bands 5,4kb and 0,4 kb.

Sequencing revealed correct orientation of the CD24 insert in clones number 3, 5 and 6.

4.3. AMAXA transfection of neurosphere cultures

4.3.1. Determination of antibiotic concentration for selection of stably transfected NSCs

Non-transfected GFP-NSCs and WT-NSCs were cultured in the presence of geneticin or zeocin at different concentrations (50, 100, 300, 400, 500, 600 or 1000 µg/ml). Analysis of culture after 10 days in the presence of antibiotics revealed surviving cells up a concentration of 300µg/ml, whereas no surviving cells were observed at higher antibiotic concentrations (Table 2). Therefore, 400µg/ml of geneticin or zeocin was used to select for stably L1-transfected cells (see below).

Concentration of geneticin	Cell survival	Concentration of zeocin	Cell survival
50µg/ml	+	50µg/ml	+
100µg/ml	+	100µg/ml	+
300µg/ml	+	300µg/ml	+
500µg/ml	-	500µg/ml	-
1000µg/ml	-	1000µg/ml	-
300µg/ml	+	300µg/ml	+
400µg/ml	-	400µg/ml	-
500µg/ml	-	500µg/ml	-
600µg/ml	-	600µg/ml	-

Table 2: Determination of geneticin and zeocin concentrations for selection of stably L1-transfected cells. +: surviving cells present; - no surviving cells present.

4.3.2. AMAXA transfection of neurosphere cultures and selection of stably L1-transfected NSCs by antibiotics

For stable transfection of GFP-NSCs cultivated as neurospheres, cultures were transfected with CMV-L1-SV40-neo. For transient transfection, GFP-NSCs were transfected with pcDNA3-L1WT. As a control, cells were sham transfected (i.e. treated as experimental cells except that DNA was omitted). As an additional control WT-NSCs propagated as neurospheres were stably transfected with CMV-EGFP-SV40-neo or transiently transfected with pEGFP-N1. After transfection NSCs were further cultivated as neurospheres. L1 expression was analyzed by immunostaining of live cells two or seven days after transfection. These experiments revealed cell surface expression of L1 on stably (Fig. 59 A-D) and transiently (not shown) transfected cells. Selection of transfected cells with antibiotics (400µg/ml geneticin) was started seven days after transfection. Attempts to expand cells that survived selection over a time period of three weeks were not successful.

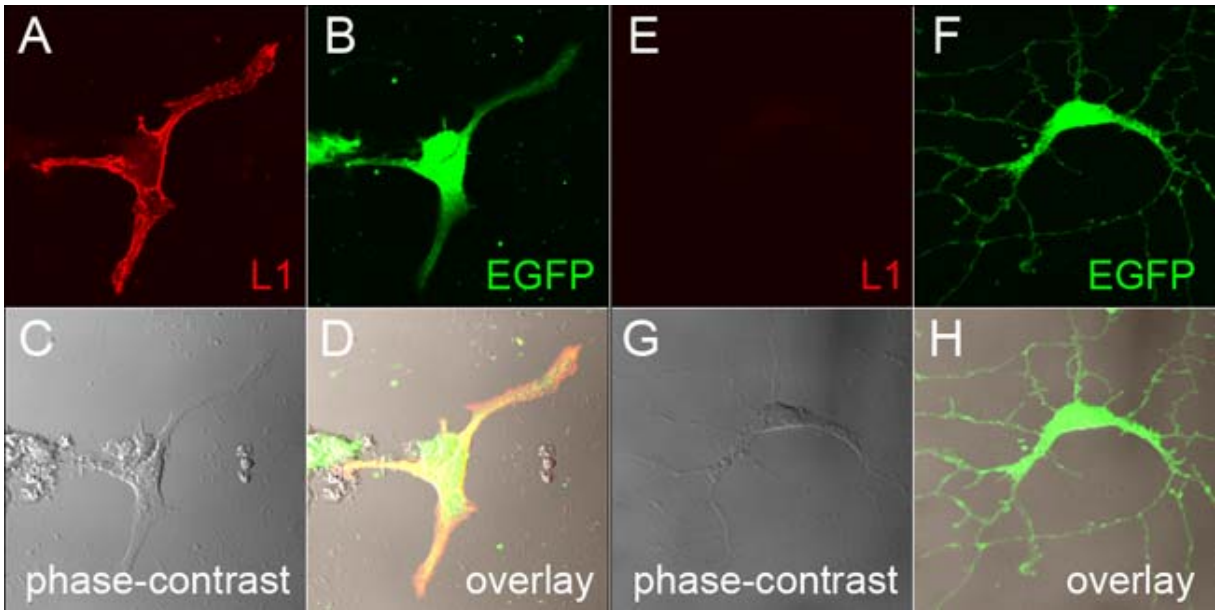

Figure 59: Immunostaining of live GFP-NSCs seven day after transfection with CMV-L1-SV40-neo using the monoclonal antibody L1555 revealed cell surface expression of L1 (A). No L1 immunoreactivity was observed on sham transfected cells (E). (B) and (F) demonstrate EGFP expression in analyzed cells. (C) and (G) are the phase contrast photomicrographs of (A) and (E), respectively. (D) and (H) are the overlays of (A, B, and C) and (E, F and G), respectively.

4.3.3. AMAXA transfection of neurosphere cultures and selection of L1-transfected NSCs by Dynabeads

For stable transfection of GFP-NSCs with L1, cells were cultivated as neurospheres and transfected with CMV-L1. WT-NSCs transfected with CMV-EGFP served as control. After transfection, NSCs were further cultivated as neurospheres. L1 expression was

examined by immunostaining of live cells two days after transfection using monoclonal antibody L1-555. Cells revealed cell surface immunostaining for L1 (Fig. 60A). Furthermore, EGFP-transfected wild-type cells revealed strong EGFP fluorescence two days after transfection (Figure 60F). On the second day after transfection L1-transfected NSCs were selected with Dynabeads coated with L1555 biotinylated antibody. Attempts to expand the selected cells were not successful, and all cells died after a further culture period of three to five days.

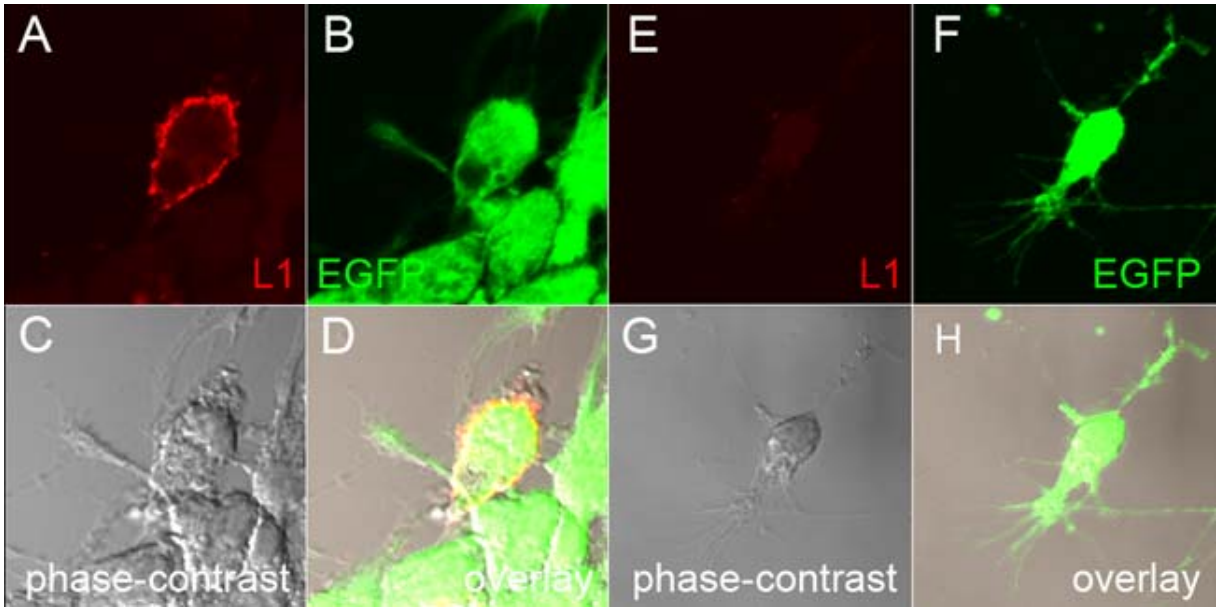

Figure 60: Immunostaining of live GFP-NSCs two days after transfection with CMV-L1 using the monoclonal antibody L1555 revealed cell surface expression of L1 (A). Analysis of fixed culture WT-NSCs two days after transfection with CMV-EGFP revealed strong EGFP expression (F). No L1 immunoreactivity was observed on CMV-EGFP transfected cells (E). (B) demonstrate EGFP expression GFP-NSCs. (C) and (G) are the phase contrast photomicrographs of (A) and (E), respectively. (D) and (H) are the overlays of (A, B, and C) and (E, F and G), respectively.

4.4. Chemical transfection of neurosphere cultures with Lipofectamin, Roti-Fect or Fugene

Three different methods were used to transfect NSCs with chemical transfection methods. To this aim, WT-NSCs were expanded as neurospheres and transiently transfected with pEGFP-N1 using Roti-Fect (2µg/ml DNA), Fugene (0, 8; 1, 6; 3, 2 µg/m DNAl) or Lipofectamin 2000 (4 or 10 µg/ml DNA). Efficacy of transfection was estimated by the percentage of EGFP-positive cells two days after transfection. Analysis revealed significant differences between the transfection efficacies of the different transfection methods (Fig. 61). The most efficient transfection of neurosphere cells was achieved using Lipofectamin 2000 (Fig. 61 I, K).

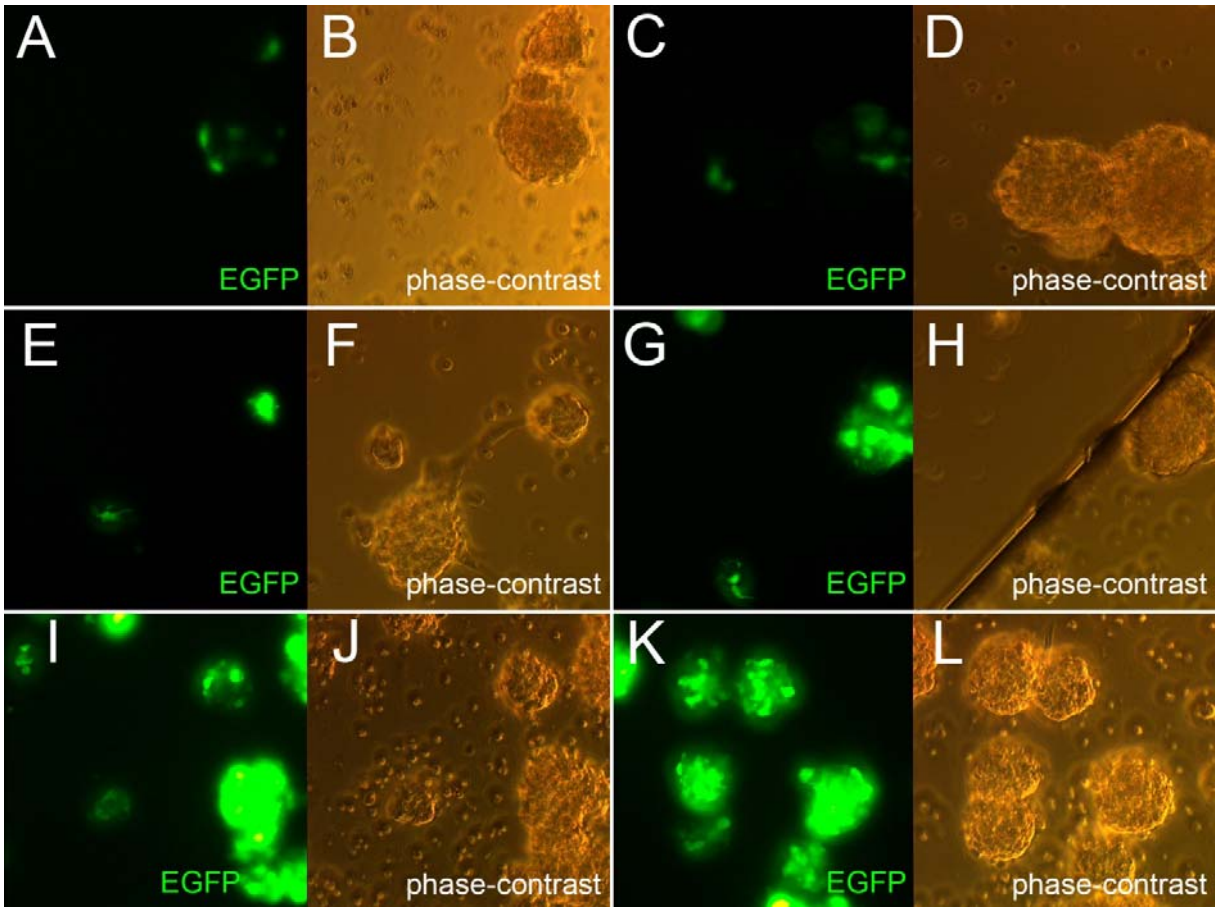

Figure 61: Expression of EGFP by WT-NCSs transfected with pEGFP-N1 using Roti-Fect reagent (2µg/ml) (A), Fugene (0, 8 µg/ml) (C), Fugene (1, 6 µg/ml) (E), Fugene (3, 2 µg/ml) (G), Lipofectamin 2000 with 4µg/ml DNA (I), Lipofectamin 2000 with 10 µg/ml DNA (K). (B, D, F, H, J, L) are the phase contrast photomicrographs of (A, C, E, G, I, K), respectively.

To further increase the transfection efficacy obtained with Lipofectamine, repeated transfections of the same cultures were performed. GFP-NSCs and WT-NSCs expanded as neurospheres were dissociated and further maintained as adherent cells on Matrigel-coated coverslips. GFP-NSCs were transfected with CMV-L1-SV40-neo, and WT-NSCs were transfected with CMV-EGFP-SV40-neo. Sham transfected (i.e. treated as experimental cells with the only exception that addition of DNA was omitted) GFP-NSCs served as control. A second and third transfection of cells with the same constructs was performed two and four days after the first transfection, respectively. Immunostaining of live cells with the monoclonal L1555 antibody revealed cell surface expression of L1 (see Fig.62A for L1 expression two days after the second transfection). In contrast, no L1 expression was detected in sham transfected cultures (Fig. 62E). Furthermore, cells transfected twice with CMV-EGFP-SV40-neo and analyzed two days after the last transfection revealed strong EGFP fluorescence (Fig.62I). Qualitative analysis of these experiments revealed no obvious difference in the number of L1 or GFP expressing cells between cultures transfected once or

twice with CMV-L1-SV40-neo or CMV-EGFP-SV40-neo, respectively. Furthermore, cultures transfected three times died within two to three days after the last transfection. Any attempts to expand L1- or GFP-transfected cells failed, irrespective of whether cells were transfected once or twice. Therefore, further experiments were performed with cells that were transfected once.

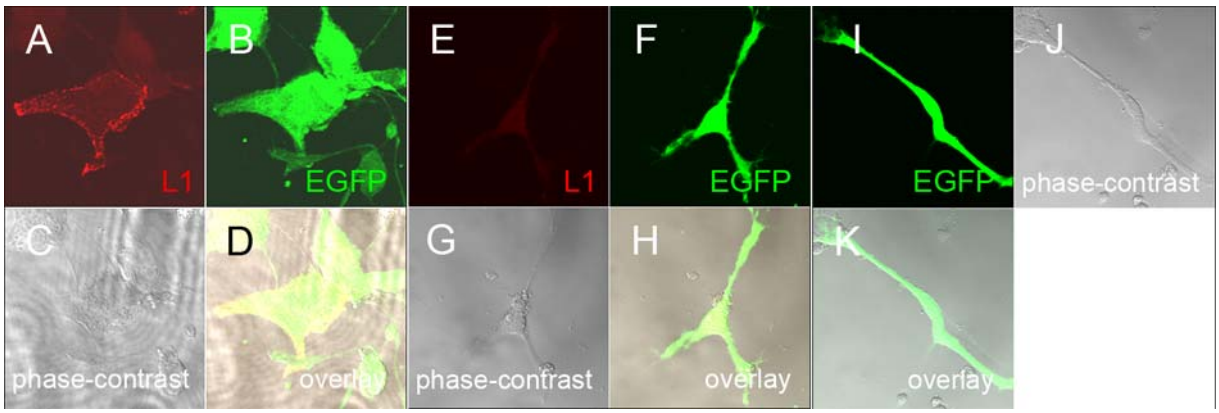

Figure 62: Immunostaining of live GFP-NSCs two days after the second transfection with CMV-L1-SV40-neo using the monoclonal antibody L1555 revealed cell surface expression of L1 (A). No L1 immunoreactivity was observed on sham transfected cells (E). WT-NCSs two days after the second transfection with CMV-EGFP-SV40-neo showed strong EGFP expression (I). (B) and (F) demonstrate EGFP expression in analyzed GFP-NSCs. (C), (G) and (J) are the phase contrast photomicrographs of (A), (E) and (I), respectively. (D), (H) and (K) are the overlays of (A, B, and C), (E, F and G) and (I, J), respectively.

L1 expression in cultures transfected once with Lipofectamine was estimated by immunostaining of live cells two (not shown) and seven days after transfection. Experiments revealed cell surface expression of L1 in cells transfected with CMV-L1-SV40-neo (Fig. 63A), whereas sham transfected cells were L1-immunonegative (Fig.63E). Similarly, WT-NSCs transfected with CMV-EGFP-SV40-neo revealed strong EGFP fluorescence seven days after a single transfection (Fig.63I). Selection of transfected cells with antibiotics (400µg/ml geneticin) was started seven days after transfection. L1 expression after selection with antibiotics for three weeks was estimated by immunostaining of live cells. Experiments revealed homogeneous L1 expression by transfected cells after selection (Fig.64A). Moreover, WT-NSC transfected with CMV-EGFP-SV40-neo and cultured for three weeks in the presence of antibiotics showed strong EGFP fluorescence (Fig.64E). However, any attempts to expand the L1- or GFP-positive cells that survived selection failed.

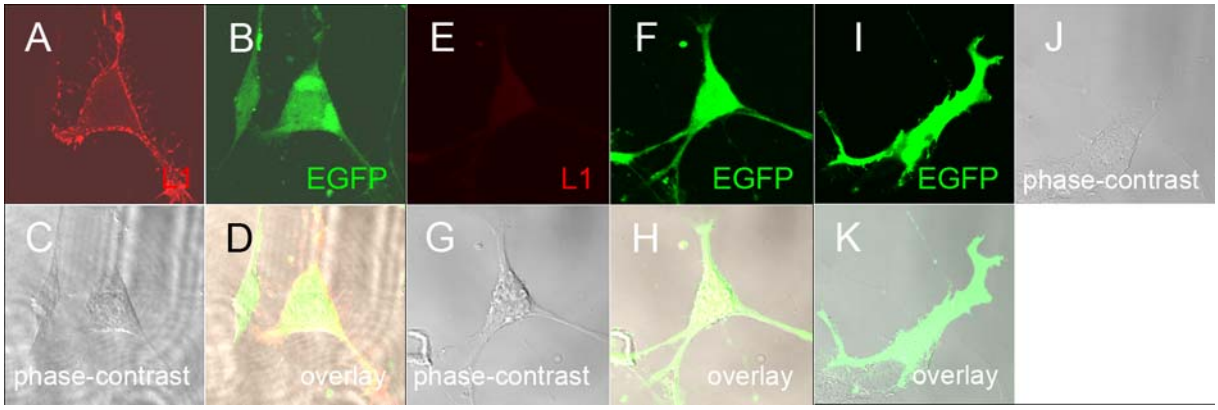

Figure 63: Immunostaining of live GFP-NSCs seven day after transfection with CMV-L1-SV40-neo using the monoclonal antibody L1555 revealed cell surface expression of L1 (A). No L1 immunoreactivity was observed on sham transfected cells (E). (B) and (F) demonstrate EGFP expression in analyzed cells. (C) and (G) are the phase contrast photomicrographs of (A) and (E), respectively. (D) and (H) are the overlays of (A, B, and C) and (E, F and G), respectively. WT-NSCs seven day after transfection with CMV-EGFP-SV40-neo showed strong EGFP expression (I). (J) is the phase contrast photomicrographs of (I). (K) is the overlay of (I) and (J).

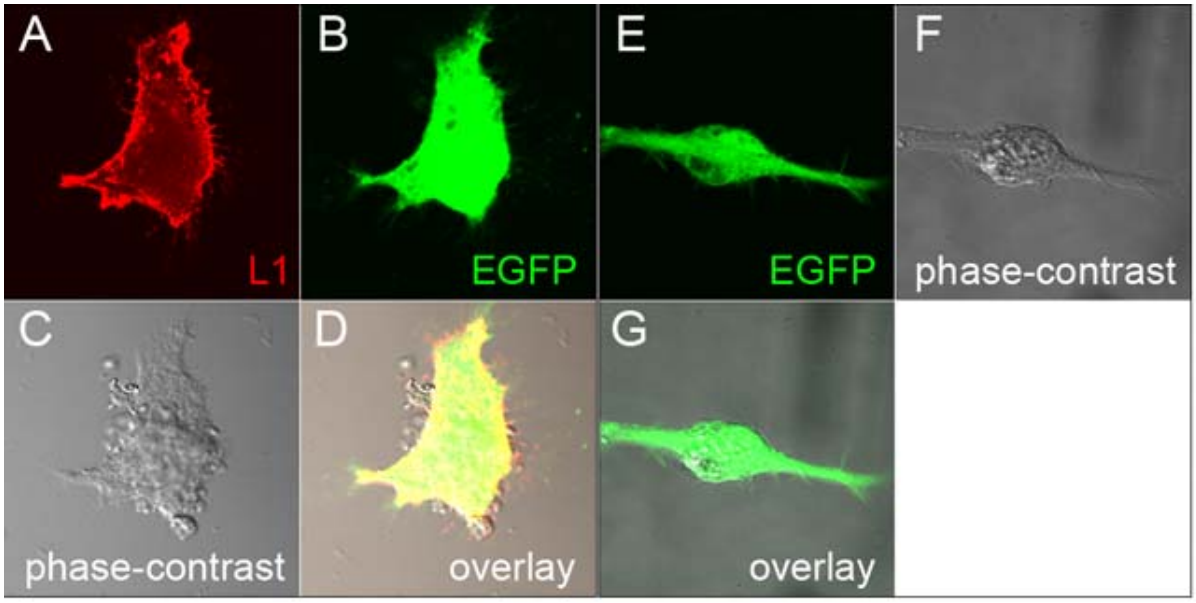

Figure 64: Immunostaining of live GFP-NSCs stably transfected with CMV-L1-SV40-neo after selection with 400 µg/ml of geneticin for three weeks using the monoclonal antibody L1555 revealed homogeneous cell surface expression of L1 (A). (B) demonstrate EGFP expression in analyzed cells. WT-NSCs stably transfected with CMV-EGFP-SV40-neo after selection with 400 µg/ml of geneticin for three weeks showed strong EGFP expression (E). (C) and (F) are the phase contrast photomicrographs of (A) and (E), respectively. (D) and (G) are the overlays of (A, B, and C) and (E and F), respectively.

4.5. AMAXA nucleofection of adherent neural stem cell cultures with L1

4.5.1. Nucleofection of adherent NSC cultures and selection of L1-transfected cells by antibiotics.

GFP-NCSs expanded as adherent cells in the presence of EGF and FGF-2 were stably nucleofected with CMV-L1-SV40-neo or SV40-neo. After nucleofection of cells with the Nucleofector device (program A33; 10µg DNA/100µl nucleofection buffer), cells was further cultivated as adherent cells. Expression of L1 was analyzed by immunostaining of live cells two days after nucleofection using the monoclonal L1 antibody 555. These experiments revealed cell surface expression of L1 in a fraction of cells (not shown). Selection of nucleofected cells was initiated three days after nucleofection with 100 µg/ml geneticin. Every second day, the concentration of geniticin was increased by 100µg/ml up to a final concentration of 400 µg/ml. L1 expression after selection was analyzed by immunostatining of live cells. Experiments revealed homogeneous L1 expression at variable levels on the cell surface of GFP-NSCs (Fig. 65A). Further expansion of nucleofected cells was routineously done in the presence of 400 µg/ml geniticin.

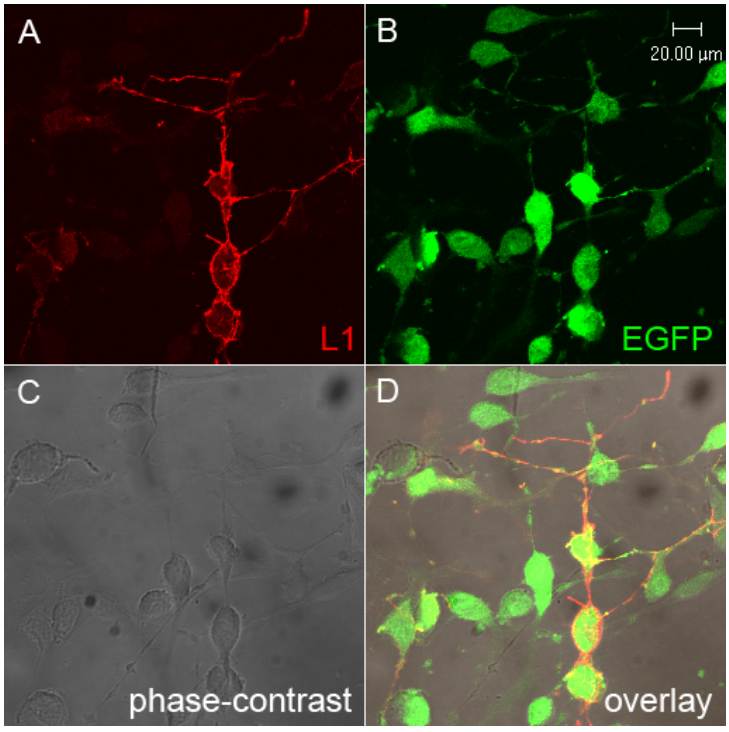

Figure 65: Immunostaining of live GFP-NSCs after nucleofection with CMV-L1-SV40-neo and selection with geneticin for one month using the monoclonal antibody L1555 revealed homogeneous cell surface expression of L1 (A). (B) demonstrate EGFP expression in analyzed cells. (C) is the phase contrast photomicrograph of (A) and (B). (D) is the overlay of (A, B, and C).

4.5.2. L1 immunostainings of L1-nucleofected NSCs with different antibodies

Immunostainings of adherently cultiviated and L1-nucleofected NSCs was performed with the monoclonal L1 antibodies L1-324, L1-555 and L1-557. All immunostaining were done in parallel on live and paraformaldehyde-fixed cells, and the percentage of cells displaying L1-immunoreactivity on the cell surface, in the cytoplasm or of cells lacking detectable levels of L1-immunreactivity was determined. Cultures nucleofected with SV40-neo served as a negative control, and no immunoreactivity was observed with any of the antibodies used.

Immunostainings of live cells with the monoclonal antibody L1-324 (Fig. 67 A and B) revealed numerous L1-immunoreactive cells. Most of these cells displayed intracellularly located L1-immunoreactivity. Quantitative analysis revealed 34% L1-negative cells, 24% cells expressing L1 at the cell surface, and 42% cells displaying intracellular L1 positivity (Fig. 66 A). Immunostainings of live cells with the monoclonal antibody L1-555 (Fig. 67 C and D) demonstrated expression of L1 in apparently all cells, with a small subpopulation expressing high levels of L1 (Fig. 67 C). Quantitative analysis revealed cell surface expression of L1 by 90% cells, and intracellular location of L1-immunoreactivity in 10% of cells (Fig. 66 B). Similarly, L1 expression by all cells (Fig. 66 C) was also observed when cultures were stained with the monoclonal antibody L1-557. (Fig. 67 E and F). Here, about 93% of cells showed cell surface expression of L1, and 7% of cells were labelled intracellularly.

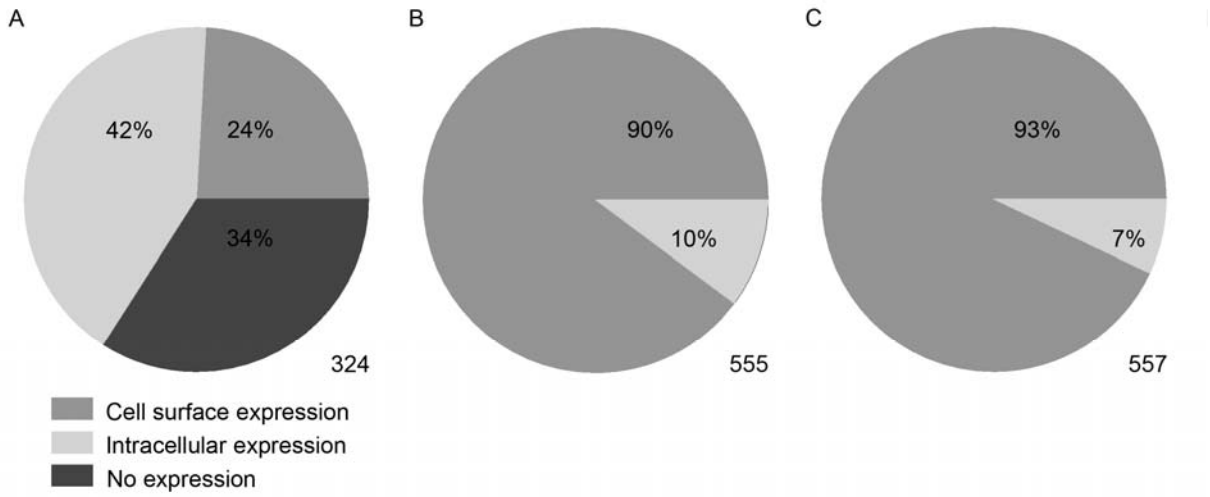

Figure 66: L1-nucleofected GFP-NSCs were stained as live cells with different L1 antibodies, and the percentage of cells displaying L1-immunoreactivity at the cell surface, in the cytoplasm or lacking detectable L1 expression was determined. (A) GFP-NSCs stained with monoclonal antibody L1-324, (B) GFP-NSCs stained with monoclonal antibody L1-555, (C) GFP-NSCs stained with monoclonal antibody L1-557.

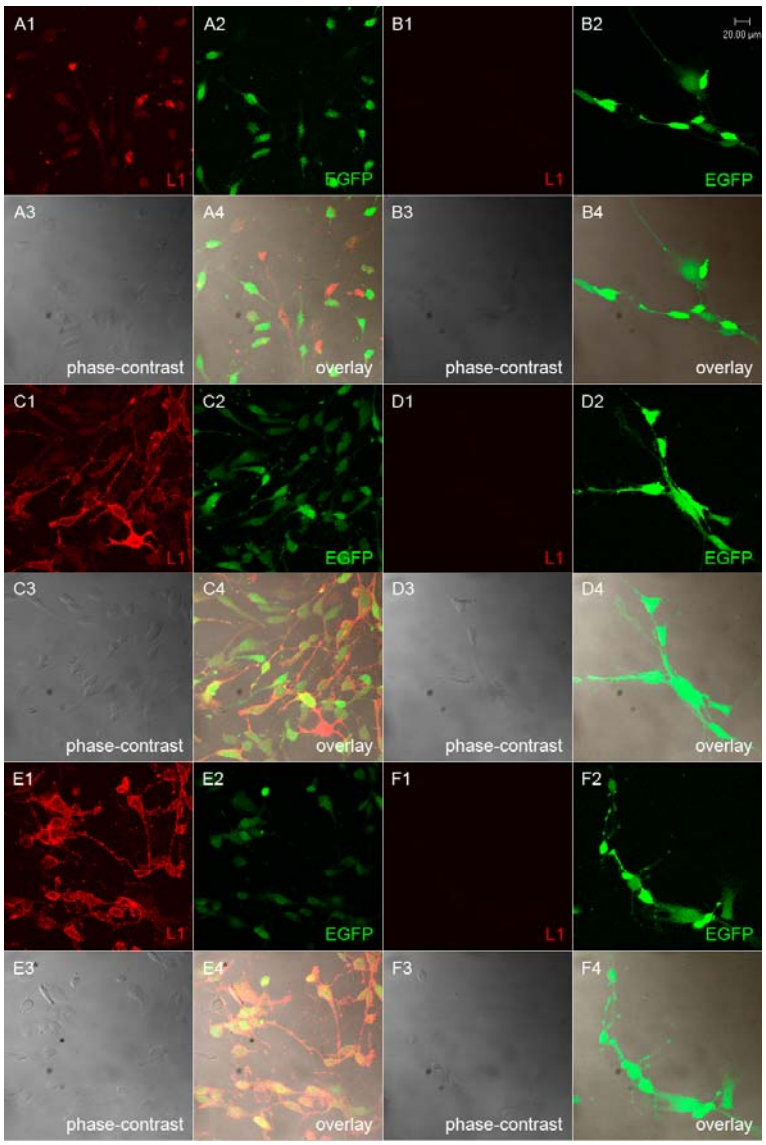

Figure 67: Immnostainings of live GFP-NSCs stably nucleofected with CMV-L1-SV40-neo and SV40-neo nucleoected cultures using different monoclonal L1 antibodies. (A1) L1 stably nucleofected GFP-NSCs stained with L1-324, (C1) L1-555, (E1) and L1-557. (B1), (D1) and (F1) show SV40-neo nucleofected GFP-NSCs stained with antibodies L1-324, L1-555 and L1-557, respectively. (A2)- (F2) demonstrates EGFP expression on analyzed cells. (A3)- (F3) are the phase contrast photomicrographs of (A1) - (F1), respectively. (A4) - (F4) are the overlays of (A1-3) - (F1-3), respectively.

Immunostainings of fixed cell cultures with L1-324 antibodies (Fig. 68 A and B) revealed a high number of cells displaying cell surface immunoreactivity (91%) and a small fraction of cells with intracellular labelling (9%; Fig.69 A). Similarly, immunostainings of fixed L1-nucleofected GFP-NSCs with monoclonal antibody L1-555 demonstrated L1 expression in virtually all cells (Fig. 68 C), with 93% of cells showing cell surface labelling and 7% showing intracellular labeling (Fig. 69 B). Fixed cultures stained with monoclonal antibody L1-557 (Fig. 68 E) contained a significant fraction of immunonegative cells (48%), 26% of cells with cell surface labelling and 26% of cells with intracellularly located L1-immunoreactivity (Fig. 69 C).

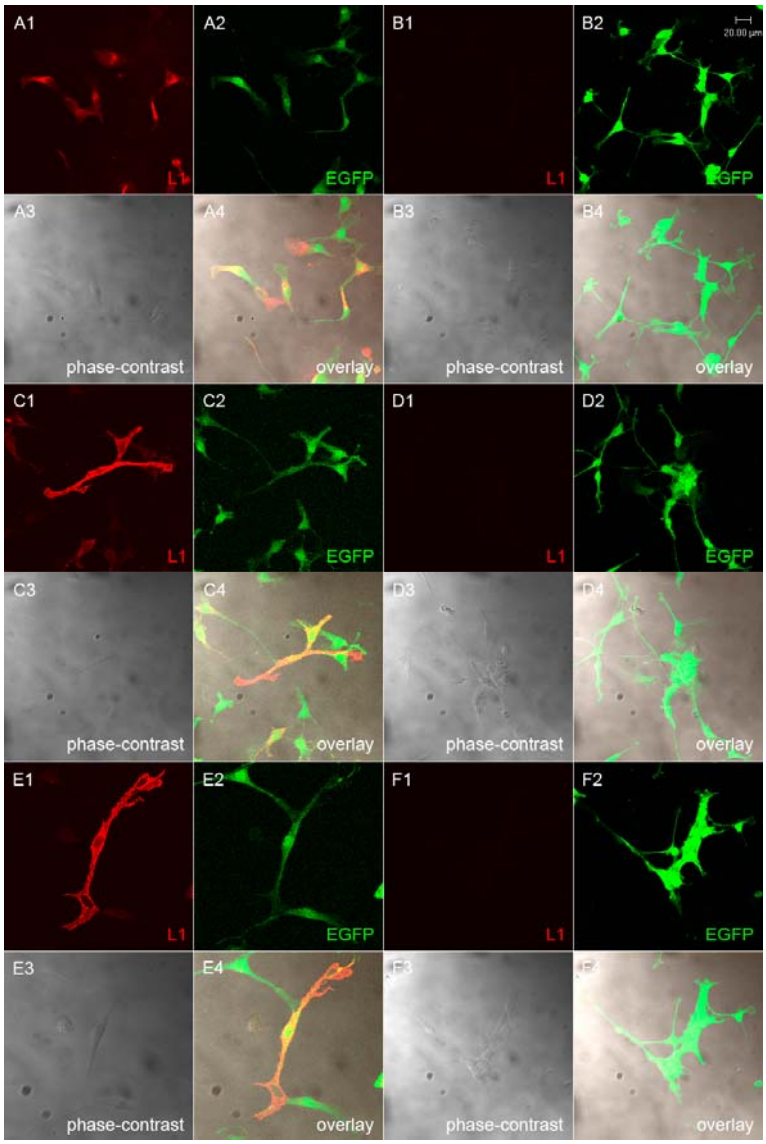

Figure 68: Immnostaining of fixed L1-nucleofected or SV40-neo nucleofected GFP-NSCs using different monoclonal L1 antibodies. (A1) L1 stably nucleofected GFP-NSCs stained with L1-324; (C1) L1-555, (E1) or L1-557. (B1), (D1) and (F1) are SV40-neo nucleofected GFP-NSCs stained with L1-324, L1-555 or L1-557, respectively. (A2) - (F2) demonstrates EGFP expression by analyzed cells. (A3) - (F3) are the phase contrast photomicrographs of (A1)-(F1), respectively. (A4) - (F4) are the overlays of (A1-3) - (F1-3), respectively.

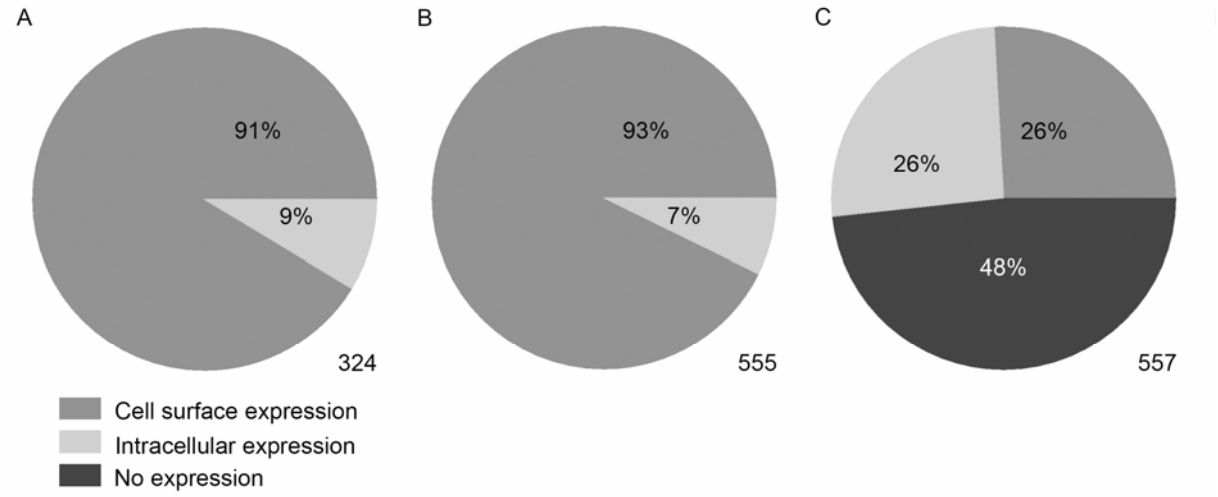

Figure 69: L1-nucleofected GFP-NSCs were fixed, stained with different L1 antibodies, and the percentage of cells displaying L1-immunoreactivity at the cell surface, in the cytoplasm or lacking detectable L1 expression was determined. (A) GFP-NSCs stained with monoclonal antibody L1-324, (B) GFP-NSCs stained with monoclonal antibody L1-555, (C) GFP-NSCs stained with monoclonal antibody L1-557.

4.6. Transplantations

4.6.1. Transplantation of adherently cultivated, stably L1-nuceofected NSCs into the retina of adult and young postnatal mice

To study the fate of stably L1-nucleofected GFP-NSCs *in vivo,* they were transplanted into the retina of 15 weeks old wild-type mice (5 animals). Sham transfected GFP-NSCs served as a control (5 animals). Analysis of host retinas four weeks after transplantation revealed the presence of GFP-positive cells that were predominantly located out of the retina (Fig. 70). Qualitative analysis of host tissues revealed no significant difference in the extent or pattern of integration between L1-nucleofected and sham nucleofected NSCs.

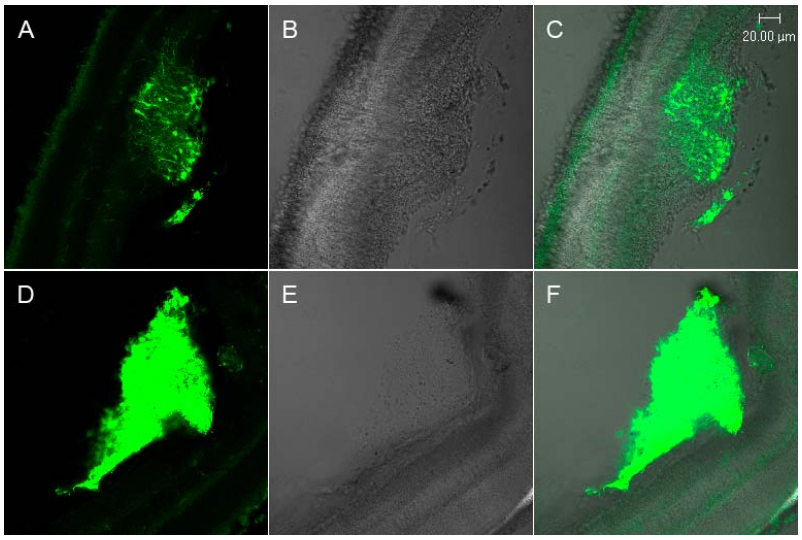

Figure 70: Stably L1-nucleofected and sham nucleofected GFP-NSCs were grafted into the retina of adult wild-type mice, and host retinas were analysed four weeks after transplantation. No significant differences in the extent of integration were detectable between L1 transfected (A) and sham transfected (D) GFP-NSCs. (B) and (E) are the phase contrast photomicrographs of (A) and (D), respectively. (C) and (F) are the overlays of (A, B) and (D, E,), respectively.

L1- and sham nucleofected GFP-NSCs were additionally transplanted into the retina of 1 day old wild-type mice (2 aminals for each cell population). Analysis of host retinas four weeks after transplantation revealed the presence of GFP-positive cells that were predominantly located out of the retina (Fig. 71). Similarly to adult host retinas, there were no obvious differences in the extent and pattern of integration between L1-positive (Fig. 71 A) and sham nucleofected (Fig. 71 D) GFP-NSCs.

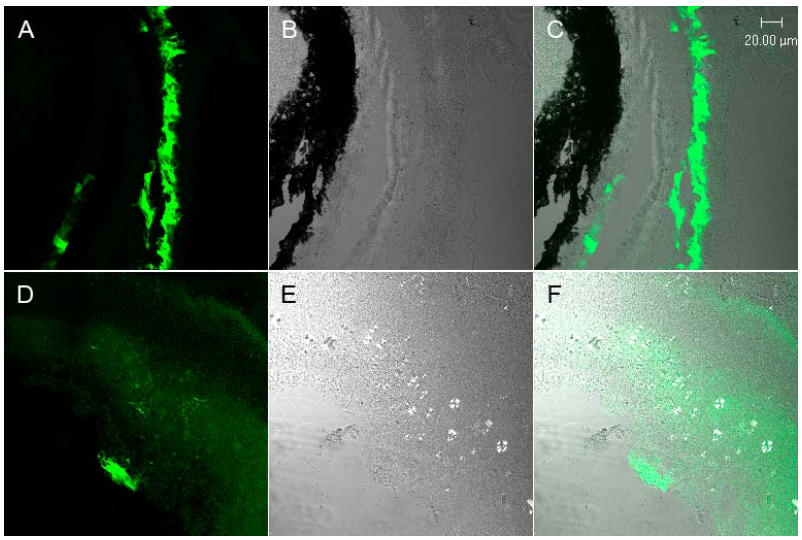

Figure 71: Stably L1-nucleofected and sham nucleofected GFP-NSCs were grafted into the retina of one day old wild-type mice, and host retinas were analysed four weeks after transplantation. No significant differences in the extent of integration were detectable between L1 nucleofected (A) and sham nucleofected (D) GFP-NSCs. (B) and (E) are the phase contrast photomicrographs of (A) and (D), respectively. (C) and (F) are the overlays of (A, B) and (D, E), respectively.

4.6.2. Transplantation of adherently cultivated, stably L1-nuceofected NSCs into the lateral ventricles of young postnatal mice

To further study the integration potential of stably L1-nucleofected GFP-NSCs, cells were transplanted into the lateral ventricles of 7 day old wild-type mice (3 animals). Sham transfected GFP-NSCs served as control (3 animals). Analysis of host tissue two weeks after transplantation revealed the presence of several GFP-positive cells in both experimental groups that were predominantly located in the periventricular region (Fig. 72). Similarly to the retina, there were no apparent differences in the integration potential or in the pattern of integration between L1-nuceofected and sham nucleofected cells.

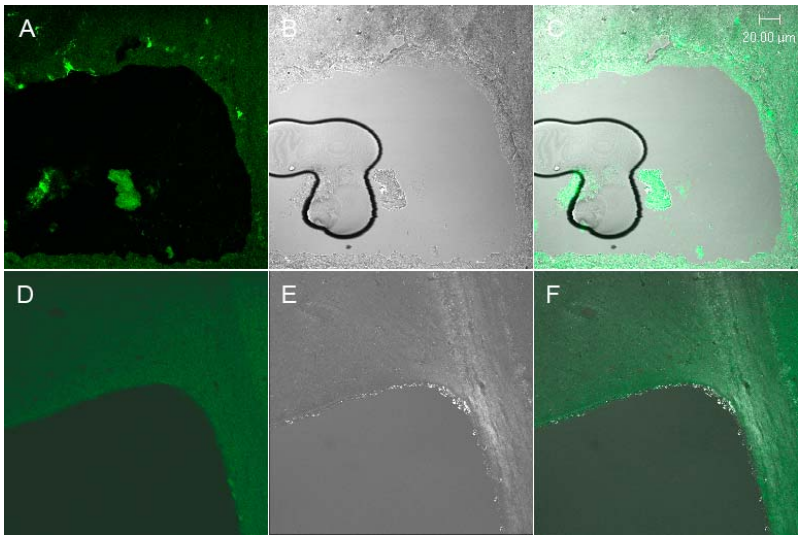

Figure 72: Stably L1-nucleofected and sham nucleofected GFP-NSCs were grafted into the lateral ventricles of seven day old wild-type mice, and host brains were analysed two weeks after transplantation. No significant differences in the extent of integration were detectable between L1 nucleofected (A) and sham nucleofected (D) GFP-NSCs. (B) and (E) are the phase contrast photomicrographs of (A) and (D), respectively. (C) and (F) are the overlays of (A, B) and (D, E) respectively.

4.6.3. Transplantation of adherently cultivated, stably L1-nuceofected NSCs into the quinolinic acid-lesioned striatum of adult mice

Finally, the effect of ectopic L1 expression on the integration potential of GFP-NSCs after transplantation into quinolinic-lesioned striatum of adult mice was analyzed. This treatment results in rapid and complete loss of GABAergic striatal neurons (Huntington's disease paradigm). Stereotaxic injection of the NMDA receptor agonist quinolinic acid into the right striatum resulted into almost complete lost of neurons in the lesioned site 3 days after injection. Three days later, NSCs were injected into the center of lesion. Serial brain sections were stained with GFP antibodies to increase the intensity of the GFP fluorescence of NSCs. Both, L1- and sham nucleofected cells were detected within the host brains 10 days after transplantation, and had extended processes into the surrounding tissue (Fig. 73). Furthermore, quantitative analysis of experimental tissues 10 days after grafting revealed a slightly but significantly increased migratory potential of L1-nucelofected NSCs when compared to sham nucleofected NSCs (Fig. 74).

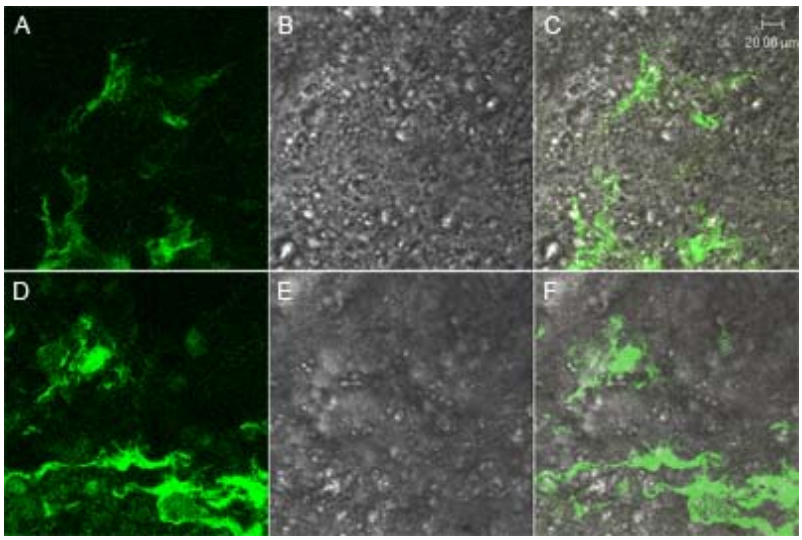

Figure 73: L1-nucleofected (A) and sham (D) nucleofected GFP-NSCs 10 days after transplantation into the lesioned stiatum of adult mice have differentiated into cells extending processes into the host brain. (B) and (E) are the phase contrast photomicrographs (A) and (D), respectively. (C) and (F) are the overlays of (A, B) and (D, E), respectively.

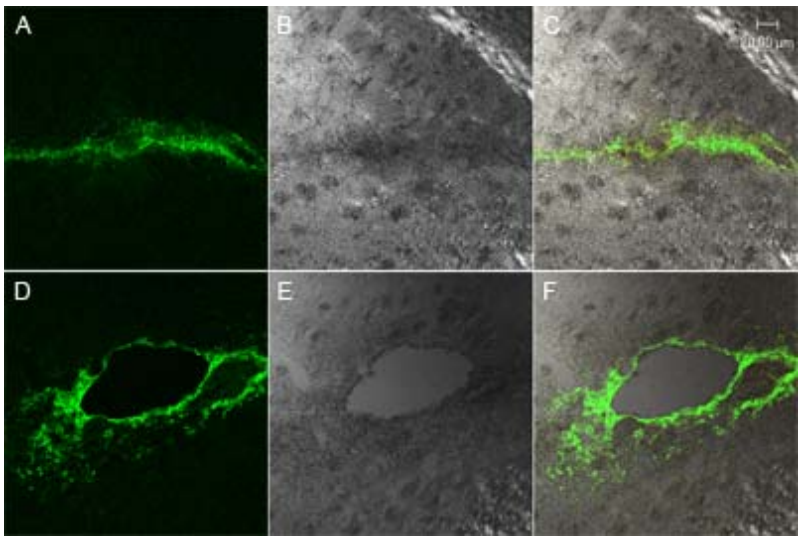

Figure 74: The distribution of L1- (A) and sham (D) nucleofected GFP-NSCs 10 days after transplantation in the lesioned striatum. (B) and (E): are the phase contrast photomicrographs (A) and (D), respectively. (C) and (F) are the overlays of (A, B) and (D, E), respectively.

To quantify migration of grafted cells within the host brains, the shortest distance between donor cells and lesion site was measured 10 days after transplantation using the Neurolucida system (MicroBrightField Europe, Magdeburg, Germany). The average migration distance observed for L1-nucleofected GFP-NSCs was 224µm ± 65,03 µm, whereas sham transfected NSCs had migrated, on average, 170 µm ± 13,30 µm away from the lesion site (Fig. 75).

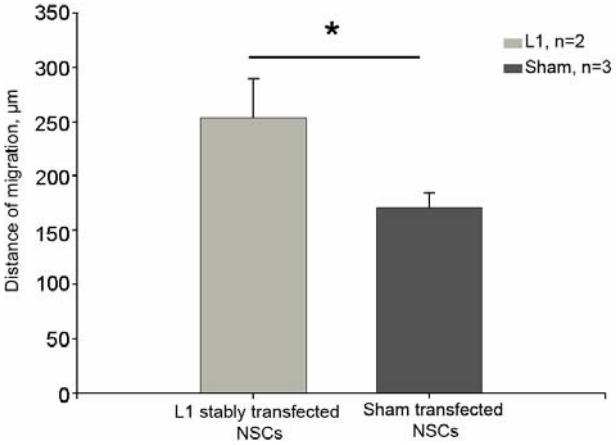

Figure 75: Average migration distance of L1- and sham nucleofected GFP-NSCs 10 days after transplantation. Note the significantly increased migration distance of L1-nucleofected NSCs when compared to sham nuleofected NSCs (asterisk: $p > 0.05$, *t* test).

The migration potential of L1-nucleofected GFP-NSCs within the quinolinic acid lesioned striatum was additionally analysed four weeks after transplantation (Fig. 76). Similar to the 10-day-survival interval, both L1- and sham-nucleofected GFP-NSCs were detected four weeks after grafting in the host brain, and had differentiated into cells extending processes into the host tissue (Fig. 77).

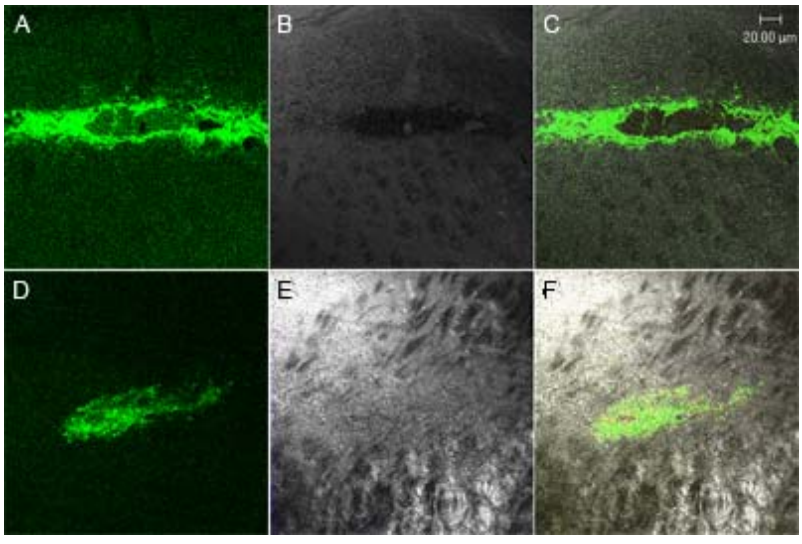

Figure 76: The distribution of L1- (A) and sham- (D) nucleofected GFP-NSCs four weeks after transplantatoion in the lesioned striatum. (B) and (E) are the phase contrast photomicrographs (A) and (D), respectively. (C) and (F) are the overlays of (A, B) and (D, E), respectively. .

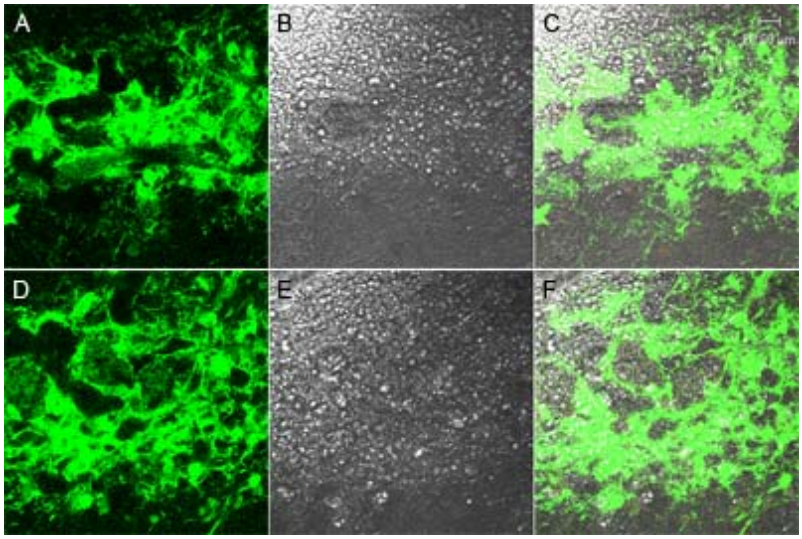

Figure 77: L1-nucleofected (A) and sham (D) nucleofected GFP-NSCs four weeks after transplantation into the lesioned stiatum of adult mice have differentiated into cells extending processes into the host brain. (B) and (E) are the phase contrast photomicrographs (A) and (D), respectively. (C) and (F) are the overlays of (A, B) and (D, E), respectively.

Similar to the 10-day-survival interval, the average migration distance four weeks after transplantation was significantly increased for L1-nucleofected cells (233µm ± 19,71 µm) when compared to sham.-nucleofected cells (152 µm ± 14,05 µm; Fig. 78).

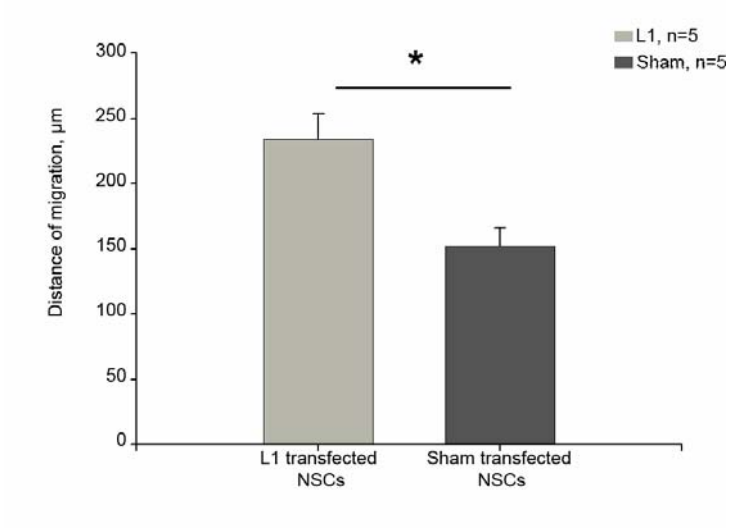

Figure 78: Average migration distance of L1- and sham nucleofected GFP-NSCs four weeks after transplantation. Note the significantly increased migration distance of L1-nucleofected NSCs when compared to sham nuleofected NSCs (asterisk: $p > 0.05$, *t* test).

To estimate the number of L1- and sham-nucleofected cells that had migrated away from the lesion site, the number of GFP-positive cells were counted four weeks after grafting. These experiments revealed similar number of GFP-positive cells in striata that received L1- or sham-nucleofected GFP-NSCs (Fig. 79).

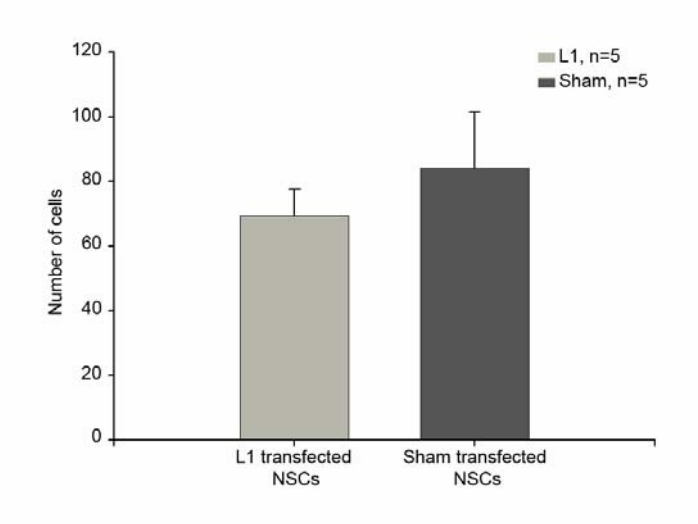

Figure 79: The average number of GFP-positive cells that had migrated away from the lesion site four weeks after transplantation of L1- or sham-nucleofected GFP-NSCs.

The survival potential of L1- and sham-nucleofected GFP-NSCs within the quinolinic acid lesioned striatum was estimated by countig profile density of live cells four weeks after grafting including cells precent in lesion site and migrated cells. Experiments reveal no difference in profile density of GFP-positive cells L1- or sham-nucleofected (Fig. 80).

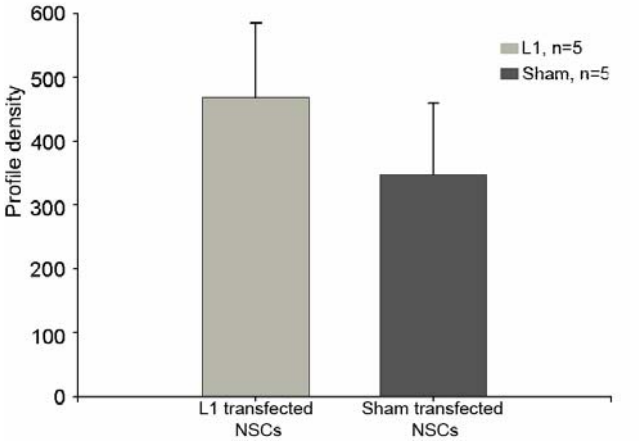

Figure 80: The average profile density of GFP-positive cells that present in the lesion site and had migrated away from the lesion site four weeks after transplantation of L1- or sham-nucleofected GFP-NSCs.

4.6.3.1. Adherently cultivated, stably L1-nuceofected NSCs show increased neuronal differentiation and decreased astrocytic differentiation after transplantation into the quinolinic acid-lesioned striatum of adult mice

The differentiation potential of L1- and sham-nucleofected GFP-NSCs *in vivo* was analyzed after transplantation into a mouse model with quinolinic acid-induced acute and selective loss of GABAergic projection neurons in the striatum.

Donor-derived neurons were identified by their co-expression of GFP and NeuN, and the percentage of GFP/NeuN-positive cells from the total number of GFP positive cells was estimated per section. These experiments revealed a significant increase in the percentage of neurons for the L1-nucleofected cells (36% ±4,51%) when compared to sham-transfected cells (19% ±4,84%) 1 month after transplantation ($p<0,001$; Fig. 81).

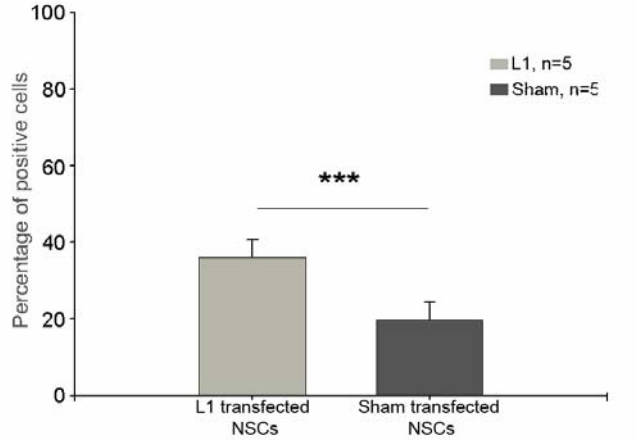

Figure 81: The percentage of GFP/NeuN-positive cells from the total number of GFP-positive cells four weeks after transplantation of L1- or sham-nucleofected GFP-NSCs (asterisks: $p<0.001$, *t* test).

Donor-derived astrocytes were identified by co-expression of GFP and S100, and the percentage of S100-positive cells was estimated per section. Analysis revealed a significant decrease in the percentage of GFP/S100-positive cells for L1-nucleofected cells (50% ±3,4%) when compared to sham-transfected cells (64% ±6,2%) 1 month after transplantation ($p<0,001$; Fig. 82).

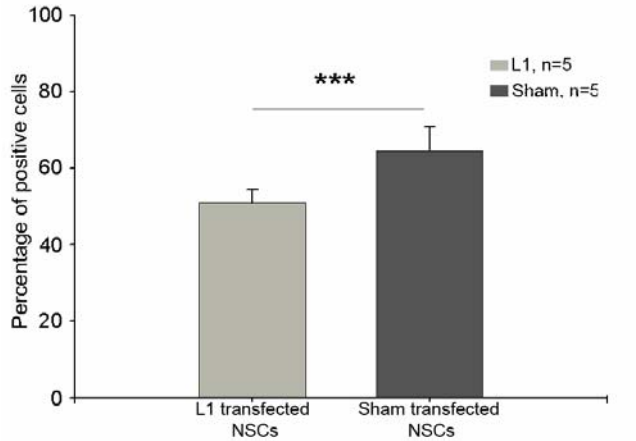

Figure 82: The percentage of GFP/S100-positive cells from the total number of GFP-positive cells four weeks after transplantation of L1- or sham-nucleofected GFP-NSCs (asterisks: $p<0.001$, *t* test).

5. Discussion

Since neural cell adhesion molecules are not only implicated in cell-cell interactions during nervous system development, but have also been recognized as important molecules being involved in cell migration and fate decision, we were interested to analyze the effect of ectopically expressed L1 on survival, migration and fate decision of NSCs *in vivo*. In this study, a method was established that allows efficient non-viral stable transfection of mouse NSCs using the nucleofection technique. When grafted into the quinolinic acid-lesioned striatum of adult mice, L1-transfected NSCs showed improved migration when compared to sham-transfected NSCs. Moreover, L1-transfected NSCs showed increased neuronal and decreased astrocytic differentiation when compared to sham-transfected NSCs.

5.1. Genetic manipulation of NSCs

Gene transfer to cells of the CNS may represent a powerful tool to treat a variety of diseases, including neurological disorders. The use of genetically modified primary NSCs for research or therapeutic uses has been greatly hampered by the difficulties involved in their successful transfection. Although several authors have reported the use and feasibility of retroviral, adenoviral, adeno-associated viral or lentiviral transduction of NSCs (Englund et al., 2000; Franceschini et al., 2001a; Vitry et al., 2001; Falk et al., 2002; Heins et al., 2002; Wu et al., 2002; Franceschini et al., 2004; Rappa et al., 2004; Copray et al., 2006; Andersson et al., 2007; Li et al., 2007; Shim et al., 2007), the safety concerns inherent in the use of engineered viruses has limited their use in the clinical setting. Besides an increase in the immunogenicity of virus-manipulated cells due to the transfer of viral proteins (Jooss et al.,1998; Trapnell and Gorziglia, 1994; Yang et al., 1995; Mincheff et al., 2001; Ojima et al., 2006; Koido et al., 2005; Cao et al., 2007; Koido et al., 2007), there is also the risk of oncogenesis, mutagenesis and cytotoxicity related to the insertion of the viral genome into host cell DNA (Gordon and Anderson, 1994; Lu et al., 1994; Ying et al.,1999; da Cruz et al., 2004; Porada et al., 2004; Okada et al., 2004).

Reports on transfections by methods such as lipid-mediated transfer, liposome-based methods, calcium phosphate co-precipitation, or standard electroporation techniques have consistently given only low transfection efficiencies of primary cells, including mitogen-expanded NSCs (Cattaneo et al., 1996; Diebold et al., 1998; 1999a, b; 2001; Irvine et al.,

2000; Haines et al., 2001; Falk et al., 2002; Kim et al., 2002; Wiesenhofer and Humpel, 2000; Ohki et al., 2001; da Cruz et al., 2004). Moreover, some findings indicate that liposome-mediated transfection procedures are fairly toxic to neural stem cells (Kim et al., 2002). In line with these data, we failed to derive stably transfected neurosphere cultures using transfection methods like Fugene, Rotifect and Lipofectamine. All these transfection methods resulted in low transfection efficiencies, and successfully transfected cells could not be expanded further. The failure to establish stably transfected cultures with these methods might relate, at least in part, to the low probability to transfect cell with stem cell characteristics, which are rare in neurosphere cultures (see below).

Nucleofection is a newly developed, electroporation-based transfection method which allows efficient transfection of a variety of proliferating, non-proliferating or difficult-to-transfect primary cell types (Dityateva et al.,2003; Gresch et al., 2004; Hamm et al., 2002; Lakshmipathy et al., 2004; Lenz et al., 2003; Maasho et al., 2004; Martinet et al., 2003; Quenneville et al., 2004; Richard et al., 2005). In fact, this method has been used in previous experiments, and transfection efficiencies of about 70% have been observed for transiently nucleofected NSCs (Richard et al., 2005). We used this method to stably introduce the gene encoding the neural recognition molecule L1 into NSCs isolated from striatum of EGFP-transgenic E14 mouse embryos. While attempt to establish L1-nucleofected NSCs from free-floating neurospheres failed, we were successful to derive stably L1 expressing cultures when adherently propagated NSCs were nucleofected with L1 (see below).

5.2. Free-floating neurospheres and adherently propagated NSCs. Are they different?

Initially NSCs were cultivated as free-floating clonal cell aggregates, so-called neurospheres (Reynolds and Weiss 1992; Reynolds et al., 1992; Weiss et al., 1996a,b). Cloning assays revealed that only a small percentage (3–4%) of the cells within these neurospheres are truly multipotent stem cells, i.e. cells that are capable to self-renew and display multipotentiality (Gritti et al., 1999; Tropepe et al., 1999). The vast majority of cells within neurospheres correspond to committed precursor cells or even mature cell. It appears that the mixed cellular environment likely provides a niche that sustains relatively few stem cells (Garcion et al., 2004). The low percentage of stem cells within neurospheres might explain why we did not succeed to derive stably transfected cultures from these cells. Given that the transfection efficacy for NSCs with the nucleofection technique is about 70%

(Richard et al., 2005) and the percentage of bone fide stem cells in neurosphere cultures is 3–4% (Gritti et al., 1999; Tropepe et al., 1999), we preferentially nucleofected precursors cells which are incapable of continued self-renewal rather than self-renewing stem cells. On the other hand experiments with neurosphere cultures that were adherently cultivated for short periods before and after transfection with Lipofectamin 2000 contained small population of stably transfected cells (i.e. cells that expressed L1 for more than 3 months) after selection with antibiotics. However, attempts to expand these cells failed.

The first adherently propagated NSCs described in the literature were derived from ES cells that were differentiated into a heterogeneous population of neuroepithelial progenitors in adherent monolayer culture (Ying et al., 2003). Over several passages, these adherently grown cells acquired a homogeneous morphology and were shown to uniformly express nestin and Sox2. Because these cells were clonogenic and indefinitely maintained the capacity to generate both neurons and astrocytes, they were termed NS cells (neural stem cells) in analogy to ES cells (embryonic stem cells). Cells with similar characteristics were later also derived from fetal brain tissue primary cell cultures or long-term expanded neurospheres. Some observations suggest that these adherently cultivated NS cells are the resident stem cells of neurospheres, rather than committed progenitor cells. For instance, adherent NSCs will readily form neurospheres if detached from a culture substrate. Some finding revealed that the complexity of neurosphere cultures, which contain a mixture of stem cells, committed progenitors, and differentiated cells like neurons and astrocytes (Suslov et al., 2002; Bez et al., 2003; Conti et al., 2005), can be eliminated by adherent culture conditions. In the present study, we were able to stably transfect adherently propagated NSCs, and this result is probably related to an enrichment of stem cells in these culture, and thus an increased probability to transfect cells which are capable to self-renew.

However, neurospheres have significant limitations (Conti et al., 2005). The stem cells maintained within neurospheres are not directly identifiable, have not been purified, and have an uncertain relationship to CNS precursor cells *in vivo* (Suslov et al., 2002). Complexity of culture is a barrier to molecular and biochemical dissection of self-renewal and commitment mechanisms (Sinor and Lillien, 2004). Furthermore, there is variation between as within cultures, which can give rise to contradictory data from different laboratories (Morshead et al., 2002). Finally, neurospheres differentiate much more readily into astrocytes than neurons *in vitro* (Morshead et al., 2002) and *in vivo* (Winkler et al., 1998), providing little enthusiasm for pharmacological screening or therapeutic applications (Rossi and Cattaneo, 2002). Neural progenitor cells are also might be propagated in adherent cultures supported by fibroblast

growth factor 2 (FGF-2) (Cattaneo and McKay, 1990; Johe et al., 1996), neuronal differentiation potential is usually progressively lost in these conditions (Temple, 1989; Qian et al., 2000).

5.3. L1 is not expressed in neural stem cell cultures

Expression of L1 was not detectable in neurosphere cultures or in adherently propagated NSC cultures. This finding is in line with the observation that expression of L1 in the developing central nervous system is restricted to postmitotic nerve cells (Rathjen and Schachner, 1984; Fushiki and Schachner, 1986), and with a previous study also demonstrating lack of L1 expression in neurosphere cultures and dissociated neural precursor cell cultures (Dihne et al., 2003)**.** Because L1 has been demonstrated to be involved in many critical steps of neural development, including cell migration, neuronal survival, outgrowth, fasciculation, pathfinding or regeneration of axons, or synaptic plasticity, ectopic expression of L1 by neural stem cells might enhance the therapeutic potential of these cells. More specifically, we hypothesized that L1 might increase the migratory potential of grafted neural stem cells, and their migratory capacity within host tissues as it has been demonstrated for ES cell-derived neural precursor cells (Dihne et al., 2003; Bernreuther et al., 2006). This hypothesis was tested by grafting stably L1-expressing, adherently propagated NSCs into the lesioned striatum of adult mice.

5.4. L1 does not influence the survival of NSCs transplanted into the quinolinic acid lesioned striatum of adult mice

In vitro studies have demonstrated that L1 promotes neurite outgrowth and survival of neurons by homophilic interactions (Chen et al., 1999; Dong et al., 2003). Furthermore, L1 as a substrate has been demonstrated to decrease proliferation, and to increase neuronal and decrease astrocytic differentiation of neural precursor cells *in vitro* by selectively enhancing neuronal differentiation of multipotential neural precursors and bipotential neuron–astrocyte precursors (Dihne et al., 2003). However, *in vivo* no difference was found with regard to proliferation and survival between non-transfected and L1-transfected ES cell-derived neural precursor cells after transplantation into the quinolinic acid-lesioned striatum of adult mice (Bernreuther et al., 2006). In agreement with these *in vivo* observations, we also did not

observe differences in the survival between L1-transfected and sham-transfected NSCs after transplantation into the same animal model.

5.5. Ectopically expressed L1 enhances the migratory capacity of neural stem cells grafted into the quinolinic acid-lesioned adult striatum

L1 promotes migration of cells *in vitro* (Lindner et al., 1983; Rathjen and Schachner, 1984). To test the impact of L1 on the migratory capacity of neural precursor cells, transplantation experiments with neural precursor cells derived from L1-transfected ES cells and non-transfected ES cells were performed. One month after transplantation of these cell populations into the quinolinic acid-lesioned striatum, precursor cells derived from non-transfected ES cells had migrated not more than 42 µm away from the graft edge. In comparison, precursor cells derived from L1-transfected ES cells had migrated about 110 µm away from the lesion site, demonstrating that ectopic L1 expression enhances the migratory capacity of neural precursor cells (Bernreuther et al., 2006).

In the present study, we tested the migratory potential of L1-nucleofected NSCs in the same animal model. When L1-transfected and sham-transfected NSCs were grafted into the lesioned striatum of adult mice, L1-nucleofected NSCs had migrated 224µm away from the graft edge 10 days after transplantation, compared to 170µm for sham-transfected NSCs. An increased migratory capacity for L1-nucleofected NSCs was also found four weeks after transplantation. At this time point, L1-nucleofected NSCs had migrated 233µm away from the graft, compared to 152µm for sham-nucleofected cells. Thus, ectopic expression of L1 enhances the migratory potential of both, ES cell-derived neural precursor cells and brain-derived adherently propagated NS cells. These data indicate that forced expression of pro-migratory proteins enhances the migration capacity of neural precursor cells, and might thus be a strategy to improve the therapeutic potential of these cells.

5.6. Influence of L1 on fate decisions of NSCs *in vivo*

A previous study has demonstrated that substrate-coated L1 decreased proliferation, increased neuronal differentiation, and decreased astrocytic differentiation of neural precursor cells *in vitro* by selectively enhancing neuronal differentiation of multipotential neural

precursors and bipotential neuron/astrocyte precursors (Dihne et al., 2003). The finding that enhanced neuronal differentiation on an L1 substrate was only observed for precursor cells prepared from wild-type mice, but not for cells prepared from L1-deficient mice, strongly suggests that the preferential neuronal differentiation is mediated by homophilic L1-L1 interactions (Dihne et al., 2003). Based on these observations, subsequent studies were performed to analyze whether forced expression of L1 in neural precursor cells might also influence fate decisions, and might result in increased neuronal differentiation. When neural progenitor cells derived from L1-transfected ES cells were grafted into the lesioned spinal cord of adult mice, differentiation of grafted cells into nerve cells was increased while differentiation into astrocytes was decreased (Chen et al., 2005). Similarly, when neural precursor cells derived from L1-transfected ES cells were grafted into the quinolinic acid-lesioned adult striatum, increased differentiation into neurons at the expense of astrocytes and neural precursor cells was observed when compared to control cells. Interestingly, the preferential neuronal differentiation resulted in an overall increase in the absolute number of GABAergic neurons (Bernreuther et al., 2006). In the present study, fate decisions of L1- and sham-nucleofected NSCs were analyzed four weeks after transplantation into the quinolinic acid-lesioned adult striatum using antibodies to NeuN and S100 for the identification of donor-derived neurons and astrocytes, respectively. Experiments revealed that differentiation of L1-nucleofected NSCs into neurons was significantly increased while differentiation into astrocytes was decreased when compared to control cells. In summary, our *in vivo* data demonstrate enhanced migratory capacity and preferential neuronal differentiation of L1-nucleofected NSCs. They thus confirm previous studies using L1-transfected ES cell-derived precursor cells and extend these results to another population of cells with therapeutic potential, neural stem cells derived from the striatum of the embryonic mouse brain.

5.7. Genetically engineered NSCs for cell replacement strategies

NSCs are candidate cells to develop cell based ex vivo gene therapies or cell replacement strategies. A rapidly growing number of reports demonstrate that genetic manipulations significantly increase the therapeutic potential of these cells. In addition to the use of genetically engineered NSCs to deliver therapeutic gene products in the diseased nervous system, these cells might be transfected with genes influencing fate decisions, improving cell survival or enhancing migration within host tissues.

In fact, previous studies have shown that NSCs can be successfully used for ex vivo gene therapeutic approaches. For instance, it has been demonstrated that genetically modified neural stem cell lines producing NGF (Kordower et al., 1997) or BDNF (Martinez-Serrano and Bjorklund, 1996) are able to protect striatal neurons against quinolinic acid-induced excitotoxic damage after transplantation into the striatum, resulting in less deterioration of behavioral function. Similarly, rescue of degenerating GABAergic host cells by neural progenitor cells secreting ciliary neurotrophic factor in the rat quinolinic acid model of Huntington's disease showed a significant decline in apomorphin-induced rotations (Weinelt et al., 2003). Furthermore, proactive transplantation of human neural stem cells transfected with ciliary neurotrophic factor has also been shown to prevent degeneration of striatal neurons in a rat model of Huntington's disease when grafted 1 week before injection of the toxic agent (Ryu et al., 2004).

In mouse model lysosomal storage disease caused by a genetic defect in the activity of b-glucuronidase, an immortalized human NSC line overexpresing b-glucuronidase was transplanted into the cerebral ventricles of MPS VII mouse brains. Transplanted human NSCs migrated extensively within the brain, produced high levels of b-glucuronidase enzyme, reduced enzyme substrate to the normal levels, and cleared the lysosomal storage in the neuronal cytoplasm. These results indicate that human NSCs might also serve as gene transfer vehicles for the treatment of diffuse CNS pathologies, such as lysosomal storage diseases (Meng et al., 2003)

In another study, human NSCs were modified to produce L-DOPA by double transduction with human TH and rat GTPCH1, and then transplanted into the brains of a rat model for PD. Production of L-DOPA in the recipient brains was enhanced, resulting in long-term functional recovery of manipulated animals (Kim et al., 2002, 2006).

There are also several studies which have genetically engineered neural stem/precursor cells with the aim to optimize their migratory potential or to direct their differentiation into particular neural cell types. For instance, one study has analyzed the effect of forced expression of GFP-tagged polysialytransferase in neural stem/precursor cells. Prolonged overexpression of PSA was observed in NSCs and oligodendrocytes, and was found to play an instructive role on the choice of a cell's migration pathway depending on the environment. Moreover, oligodendrocytes derived from the transduced NSCs were able to down-regulate PSA and to differentiate into myelin-forming cells when exposed to myelinating signals, indicating that PSA expression can be manipulated without causing irreversible deleterious effects. Furthermore, using a chick xenograft assay for migration, it was shown that PSA can

instruct precursor migration along the ventral pathway. Persistent overexpression of PSA did not change neural precursor multipotentiality *in vitro*, but induced a delay in oligodendrocyte differentiation. Finally, PSA-overexpressing NSCs showed widespread engraftment in brains of the myelin mutant *shiverer*. However, PSA overexpression did not profoundly modify the ability of grafted precursors to incorporate into many different brain regions of this mutant mouse (Franceschini et al., 2004).

Forced expression of Nurr1, a transcriptional factor critical for midbrain dopamine (DA) neuron development, in adult NSCs induced the cells to acquire a DA neurotransmitter phenotype and differentiation towards morphologically, phenotypically, and ultrastructurally mature DA neurons. Co-expression of Nurr1 and the neurogenic transcription factor Mash1, in combination with a treatment of cells with neurogenic cytokines brain-derived neurotrophic factor and neurotrophin-3 greatly enhanced the Nurr1-induced DA neuron yield. The Nurr1-induced DA neurons demonstrated presynaptic DA neuronal functionality, in that they released DA neurotransmitter in response to depolarization stimuli and in that they showed a specific DA reuptake. Furthermore, Nurr1-engineered adult NSCs survived, integrated, and differentiated into DA neurons *in vivo* and ameliorated the behavioral deficit of parkinsonian rats. Together, these findings indicate that genetically engineered NSCs from the adult brain might serve as a cell population to develop cell replacement therapies for Parkinson disease (Shim et al., 2007).

In view of the possible application of NSCs as a source for remyelinating cell transplants in demyelinating diseases (e.g., multiple sclerosis), NSCs were transfected with the Olig2 gene. Forced expression of Olig2 induced the development of fully mature oligodendrocytes expressing the transcription factor Nkx2.2 and all major myelin-specific proteins. Moreover, Olig2-transfected NSCs, in contrast to nontransfected NSCs, developed into actively remyelinating oligodendrocytes after transplantation into the corpus callosum of long-term cuprizone-fed mice, an animal model for demyelination. These results show that transfection of genes encoding for oligodendrogenic transcription factors can be an efficient way to induce the differentiation of NSCs into functional oligodendrocytes (Copray et al., 2006).

The requirement for broader approaches is illustrated by the example of Huntington's disease. Mutations in huntingtin are suggested to exert their toxic activity largely through cell-autonomous mechanisms, so the transplantation of healthy cells that are able to turn into functionally integrated striatal neurons should, in theory, be a realistic goal. But, even in this case, recent advances in understanding of pathogenic mechanisms indicate that mutations in

huntingtin cause the loss of physiological BDNF (Zuccato et al, 2001) indicating that newly implanted striatal neurons might eventually suffer from the depletion of cortically derived BDNF, which they depend on for their activity.

6. Summary

Neural stem/precursor cells either derived from ES cells or the developing or adult brain are considered as candidate cells to develop cell based ex vivo gene therapies and cell replacement strategies for a variety of neurological disorders. However, when these cells are grafted to the normal or diseased adult brain, they usually show a limited migratory capacity and a limited neuronal differentiation potential. Genetic manipulations prior to transplantations might provide a strategy to improve the therapeutic potential of these cells. The neural recognition molecule L1 is implicated in migration of nerve cells, outgrowth, pathfinding and fasciculation of axons, and adhesion between neurons and between neurons and Schwann cells (Faissner et al., 1984; Rathjen and Schachner, 1984; Fischer et al., 1986; Chang et al., 1987; Lagenaur and Lemmon, 1987; Persohn and Schachner, 1987; Kunz et al., 1998). In addition, L1 has been implicated in axonal regeneration (Martini and Schachner, 1988), neuronal cell survival (Chen et al., 1999; Nishimune et al., 2005), proliferation and fate decisions of neural precursor cells (Dihne et al., 2003). In the present study, we analyzed whether forced expression of L1 in neural stem cells isolated from the embryonic mouse brains enhances the therapeutic potential of these cells after transplantation into a lesioned adult brain structure, the quinolinic acid-lesioned striatum. To this aim, we genetically engineered adherently propagated neural stem cells to stably express L1 using the nucleofection technique. When these cells were grafted into the lesioned striatum of adult mice, we observed enhanced migration and preferential neuronal differentiation of L1-nucleofected cells when compared to non-transfected control cells. These results demonstrate that genetic manipulations provide a promising strategy to modify the properties of neural stem/precursor cells, eventually resulting in the development of optimized cell replacement strategies.

References

Acarin L, Gonzalez B, Castellano B (2000) Neuronal, astroglial and microglial cytokine expression after an excitotoxic lesion in the immature rat brain. Eur. J. Neurosci. 12:3505–3520.

Ader M, Meng J, Schachner M, Bartsch U (2000) Formation of myelin after transplantation of neural precursor cells into the retina of young postnatal mice. Glia 30, 301-310.

Ader M, Schachner M, Bartsch U (2001) Transplantation of neural precursor cells into the dysmyelinated CNS of mutant mice deficient in the myelin-associated glycoprotein and Fyn tyrosine kinase. Eur. J. Neurosci. 14:561–566.

Ader M, Schachner M, Bartsch U (2004) Integration and differentiation of neural stem cells after transplantation into the dysmyelinated central nervous system of adult mice. Eur. J. Neurosci. 20:1205–1210.

Albe-Fessard D, Sanderson P, Mavoungou R (1990). The influence of striatum on the substantia nigra: a study using the spreading depression technique. Brain Res. Bull. 24(2):213-9.

Albin RL, Young AB, Penney JB (1989). The functional anatomy of basal ganglia disorders. Trends Neurosci. 10:366-75.

Alexander GE, Crutcher MD (1990). Functional architecture of basal ganglia circuits: neural substrates of parallel processing. Trends Neurosci. 7:266-71.

Altman J (1969) Autoradiographic and histological studies of postnatal neurogenesis. IV. Cell proliferation and migration in the anterior forebrain, with special reference to persisting neurogenesis in the olfactory bulb. J. Comp. Neurol. 137 (4):433-457.

Altman J, Das GD (1965) Autoradiographic and histological evidence of postnatal hippocampal neurogenesis in rats. J. Comp. Neurol. 124 (3):319-335.

Alvarez-Buylla A, Garcia-Verdugo J M, Tramontin AD (2001) A unified hypothesis on the lineage of neural stem cells. Nat. Rev. Neurosci. 2, 287–293.

Amaral D. and Witter M.(1989) The three-dimensional organization of the hippocampal formation: a review of anatomical data. Neuroscience 31:571-591.

Amaral D. and Witter M.(1995) Hippocampal formation. In: Paxinos G, ed. The rat nervous system. San Diego: Academic Press, 1995, pp. 443-492.

Andreassen OA, Ferrante RJ, Aamo TO, Beal MF, Jørgensen HA (2003) Oral dyskinesias and histopathological alterations in substantia nigra after long-term haloperidol treatment of old rats. Neuroscience. 122(3):717-25.

Andersen P, Bland H, Myhrer T and Schwartzkroin P (1979) Septo-hippocampal pathway necessary for dentate theta production. Brain Res. 165:13-22.

Anderson DJ, Gage FH, Weissman IL (2001) Can stem cells cross lineage boundaries? Nat. Med. 7, 393-5.

Andersson EK, Irvin DK, Ahlsiö J, Parmar M (2007) Ngn2 and Nurr1 act in synergy to induce midbrain dopaminergic neurons from expanded neural stem and progenitor cells.Exp. Cell Res. 313(6):1172-80.

Angst BD, Marcozzi C, Magee AI (2001) The cadherin superfamily: diversity in form and function. J. Cell Sci. 114, 629-641.

Aplin AE, Howe A, Alahari SK, Juliano RL (1998) Signal transduction and signal modulation by cell adhesion receptors: the role of integrins, cadherins, immunoglobulin-cell adhesion molecules, and selectins. Pharmacol. Rev. 50, 197-263.

Appel F, Holm J, Conscience JF, Schachner M (1993) Several extracellular domains of the neural cell adhesion molecule L1 are involved in neurite outgrowth and cell body adhesion. J Neurosci 13, 4764-4775.

Arenas, E., Trupp, M., Akerud, P., Ibanez, C.F. (1995) GDNF prevents degeneration and promotes the phenotype of brain noradrenergic neurons *in vivo*. Neuron. 15, 1465-1473.

Asou H, Miura M, Kobayashi M, Uyemura K, Itoh K (1992) Cell adhesion molecule L1 guides cell migration in primary reaggregation cultures of mouse cerebellar cells. Neurosci. Lett .144, 221-224.

Atherton JF, Bevan MD (2005). Ionic mechanisms underlying autonomous action potential generation in the somata and dendrites of GABAergic substantia nigra pars reticulata neurons *in vitro*. J. Neurosci. 25 (36): 8272–8281.

Angulo JA, McEwen BS (1994). Molecular aspects of neuropeptide regulation and function in the corpus striatum and nucleus accumbens. Brain Res. Brain Res. Rev. 1:1-28.

Bachoud-Levi AC, Remy P, Nguyen JP, Brugieres P, Lefaucheur JP, Bourdet C, Baudic S, Gaura V, Maison P, Haddad B, Boisse MF, Grandmougin T, Jeny R, Bartolomeo P, Dalla BG, Degos JD, Lisovoski F, Ergis AM, Pailhous E, Cesaro P, Hantraye P, Peschanski M (2000) Motor and cognitive improvements in patients with Huntington's disease after neural transplantation. Lancet 356:1975–1979.

Balak K, Jacobson M, Sunshine J and Rutishauser U. (1987). Neural cell adhesion molecule expression in Xenopus embryos. Dev. Biol. 119:540-50.

Bartsch U, Kirchhoff F, Schachner M (1989) Immunohistological localization of the adhesion molecules L1, NCAM, and MAG in the developing and adult optic nerve of mice. J. Comp. Neurol. 284, 451-462.

Beal MF, Kowall NW, Ellison DW, Mazurek MF, Swartz KJ, Martin JB (1986) Replication of the neurochemical characteristics of Huntington's disease by quinolinic acid. Nature 321:168–171.

Beal MF, Kowall NW, Swartz KJ, Ferrante RJ, Martin JB (1989) Differential sparing of somatostatin-neuropeptide Y and cholinergic neurons following striatal excitotoxin lesions. Synapse 3:38–47.

Becker CG, Artola A, Gerardy-Schahn R, Becker T, Welzl H, Schachner M (1996) The polysialic acid modification of the neural cell adhesion molecule is involved in spatial learning and hippocampal long-term potentiation. J. Neurosci. Res. 45: 143-152.

Belin D, Deroche-Gamonet V, Jaber M (2007) Cocaine-induced sensitization is associated with altered dynamics of transcriptional responses of the dopamine transporter, tyrosine hydroxylase, and dopamine D2 receptors in C57Bl/6J mice. Psychopharmacology (Berl). 193(4):567-78. Epub 2007 May 17.

Bennett TL, Nunn PJ and Inman DP (1971) Effects of scopolamine on hippocampal theta and correlated discrimination performance. Physiol. Behav. 7:451-454.

Bernreuther C, Dihne M, Johann V, Schiefer J, Cui Y, Hargus G, Schmid JS, Xu J, Kosinski CM, Schachner M (2006) Neural cell adhesion molecule L1-transfected embryonic stem cells promote functional recovery after excitotoxic lesion of the mouse striatum. J. Neurosci. 26(45):11532-9.

Berretta N, Paolucci E, Bernardi G, Mercuri NB (2001)Glutamate receptor stimulation induces a persistent rhythmicity of the GABAergic inputs to rat midbrain dopaminergic neurons. Eur. J. Neurosci. 14(5):777-84

Bez A, Corsini E, Curti D, Biggiogera M, Colombo A, Nicosia RF, Pagano SF, Parati EA (2003) Neurosphere and neurosphere-forming cells: morphological and ultrastructural characterization. Brain Res. 993(1-2):18-29.

Bickers D, Adams R (1949) Hereditary stenosis of the aqueduct of Sylvius as a cause of congenital hydrocephalus. Brain 72, 246-262.

Bonfanti L, Olive S, Poulain D and Theodosis D(1992). Mapping of the distribution of polysialylated neural cell adhesion molecule throughout the central nervous system of the adult rat: an immunohistochemical study. Neuroscience 49:419-36.

Bronner-Fraser M, Wolf J, Murray B (1992) Effects of antibodies against N-cadherin and N-CAM on the cranial neural crest and neural tube. Dev. Biol. 153: 291-301.

Brackenbury R, Thiery JP, Rutishauser U, Edelman GM (1977) Adhesion among neural cells of the chick embryo. I. An immunological assay for molecules involved in cell-cell binding. J. Biol. Chem. 252, 6835-6840.

Brasted PJ, Watts C, Robbins TW, Dunnett SB (1999) Associative plasticity in striatal transplants. Proc. Natl. Acad. Sci. USA 96:10524–10529.

Brown M (1991) Essentials of neural development.Anonymous. Anonymous. Cambridge University Press.

Brummendorf T, Rathjen FG (1995). Cell adhesion molecules 1: immunoglobulin superfamily. Protein Profile. 2, 963-1108.

Brümmendorf T, Kenwrick S, Rathjen FG (1998) Neural cell recognition molecule L1: from cell biology to human hereditary brain malformations. Curr. Opin. Neurobiol. 8:87-97.

Bruses JL, Chauvet N, Rutishauser U (2001 a) Membrane lipid rafts are necessary for the maintenance of the (alpha) 7 nicotinic acetylcholine receptor in somatic spines of ciliary neurons. J Neurosci. 21:504-512.

Bruses JL and Rutishauser U (2001) Roles, regulation, and mechanism of polysialic acid function during neural development. Biochimie 83:635-643.

Bukalo O, Fentrop N, Lee A, Salmen B, Law JWS, Wotjak CT, Schweizer M, Dityatev A, Schachner M (2004) Conditional ablation of the neural cell adhesion molecule NCAM reduces precision of spatial learning, long-term potentiation and depression in the CA1 subfield of mouse hippocampus. J. Neurosci. 24: 1565-1577.

Bunney BS, Chiodo LA, Grace AA (1991). Midbrain dopamine system electrophysiological functioning: a review and new hypothesis. Synapse. 2:79-94.

Bunsey M and Eichenbaum H. (1996) Conservation of hippocampal memory function in rats and humans. Nature 379:255-257.

Burden-Gulley SM, Payne HR, Lemmon V (1995) Growth cones are actively influenced by substrate-bound adhesion molecules. J. Neurosci. 15, 4370-4381.

Burke RE (2004) Ontogenic cell death in the nigrostriatal system. Cell Tissue Res. 318:63-72.

Cameron H.A, Woolley C.S, McEwen B.S, Gould E (1993) Differentiation of newly born neurons and glia in the dentate gyrus of the adult rat. Neuroscience 56 (2):337-344.

Canals JM, Marco S, Checa N, Michels A, Perez-Navarro E, Arenas E, Alberch J (1998) DiVerential regulation of the expression of nerve growth factor, brain-derived neurotrophic factor, and neurotrophin-3 after excitotoxicity in a rat model of Huntington's disease. Neurobiol. Dis. 5:357–364.

Cao DY, Yang JY, Dou KF, Ma LY, Teng ZH (2007) Alpha-fetoprotein and interleukin-18 gene-modified dendritic cells effectively stimulate specific type-1 CD4- and CD8-mediated T-Cell response from hepatocellular carcinoma patients *in Vitro*. Hum. Immunol. 68(5):334-41.

Carpenter MK, Winkler C, Fricker R, Emerich DF, Wong SC, Greco C, Chen EY, Chu Y, Kordower JH, Messing A, Bjorklund A, Hammang JP (1997) Generation and transplantation of EGF-responsive neural stem cells derived from GFAP-hNGF transgenic mice. Exp. Neurol. 148:187–204.

Cattaneo E, McKay R (1990) Proliferation and differentiation of neuronal stem cells regulated by nerve growth factor. Nature 347: 762–765.

Cattaneo E, Conti L, Gritti A, Frolichsthal P, Govoni S, Vescovi A (1996) Non-virally mediated gene transfer into human central nervous system precursor cells. Brain Res. Mol. Brain Res. 42(1):161-6.

Chang S, Rathjen FG, Raper JA (1987) Extension of neurites on axons is impaired by antibodies against specific neural cell surface glycoproteins. J. Cell. Biol. 104, 355-362.

Chapman VM, Keitz BT, Stephenson DA, Mullins LJ, Moos M, Schachner M (1990) Linkage of a gene for neural cell adhesion molecule, L1 (CamL1) to the Rsvp region of the mouse X chromosome. Genomics 8, 113-118.

Chen S, Mantei N, Dong L, Schachner M (1999) Prevention of neuronal cell death by neural adhesion molecules L1 and CHL1. J Neurobiol. 38, 428-439.

Chen J, Bernreuther C, Dihne M, Schachner M (2005) Cell adhesion molecule l1-transfected embryonic stem cells with enhanced survival support regrowth of corticospinal tract axons in mice after spinal cord injury.J. Neurotrauma. 8:896-906.

Chao CC, Ma YL, Chu KY, Lee EH (2003) Integrin alphav and NCAM mediate the effects of GDNF on DA neuron survival, outgrowth, DA turnover and motor activity in rats. Neurobiol. Aging 24:105-116.

Chrobak JJ. (2000) Septal orchestration of hippocampal network dynamics. In: Numan R, ed. The behavioral neuroscience of the septal region. New York: Springer-Verlag: 71-91.

Chen XY, Li J, Qi WQ, Shen SH. (2007) Experimental change on dopaminergic neurons in striatum of Parkinson disease rats. Histol Histopathol. 22(10):1085-90.

Chuong CM and Edelman GM.(1984). Alterations in neural cell adhesion molecules during development of different regions of the nervous system. J. Neurosci. 4:2354-68

Clark EA, Brugge JS (1995) Integrins and signal transduction pathways: the road taken. Science 268, 233-239.

Clarke DJ, Dunnett SB, Isacson O, Sirinathsinghji DJ, Bjorklund A (1988) Striatal grafts in rats with unilateral neostriatal lesions—I. Ultrastructural evidence of afferent synaptic inputs from the host nigrostriatal pathway. Neuroscience 24:791–801.

Cohen NR, Taylor JS, Scott LB, Guillery RW, Soriano P, Furley AJ (1998) Errors in corticospinal axon guidance in mice lacking the neural cell adhesion molecule L1. Curr. Biol. 8, 26-33.

Colom LV, Nassif-Caudarella S, Dickson CT, Smythe JW and Bland BH. (1991) *In vivo* intrahippocampal microinfusion of carbachol and bicuculline induces theta-like oscillations in the septally deafferented hippocampus. Hippocampus 1:381-390.

Conti L, Pollard SM, Gorba T, Reitano E, Toselli M, Biella G, Sun Y, Sanzone S, Ying QL, Cattaneo E, Smith A (2005) Niche-independent symmetrical self-renewal of a mammalian tissue stem cell. PLoS Biol 3(9): e283.

Copray S, Balasubramaniyan V, Levenga J, de Bruijn J, Liem R, Boddeke E (2006) Olig2 overexpression induces the *in vitro* differentiation of neural stem cells into mature oligodendrocytes. Stem Cells. 4:1001-10.

Corotto F.S, Henegar J.A, Maruniak J.A (1993) Neurogenesis persists in the subependymal layer of the adult mouse brain. Neurosci.Lett. 149 (2):111-114.

Coutelle O, Nyakatura G, Taudien S, Elgar G, Brenner S, Platzer M, Drescher B, Jouet M, Kenwrick S, Rosenthal A (1998) The neural cell adhesion molecule L1: genomic organisation and differential splicing is conserved between man and the pufferfish Fugu. Gene 208, 7-15.

Cragg SJ, Baufreton J, Xue Y, Bolam JP, Bevan MD (2004). Synaptic release of dopamine in the subthalamic nucleus. Eur. J. Neurosci. 20 (7): 1788–1802.

Cremer H, Lange R, Christoph A, Plomann M, Vopper G, Roes J, Brown R, Baldwin S, Kraemer P, Scheff S (1994). Inactivation of the N-CAM gene in mice results in size reduction of the olfactory bulb and deficits in spatial learning. Nature 367, 455- 459.

Cremer H, Chazal G, Goridis C and Represa A (1997). NCAM is essential for axonal growth and fasciculation in the hippocampus. Mol. Cell Neurosci. 8, 323-335.

Cremer H, Chazal G, Carleton A, Goridis C, Vincent JD, Lledo PM (1998) Long-term but not short-term plasticity at mossy fiber synapses is impaired in neural cell adhesion molecule-deficient mice. Pro. Natl. Acad. Sci. USA 95: 13242-13247.

Cunningham BA, Hemperly JJ, Murray BA, Prediger EA, Brackenbury R, Edelman GM (1987) Neural cell adhesion molecule: structure, immunoglobulin-like domains, cell surface modulation, and alternative RNA splicing. Science 236: 799-806.

Cunningham BA (1995) Cell adhesion molecules as morphoregulators. Curr Opin Cell Biol 7, 628-633.

da Cruz MT, Simões S, de Lima MC (2004) Improving lipoplex-mediated gene transfer into C6 glioma cells and primary neurons. Exp. Neurol. 187(1):65-75.

Dahme M, Bartsch U, Martini R, Anliker B, Schachner M, Mantei N (1997) Disruption of the mouse L1 gene leads to malformations of the nervous system. Nat. Genet. 17, 346-349.

Dale AS (1935). The relation between metabolic processes and the ventricular electrogram. J. Physiol. 84(4):433-453.

Das G.D (1977) Gliogenesis during embryonic development in the rat. Experientia 33 (12):1648- 1649.

Davis AA, Temple S (1994) A self-renewing multipotential stem cell in embryonic rat cerebral cortex. Nature 372: 263–266.

Dayhoff MO, Barker WC, Hunt LT (1983) Establishing homologies in protein sequences. Methods. Enzymol. 91, 524-545.

Delling M, Wischmeyer E, Dityatev A, Sytnyk V, Veh RW, Karschin A, Schachner M (2002) The neural cell adhesion molecule regulates cell-surface delivery of G-protein-activated inwardly rectifying potassium channels via lipid rafts. J Neurosci. 22: 7154-7164.

D'Eustachio P, Owens GC, Edelman GM and Cunningham BA (1985). Chromosomal location of the gene encoding the neural cell adhesion molecule (N-CAM) in the mouse. Proc. Natl. Acad. Sci. U S A 82:7631-5.

Debiec H, Christensen EI, Ronco PM (1998) The cell adhesion molecule L1 is developmentally regulated in the renal epithelium and is involved in kidney branching morphogenesis. J. Cell. Biol. 143, 2067-2079.

Demyanenko GP, Tsai AY, Maness PF (1999) Abnormalities in neuronal process extension, hippocampal development, and the ventricular system of L1 knockout mice. J, Neurosci, 19, 4907-4920.

Diebold SS, Cotten M, Wagner E, Zenke M (1998) Gene-modified dendritic cells by receptor-mediated transfection. Adv. Exp. Med. Biol. 451:449-55.

Diebold SS, Kursa M, Wagner E, Cotten M, Zenke M (1999a) Mannose polyethylenimine conjugates for targeted DNA delivery into dendritic cells. J. Biol. Chem. 274(27):19087-94.

Diebold SS, Lehrmann H, Kursa M, Wagner E, Cotten M, Zenke M (1999b) Efficient gene delivery into human dendritic cells by adenovirus polyethylenimine and mannose polyethylenimine transfection. Hum Gene Ther. 10(5):775-86.

Diebold SS, Cotten M, Koch N, Zenke M (2001) MHC class II presentation of endogenously expressed antigens by transfected dendritic cells. Gene Ther. 6:487-93.

Dihne M, Bernreuther C, Sibbe M, Paulus W, Schachner M (2003) A new role for the cell adhesion molecule L1 in neural precursor cell proliferation, differentiation, and transmitter-specific subtype generation. J. Neurosci. 23(16):6638-50.

Dityatev A, Dityateva G, Schachner M (2000) Synaptic strength as a function of post- versus presynaptic expression of the neural cell adhesion molecule NCAM. Neuron 26: 207-217.

Dityatev A, Dityateva G, Sytnyk V, Delling M, Toni N, Nikonenko I, Muller D, Schachner M (2004) Polysialylated neural cell adhesion molecule promotes remodeling and formation of hippocampal synapses. J. Neurosci. 24: 9372-82.

Dityateva G, Hammond M, Thiel C, Ruonala MO, Delling M, Siebenkotten G, Nix M, Dityatev A (2003) Rapid and efficient electroporation-based gene transfer into primary dissociated neurons. J. Neurosci. Methods 130(1):65-73.

Djabali M, Mattei MG, Nguyen C, Roux D, Demengeot J, Denizot F, Moos M, Schachner M, Goridis C, Jordan BR (1990) The gene encoding L1, a neural adhesion molecule of the immunoglobulin family, is located on the X chromosome in mouse and man. Genomics 7, 587-593.

Dobrossy MD, Dunnett SB (2004) Environmental enrichment affects striatal graft morphology and functional recovery. Eur. J. Neurosci. 19:159–168.

Doherty P, Cohen J, Walsh FS (1990) Neurite outgrowth in response to transfected N-CAM changes during development and is modulated by polysialic acid. Neuron 5: 209-219.

Doetschman TC, Eistetter H, Katz M, Schmidt W, Kemler R (1985) The *in vitro* development of blastocyst-derived embryonic stem cell lines: formation of visceral yolk sac, blood islands and myocardium. J. Embryol. Exp. Morphol. 87:27-45.

Dong L, Chen S, Schachner M (2003). Single chain Fv antibodies against neural cell adhesion molecule L1 trigger L1 functions in cultured neurons. Mol. Cell. Neurosci. 22: 234–247.

Dunnett SB, Isacson O, Sirinathsinghji DJ, Clarke DJ, Bjorklund A (1988) Striatal grafts in rats with unilateral neostriatal lesions—III. Recovery from dopamine-dependent motor asymmetry and deWcits in skilled paw reaching. Neuroscience 24:813–820.

Dunnett SB, Bjorklund A (1992) Neural transplantation: a practical approach. IRL Press, Oxford. Ref Type: serial (Book, Monograph).

Dunnett SB, Boulton AA, Baker GB (2000) Neural transplantation methods. Neuromethods, vol. 36. Humana Press, Totowa. Ref Type: serial (Book, Monograph).

Dusart I, Marty S, Peschanski M (1991) Glial changes following an excitotoxic lesion in the CNS—I. Astrocytes. Neuroscience 45:541–549.

Dutar P, Bassant MH, Senut MC and Lamour Y (1995). The septohippocampal pathway: structure and function of a central cholinergic system. Physiol Rev. 75:393-427.

Dusek JA and Eichenbaum H. The hippocampus and memory for orderly stimulus relations (1997) Proc. Natl. Acad. Sci. U S A 94:7109-7114.

Ebeling O, Duczmal A, Aigner S, Geiger C, Schollhammer S, Kemshead JT, Moller P, Schwartz-Albiez R, Altevogt P (1996) L1 adhesion molecule on human lymphocytes and monocytes: expression and involvement in binding to alpha v beta 3 integrin. Eur. J. Immunol. 26, 2508-2516.

Eccles JC (1976a). From electrical to chemical transmission in the central nervous system. Notes Rec. R. Soc. Lond. 2:219-30.

Eccles JC (1976b). The plasticity of the mammalian central nervous system with special reference to new growths in response to lesions. Naturwissenschaften. 1:8-15.

Eckhardt M, Bukalo O, Chazal G, Wang L, Goridis C, Schachner M, Gerardy-Schahn R, Cremer H, Dityatev A (2000) Mice deficient in the polysialyltransferase ST8SiaIV/PST-1 allow discrimination of the roles of neural cell adhesion molecule protein and polysialic acid in neural development and synaptic plasticity. J. Neurosci. 20: 5234-5244.

Edelman GM, Cunningham BA, Gall WE, Gottlieb PD, Rutishauser U, Waxdal MJ (1969) The covalent structure of an entire gammaG immunoglobulin molecule. Proc. Natl. Acad. Sci. U S A 63, 78-85.

Edelman G, (1986) Cell adhesion and the molecular processes of morphogenesis. Annu. Rev. Biochem. 54, 135-169.

Eichenbaum H and Cohen NJ. (1988) Representation in the hippocampus: what do hippocampal neurons code? Trends Neurosci. 11:244-248.

Engel J (1991) Common structural motifs in proteins of the extracellular matrix. Curr. Opin. Cell. Biol. 3, 779-785.

Englund U, Ericson C, Rosenblad C, Mandel RJ, Trono D, Wictorin K, Lundberg C (2000) The use of a recombinant lentiviral vector for ex vivo gene transfer into the rat CNS. Neuroreport. 11(18):3973-7.

Englund U, Bjorklund A, Wictorin K (2002) Migration patterns and phenotypic differentiation of long-term expanded human neural progenitor cells after transplantation into the adult rat brain. Brain Res.Dev.Brain Res. 134 (1-2):123-141.

Eriksson C, Bjorklund A, Wictorin K (2003) Neuronal differentiation following transplantation of expanded mouse neurosphere cultures derived from different embryonic forebrain regions. Exp. Neurol. 184:615–635.

Fachinetto R, Burger ME, Wagner C, Wondracek DC, Brito VB, Nogueira CW, Ferreira J, Rocha JB (2005) High fat diet increases the incidence of orofacial dyskinesia and oxidative stress in specific brain regions of rats. Pharmacol. Biochem. Behav. 81(3):585-92.

Faissner A, Kruse J, Nieke J, Schachner M (1984) Expression of neural cell adhesion molecule L1 during development, in neurological mutants and in the peripheral nervous system. Brain. Res. 317, 69-82.

Faissner A, Teplow DB, Kubler D, Keilhauer G, Kinzel V, Schachner M (1985) Biosynthesis and membrane topography of the neural cell adhesion molecule L1. EMBO J 4, 3105-3113.

Falk A, Holmström N, Carlén M, Cassidy R, Lundberg C, Frisén J (2002) Gene delivery to adult neural stem cells. Exp. Cell Res. 279(1):34-9.

Fallon J (1987a). Growth factors in the basal ganglia. In: Carpenter MB. Basal ganglia:structure and function. New York: Plenum, pp.247-260.

Fallon J. (1987b). The ghost in the machine: What if the midbrainnoutput is excitatory? Behav. Brain Sci. 10, 210-211.

Fallon JH, Moore RY (1978a). Catecholamine innervation of the basal forebrain. III. Olfactory bulb, anterior olfactory nuclei, olfactory tubercle and piriform cortex. J. Comp. Neurol. 180(3): 533-44.

Fallon JH, Moore RY (1978b). Catecholamine innervation of the basal forebrain. IV. Topography of the dopamine projection to the basal forebrain and neostriatum. J. Comp. Neurol. 180(3): 545-80.

Fallon J, Loughlin S (1982). Cortico-striato-pallidal systems: How many are there? Neurosci. Abstr. 8, 934.

Fallon J, Loughlin S (1985). The substantia nigra. In: Paxinos G. and Watson J., ed. The rat central nervous system: a handbook for neuroscientists. Sydney: Academic Press, 1985, pp. 353-374.

Fallon J, Loughlin S (1987). Monoamine innnervation of cerebral cortex and a theory of the role of monoamines in cerebral cortex and basal ganglia. In: Jones EG., Peters A. ed. Cerebral cortex. New York: Plenum, Vol.6, pp. 41-127.

Fallon J, Loughlin S (1995). Substantia nigra. In: Paxinos G, ed. The rat nervous system. San Diego: Academic Press, 1995, pp. 443-492.

Fannon AM, Colman DR (1996) A model for central synaptic junctional complex formation based on the differential adhesive specificities of the cadherins. Neuron 17, 423-434.

File SE, Kenny PJ, Cheeta S (2000). The role of the dorsal hippocampal serotonergic and cholinergic systems in the modulation of anxiety. Pharmacol Biochem. Behav. 66:65-72.

Filiz S, Dalcik H, Yardimoglu M, Gonca S, Ceylan S (2002). Localization of neural cell adhesion molecule (N-CAM) immunoreactivity in adult rat tissues. Biotech. Histochem. 77(3):127-35.

Fischer G, Kunemund V, Schachner M (1986) Neurite outgrowth patterns in cerebellar microexplant cultures are affected by antibodies to the cell surface glycoprotein L1. J. Neurosci 6, 605-612.

Franceschini IA, Feigenbaum-Lacombe V, Casanova P, Lopez-Lastra M, Darlix JL, Dalcq MD (2001a) Efficient gene transfer in mouse neural precursors with a bicistronic retroviral vector. J. Neurosci. Res. 65(3):208-19.

Franceschini I, Angata K, Ong E, Hong A, Doherty P and Fukuda M (2001b). Polysialyltransferase ST8Sia II (STX) polysialylates all of the major isoforms of NCAM and facilitates neurite outgrowth. Glycobiology 11:231-9.

Franceschini I, Vitry S, Padilla F, Casanova P, Tham TN, Fukuda M, Rougon G, Durbec P, Dubois-Dalcq M (2004) Migrating and myelinating potential of neural precursors engineered to overexpress PSA-NCAM. Mol. Cell. Neurosci. 2:151-62.

Francois C, Percheron G, Yelnik J (1984). Localization of nigrostriatal, nigrothalamic and nigrotectal neurons in ventricular coordinates in macaques. Neuroscience 13 (1): 61–76.

Francois C, Yelnik J, Percheron G (1987). Golgi study of the primate substantia nigra. II. Spatial organization of dendritic arborizations in relation to the cytoarchitectonic boundaries and to the striatonigral bundle. J. Comp. Neurol. 265 (4): 473–493.

Francois C, Yelnik J, Tande D, Agid Y, Hirsch EC (1999). Dopaminergic cell group A8 in the monkey: anatomical organization and projections to the striatum. J. Comp. Neurol. 414 (3): 334–347.

Fransen E, Schrander-Stumpel C, Vits L, Coucke P, van Camp G, Willems PJ (1994) X-linked hydrocephalus and MASA syndrome present in one family are due to a single missense mutation in exon 28 of the L1CAM gene. Hum. Mol. Genet. 3, 2255-2256.

Fransen E, Lemmon V, van Camp G, Vits L, Coucke P, Willems PJ (1995) CRASH syndrome: clinical spectrum of corpus callosum hypoplasia, retardation, adducted thumbs, spastic paraparesis and hydrocephalus due to mutations in one single gene, L1. Eur. J. Hum. Genet. 3, 273-284.

Fransen E, Vits L, van Camp G, Willems PJ (1996) The clinical spectrum of mutations in L1, a neuronal cell adhesion molecule. Am. J. Med. Genet. 64, 73-77.

Fransen E, van Camp G, Vits L, Willems PJ (1997) L1-associated diseases: clinical geneticists divide, molecular geneticists unite. Hum. Mol. Genet. 6, 1625-1632.

Fransen E, D'Hooge R, van Camp G, Verhoye M, Sijbers J, Reyniers E, Soriano P, Kamiguchi H, Willemsen R, Koekkoek SK, De Zeeuw CI, De Deyn PP, Van der LA, Lemmon V, Kooy RF, Willems PJ (1998) L1 knockout mice show dilated ventricles, vermis hypoplasia and impaired exploration patterns. Hum. Mol. Genet. 7, 999-1009.

Freund TF and Antal M (1988) GABA-containing neurons in the septum control inhibitory interneurons in the hippocampus. Nature 336:170-173.

Freund TF and Gulyas AI (1997) Inhibitory control of GABAergic interneurons in the hippocampus. Can. J. Physiol. Pharmacol. 75:479-487.

Fricker RA, Carpenter MK, Winkler C, Greco C, Gates MA, Bjorklund A (1999) Site-specific migration and neuronal differentiation of human neural progenitor cells after transplantation in the adult rat brain. J. Neurosci. 19:5990–6005.

Fricker-Gates RA, Muir JA, Dunnett SB (2004) Transplanted hNT cells ("LBS neurons") in a rat model of huntington's disease: good survival, incomplete diVerentiation, and limited functional recovery. Cell. Transplant. 13:123–136.

Frotscher M and Leranth C (1985) Cholinergic innervation of the rat hippocampus as revealed by choline acetyltransferase immunocytochemistry: a combined light and electron microscopic study. J. Comp. Neurol. 239:237-246.

Fuchs E, Tumbar T, Guasch G (2004) Socializing with the neighbors: stem cells and their niche. Cell 116: 769–778.

Fushiki S, Schachner M (1986) Immunocytological localization of cell adhesion molecules L1 and N-CAM and the shared carbohydrate epitope L2 during development of the mouse neocortex. Brain Res. 389, 153-167.

Fux CM, Krug M, Dityatev A, Schuster T, Schachner M (2003) NCAM180 and glutamate receptor subtypes in potentiated spine synapses: an immunogold electron microscopic study. Mol. Cell. Neurosci. 24: 939-950.

Gage FH, Ray J, Fisher LJ (1995) Isolation, characterization, and use of stem cells from the CNS. Annu. Rev. Neurosci. 18, 159–192

Gage FH (2000) Mammalian neural stem cells. Science 287, 1433–1438.

Garcion E, Halilagic A, Faissner A, ffrench-Constant C (2004) Generation of an environmental niche for neural stem cell development by the extracellular matrix molecule tenascin C. Development 131: 3423–3432.

Gaykema RP, Luiten PG, Nyakas C and Traber J (1990) Cortical projection patterns of the medial septum-diagonal band complex. J. Comp. Neurol. 293:103-124.

Gennarini G, Hirn M, Deagostini-Bazin H and Goridis C (1984a). Studies on the transmembrane disposition of the neural cell adhesion molecule N-CAM. The use of liposome-inserted radioiodinated N-CAM to study its transbilayer orientation. Eur. J. Biochem. 2;142:65-73.

Gennarini G, Rougon G, Deagostini-Bazin H, Hirn M and Goridis C (1984b). Studies on the transmembrane disposition of the neural cell adhesion molecule N-CAM. A monoclonal antibody recognizing a cytoplasmic domain and evidence for the presence of phosphoserine residues. Eur J Biochem 2;142:57-64.

Gerfen CR (1992a). The neostriatal mosaic: multiple levels of compartmental organization. Trends Neurosci. 15(4):133-9.

Gerfen CR (1992b). The neostriatal mosaic: multiple levels of compartmental organization in the basal ganglia. Annu. Rev. Neurosci..15:285-320.

Gerfen CR, Herkenham M, Thibault J (1987a). The neostriatal mosaic: II. Patch- and matrix-directed mesostriatal dopaminergic and non-dopaminergic systems. J. Neurosci. (12):3915-34.

Gerfen CR, Herkenham M, Thibault J (1987b). The neostriatal mosaic: II. Patch- and matrix-directed mesostriatal dopaminergic and non-dopaminergic systems. J. Neurosci. (12):3915-34.

Gerfen CR, Engber TM, Mahan LC, Susel Z, Chase TN, Monsma FJ Jr, Sibley DR (1990). D1 and D2 dopamine receptor-regulated gene expression of striatonigral and striatopallidal neurons. Science. 250(4986):1429-32.

Gerfen CR, McGinty JF, Young WS 3rd (1991). Dopamine differentially regulates dynorphin, substance P, and enkephalin expression in striatal neurons: in situ hybridization histochemical analysis. J. Neurosci. 11(4):1016-31.

Glaser T, Pollard SM, Smith A, Brüstle O (2007) Tripotential differentiation of adherently expandable neural stem (NS) cells. PLoS ONE. 2(3):e298.

Goodman CS, Shatz CJ (1993) Developmental mechanisms that generate precise patterns of neuronal connectivity. Cell 72 Suppl, 77-98.

Gold PE (2003) Acetylcholine modulation of neural systems involved in learning and memory. Neurobiol. Learn. Mem. 80:194-210.

Gordon EM, Anderson WF (1994) Gene therapy using retroviral vectors. Curr. Opin. Biotechnol. (6):611-6.

Gordon T, Hegedus J, Tam SL (2004) Adaptive and maladaptive motor axonal sprouting in aging and motoneuron disease. Neurol. Res. 26:174-185.

Gordon-Weeks PR, Fischer I (2000) MAP1B expression and microtubule stability in growing and regenerating axons. Microsc. Res. Tech. 48, 63-74.

Götz M (2003) Glial cells generate neurons--master control within CNS regions: developmental perspectives on neural stem cells. Neuroscientist. 5:379-97.

Gould E, Reeves A.J, Graziano M.S, Gross C.G (1999) Neurogenesis in the neocortex of adult primates. Science 286 (5439):548-552.

Graeff, F. G., Guimaraes, F. S., De Andrade, T. G., and Deakin, J. F. (1996). Role of 5-HT in stress, anxiety, and depression. Pharmacol. Biochem. Behav. 54, 129-141.

Grace AA, Onn SP (1989). Morphology and electrophysiological properties of immunocytochemically identified rat dopamine neurons recorded *in vitro*. J. Neurosci. 10:3463-81.

Granholm AC, Srivastava N, Mott JL, Henry S, Henry M, Westphal H, Pichel JG, Shen L, Hoffer BJ (1997) Morphological alterations in the peripheral and central nervous systems of mice lacking glial cell line-derived neurotrophic factor (GDNF): immunohistochemical studies. J Neurosci 17:1168-1178.

Gresch O, Engel FB, Nesic D, Tran TT, England HM, Hickman ES, Körner I, Gan L, Chen S, Castro-Obregon S, Hammermann R, Wolf J, Müller-Hartmann H, Nix M, Siebenkotten G, Kraus G, Lun K (2004) New non-viral method for gene transfer into primary cells. Methods 33(2):151-63.

Gritti A, Parati EA, Cova L, Frolichsthal P, Galli R, Wanke E, Faravelli L, Morassutti DJ, Roisen F, Nickel DD, Vescovi AL (1996) Multipotential stem cells from the adult mouse brain proliferate and self-renew in response to basic fibroblast growth factor. J. Neurosci. 16(3): 1091–1100.

Gritti A, Frolichsthal-Schoeller P, Galli R, Parati EA, Cova L, Pagano SF, Bjornson CR, Vescovi AL (1999) Epidermal and fibroblast growth factors behave as mitogenic regulators for a single multipotent stem cell-like population from the subventricular region of the adult mouse forebrain. J. Neurosci. 19(9): 3287–3297.

Gundersen HJ (1986) Stereology of arbitrary particles. A review of unbiased number and size estimators and the presentation of some new ones, in memory of William R. Thompson. J. Microsc. 143: 3-45.

Gubkina O, Cremer H and Rougon G.(2001). Mutation in the neural cell adhesion molecule interferes with the differentiation of anterior pituitary secretory cells. Neuroendocrinology 74:335-46.

Haas SJP, Ahrens A, Petrov S, Schmitt O, Wree A (2004) Quinolinic acid lesions of the caudate putamen in the rat lead to a local increase of ciliary neurotrophic factor. J. Anatomy 204:271–281.

Haines AM, Irvine AS, Mountain A, Charlesworth J, Farrow NA, Husain RD, Hyde H, Ketteringham H, McDermott RH, Mulcahy AF, Mustoe TL, Reid SC, Rouquette M, Shaw JC, Thatcher DR, Welsh JH, Williams DE, Zauner W, Phillips RO (2001) CL22 - a novel cationic peptide for efficient transfection of mammalian cells. Gene Ther. 2:99-110.

Hajos M, Greenfield SA (1993). Topographic heterogeneity of substantia nigra neurons: diversity in intrinsic membrane properties and synaptic inputs. Neuroscience. 55(4):919-34.

Hajos M, Greenfield SA (1994). Synaptic connections between pars compacta and pars reticulata neurones: electrophysiological evidence for functional modules within the substantia nigra. Brain Res. 660 (2): 216–224.

Halliday GM, Tork I (1986). Comparative anatomy of the ventromedial mesencephalic tegmentum in the rat, cat, monkey and human. J. Comp. Neurol. 252(4): 423-45.

Halliday J, Chow CW, Wallace D, Danks DM (1986) X linked hydrocephalus: a survey of a 20 year period in Victoria, Australia. J. Med. Genet. 23, 23-31.

Hamm A, Krott N, Breibach I, Blindt R, Bosserhoff AK (2002) Efficient transfection method for primary cells. Tissue Eng. 8(2):235-45.

Hammang JP, Archer DR, Duncan ID (1997) Myelination following transplantation of EGF-responsive neural stem cells into a myelin-deficient environment. Exp. Neurol. 147:84–95.

Hammond MS, Sims C, Parameshwaran K, Suppiramaniam V, Schachner M, Dityatev A (2006) Neural cell adhesion molecule-associated polysialic acid inhibits NR2B-containing N-methyl-D-aspartate receptors and prevents glutamate-induced cell death. J. Biol. Chem. 2006 Nov 17;281(46):34859-69. Epub 2006 Sep 20.

Haney CA, Sahenk Z, Li C, Lemmon VP, Roder J, Trapp BD (1999) Heterophilic binding of L1 on unmyelinated sensory axons mediates Schwann cell adhesion and is required for axonal survival. J. Cell. Biol. 146, 1173-1184.

Hattori T, Takada M, Moriizumi T, Van der Kooy D (1991). Single dopaminergic nigrostriatal neurons form two chemically distinct synaptic types: possible transmitter segregation within neurons. J. Comp. Neurol. 309(3):391-401.

Heimer L, Wilson RD (1975). The subcortical projections of allocortex: Similarities in the neural associations of the hippocampus, the piriform cortex and the neocortex. In Santini M: Golgi Centenniel Symposium Proceedeng. New York: Raven, pp.177-193.

Heins N, Malatesta P, Cecconi F, Nakafuku M, Tucker KL, Hack MA, Chapouton P, Barde YA, Götz M (2002) Glial cells generate neurons: the role of the transcription factor Pax6. Nat. Neurosci. 4:308-15.

Hikosaka O, Wurtz RH (1983). Visual and oculomotor functions of monkey substantia nigra pars reticulata. I to IV. J. Neurophysiol. 49 (5): 1230–1301.

Hlavin ML, Lemmon V (1991) Molecular structure and functional testing of human L1CAM: an interspecies comparison. Genomics 11, 416-423.

Holm PC, Rodriguez FJ, Kresse A, Canals JM, Silos-Santiago I, Arenas E (2003) Crucial role of TrkB ligands in the survival and phenotypic differentiation of developing locus coeruleus noradrenergic neurons. Development 130:3535-3545.

Holst BD, Vanderklish PW, Krushel LA, Zhou W, Langdon RB, McWhirter JR, Edelman GM, Crossin KL (1998) Allosteric modulation of AMPA-type glutamate receptors increases activity of the promoter for the neural cell adhesion molecule, N-CAM. Proc. Natl. Sci .USA 95: 2597-2602.

Hopkins WF, Johnston D (1988) Noradrenergic enhancement of long-term potentiation at mossy fiber synapses in the hippocampus. J Neurophysiol 59: 667-687.

Hortsch M (1996). The L1 family of neural cell adhesion molecules: old proteins performing new tricks. Neuron 17, 587-593.

Hortsch M (2000) Structural and functional evolution of the L1 family: are four adhesion molecules better than one? Mol.Cell. Neurosci. 15, 1-10.

Howard CV, Reed MG (1998) Unbiased Stereology. Three-Dimensional Measurement in Microscopy. BIOS Scientific Publishers, Oxford.

Huang L.B., Lim R (1990) Identification of injuryinduced mitotic cells in adult rat cerebral cortex by neuron-specific markers. Brain. Res.Dev.Brain. Res. 51 (1):123-127.

Huh KH, Fuhrer C (2002) Clustering of nicotinic acetylcholine receptors: from the neuromuscular junction to interneuronal synapses. Mol. Neurobiol. 25:79-112.

Hurelbrink CB, Armstrong RJ, Dunnett SB, Rosser AE, Barker RA (2002) Neural cells from primary human striatal xenografts migrate extensively in the adult rat CNS. Eur. J. Neurosci. 15:1255–1266.

Iacovelli L, Fulceri F, De Blasi A, Nicoletti F, Ruggieri S, Fornai F (2006) The neurotoxicity of amphetamines: bridging drugs of abuse and neurodegenerative disorders. Exp. Neurol. 201(1):24-31. Epub 2006 May 5.

Irintchev A, Salvini TF, Faissner A, Wernig A (1993) Differential expression of tenascin after denervation, damage or paralysis of mouse soleus muscle. J. Neurocytol. 22:955--965.

Irintchev A, Zeschnigk M, Starzinski-Powitz A, Wernig A (1994) Expression pattern of M-cadherin in normal, denervated, and regenerating mouse muscles. Dev. Dyn. 199:326-337.

Irintchev A, Rosenblatt JD, Cullen MJ, Zweyer M, Wernig A (1998) Ectopic skeletal muscles derived from myoblasts implanted under the skin. J .Cell. Sci. 111:3287- 3297.

Irintchev A, Koch M, Needham LK, Maness P and Schachner M (2004) Impairment of sensorimotor gating in mice deficient in the cell adhesion molecule L1 or its close homologue, CHL1. Brain Res. 1029: 131-134.

Irintchev A, Rollenhagen A, Troncoso E, Kiss JZ, Schachner M (2005) Structural and functional aberrations in the cerebral cortex of tenascin-C deficient mice. Cereb. Cortex 15: 950-962.

Irvine AS, Trinder PK, Laughton DL, Ketteringham H, McDermott RH, Reid SC, Haines AM, Amir A, Husain R, Doshi R, Young LS, Mountain A (2000) Efficient nonviral transfection of dendritic cells and their use for *in vivo* immunization. Nat Biotechnol. 12:1273-8.

Isacson O, Fischer W, Wictorin K, Dawbarn D, Bjorklund A (1987) Astroglial response in the excitotoxically lesioned neostriatum and its projection areas in the rat. Neuroscience 20:1043–1056.

Itoh K, Sakurai Y, Asou H, Umeda M (2000) Differential expression of alternatively spliced neural cell adhesion molecule L1 isoforms during oligodendrocyte maturation. J. Neurosci. Res. 60, 579-586.

Jakab RL and Leranth C. (1995) Septum. In: Paxinos G, ed. The rat nervous system. San Diego: Academic Press 405-442.

Johansson CB, Momma S, Clarke DL, Risling M, Lendahl U, Frisén J (1999a) Identification of a neural stem cell in the adult mammalian central nervous system. Cell 96: 25–34.

Johansson C.B, Svensson M, Wallstedt L, Janson A.M, Frisen J (1999b) Neural stem cells in the adult human brain. Exp.Cell. Res. 253 (2):733-736.

Johe KK, Hazel TG, Muller T, Dugich-Djordjevic MM, McKay RD (1996) Single factors direct the differentiation of stem cells from the fetal and adult central nervous system. Genes Dev. 10: 3129–3140.

Jooss K, Yang Y, Fisher KJ, Wilson JM (1998) Transduction of dendritic cells by DNA viral vectors directs the immune response to transgene products in muscle fiber. J. Virol. 72(5):4212-23.

Jouet M, Rosenthal A, Armstrong G, MacFarlane J, Stevenson R, Paterson J, Metzenberg A, Ionasescu V, Temple K, Kenwrick S (1994) X-linked spastic paraplegia (SPG1), MASA syndrome and X-linked hydrocephalus result from mutations in the L1 gene. Nat. Genet. 7, 402-407.

Jouet M, Rosenthal A, Kenwrick S (1995) Exon 2 of the gene for neural cell adhesion molecule L1 is alternatively spliced in B cells. Mol. Brain. Res. 30, 378-380.

Juliano RL (2002) Signal transduction by cell adhesion receptors and the cytoskeleton: functions of integrins, cadherins, selectins, and immunoglobulin-superfamily members. Annu. Rev. Pharmacol. Toxicol. 42, 283-323.

Kalivas PW (1993). Neurotransmitter regulation of dopamine neurons in the ventral tegmental area. Brain Res. Brain Res. Rev. 18(1):75-113.

Kallunki P, Edelman GM, Jones FS (1997) Tissue-specific expression of the L1 cell adhesion molecule is modulated by the neural restrictive silencer element. J.Cell.Biol. 138, 1343-1354.

Kalyani A, Hobson K, Rao M.S (1997) Neuroepithelial stem cells from the embryonic spinal cord: isolation, characterization, and clonal analysis. Dev.Biol. 186 (2):202-223.

Kamiguchi H, Long KE, Pendergast M, Schaefer AW, Rapoport I, Kirchhausen T, Lemmon V (1998) The neural cell adhesion molecule L1 interacts with the AP-2 adaptor and is endocytosed via the clathrin-mediated pathway. J. Neurosci 18, 5311-5321.

Kanda T, Iwasaki T, Nakamura S, Kurokawa T, Ikeda K, Mizusawa H (2000) Self-secretion of fibroblast growth factor-9 supports basal forebrain cholinergic neurons in an autocrine/paracrine manner. Brain Res. 876:22-30.

Kaplan M.S and Hinds J.W (1977) Neurogenesis in the adult rat: electron microscopic analysis of light radioautographs. Science 197 (4308):1092-1094.

Kaplan M.S (1981) Neurogenesis in the 3-month-old rat visual cortex. J.Comp. Neurol. 195 (2):323-338.

Kaplan P (1983) X linked recessive inheritance of agenesis of the corpus callosum 5. J. Med. Genet. 20, 122-124.

Kater SB, Rehder V (1995) The sensory-motor role of growth cone filopodia. Curr. Opin. Neurobiol. 5, 68-74.

Kenwrick S, Ionasescu V, Ionasescu G, Searby C, King A, Dubowitz M, Davies KE (1986) Linkage studies of X-linked recessive spastic paraplegia using DNA probes. Hum. Genet. 73, 264-266.

Kenwrick S, Watkins A, De Angelis E (2000). Neural cell recognition molecule L1: relating biological complexity to human disease mutations. Hum.Mol.Genet. 9, 879-886.

Kilpatrick TJ, Bartlett PF (1993) Cloning and growth of multipotential neural precursors: requirements for proliferation and differentiation. Neuron 10: 255–265.

Kim YC, Shim JW, Oh YJ, Son H, Lee YS, Lee SH (2002) Co-transfection with cDNA encoding the Bcl family of anti-apoptotic proteins improves the efficiency of transfection in primary fetal neural stem cells. J. Neurosci. Methods. 117(2):153-8.

Kim JH, Lee JH, Park JY, Park CH, Yun CO, Lee SH, Lee YS, Son H (2005) Retrovirally transduced NCAM140 facilitates neuronal fate choice of hippocampal progenitor cells. J. Neurochem. 94: 417-424.

Kim SU, Park IH, Kim TH, Kim KS, Choi HB, Hong SH, Bang JH, Lee MA, Joo IS, Lee CS, Kim YS (2006) Brain transplantation of human neural stem cells transduced with tyrosine hydroxylase and GTP cyclohydrolase 1 provides functional improvement in animal models of Parkinson disease. Neuropathology 26:129–40.

Kiss JZ, Troncoso E, Djebbara Z, Vutskits L and Muller D.(2001). The role of neural cell adhesion molecules in plasticity and repair. Brain Res. Rev. 36:175-84.

Kitai ST, Sugimori M, Kocsis JD (1976). Excitatory nature of dopamine in the nigro-caudate pathway. Exp. Brain Res. 24(4):351-63.

Kohl A, Giese KP, Mohajeri MH, Montag D, Moos M, Schachner M (1992) Analysis of promoter activity and 5' genomic structure of the neural cell adhesion molecule L1. J.Neurosci.Res. 32, 167-177.

Koido S, Hara E, Homma S, Torii A, Toyama Y, Kawahara H, Watanabe M, Yanaga K, Fujise K, Tajiri H, Gong J, Toda G (2005) Dendritic cells fused with allogeneic colorectal cancer cell line present multiple colorectal cancer-specific antigens and induce antitumor immunity against autologous tumor cells. Clin. Cancer Res. 11(21):7891-900.

Koido S, Hara E, Homma S, Torii A, Mitsunaga M, Yanagisawa S, Toyama Y, Kawahara H, Watanabe M, Yoshida S, Kobayashi S, Yanaga K, Fujise K, Tajiri H (2007) Streptococcal preparation OK-432 promotes fusion efficiency and enhances induction of antigen-specific CTL by fusions of dendritic cells and colorectal cancer cells. J. Immunol. 178(1):613-22.

Konopacki J, Maciver MB, Bland BH and Roth SH (1987) Theta in hippocampal slices: relation to synaptic responses of dentate neurons. Brain . Bull. 18:25-27.

Kordower JH, Mufson EJ, Fox N, Martel L, Emerich DF (1997) Cellular delivery of NGF does not alter the expression of beta-amyloid immunoreactivity in young or aged nonhuman primates. Exp. Neurol. 145(2 Pt 1):586-91.

Kornblihtt AR, Umezawa K, Vibe-Pedersen K, Baralle FE (1985) Primary structure of human fibronectin: differential splicing may generate at least 10 polypeptides from a single gene. EMBO J 4: 1755-1759.

Kowitz A, Kadmon G, Eckert M, Schirrmacher V, Schachner M, Altevogt P (1992) Expression and function of the neural cell adhesion molecule L1 in mouse leukocytes. Eur.J.Immunol. 22, 1199-1205.

Kramis R, Vanderwolf CH and Bland BH (1975) Two types of hippocampal rhythmical slow activity in both the rabbit and the rat: relations to behavior and effects of atropine, diethyl ether, urethane, and pentobarbital. Exp. Neurol. 49:58-85.

Kruse J, Mailhammer R, Wernecke H, Faissner A, Sommer I, Goridis C, Schachner M (1984) Neural cell adhesion molecules and myelin-associated glycoprotein share a common carbohydrate moiety recognized by monoclonal antibodies L2 and HNK-1. Nature 311: 153-155.

Kujat R, Miragall F, Krause D, Dermietzel R, Wrobel KH (1995) Immunolocalization of the neural cell adhesion molecule L1 in non- proliferating epithelial cells of the male urogenital tract. Histochem. Cell. Biol. 103, 311-321.

Kumamoto N, Matsuzaki S, Inoue K, Hattori T, Shimizu S, Hashimoto R, Yamatodani A, Katayama T, Tohyama M (2006) Hyperactivation of midbrain dopaminergic system in schizophrenia could be attributed to the down-regulation of dysbindin. Biochem Biophys Res Commun. 30; 345(2):904-9. Epub 2006 May 6.

Kunz S, Spirig M, Ginsburg C, Buchstaller A, Berger P, Lanz R, Rader C, Vogt L, Kunz B, Sonderegger P (1998) Neurite fasciculation mediated by complexes of axonin-1 and Ng cell adhesion molecule. J. Cell. Biol. 143, 1673-1690.

Laeng P, Molthagen M, Yu EG, Bartsch U (1996) Transplantation of oligodendrocyte progenitor cells into the rat retina: extensive myelination of retinal ganglion cell axons. Glia 18: 200-210.

Laemmli (1970) Cleavage of structural proteins during the assembly of the head of bacteriophage T4. Nature, 227(5259), 680-685.

Lagenaur C, Lemmon V (1987) An L1-like molecule, the 8D9 antigen, is a potent substrate for neurite extension. Proc. Natl. Acad. Sci. U S A 84, 7753-7757.

Lakshmipathy U, Pelacho B, Sudo K, Linehan JL, Coucouvanis E, Kaufman DS, Verfaillie CM (2004) Efficient transfection of embryonic and adult stem cells. Stem Cells 22(4):531-43.

Landmesser L, Dahm L, Schultz K, Rutishauser U (1988) Distinct roles for adhesion molecules during innervation of embryonic chick muscle. Dev. Biol. 103: 645-670.

Langer LF, Jimenez-Castellanos J, Graybiel AM (1991). The substantia nigra and its relations with the striatum in the monkey. Prog. Brain Res. 87: 81-99.

Lahrtz F, Horstkorte R, Cremer H, Schachner M and Montag D.(1997). VASEencoded peptide modifies NCAM- and L1-mediated neurite outgrowth. J. Neurosci. Res. 1;50:62-8.

Lauterbach EC (1996) Bipolar disorders, dystonia, and compulsion after dysfunction of the cerebellum, dentatorubrothalamic tract, and substantia nigra. Biol Psychiatry. 15;40(8):726-30.

Lavoie B, Smith Y, Parent A (1989). Dopaminergic innervation of the basal ganglia in the squirrel monkey as revealed by tyrosine hydroxylase immunohistochemistry. J. Comp. Neurol. 289(1): 36–52.

Lee MG, Chrobak JJ, Sik A, Wiley RG and Buzsaki G (1994) Hippocampal theta activity following selective lesion of the septal cholinergic system. Neuroscience 62:1033-1047.

Lee TH, Ellinwood EH Jr, Einstein G (1992). Intracellular recording from dopamine neurons in the substantia nigra: double labelling for identification of projection site and morphological features. J. Neurosci. Methods. 43(2-3):119-27.

Lenz P, Bacot SM, Frazier-Jessen MR, Feldman GM (2003) Nucleoporation of dendritic cells: efficient gene transfer by electroporation into human monocyte-derived dendritic cells FEBS Lett. 538(1-3):149-54.

Leung LS, Martin LA and Stewart DJ (1994) Hippocampal theta rhythm in behaving rats following ibotenic acid lesion of the septum. Hippocampus 4:136-147.

Li XJ (1999) The early cellular pathology of Huntington's disease. Mol. Neurobiol. 20:111–124.

Li L, Xie T (2005) Stem cell niche: structure and function. Annu. Rev. Cell. Dev. Biol. 21: 605–631.

Li QJ, Tang YM, Liu J, Zhou DY, Li XP, Xiao SH, Jian DX, Xing YG (2007) Treatment of Parkinson disease with C17.2 neural stem cells overexpressing NURR1 with a recombined republic-deficit adenovirus containing the NURR1 gene. Synapse. 61(12):971-7.

Lindner J, Rathjen FG, Schachner M (1983) L1 mono- and polyclonal antibodies modify cell migration in early postnatal mouse cerebellum. Nature 305, 427-430.

Linke R, Schwegler H and Boldyreva M (1994) Cholinergic and GABAergic septo-hippocampal projection neurons in mice: a retrograde tracing study combined with double immunocytochemistry for choline acetyltransferase and parvalbumin. Brain Res. 653:73 - 80.

Llinas R, Greenfield SA, Jahnsen H (1984). Electrophysiology of pars compacta cells in the *in vitro* substantia nigra--a possible mechanism for dendritic release. Brain Res. 294(1):127-32.

Loeffler M, Bratke T, Paulus U, Li Y. Q, Potten C.S (1997) Clonality and life cycles of intestinal crypts explained by a state dependent stochastic model of epithelial stem cell organization. J.Theor.Biol. 186 (1):41-54.

Lois C, Alvarez-Buylla A (1993) Proliferating subventricular zone cells in the adult mammalian forebrain can differentiate into neurons and glia. Proc. Natl. Acad. Sci. USA 90, 2074–2077.

Lois C, Alvarez-Buylla A (1994) Long-distance neuronal migration in the adult mammalian brain. Science 264 (5162):1145-1148.

Loudes C, Rougon G, Kordon C, Faivre-Bauman A (1997) Polysialylated neural cell adhesion is involved in target-induced morphological differentiation of arcuate dopaminergic neurons. Eur. J. Neurosci. 9:2323-2333.

Lu D, Benjamin R, Kim M, Conry RM, Curiel DT (1994) Optimization of methods to achieve mRNA-mediated transfection of tumor cells *in vitro* and *in vivo* employing cationic liposome vectors. Cancer Gene Ther. (4):245-52.

Lundberg C, MartinezSerrano A, Cattaneo E, Mckay RDG, Bjorklund A (1997) Survival, integration, and differentiation of neural stem cell lines after transplantation to the adult rat striatum. Exp. Neurol. 145:342–360.

Luskin M.B (1993) Restricted proliferation and migration of postnatally generated neurons derived from the forebrain subventricular zone. Neuron 11 (1):173-189.

Luthi A, Laurent JP, Figurov A, Muller D, Schachner M (1994) Hippocampal long-term potentiation and neural cell adhesion molecules L1 and NCAM. Nature 372, 777-779.

Luthi A, Mohajeri H, Schachner M, Laurent JP (1996) Reduction of hippocampal long-term potentiation in transgenic mice ectopically expressing the neural cell adhesion molecule L1 in astrocytes. J. Neurosci. Res. 46, 1-6.

Maasho K, Marusina A, Reynolds NM, Coligan JE, Borrego F (2004) Efficient gene transfer into the human natural killer cell line, NKL, using the Amaxa nucleofection system. J. Immunol. Methods. 284(1-2):133-40.

Mangiarini L, Sathasivam K, Seller M, Cozens B, Harper A, Hetherington C, Lawton M, Trottier Y, Lehrach H, Davies S, Bates G (1996) Exon 1 of the HD gene with an expanded CAG repeat is sufficient to cause a progressive neurological phenotype in transgenic mice. Cell 87:493–506.

Martinet W, Schrijvers DM, Kockx MM (2003) Nucleofection as an efficient nonviral transfection method for human monocytic cells. Biotechnol. Lett. 25(13):1025-9.

Martinez-Serrano A, Björklund A (1996) Protection of the neostriatum against excitotoxic damage by neurotrophin-producing, genetically modified neural stem cells. J. Neurosci. 16(15):4604-16.

Martini R, Schachner M (1986) Immunoelectron microscopic localization of neural cell adhesion molecules (L1, N-CAM, and MAG) and their shared carbohydrate epitope and myelin basic protein in developing sciatic nerve. J. Cell. Biol. 103, 2439-2448.

Martini R, Schachner M (1988) Immunoelectron microscopic localization of neural cell adhesion molecules (L1, N-CAM, and myelin-associated glycoprotein) in regenerating adult mouse sciatic nerve. J. Cell. Biol .106, 1735-1746.

Marty S, Dusart I, Peschanski M (1991) Glial changes following an excitotoxic lesion in the CNS—I. Microglia/macrophages. Neuroscience 45:529–539.

McBride JL, Behrstock SP, Chen EY, Jakel RJ, Siegel I, Svendsen CN, Kordower JH (2004) Human neural stem cell transplants improve motor function in a rat model of Huntington's disease. J. Comp. Neurol. 475:211–219.

McCormick SE, Stoessl AJ (2002) Blockade of nigral and pallidal opioid receptors suppresses vacuous chewing movements in a rodent model of tardive dyskinesia. Neuroscience 112(4):851-9.

McKay R (1997) Stem cells in the central nervous system. Science 276, 66–71.

Meli ML, Carrel F, Waibel R, Amstutz H, Crompton N, Jaussi R, Moch H, Schubiger PA, Novak-Hofer I (1999) Anti-neuroblastoma antibody chCE7 binds to an isoform of L1-CAM present in renal carcinoma cells. Int. J. Cancer 83, 401-408.

Meng XL, Shen JS, Ohashi T, Maeda H, Kim SU, Eto Y (2003) Brain transplantation of genetically engineered human neural stem cells globally corrects brain lesions in mucopolysaccharidosis VII mice. J. Neurosci. Res.74:266–77.

Mesulam MM, Mufson EJ, Wainer BH and Levey AI (1983) Central cholinergic pathways in the rat: an overview based on an alternative nomenclature (Ch1-Ch6). Neuroscience 10:1185- 1201.

Miller P.D., Chung,W.W., Lagenaur,C.F., and DeKosky,S.T. (1993). Regional distribution of neural cell adhesion molecule (N-CAM) and L1 in human and rodent hippocampus. J. Comp. Neurol. 327, 341-349.

Milner TA and Amaral DG (1984) Evidence for a ventral septal projection to the hippocampal formation of the rat. Exp. Brain. Res. 55:579-585.

Mincheff M, Altankova I, Zoubak S, Tchakarov S, Botev C, Petrov S, Krusteva E, Kurteva G, Kurtev P, Dimitrov V, Ilieva M, Georgiev G, Lissitchkov T, Chernozemski I, Meryman HT (2001) *In vivo* transfection and/or cross-priming of dendritic cells following DNA and adenoviral immunizations for immunotherapy of cancer--changes in peripheral mononuclear subsets and intracellular IL-4 and IFN-gamma lymphokine profile. Crit. Rev. Oncol. Hematol. 39(1-2):125-32.

Mitchell IJ, Cooper AC, Griffiths MR, Cooper AJ (2002) Acute administration of haloperidol induces apoptosis of neurones in the striatum and substantia nigra in the rat. Neuroscience 109(1):89-99.

Miura M, Kobayashi M, Asou H, Uyemura K (1991) Molecular cloning of cDNA encoding the rat neural cell adhesion molecule L1. Two L1 isoforms in the cytoplasmic region are produced by differential splicing. FEBS Lett. 289, 91-95.

Mizuno K, Carnahan J, Nawa H (1994) Brain-derived neurotrophic factor promotes diVerentiation of striatal GABAergic neurons. Dev. Biol. 165:243–256.

Monmaur P and Breton P (1991) Elicitation of hippocampal theta by intraseptal carbachol injection in freely moving rats. Brain Res. 544:150-155.

Moore SE and Walsh FS (1986). Nerve dependent regulation of neural cell adhesion molecule expression in skeletal muscle. Neuroscience 18:499-505.

Moos M, Tacke R, Scherer H, Teplow D, Fruh K, Schachner M (1988) Neural adhesion molecule L1 as a member of the immunoglobulin superfamily with binding domains similar to fibronectin. Nature 334, 701-703.

Morris RG, Garrud P, Rawlins JN and Keefe O (1982) Place navigation impaired in rats with hippocampal lesions. Nature 297:681-683.

Morrison SJ, Shah NM, Anderson DJ (1997a) Regulatory mechanisms in stem cell biology. Cell 88: 287–298.

Morrison S.J, Wright D.E, Cheshier S.H, Weissman I.L(1997b). Hematopoietic stem cells: challenges to expectations. Curr.Opin.Immunol. 9 (2):216-221.

Morshead CM, Benveniste P, Iscove NN, van der Kooy D (2002) Hematopoietic competence is a rare property of neural stem cells that may depend on genetic and epigenetic alterations. Nat Med 8: 268–273.

Moya GE, Michaelis RC, Holloway LW, Sanchez JM (2002) Prenatal Diagnosis of L1 Cell Adhesion Molecule Mutations. capabilities and limitations. Fetal. Diagn. Ther. 17, 115-119.

Mueller HT, Haroutunian V, Davis KL, Meador-Woodruff JH (2004) Expression of the ionotropic glutamate receptor subunits and NMDA receptor-associated intracellular proteins in the substantia nigra in schizophrenia Brain Res. Mol. Brain Res. 5;121(1-2):60-9.

Muller D, Wang C, Skibo G, Toni N, Cremer H, Calaora V, Rougon G, Kiss JZ (1996) PSA-NCAM is required for activity-induced synaptic plasticity. Neuron 17: 413-422.

Muller D, Djebbara-Hannas Z, Jourdain P, Vutskits L, Durbec P, Rougon G, Kiss JZ. (2000) Brain-derived neurotrophic factor restores long-term potentiation in polysialic acid-neural cell adhesion molecule-deficient hippocampus. Proc. Natl. Acad. Sci. USA 97: 4315-4320.

Murer MG, Yan Q, Raisman-Vozari R (2001) Brain-derived neurotrophic factor in the control human brain, and in Alzheimer's disease and Parkinson's disease. Prog. Neurobiol. 63:71-124.

Murray GK, Corlett PR, Clark L, Pessiglione M, Blackwell AD, Honey G, Jones PB, Bullmore ET, Robbins TW, Fletcher PC (2007) Substantia nigra/ventral tegmental reward prediction error disruption in psychosis. Mol. Psychiatry. Aug 7.

Nakao N, Brundin P, Funa K, Lindvall O, Odin P (1995) Trophic and protective actions of brain-derived neurotrophic factor on striatal DARPP-32-containing neurons *in vitro*. Brain Res. Dev. Brain Res. 90:92–101.

Nedergaard S, Greenfield SA (1992). Sub-populations of pars compacta neurons in the substantia nigra: the significance of qualitatively and quantitatively distinct conductances. Neuroscience. 48(2):423-37.

Neugebauer KM, Tomaselli KJ, Lilien J and Reichardt LF.(1988). N-cadherin, NCAM, and integrins promote retinal neurite outgrowth on astrocytes *in vitro*. J. Cell Biol. 107:1177-8

Niethammer P, Delling M, Sytnyk V, Dityatev A, Fukami K, Schachner M (2002) Cosignaling of NCAM via lipid rafts and the FGF receptor is required for neuritogenesis. J. Cell Biol. 157: 521-532.

Nikonenko AG, Sun M, Lepsveridze E, Apostolova I, Petrova I, Irintchev A, Dityatev A, Schachner M. (2006) Enhanced perisomatic inhibition and impaired long-term potentiation in the CA1 region of juvenile CHL1 deficient mice. Eur J Neurosci 23: 1839-1852.

Nishimune H, Bernreuther C, Carroll P, Chen S, Schachner M, Henderson CE (2005) Neural adhesion molecules L1 and CHL1 are survival factors for motoneurons. J. Neurosci. Res. 80, 593-599.

Nguyen C, Mattei MG, Mattei JF, Santoni MJ, Goridis C and Jordan BR (1986). Localization of the human NCAM gene to band q23 of chromosome 11: the third gene coding for a cell interaction molecule mapped to the distal portion of the long arm of chromosome 11. J. Cell Biol. 102:711-5.

Nolte C, Moos M, Schachner M (1999) Immunolocalization of the neural cell adhesion molecule L1 in epithelia of rodents. Cell. Tissue. Res .298, 261-273.

Ohki EC, Tilkins ML, Ciccarone VC, Price PJ (2001) Improving the transfection efficiency of post-mitotic neurons. J. Neurosci. Methods. 112(2):95-9.

Ojima T, Iwahashi M, Nakamura M, Matsuda K, Naka T, Nakamori M, Ueda K, Ishida K, Yamaue H (2006) The boosting effect of co-transduction with cytokine genes on cancer vaccine therapy using genetically modified dendritic cells expressing tumor-associated antigen. Int. J. Oncol. (4):947-53.

Okabe M, Ikawa M, Kominami K, Nakanishi T, Nishimune Y, (1997) "Green Mice" as a source of ubiquitous green cells, FEBS Lett. 407, 313-319.

Okada T, Caplen NJ, Ramsey WJ, Onodera M, Shimazaki K, Nomoto T, Ajalli R, Wildner O, Morris J, Kume A, Hamada H, Blaese RM, Ozawa K (2004) In situ generation of pseudotyped retroviral progeny by adenovirus-mediated transduction of tumor cells enhances the killing effect of HSV-tk suicide gene therapy *in vitro* and *in vivo*. J. Gene Med. (3):288-99.

Ong E, Nakayama J, Angata K, Reyes L, Katsuyama T, Arai Y and Fukuda M(1998). Developmental regulation of polysialic acid synthesis in mouse directed by two polysialyltransferases, PST and STX. Glycobiology 8:415-24.

Ono K, Tomasiewicz H, Magnuson T, and Rutishauser U (1994). N-CAM mutation inhibits tangential neuronal migration and is phenocopied by enzymatic removal of polysialic acid. Neuron 13: 595-609.

Orr HT, Lancet D, Robb RJ, Lopez de Castro JA, Strominger JL (1979) The heavy chain of human histocompatibility antigen HLA-B7 contains an immunoglobulin-like region. Nature 282, 266-270.

Palmer TD, Ray J, Gage FH (1995) FGF-2-responsive neuronal progenitors reside in proliferative and quiescent regions of the adult rodent brain. Mol. Cell. Neurosci. 6, 474–486.

Palmer TD, Takahashi J, Gage FH (1997) The adult rat hippocampus contains primordial neural stem cells. Mol. Cell Neurosci. 8: 389–404.

Palmer TD, Markakis EA, Willhoite AR, Safar F, Gage FH (1999) Fibroblast growth factor-2 activates a latent neurogenic program in neural stem cells from diverse regions of the adult CNS. J. Neurosci. 19, 8487–8497.

Paratcha G, Ledda F, Ibanez CF (2003) The neural cell adhesion molecule NCAM is an alternative signaling receptor for GDNF family ligands. Cell 113: 867-879.

Payne HR, Burden SM, Lemmon V (1992) Modulation of growth cone morphology by substrate-bound adhesion molecules. Cell. Motil. Cytoskeleton. 21, 65-73.

Pereda A, Triller A, Korn H, Faber DS (1992). Dopamine enhances both electrotonic coupling and chemical excitatory postsynaptic potentials at mixed synapses. Proc. Natl. Acad. Sci. U S A. 89(24):12088-92.

Perez-Navarro E, Canudas AM, Akerund P, Alberch J, Arenas E (2000) Brain-derived neurotrophic factor, neurotrophin-3, and neurotrophin-4/5 prevent the death of striatal projection neurons in a rodent model of Huntington's disease. J. Neurochem. 75:2190–2199.

Perrin FE, Rathjen FG, Stoeckli ET (2001) Distinct subpopulations of sensory afferents require F11 or axonin-1 for growth to their target layers within the spinal cord of the chick. Neuron 30, 707-723.

Persohn E, Schachner M (1987) Immunoelectron microscopic localization of the neural cell adhesion molecules L1 and N-CAM during postnatal development of the mouse cerebellum. J. Cell. Biol. 105, 569-576.

Persohn E, Pollerberg GE and Schachner M (1989). Immunoelectron-microscopic localization of the 180 kD component of the neural cell adhesion molecule N-CAM in postsynaptic membranes. J. Comp. Neurol. 1;288:92-100.

Persohn E, Schachner M (1990) Immunohistological localization of the neural adhesion molecules L1 and NCAM in the developing hippocampus of the mouse. J. Neurocytol. 19, 807-819.

Peschanski M, Bachoud-Levi AC, Hantraye P (2004) Integrating fetal neural transplants into a therapeutic strategy: the example of Huntington's disease. Brain 127:1219–1228.

Petersén A, Hansson O, Puschban Z, Sapp E, Romero N, Castilho RF, Sulzer D, Rice M, DiFiglia M, Przedborski S, Brundin P (2001) Mice transgenic for exon 1 of the Huntington's disease gene display reduced striatal sensitivity to neurotoxicity induced by dopamine and 6-hydroxydopamine. Eur. J. Neurosci. 14(9):1425-35.

Petsche H, Stumpf C and Gogolak G (1962) The significance of the rabbit's septum as a relay station between midbrain and the hippocampus: I. The control of hippocampus arousal activity by the septum cells. Electroenceph. clin. Neurophysiol. 14:202-211.

Pollard SM, Conti L, Sun Y, Goffredo D, Smith A (2006) Adherent neural stem (NS) cells from fetal and adult forebrain. Cereb. Cortex 1: i112–120.

Pollerberg GE, Burridge K, Krebs KE, Goodman SR and Schachner M.(1987). The 180-kD component of the neural cell adhesion molecule N-CAM is involved in a cellcell contacts and cytoskeleton-membrane interactions. Cell Tissue Res 250(1):227-36.

Polo-Parada L, Bose CM, Landmesser LT. (2001) Alterations in transmission, vesicle dynamics, and transmitter release machinery at NCAM-deficient neuromuscular junctions. Neuron 32: 815-828.

Porada CD, Park P, Almeida-Porada G, Zanjani ED (2004) The sheep model of in utero gene therapy. Fetal Diagn. Ther. (1):23-30.

Price ML, Hoffer BJ, Granholm AC (1996) Effects of GDNF on fetal septal forebrain transplants in oculo. Exp. Neurol. 141:181-189.

Purves D, Lichtman JW (1983) Specific connections between nerve cells. Annu. Rev. Physiol. 45, 553-565.

Qian X, Shen Q, Goderie SK, He W, Capela A, Davis AA, Temple S (2000) Timing of CNS cell generation: A programmed sequence of neuron and glial cell production from isolated murine cortical stem cells. Neuron 28: 69–80.

Quenneville SP, Chapdelaine P, Rousseau J, Beaulieu J, Caron NJ, Skuk D, Mills P, Olivares EC, Calos MP, Tremblay JP (2004) Nucleofection of muscle-derived stem cells and myoblasts with phiC31 integrase: stable expression of a full-length-dystrophin fusion gene by human myoblasts. Mol. Ther. 10(4):679-87.

Quintero EM, Willis LM, Zaman V, Lee J, Boger HA, Tomac A, Hoffer BJ, Stromberg I, Granholm AC (2004) Glial cell line-derived neurotrophic factor is essential for neuronal survival in the locus coeruleus-hippocampal noradrenergic pathway. Neuroscience 124:137-146.

Rakic P (2003) Elusive radial glial cells: historical and evolutionary perspective. Glia 43(1):19-32.

Rafuse VF, Polo-Parada L, Landmesser LT (2000) Structural and functional alterations of neuromuscular junctions in NCAM-deficient mice. J. Neurosci. 20:6529-6539.

Rappa G, Kunke D, Holter J, Diep DB, Meyer J, Baum C, Fodstad O, Krauss S, Lorico A (2004) Efficient expansion and gene transduction of mouse neural stem/progenitor cells on recombinant fibronectin. Neuroscience 124(4):823-30.

Rathjen FG, Schachner M (1984) Immunocytological and biochemical characterization of a new neuronal cell surface component (L1 antigen) which is involved in cell adhesion. EMBO J 3: 1-10.

Reynolds B A, Weiss S (1992) Generation of neurons and astrocytes from isolated cells of the adult mammalian central nervous system. Science 255 (5052):1707-1710.

Reynolds B A, Tetzlaff W, Weiss S (1992) A multipotent EGF-responsive striatal embryonic progenitor cell produces neurons and astrocytes. J. Neurosci. 12: 4565–4574.

Richard I, Ader M, Sytnyk V, Dityatev A, Richard G, Schachner M, Bartsch U (2005) Electroporation-based gene transfer for efficient transfection of neural precursor cells. Brain Res. Mol. Brain Res. 138(2):182-90.

Rolf B, Kutsche M, Bartsch U (2001) Severe hydrocephalus in L1-deficient mice. Brain. Res. 891, 247-252.

Rose SP (1995) Cell-adhesion molecules, glucocorticoids and long-term-memory formation. Trends. Neurosci. 18, 502-506.

Rosenthal A, Jouet M, Kenwrick S (1992) Aberrant splicing of neural cell adhesion molecule L1 mRNA in a family with X-linked hydrocephalus. Nat. Genet. 2, 107-112.

Rossi F, Cattaneo E (2002) Opinion: Neural stem cell therapy for neurological diseases: Dreams and reality. Nat. Rev. Neurosci. 3: 401–409.

Rowntree CI and Bland BH (1986) An analysis of cholinoceptive neurons in the hippocampal formation by direct microinfusion. Brain. Res. 362:98-113.

Ruoslahti E, Pierschbacher MD (1987) New perspectives in cell adhesion: RGD and integrins. Science 238, 491-497.

Rutishauser U, Edelman GM (1980) Effects of fasciculation on the outgrowth of neurites from spinal ganglia in culture. J. Cell Biol. 87: 370-378.

Rutishauser U and Landmesser L(1996). Polysialic acid in the vertebrate nervous system: a promoter of plasticity in cell-cell interactions. Trends Neurosci. 19:422-7.

Ryu JK, Kim J, Cho SJ, Hatori K, Nagai A, Choi HB, Lee MC, McLarnon JG, Kim SU (2004) Proactive transplantation of human neural stem cells prevents degeneration of striatal neurons in a rat model of Huntington disease. Neurobiol. Dis. 1:68-77.

Sadoul K, Sadoul R, Faissner A, Schachner M (1988) Biochemical characterization of different molecular forms of the neural cell adhesion molecule L1. J, Neurochem, 50, 510-521.

Salzer JL, Holmes WP and Colman DR (1987). The amino acid sequences of the myelin-associated glycoproteins: homology to the immunoglobulin gene superfamily. J. Cell Biol. 104:957-65.

Salton SR, Shelanski ML, Greene LA (1983) Biochemical properties of the nerve growth factor-inducible large external (NILE) glycoprotein. J. Neurosci. 3, 2420-2430.

Sambrook J., Fritsch E. F., Maniatis T. (1989). Molecular cloning: A Laboratory Manual. (Cold Spring Harbor: Cold Spring Harbor Laboratory).

Sariola H, Saarma M (2003) Novel functions and signalling pathways for GDNF. J. Cell Sci. 116:3855-3862.

Satoh K, Armstrong DM and Fibiger HC (1983) A comparison of the distribution of central cholinergic neurons as demonstrated by acetylcholinesterase pharmacohistochemistry and choline acetyltransferase immunohistochemistry. Brain Res. Bull. 11:693-720.

Schiefer J, Topper R, Schmidt W, Block F, Heinrich PC, Noth J, Schwarz M (1998) Expression of interleukin 6 in the rat striatum following stereotaxic injection of quinolinic acid. J. Neuroimmunol. 89:168–176.

Schrander-Stumpel C, Fryns JP (1998) Congenital hydrocephalus: nosology and guidelines for clinical approach and genetic counselling. Eur. J. Pediatr. 157, 355-362.

Schuch U, Lohse MJ, Schachner M (1989) Neural cell adhesion molecules influence second messenger systems. Neuron 3: 13-20.

Schultz W (1986). Activity of pars reticulata neurons of monkey substantia nigra in relation to motor, sensory and complex events. J. Neurophysiol. 55 (4): 660–677.

Schurmann G, Haspel J, Grumet M, Erickson HP (2001) Cell adhesion molecule L1 in folded (horseshoe) and extended conformations. Mol. Biol. Cell. 12, 1765-1773.

Schuster T., Krug,M., Hassan,H., and Schachner,M. (1998). Increase in proportion of hippocampal spine synapses expressing neural cell adhesion molecule NCAM180 following long-term potentiation. J. Neurobiol. 37, 359-372.

Schuster T, Krug M, Stalder M, Hackel N, Gerardy-Schahn R, and Schachner M (2001). Immunoelectron microscopic localization of the neural recognition molecules L1, NCAM, and its isoform NCAM180, the NCAM-associated polysialic acid, beta1 integrin and the extracellular matrix molecule tenascin-R in synapses of the adult rat hippocampus. J. Neurobiol. 49: 142-158.

Scoville WB and Milner B (1957) Loss of recent memory after bilateral hippocampal lesions. J. Neurol. Neurosurg. Psychiatry 20:11-12.

Seaberg RM, van der Kooy D (2003) Stem and progenitor cells: the premature desertion of rigorous definitions. Trends. Neurosci. 26, 125–131.

Seilheimer B and Schachner M.(1988). Studies of adhesion molecules mediating interactions between cells of peripheral nervous system indicate a major role for L1 in mediating sensory neuron growth on Schwann cells in culture. J. Cell Biol. 107:341-51.

Seilheimer B, Persohn E, Schachner M (1989) Neural cell adhesion molecule expression is regulated by Schwann cell-neuron interactions in culture. J. Cell. Biol. 108, 1909-1915.

Seki T, Arai Y (1991) The persistent expression of a highly polysialylated NCAM in the dentate gyrus of the adult rat. Neurosci Res.12: 503-513.

Serville F, Lyonnet S, Pelet A, Reynaud M, Louail C, Munnich A, Le Merrer M (1992) X-linked hydrocephalus: clinical heterogeneity at a single gene locus. Eur. J. Pediatr. 151, 515-518.

Sharp AH, Ross CA (1996) Neurobiology of Huntington's disease. Neurobiol. Dis. 3:3–15.

Shim JW, Park CH, Bae YC, Bae JY, Chung S, Chang MY, Koh HC, Lee HS, Hwang SJ, Lee KH, Lee YS, Choi CY, Lee SH (2007). Generation of functional dopamine neurons from neural precursor cells isolated from the subventricular zone and white matter of the adult rat brain using Nurr1 overexpression. Stem Cells. 25(5):1252-62.

Shepard JD, Chuang DT, Shaham Y, Morales M (2006) Effect of methamphetamine self-administration on tyrosine hydroxylase and dopamine transporter levels in mesolimbic and nigrostriatal dopamine pathways of the rat. Psychopharmacology (Berl). 185(4):505-13. Epub 2006 Mar 23.

Shults C, Kimber TA (1992) Mesencephalic dopaminergic cells exhibit increased density of neural cell adhesion molecule and polysialic acid during development. Brain. Res. Dev. Brain. Res. 65:161-172.

Sidman RL, Angevine JB and Peirce ET (1971) Atlas of the mouse brain and spinal cord. Harvard University Press, Cambridge, Massachusetts.

Sinor AD, Lillien L (2004) Akt-1 expression level regulates CNS precursors. J. Neurosci. 24: 8531–8541.

Sirinathsinghji DJ, Dunnett SB, Isacson O, Clarke DJ, Kendrick K, Bjorklund A (1988) Striatal grafts in rats with unilateral neostriatal lesions—II. *In vivo* monitoring of GABA release in globus pallidus and substantia nigra. Neuroscience 24:803–811.

Skibo GG, Davies HA, Rusakov DA, Stewart MG, Schachner M (1998) Increased immunogold labeling of neural cell adhesion molecule isoforms in synaptic active zones of the chick striatum 5-6 h after one-trial passive avoidance training. Neuroscience 82: 1-5.

Small SJ and Akeson R.(1990). Expression of the unique NCAM VASE exon is independently regulated in distinct tissues during development. J. Cell Biol. 111:2089-96.

Small SJ, Haines SL and Akeson RA.(1988). Polypeptide variation in an N-CAM extracellular immunoglobulin-like fold is developmentally regulated through alternative splicing. Neuron 1:1007-17.

Song H, Stevens CF, Gage FH (2002) Astroglia induce neurogenesis from adult neural stem cells. Nature 417, 39–44.

Squire LR and Zola-Morgan S (1991) The medial temporal lobe memory system. Science 253:1380-1386.

Staubli U, Chun D, Lynch G (1998) Time-dependent reversal of long-term potentiation by an integrin antagonist. J.Neurosci. 18, 3460-3469.

Stoenica L, Senkov O, Gerardy-Schahn R, Weinhold B, Schachner M, Dityatev A (2006) *In vivo* synaptic plasticity in the dentate gyrus of mice deficient in the neural cell adhesion molecule NCAM or its polysialic acid. Eur J Neurosci 23: 2255-2264.

Stork, O., Welzl, H., Cremer, H., and Schachner, M. (1997). Increased intermale aggression and neuroendocrine response in mice deficient for the neural cell adhesion molecule (NCAM). Eur. J. Neurosci. 9, 1117-1125.

Stork, O., Welzl, H., Wotjak, C. T., Hoyer, D., Delling, M., Cremer, H., and Schachner, M. (1999). Anxiety and increased 5-HT1A receptor response in NCAM null mutant mice. J. Neurobiol. 40, 343-355.

Strekalova H, Buhmann C, Kleene R, Eggers C, Saffell J, Hemperly J, Weiller C, Mueller-Thomsen T, Schachner M (2005) Elevated levels of neural recognition molecule L1 in the cerebrospinal fluid of patients with Alzheimer disease and other dementia syndromes. Neurobiol. Aging 27(1):1-9.

Sun W, Akins CK, Mattingly AE, Rebec GV (2005) Ionotropic glutamate receptors in the ventral tegmental area regulate cocaine-seeking behavior in rats. Neuropsychopharmacology. 30(11):2073-81.

Super H, Soriano E, Uylings H. B (1998) The functions of the preplate in development and evolution of the neocortex and hippocampus. Brain Res.Brain Res.Rev. 27 (1):40-64.

Suslov ON, Kukekov VG, Ignatova TN, Steindler DA (2002) Neural stem cell heterogeneity demonstrated by molecular phenotyping of clonal neurospheres. Proc. Natl. Acad. Sci. U S A 99: 14506–14511.

Svendsen CN, Clarke DJ, Rosser AE, Dunnett SB (1996) Survival and differentiation of rat and human epidermal growth factor-responsive precursor cells following grafting into the lesioned adult central nervous system. Exp. Neurol. 137:376–388.

Sytnyk V, Leshchyns'ka I, Nikonenko AG, Schachner M (2006) NCAM promotes assembly and activity-dependent remodeling of the postsynaptic signaling complex. J. Cell. Biol. 25;174(7):1071-85.

Takeda Y, Asou H, Murakami Y, Miura M, Kobayashi M, Uyemura K (1996) A nonneuronal isoform of cell adhesion molecule L1: tissue-specific expression and functional analysis. J.Neurochem. 66, 2338-2349.

Tamamaki N, Nakamura K, Okamoto K, Kaneko T (2001) Radial glia is a progenitor of neocortical neurons in the developing cerebral cortex. Neurosci.Res. 41 (1):51-60.

Tang L, Hung CP, Schuman EM (1998) A role for the cadherin family of cell adhesion molecules in hippocampal long-term potentiation. Neuron 20, 1165-1175.

Tang TS, Chen X, Liu J, Bezprozvanny I (2007). Dopaminergic signaling and striatal neurodegeneration in Huntington's disease. J Neurosci. 25;27(30):7899-910.

Taupin P and Gage F.H (2002) Adult neurogenesis and neural stem cells of the central nervous system in mammals. J.Neurosci.Res. 69 (6):745-749.

Teitelbaum H, Lee JF and Johannessen JN (1975) Behaviorally evoked hippocampal theta waves: a cholinergic response. Science 188:1114-1116.

Temple S (1989) Division and differentiation of isolated CNS blast cells in microculture. Nature 340: 471–473.

Tepass U, Truong K, Godt D, Ikura M, Peifer M (2000) Cadherins in embryonic and neural morphogenesis. Nat. Rev. Mol. Cell. Biol. 1, 91-100.

The Huntington's Disease Collaborative Research Group (1993) A novel gene containing a trinucleotide repeat that is expanded and unstable on Huntington's disease chromosomes. Cell 72:971–983.

Thiery JP, Brackenbury R, Rutishauser U, Edelman GM (1977) Adhesion among neural cells of the chick embryo. II. Purification and characterization of a cell adhesion molecule from neural retina. J. Biol. Chem. 252, 6841-6845.

Thomas SN, Soreghan BA, Nistor M, Sarsoza F, Head E, Yang AJ (2005) Reduced neuronal expression of synaptic transmission modulator HNK-1/neural cell adhesion molecule as a potential consequence of amyloid beta-mediated oxidative stress: a proteomic approach. J. Neurochem. 92:705-717.

Thor G, Probstmeier R, Schachner M (1987) Characterization of the cell adhesion molecules L1, N-CAM and J1 in the mouse intestine. EMBO J 6, 2581-2586.

Todaro L, Puricelli L, Gioseffi H, Guadalupe PM, Lastiri J, Bal de Kier JE, Varela M, Sacerdote dL (2004) Neural cell adhesion molecule in human serum. Increased levels in dementia of the Alzheimer type. Neurobiol. Dis. 15:387-393.

Tomasiewicz H, Ono K, Yee D, Thompson C, Goridis C, Rutishauser U, and Magnuson T (1993). Genetic deletion of a neural cell adhesion molecule variant (N-CAM- 180) produces distinct defects in the central nervous system. Neuron 11: 1163-1174.

Topper R, Gehrmann J, Schwarz M, Block F, Noth J, Kreutzberg GW (1993) Remote microglial activation in the quinolinic acid model of Huntington's disease. Exp. Neurol. 123:271–283.

Towbin H, Staehelin T, Gordon J (1979) Electrophoretic transfer of proteins from polyacrylamide gels to nitrocellulose sheets: procedure and some applications. Proc. Natl. Acad. Sci. U S A. 76(9), 4350-4.

Trapnell BC, Gorziglia M (1994) Gene therapy using adenoviral vectors. Curr. Opin. Biotechnol. 6:617-25.

Tropepe V, Sibilia M, Ciruna BG, Rossant J, Wagner EF, van der Kooy D (1999) Distinct neural stem cells proliferate in response to EGF and FGF in the developing mouse telencephalon. Dev. Biol. 208: 166–188.

Tropepe V, Hitoshi S, Sirard C, Mak TW, Rossant J, van der Kooy D (2001) Direct neural fate specification from embryonic stem cells: a primitive mammalian neural stem cell stage acquired through a default mechanism. Neuron 30: 65–78.

Uchida N, Buck DW, He D, Reitsma MJ, Masek M, Phan TV, Tsukamoto AS, Gage FH, Weissman IL (2000) Direct isolation of human central nervous system stem cells. Proc. Natl. Acad. Sci. U S A 97:14720–14725.

Ulla M, Thobois S, Lemaire JJ, Schmitt A, Derost P, Broussolle E, Llorca PM, Durif F (2006) Manic behaviour induced by deep-brain stimulation in Parkinson's disease: evidence of substantia nigra implication? J. Neurol. Neurosurg. Psychiatry. 77(12):1363-6.

Uylings HB, van Pelt J, Parnavelas JG, Ruiz-Marcos A (1994) Geometrical and topological characteristics in the dendritic development of cortical pyramidal and non-pyramidal neurons. Prog. Brain Res. 102:109-23.

Vaccarino FJ, Franklin KB, Prupas D (1985). Opposite locomotor asymmetries elicited from the medial and lateral substantia nigra: role of the superior colliculus. Physiol. Behav. 35(5):741-7.

Vaithianathan T, Matthias K, Bahr B, Schachner M, Suppiramaniam V, Dityatev A, Steinhauser C (2004) Neural cell adhesion molecule-associated polysialic acid potentiates alpha-amino-3-hydroxy-5-methylisoxazole-4-propionic acid receptor currents. J. Biol. Chem. 279:47975-47984.

van der Kooy D, Weiss S (2000) Why stem cells? Science 287, 1439–1441.

Venero C, Tilling T, Hermans-Borgmeyer I, Herrero AI, Schachner M, Sandi C (2004) Water maze learning and forebrain mRNA expression of the neural cell adhesion molecule L1. J. Neurosci .Res. 75, 172-181.

Ventimiglia R, Mather PE, Jones BE, Lindsay RM (1995) The neurotrophins BDNF, NT-3 and NT-4/5 promote survival and morphological and biochemical differentiation of striatal neurons *in vitro*. Eur. J. Neurosci. 7:213–222.

Vescovi AL, Parati EA, Gritti A, Poulin P, Ferrario M, Wanke E, Frölichsthal-Schoeller P, Cova L, Arcellana-Panlilio M, Colombo A, Galli R (1999) Isolation and cloning of multipotential stem cells from the embryonic human CNS and establishment of transplantable human neural stem cell lines by epigenetic stimulation. Exp. Neurol. 156: 71–83.

Vitry S, Avellana-Adalid V, Lachapelle F, Evercooren AB (2001) Migration and multipotentiality of PSA-NCAM+ neural precursors transplanted in the developing brain. Mol. Cell. Neurosci. 6:983-1000.

Vits L, van Camp G, Coucke P, Fransen E, De Boulle K, Reyniers E, Korn B, Poustka A, Wilson G, Schrander-Stumpel C (1994) MASA syndrome is due to mutations in the neural cell adhesion gene L1CAM. Nat. Genet. 7, 408-413.

Vutskits L, Djebbara-Hannas Z, Zhang H, Paccaud JP, Durbec P, Rougon G, Muller D, Kiss JZ (2001) PSA-NCAM modulates BDNF-dependent survival and differentiation of cortical neurons. Eur. J. Neurosci. 13:1391-1402.

Wainer BH, Bolam JP, Freund TF, Henderson Z, Totterdell S and Smith AD (1984) Cholinergic synapses in the rat brain: a correlated light and electron microscopic immunohistochemical study employing a monoclonal antibody against choline acetyltransferase. Brain. Res. 308:69-76.

Walmod PS, Kolkova K, Berezin V, Bock E (2004) Zippers make signals: NCAm-mediated molecular interactions and signal transduction. Neurochem Res 29: 2015-2035.

Walsh FS and Doherty P.(1991). Glycosylphosphatidylinositol anchored recognition molecules that function in axonal fasciculation, growth and guidance in the nervous system. Cell Biol. Int. Rep. 15:1151-66.

Walsh FS, Meiri K, Doherty P (1997) Cell signalling and CAM-mediated neurite outgrowth. Soc. Gen. Physiol. Ser. 52:221-226.

Ward NL, Hagg T (2000) BDNF is needed for postnatal maturation of basal forebrain and neostriatum cholinergic neurons *in vivo*. Exp. Neurol. 162:297-310.

Watt FM, Hogan BL (2000) Out of Eden: stem cells and their niches. Science 287: 1427–1430.

Weinelt S, Peters S, Bauer P, Mix E, Haas SJ, Dittmann A, Petrov S, Wree A, Cattaneo E, Knoblich R, Strauss U, Rolfs A (2003) Ciliary neurotrophic factor overexpression in neural progenitor cells (ST14A) increases proliferation, metabolic activity, and resistance to stress during differentiation. J. Neurosci. Res. 71(2):228-36.

Weis C, Marksteiner J, Humpel C (2001) Nerve growth factor and glial cell line-derived neurotrophic factor restore the cholinergic neuronal phenotype in organotypic brain slices of the basal nucleus of Meynert. Neuroscience 102:129-138.

Weiss S, Dunne C, Hewson J, Wohl C, Wheatley M, Peterson AC, Reynolds BA (1996a) Multipotent CNS stem cells are present in the adult mammalian spinal cord and ventricular neuroaxis. J. Neurosci. 16(23): 7599–7609.

Weiss S, Reynolds B A, Vescovi AL, Morshead C, Craig CG, van der Kooy D (1996b) Is there a neural stem cell in the mammalian forebrain? Trends. Neurosci. 19, 387–393.

Wiesenhofer B, Humpel C (2000) Lipid-mediated gene transfer into primary neurons using FuGene: comparison to C6 glioma cells and primary glia. Exp. Neurol. 164(1):38-44.

Williams AF, Barclay AN (1988) The immunoglobulin superfamily--domains for cell surface recognition. Annu. Rev. Immunol. 6, 381-405.

Williams LR, Inouye G, Cummins V, Pelleymounter MA (1996) Glial cell line-derived neurotrophic factor sustains axotomized basal forebrain cholinergic neurons *in vivo*: dose-response comparison to nerve growth factor and brain-derived neurotrophic factor. J. Pharmacol. Exp. Ther. 277:1140-1151.

Winkler C, Fricker RA, Gates MA, Olsson M, Hammang JP, Carpenter MK, Bjorklund A (1998) Incorporation and glial differentiation of mouse EGF-responsive neural progenitor cells after transplantation into the embryonic rat brain. Mol. Cell .Neurosci. 11(3):99–116.

Wenk GL, Stoehr JD, Quintana G, Mobley S and Wiley RG (1994) Behavioral, biochemical, histological, and electrophysiological effects of 192 IgG-saporin injections into the basal forebrain of rats. J. Neurosci. 14:5986-5995.

Wood ER, Dudchenko PA and Eichenbaum H (1999) The global record of memory in hippocampal neuronal activity. Nature 397:613-616.

Wong EV, Schaefer AW, Landreth G, Lemmon V (1996a) Casein kinase II phosphorylates the neural cell adhesion molecule L1. J.Neurochem. 66, 779-786.

Wong EV, Schaefer AW, Landreth G, Lemmon V (1996b). Involvement of p90rsk in neurite outgrowth mediated by the cell adhesion molecule L1. J.Biol.Chem. 271, 18217-18223.

Wu P, Ye Y, Svendsen CN (2002) Transduction of human neural progenitor cells using recombinant adeno-associated viral vectors. Gene Ther. 9(4):245-55.

Yamasaki M, Arita N, Hiraga S, Izumoto S, Morimoto K, Nakatani S, Fujitani K, Sato N, Hayakawa T (1995) A clinical and neuroradiological study of X-linked hydrocephalus in Japan. J. Neurosurg. 83, 50-55.

Yang Y, Li Q, Ertl HC, Wilson JM (1995) Cellular and humoral immune responses to viral antigens create barriers to lung-directed gene therapy with recombinant adenoviruses. J. Virol. 69(4):2004-15.

Ying H, Zaks TZ, Wang RF, Irvine KR, Kammula US, Marincola FM, Leitner WW, Restifo NP (1999) Cancer therapy using a self-replicating RNA vaccine. Nat. Med. (7):823-7.

Ying QL, Stavridis M, Griffiths D, Li M, Smith A (2003) Conversion of embryonic stem cells into neuroectodermal precursors in adherent monoculture. Nat. Biotechnol. 21: 183–186.

Yohrling GJ 4th, Jiang GC, DeJohn MM, Miller DW, Young AB, Vrana KE, Cha JH. (2004) Analysis of cellular, transgenic and human models of Huntington's disease reveals tyrosine hydroxylase alterations and substantia nigra neuropathology. Brain Res Mol Brain Res. 6;119(1):28-36.

Zaborszky L, Vadasz C (2001) The midbrain dopaminergic system: anatomy and genetic variation in dopamine neuron number of inbred mouse strains. Behav Genet 31: 47-59.

Zola-Morgan S and Squire LR (1986) Memory impairment in monkeys following lesions limited to the hippocampus. Behav. Neurosci. 100:155-160.

Zold CL, Larramendy C, Riquelme LA, Murer MG (2007) Distinct changes in evoked and resting globus pallidus activity in early and late Parkinson's disease experimental models. Eur. J. Neurosci. 2007 26(5):1267-79.

Zuccato C, Ciammola A, Rigamonti D, Leavitt BR, Goffredo D, Conti L, MacDonald ME, Friedlander RM, Silani V, Hayden MR, Timmusk T, Sipione S, Cattaneo E (2001) Loss of Huntingtin–mediated BDNF gene transcription in Huntington's disease. Science 293: 493–498.

Abbreviations

ANOVA	Analysis of variance
Amp	Ampicillin
BDNF	Brain derived neurotrophic factor
bFGF	Basic fibroblast growth factor
BLBP	Brain lipid binding protein
BME	Eagle's basal medium
bp	Base pairs
BrdU	Bromodeoxyuridine
BSA	Bovine serum albumine
CA	Cornu ammonis
$CaCl_2$	Calcium chloride
CAM	Cell adhesion molecule
cAMP	Cyclic adenosine monophosphate
cDNA	Complementary deoxyribonucleic acid
ChAT	Choline acetyltransferase
CHO	Chinese Hamster Ovarian
CMV	Cytomegalovirus
CNS	Central nervous system
D	Dalton (g / mol)
dd	Double distilled
DB	Diagonal band of Broca
DG	Dentate gyrus
DMEM	Dulbecco's modified Eagle's medium
DMSO	Dimethylsulfoxide
DNA	Desoxyribonucleic acid
dNTP	2’-desoxyribonucleotide-5’-triphosphate
dsDNA	Double-stranded DNA
E	Embryonic
ECL	Enhanced chemiluminescence
EDTA	Ethylendiamintetraacetic acid
e.g	For example
EGF	Epidermal growth factor
EGFL	EGF-like
EGFR	Epidermal growth factor receptor
EGFP	Enhanced green fluorescence protein
ES	Embryonic stem
FCS	Fetal calf serum

FGF	Fibroblast growth factor
FGF-2	Fibroblast growth factor-2
FNIII	Fibronectin type III
g	Gram
GABA	Gamma amino butyric acid
GDNF	Glial-cell-line-derived neurotrophic factor
GFAP	Glial fibrilary acidic protein
GFP	Green fluorescence protein
GLAST	Solute carrier family 1 (glial high affinity glutamate transporter), member 3
GPI	Glycosylphosphaditylinositol
GTPCH1	GTP cyclohydrolase 1
h	hour(s)
HBSS	Hank´s balanced salt solution
HD	Huntington's disease
hDB	Horizontal limb of the diagonal band of Broca
HEPES	2-(4-(2-Hydroxyethyl)-piperzino)-ethansulfonic acid
HRP	Horseradish peroxidase
Hz	Hertz
Ig	Immunoglobulin
i.e.	Id est (that is)
Kan	Kanamycin
kb	Kilo base pairs
KD	Kilo Dalton
l	Liter
LB	Luria Bertani
L-DOPA	L-dihydroxyphenyl alanine
LTP	Long-term potentiation
LTD	Long-term depression
LS	Lateral septum
LSM	Laser scanning microscope
m	milli (10^{-3})
M	Mole
MAG	Myelin-associated glycoprotein
MEM	Minimal essential medium
min	Minute
ml	Milliliter (Litre × 10^{-3})
MOPS	(4-(N-morpholino)-propan)-sulfonic acid
mRNA	Messenger ribonucleic acid
MS	Medial septum

MSDB	Medial septum / diagonal band of Broca
MSDbBnc	Medial septum / diagonal band of Broca nuclear complex
n	nano (10^{-9})
NaCl	Sodium chloride
NaOH	Sodium hydroxide solution
NB	Nucleus basalis
NCAM	Neural cell adhesion molecule
NCAM-/-	NCAM deficient
NCAM+/+	NCAM non-deficient
NDS	Normal donkey serum
NSC	Neural stem cell
Nm	Nanometers
NMDA	N-methyl-D-aspartate
OD	Optic density
p	pico (10^{-12})
P	Postnatal
PAGE	polyacrylamide gel electrophoresis
Pax6	Paired box gene 6
PBS	Phosphate-buffered saline
PCR	Polymerase chain reaction
PD	Parkinson disease
PDGF	Platelet-derived growth factor
PFA	Paraformaldehyde
pH	p(otential) of H(ydrogen), the logarithm of the reciprocal of hydrogen-ion concentration in gram atoms per liter
PLL	Poly-l-lysine
PSA	Polysialic acid
PSA-NCAM	Polysialated neural cell adhesion molecule
QA	Quinolinic acid
RC2	Intermediate filament-associated protein RC2
RGB	Red green blue
RNA	Ribonucleic acid
rpm	Rounds per minute
RT	Room temperature
SEM	Standard error of mean
SD	Standard deviation
SDS	Sodium dodecyl sulfate
SDS-PAGE	SDS-polyacrylamide gel electrophoresis
Sox1	Official symbol of SRY (sex determining region Y)-

	box 1
Sox2	Official symbol of SRY (sex determining region Y)-box 2
SVZ	Subventricular zone
TAE	Tris-acetate buffer
TBS	Tris-buffered saline
TEMED	N,N,N',N'-Tetramethylethylendiamin
Tris	Tris(-hydroxymethyl)-aminomethane
U	Unit
UV	Ultra-violett
V	Volt
VASE	Variable alternative spliced exon
vDB	Vertical limb of diagonal band of Broca
vol	Volume
VZ	Ventricular zone
v/v	Volume/volume
w/v	Weight/volume
µ	Micro (10-6)
°C	Grad Celsius
%	Percent

Acknowlegment

This study has been performed in the Institute for Biosynthesis of Neuronal Structures of the Center for Molecular Neurobiology (ZMNH) at the University of Hamburg. I would like to thank sincerely Prof. Melitta Schachner for providing facilities for this research, fruitful discussions and for constant support and guidance during these years.

I would also like to thank Prof. Konrad Wiese for the external supervision of this thesis.

I am especially grateful to Dr. Andrey Irintchev for nice supervision, for providing me with a big source of ideas, fruitful discussions and for his constant support during all years.

I would also like to thank Dr. Udo Bartsch for supervision, for providing new ideas and for helpful discussions.

I also wish to thank the present and former colleagues in the lab for their help during this work. I thank Ines Richard for introducing me in the new methods and helping me to overcome all kinds of problems at the beginning. I would also like to thank Dr. Christian Bernreuther for introducing me in molecular biology technique and Dr. Gabriele Loers for introducing me in biochemistry technique. Thanks to all present and former members of the morphology and stem cells groups for providing a nice and inspiring working atmosphere. Especially I would like to thank my lab mates Elena Uliyanova, Tatjana Makhina, Galina Dityateva, Dr. Daria Guseva, Dr. Elena Sivukhina, Dr. Alexander Dityatev, Dr. Olena Bukalo**,** Dr. Mirjam Sibbe, Ivayla Apostolova, Olga Simova, Emmanuela Szpotowicz, Dr. Gunnar Hargus.

I am grateful to Dr. Fabio Morellini for breeding of NCAM deficient mice, Achim Dahlmann for their genotyping and Eva Kronberg for great animal care.

For the correction and help with this manuscript I would like to thank Drs. A. Irintchev and U. Bartsch.

For checking up my English I would like to thanks Dr. Andrew Sharott.

I am grateful to my family and my friends in Ukraine who supported me at the thousands kilometer distance all this time. I also wish to thank my friends in Hamburg for making this time special and support. My special thanks to my friend Andrii for his trust in me, patience and love.

Publications and poster presentations

Publications

Tereshchenko Y, Dityatev A, Schachner M, Irintchev A. Hippocampal dysplasia and aberrations in cholinergic and catecholaminergic nuclei and their hippocampal projections in NCAM-deficient mice (in preparation).

Tereshchenko Y, Brandewiede J, Schachner M, Irintchev A, Morellini F. Stereological estimation of noradrenergic neurons in locus coeruleus and septal cholinergic neurons in C57BL/6 mice and their relation to novelty-induced behavior (in preparation).

Poster presentations

Yuliya Tereshchenko, Joerg Brandewiede, Fabio Morellini, Alexander Dityatev, Melitta Schachner, Andrey Irintchev (2007). Hippocampal dysplasia and aberrations in cholinergic and catecholaminergic nuclei and their hippocampal projections in NCAM-deficient mice: Implications for behavior. 31th Göttingen Neurobiology Conference, March 29 – April 1, 2007, Göttingen, Germany.

Certification

Universitätsklinikum Hamburg-Eppendorf

Institut für Neurophysiologie und Pathophysiologie

Zentrum für Experimentelle Medizin

Martinistraße 52
20246 Hamburg
Telefon: (040) 42803-7238
Telefax: (040) 42803-7752
www.uke.uni-hamburg.de

Institut für Neurophysiologie und Pathophysiologie
Universitätsklinikum Hamburg-Eppendorf, Martinistr. 52, 20246 Hamburg

2. Dezember 2007

I, Dr. Andrew Sharott, from the institute of Neurophysiology and Pathophysiology, at the University Medical Centre Hamburg-Eppendorf, do confirm as an English native speaker that the PhD thesis "Neural stem cells from embryonic brain of mice and neural cell adhesion molecule L1 and projection aberrations to the hippocampus in NCAM deficient mice (Mus musculus L., 1758) by Yulyia Tereshchenko is written in appropriate and correct English.

Dr Andrew Sharott